Photoswitchable Sensors:
Reversible Ion Detection Using Optical Fibres

by
Daniel Stubing

A thesis submitted in fulfilment of the requirements for the degree of Doctor of Philosophy

At The University of Adelaide

School of Physical Sciences

2017

Contents

Abstract ..... **v**

Declaration ..... **vii**

Publications During Candidature ..... **ix**

Acknowledgements ..... **xi**

Contributions ..... **xiii**

Abbreviations ..... **xv**

Chapter 1 Introduction **1**

1.1 Background and Motivation 3

1.1.1 Importance of Sensors for Metal Ions in Biology 3

1.1.2 Current Techniques for Biological Metal Ion Sensing 5

1.1.3 The Design of a New Sensor Platform for Biological Metal Ions 6

1.2 The Microstructured Optical Fibre Component 8

1.2.1 Optical Fibres as Sensors 9

1.2.2 The Principles of MOFs as Fluorescence Sensors 10

1.3 Surface Chemistry 14

1.3.1 Chemical Properties of Silica Glass 14

1.3.2 Silanization: Basic overview of the chemistry and protocols 15

1.4 The Photoswitchable Component 17

1.5 Outline of Thesis 19

1.5.1 Chapter 2 19

1.5.2 Chapter 3 19

1.5.3 Chapter 4 19

1.5.4 Chapter 5 20

1.5.5 Appendices 20

1.6 References for Chapter 1 21

Chapter 2 Suitability of Photoswitches for MOF Devices **31**

2.1 Overview of Chapter 33

2.2 PAPER 1: A Comparative Study of the Fluorescence and Photostability of Common Photoswitches in Microstructured Optical Fibre 34
2.3.1 Abstract 37
2.3.2 Introduction 37
2.3.3 Results and Discussion 42
2.3.4 Conclusions/Outlook 51
2.3.5 Materials and Methods 52
2.3.6 Supporting Information 54
2.4 Discussion of Photoswitch Properties for use as Sensors. 57
2.4.1 Structural Properties of the Photoswitches: Useable changes upon photoswitching 57
2.4.2 Wavelengths of Photoswitching 61
2.4.3 Yields of Photoswitching 63
2.4.4 High Switching Fatigue Resistance 63
2.4.5 Ease of Synthesis and Versatility in Structure Diversification 64
2.5 Conclusions to Chapter 2 66
2.6 References Chapter 2 68
Chapter 3 Photoswitchable Spiropyran Sensors for Lithium Metal Ions 77
PAPER 2: Crowned Spiropyran Fluoroionophores with a Carboxyl Moiety for the Selective Detection of Lithium Ions 79
3.1 Abstract 83
3.2 Introduction 83
3.3 Results and Discussion 85
3.3.1 Influence of the Aza-1-crown ether Group On Absorbance and Fluorescence of the Spiropyran Base-unit. 86
3.3.2 Absorbance Changes Upon Binding Alkali Metal Ions .. 87
3.3.3 Fluorescence Detection of Alkali Metal Ion Binding 90
3.4 Conclusions 93
3.5 Experimental 94
3.5.1 Materials and Methods 94
3.5.2 Synthesis of Aza-crowncrown ether Spiropyrans 94
3.5.3 Comparative Assay Procedure 97
3.5.4 Li^+ Concentration Dependence Assay Procedure 98

3.5.5 Job's Plot 98
3.6 Supplementary Information 99
3.7 References for Chapter 3 103
Chapter 4 Photoswitchable Spiropyran Sensors for the detection of Calcium Ions 105
4.1 Introduction 107
4.1.1 The Design of a Spiropyran Metal Ion Sensor 107
4.2 Extended Comparison of the Selectivity of 1-aza-12-crown-4 spiropyran (SP-1) to Divalent Metal Ions 110
4.2.1 Results and Discussion 110
4.2.2 Conclusions to Section 4.2 124
4.3 Comparison of the Influence of a N-indoline ethoxy Moiety on Sensing Metal Ions Between SP-3 and SP-4 126
4.3.1 Results and Discussion 127
4.4 Conclusions to Chapter 4 152
4.5 Materials and Methods 153
4.5.1 Synthesis of Spiropyran Fluoroionophores 153
4.5.2 Ion Binding Studies 155
4.5.3 Computational Modelling 158
4.6 References for Chapter 4 159
Chapter 5 Surface Functionalisation and MOF sensors 163
5.1 Introduction 165
5.1.1 The Current Literature on Photoswitchable Sensing Surfaces 165
5.1.2 Functionalisation of Silica Surfaces 167
5.1.3 Glass Slide Surface Characterisation Techniques 170
5.2 Attachment of Photoswitches to Glass Surfaces 173
5.2.1 Results and Discussion 174
5.2.2 Conclusions to Section 5.2 184
5.3 Investigation of Photoswitchable Sensors in MOFs 186
5.3.1 Results and Discussion 186
5.3.2 Conclusions to Section 5.3 204
5.4 Photoswitchable MOF Metal Ion Sensors in Published Articles. 205

5.4.1 PAPER 3: A Dual Sensor for Cd(II) and Ca(II): Selective nanoliter-scale sensing of metal ions 205

5.4.2 PAPER 4: Microstructured Optical Fibres and Live Cells: A Water-Soluble, Photochromic Zinc Sensor 209

5.5 Conclusion to Chapter 5 213

5.6 Materials and Methods 215

5.6.1 Glass Slide Experiments 215

5.6.2 Microstructured Optical Fibre Experiments 218

5.7 References for Chapter 5 224

Chapter 6 Overall Conclusions 229

Appendix 235

Appendix A: Synthesis and Characterisation of CF_3-fulgide 237

Appendix B: Surface Potential Experiments on Quartz Glass 255

Appendix C: Computational Models of Spiropyran-Metal Ion 1:1 Complexes 265

Appendix D: Other Publications 269

D.1 A Dual Sensor for Cd(II) and Ca(II): Selective nanolitre-scale sensing of metal ions 273

D.2 Microstructured Optical Fibres and Live Cells: A Water-Soluble, Photochromic Zinc Sensor 299

D.3 A Selective and Reversible Calcium Sensor for Biological Applications 317

Abstract

In studying and diagnosing cellular systems and diseases, the ability to accurately detect and monitor the concentrations and fluctuations of metal ions is of particular importance. Fluorescent photoswitchable sensors provide a means to reversibly detect metal ions in solution. This class of sensors uses a light stimulus to chemically switch between two distinct species, one that can bind to an analyte of choice and one that cannot bind. This then provides sensors that can be turned off at will, allowing the sensor to be reset and used again at a different time point. This thesis investigates the design, synthesis and metal ion selectivity of a series of photoswitchable sensors. These sensors contain a spiropyran core unit with differing ion binding domains, such as an aza-crown ether, providing ion specificity, as well as a free carboxyl group that allows for attachment to a solid support. A discussion on the choice of this photoswitchable moiety and subsequent design and synthesis as a new metal ion sensor is presented in Chapters 2, and 3 and 4, respectively.

These photoswitchable sensor molecules were then used within a microstructured optical fibre (MOF) sensing platform. Suspended core microstructured optical fibres provide a biologically suitable platform that provides a very sensitive means to sense in nanolitre volumes of sample. Covalently attaching these photoswitchable sensors to the light guiding core, via APTES silanization, provided a reversible sensing system capable of detecting picomolar concentrations of metal ions, such as Ca^{2+} in a biological sample while not contaminating the sample. The MOF not only provided a means to detect a fluorescence signal, it also allowed for repetitive on/off photocycling of the photoswitch, both in solution and attached to the surface.

Declaration

I certify that this work contains no material which has been accepted for the award of any other degree or diploma in any university or other tertiary institution and, to the best of my knowledge and belief, contains no material previously published or written by another person, except where due reference has been made in the text. In addition, I certify that no part of this work will, in the future, be used in a submission for any other degree or diploma in any university or other tertiary institution without the prior approval of the University of Adelaide and where applicable, any partner institution responsible for the joint-award of this degree.

I give consent to this copy of my thesis when deposited in the University Library, being made available for loan and photocopying, subject to the provisions of the Copyright Act 1968.

The author acknowledges that copyright of published works contained within this thesis resides with the copyright holder(s) of those works.

I also give permission for the digital version of my thesis to be made available on the web, via the University's digital research repository, the Library catalogue and also through web search engines, unless permission has been granted by the University to restrict access for a period of time.

Signed: _____ Date: _____

Daniel Stubing

Publications During Candidature

PAPER 1: p37

Stubing, D. B.; Heng, S.; Monro, T. M.; Abell, A. D. A comparative study of the fluorescence and photostability of common photoswitches in microstructured optical fibre. *Sensors and Actuators B: Chemical* 2017, *239*, 474-480.

PAPER 2: p79

Stubing, D. B.; Heng, S.; Abell, A. D. Crowned spiropyran fluoroionophores with a carboxyl moiety for the selective detection of lithium ions. *Organic & biomolecular chemistry* 2016, 14 (15), 3752-7.

PAPER 3: p269

Heng, S.; Mak, A. M.; **Stubing, D. B.**; Monro, T. M.; Abell, A. D. Dual Sensor for Cd(II) and Ca(II): Selective Nanolitre-Scale Sensing of Metal Ions. *Analytical Chemistry* 2014, *86* (7), 3268-3272.

PAPER 4: p273

Heng, S.; McDevitt, C. A.; **Stubing, D. B.**; Whittall, J. J.; Thompson, J. G.; Engler, T. K.; Abell, A. D.; Monro, T. M. Microstructured optical fibers and live cells: a water-soluble, photochromic zinc sensor. *Biomacromolecules* 2013, 14 (10), 3376-9.

PAPER 5: p274

Heng, S.; Zhang X.; Kostecki R.; Mak A. M.; Pei J.; **Stubing D. B.**; Ebendorff-Heidepriem H.; Abell A. D.; A Selective and Reversible Calcium Sensor for Biological Applications. (Submitted for publication)

Acknowledgements

First and foremost, I would like to thank my supervisors, if it was not for you this project would not have been possible. Dr Sabrina Heng for always being very helpful, supportive and mentoring in almost all matters throughout my PhD. Prof. Andrew Abell for taking me on and allowing me this opportunity, and for being a mentor throughout. Prof. Tanya Monro for being available as required and providing important information and contacts relating to the optics and fibre side of this project, which was the field most foreign and new to me at the start of this project.

I would also like to thank the entire Abell research group for the support that you have given me. It was great to be able to work in such a friendly and helpful environment. Even though our areas of our research are very diverse and at times the nature of my work was quite unrelated, you were always open for listening and providing assistance and feedback. Your company and friendship throughout this PhD made this experience enjoyable, in particular the friendship from Kelly Keeling and Malcolm Purdey.

I would also like to acknowledge the IPAS research team for creating a good multi-disciplinary workplace, which allows for easy collaboration with people in other fields of research. I would like to thank Dr Herbert Foo, Roman Kostecki, and Dr Eric Schartner for assistance in the lab at almost any time.

On a personal side, I would like to thank my family for always being supportive of me in this endeavour, not just mentally, but for allowing me to have the freedom I have needed, particularly through the busy and stressful times. Finally, I would like to thank all the rest my friends for giving me a social life to de-stress with. In particular, Geoff for always being someone to talk with and grab a drink/movie and Simon for helping me stay motivated to get/stay fit through this time, thereby being also able to complete two Olympic triathlons.

Finally, thank you to everyone else that provided me with support, both in and out of the lab.

Contributions

Further from those acknowledged within the text I would like to acknowledge and thank the following people for providing assistance in the work presented in this thesis.

- Roman Kostecki and Mai-Chi Ngyuen for providing assistance and training, respectively, with the MOF optics setup.
- Dr John Horsley and Georgina Sylvia for performing mass spectrometry of some synthesised compounds.
- Dr Herbert Foo for general assistance with glass based chemistry, in particular for assistance in setting up Zetasizer and for assistance when attempting to prepare fire polished F300 glass slides (not presented).
- Mellissa Keeling who assisted in some fibre functionalisation procedures.

Contributions relating to specific work presented in published work are addressed in the relevant sections.

Abbreviations

^{13}C NMR	–	carbon nuclear magnetic resonance spectroscopy
^{19}F NMR	–	fluorine nuclear magnetic resonance spectroscopy
^{1}H NMR	–	proton nuclear magnetic resonance spectroscopy
AAS	–	atomic absorption spectroscopy
ACN	–	acetonitrile
AFM	–	atomic force microscopy
APTES	–	aminopropyl triethoxysilane
Azo1	–	azobenzene lumogallion derivative (Chapter 2 and 5)
$CDCl_3$	–	deuterated chloroform
CF_3-Fulgide	–	trifluromethyl indolylfulgide (Chapter 2)
CTES	–	carboxy triethoxysilane
DA1	–	diphenythienyl perfluoropentene (Chapter 2)
DASAs	–	donor acceptor Stenhouse abducts (furfural based photoswitch)
DIPEA	–	diisopropylethylamine
DMF	–	dimethyl formamide
DMSO	–	dimethyl sulfoxide
DMSO-d_6	–	hexa-deuterated dimethyl sulfoxide (DMSO)
EDC	–	N-Ethyl-N′-(3-dimethylaminopropyl)carbodiimide hydrochloride
EDTA	–	ethylenediaminetetraacetic acid
F2	–	a type of lead silicate glass
F300	–	high purity silica glass produced by Heraeus Quartzglas
FCF	–	fluorescence capture fraction
FRET	–	Förster (fluorescence) resonance electron transfer
FT-IR	–	Fourier transform infrared
HATU	–	1-[Bis(dimethylamino)methylene]-1H-1,2,3-triazolo[4,5-b]pyridinium 3-oxid hexafluorophosphate
HBDI	–	4-hydroxybenzylidene-1,2 dimethylimidazolinone
HOMO	–	highest occupied molecular orbital
HPLC	–	high pressure liquid chromatography
ICP-MS	–	inducted coupled plasma mass spectroscopy

IR	–	infra-red
IVF	–	*in vitro* fertilisation
LDA	–	lithium diisopropylamide
MC	–	merocyanine isomer of spiropyran
MCT	–	mercury cadmium telluride
MOF	–	microstructured optical fibre
MS	–	mass spectrometry
n-BuLi	–	n-Butyllithium
ND	–	neutral-density filter
NHS	–	N-Hydroxysuccinimide
PAINT	–	point accumulation for imaging in nanoscale topography
PALM	–	photo-activated localisation microscopy
Piranha	–	a 7:3 solution of H_2SO_4 and 30 % $H_2O_{2(aq)}$
PMMA	–	poly (methyl methacrylate)
PMT	–	photomultiplier tube
PSS	–	photo-stationary state
RFU	–	relative fluorescence units
RP-HPLC	–	reverse-phase high pressure liquid chromatography
SAM	–	self-assembled monolayer
SCF (SC-MOF)	–	suspended core fibre
SP	–	spiropyran
SP1	–	zinc selective spiropyran (Chapter 2 and 5)
SP-1	–	spiropyran with methyl-1-aza-12-crown-4 (Chapter 3 and 4)
SP-2	–	spiropyran with methyl-1-aza-15-crown-5 (Chapter 3 and 4)
SP-3	–	spiropyran with methyl-1-aza-18-crown-6 (Chapter 3, 4, and 5)
SP-4	–	spiropyran with N-ethoxy and methyl-1-aza-18-crown-6 (Chapter 4)
SP-5	–	spiropyran with N-ethoxy and methyl-(tetrahydro-2H-pyran-2-ylmethoxy) (Chapter 5)
SP-6	–	spiropyran with N-butanoic acid and diether alkyl chain (Chapter 5)
SP-7	–	spiropyran with N-ethoxy and diether alkyl chain (Chapter 5)
STED	–	stimulated emission depletion microscopy
STORM	–	stochastic optical reconstruction microscopy
TOF-SIM	–	time-of-fight secondary ion mass spectrometry
UV	–	ultra-violet

UV254nm	–	irradiation from a germicidal UV source (Hg 254 nm emission band)
UV352nm	–	irradiation from a UV blacklight source (Hg 352 nm emission band)
UV-vis	–	ultra-violet to visible absorption spectroscopy
XPS	–	x-ray photoelectron spectroscopy
λ_{em}	–	peak emission wavelength
λ_{ex}	–	excitation wavelength
λ_{max}	–	peak absorption wavelength

CHAPTER 1

INTRODUCTION

1.1 BACKGROUND AND MOTIVATION

This thesis describes an investigation into new photoswitchable molecular metal ion sensors based upon a fibre optic sensing platform. Motivation for this work derives from an increasing need, both clinically and in research, for new tools and instruments for studying and measuring biological process; particularly towards the real time study of metal ions in biological samples. This research was performed in collaboration with researchers within the Institute of Photonics and Advanced Sensing (IPAS), as well as the ARC Centre of Excellence for Nanoscale BioPhotonics (CNBP); both institutes recognising the need for new photonic tools for advanced sensing in order to better biological research.

1.1.1 IMPORTANCE OF SENSORS FOR METAL IONS IN BIOLOGY

The main foreseeable application of the research presented in this thesis is in the study of the concentrations and fluctuations of metal ions in cellular systems in order to understand their role within the cell; in both healthy cell processes and in disease states. It is already well established that metal ions, in particular sodium (Na^{+}), potassium (K^{+}), magnesium (Mg^{2+}), and calcium (Ca^{2+})[1, 2] exist in large quantities in the human body and are vital for many processes;[3] such as in inter- and extra-cellular signalling, where controlled fluctuations of their concentrations cause a cellular response.[4, 5] Other essential metal ions are the transition metals vanadium ($V^{1+/3+/4+}$), chromium (Cr^{2+}), and molybdenum (Mo^{4+}) all found in trace quantities, as well as the more common manganese (Mn^{2+}), zinc (Zn^{2+}), iron ($Fe^{2+/3+}$),[6] cobalt (Co^{2+}), and copper (Cu^{2+})[6, 7]. Other non-essential ions, such as cadmium (Cd^{2+}), mercury (Hg^{2+}), lead (Pb^{2+})[8] and arsenic ($As^{3+/5+}$) are toxic.[5, 9-15] Metal ions bind to proteins known as metalloproteins and are essential to their function. A normal homeostasis of these metals is vital to cell health. Any disruption of metal ion homeostasis can lead to, or be a result of, poor cell health and disease. For example, Zn^{2+} is known to be involved in cell apoptosis, regulation of the immune system, as well as in Alzheimer's disease.[6, 7, 16-23] Cd^{2+} toxicity arises due to it replacing Ca^{2+}, disrupting normal calcium processes causing diseases such as osteoporosis, hypercalciuria, osteomalacia, renal tubular cell dysfunction, cancer, and neurodegenerative disorders.[1, 24-34]

Two more examples of the need for understanding the roles of metal ions in biological systems are: the role of Ca^{2+} fluctuations in a developing embryo, or the mechanism of lithium's (Li^{+}) influence in neurodegenerative disorders, such as manic depression.

One of the most common metal ions in biology is Ca^{2+}. Commonly known as being critical for bone structure it is also a ubiquitous intracellular signalling ion responsible for controlling numerous cellular processes; including cell proliferation, differentiation, and survival/death.[24, 35-38] An ability to sense and determine its intracellular concentration is thus important to understand cell growth processes as well as disease proliferation and progression. One example of how understanding the role of Ca^{2+} is important in biological systems, which is of particular interest for *in vitro* fertilisation (IVF) and reproductive research, is the role of Ca^{2+} in developing embryos.[39-42] Ca^{2+} is released from the endoplasmic reticulum following sperm penetration (fertilisation), a major signalling event in oocyte activation. Oocyte activation allows oocyte-embryo transition to occur via hardening of the oocyte membrane (zona pellucida) to prevent polyspermy (fertilisation of multiple sperm); and resumption of meiosis, to allow shedding of the half the maternal chromosomes to accommodate paternal chromosomes and DNA synthesis for the fusion of the female and male pro-nuclei (syngamy). Hence, the release of Ca^{2+} by an oocyte provides a potential marker for defining successful fertilisation. Therefore, being able to monitor fluctuations of Ca^{2+} around an oocyte should be able to confirm fertilisation and possibly be a marker for predicting embryonic health in IVF. However, current technologies are limited in the ability to sense around IVF samples due to the risk of contamination or of damaging the oocyte/embryo.

Li^{+} is a vital trace metal ion found in mammalian tissues at approx. 0.001 – 0.01 mM, yet little is known about its biological role. It is believed to be involved in cell signalling as a neurotransmitter, possibly replacing Na^{2+}.[43] Nonetheless, it has been proven effective in the treatment of psychological disorders such as depression.[43, 44] However, it is toxic at higher concentrations and is therefore only administrable within a narrow therapeutic window of 0.6 – 1.2 mM.[45, 46] Understanding how Li^{+} is an effective drug for manic depression could lead to better understanding of what causes manic depression and lead to safer, better targeted, treatments and

therapeutics.[44] Therefore, from these two examples it is clear that it is of clinical interest to be able to study the biochemical role of metal ions.

1.1.2 CURRENT TECHNIQUES FOR BIOLOGICAL METAL ION SENSING

The current state of detection of metal ions, in particular toxic metal ions, in a human subject is performed through extensive pathology measurements. This requires extensive sample preparation and lengthy processing time. For example, a biosample (e.g. whole blood, salvia, urine, or hair) is transferred to an external laboratory where analysis often takes days to weeks to process. During processing, the sample undergoes extensive preparation, before trace metals analysis is performed via inductive coupled plasma mass spectroscopy (ICPMS), which is a large and expensive device, or atomic absorption spectroscopy (AAS).[47, 48] As the process required to get from the subject to the measurement requires many steps it can lead to contamination of the sample, which for trace metals can lead to large errors.[49] In most situations, a treating doctor needs initially only a yes or no answer, or a rough guide, as to whether further investigation and a detailed accurate analysis is needed. Ideally, this would be done on site in a quick, non-invasive manner. To achieve this, new sensing technologies are required.

In clinical research, it is a common desire to be able to understand biological processes going on in real time in a live sample. However, while many analytical techniques for detecting metal ions, such as X-ray spectroscopy or mass spectroscopy, give valuable information, they are very intrusive and generally require destruction of the system. As technologies improve, optical based techniques are becoming more useful to study biological systems.[6, 17, 50-52] While in the past optical sensing systems have been highly limited in spatial resolution, new technologies are allowing more detailed imaging of samples with light.[53-55] For example, advances in confocal microscopy techniques and analysis such as STED, [56, 57] STORM,[58] PALM, and PAINT allow sub wavelength resolution.[59-65] However, these systems are still greatly limited in sample preparation and in the optical fluorescent dyes used; as the cells need to be cultured or removed from the host, then treated with the dye. Also, the dye may not show a true approximation of the concentration of the analyte in the sample due to difference in cell permeability, localisation in the cell, or false readings of a positive (or negative) signal due to other

interferences. Some of these issues are avoided through use of a ratiometric dye (a dye that produces two signals, binding and non-binding, which can be compared).[17, 50, 66] Also these dyes mostly only give a snapshot of the system and are not able to quantify fluctuations in analyte concentrations.

New technologies which allow measurement of a specific analyte in living samples, using optical devices with dyes that do not interfere or contaminate the system, would be advantageous to understanding the role of that analyte in the system. Therefore, it would be desirable to have a device that could be inserted into a functioning biological system and monitor the current state of that system in a time dependent manner.

1.1.3 THE DESIGN OF A NEW SENSOR PLATFORM FOR BIOLOGICAL METAL IONS

We aimed to design and develop a new sensing platform for real time optical measurements of metal ions in a biological medium. This sensor must be: highly sensitive and selective to metal ions, so that trace metals can be detected; small, portable, and accessible, so that it can be used in the field or by clinicians; and non-interfering, so as not to damage or contaminate the sample. To achieve this, a microstructured optical fibre (MOF) was the chosen sensing platform.[67-69]

The sensor design can be divided into three core components: 1) the MOF light-guide, 2) the surface attachment linker, and 3) the ion selective photoreversible ionophores (as shown in the cartoon in Figure 1-1). The underlying principles of each of these components are introduced in Sections 1.2, 1.3 and 1.4, respectively. The three components give the sensor the required sensitivity, versatility, selectivity and reusability.

The photoswitchable ionophore provides selectivity. By specifically designing the chemical structure of the ionophore, the photoswitches can be tailored for a specific purpose and selectively bind to a target of choice (e.g., a metal ion). In one structural conformation the sensing ability is ‘off’, however, when the photoswitch is activated with light the switch turns ‘on’ and it is able to bind the target and give a signal. Then the process can be reversed with another photon of an alternative wavelength.

Thereby, the sensor is reset and can later be reactivated to provide sensing at another time point.

The photoswitch as well as its attachment to the surface provides reusability, as the analyte can be washed from the fluorophore. The surface attachment also serves to concentrate the photoswitch on the light rich surface, and fix it to the surface so that it cannot leach into the solution and contaminate the sample.

The MOF component provides a highly sensitive remote sensing platform as well as a sample chamber. As a dip sensor only the tip of the MOF needs to be inserted to the sample and only nanolitres of sample are tested at any time. The MOF not only provides a method to produce and detect fluorescence, it can also be used to guide the required switching light, with all required optics at a distance well away from the sample.

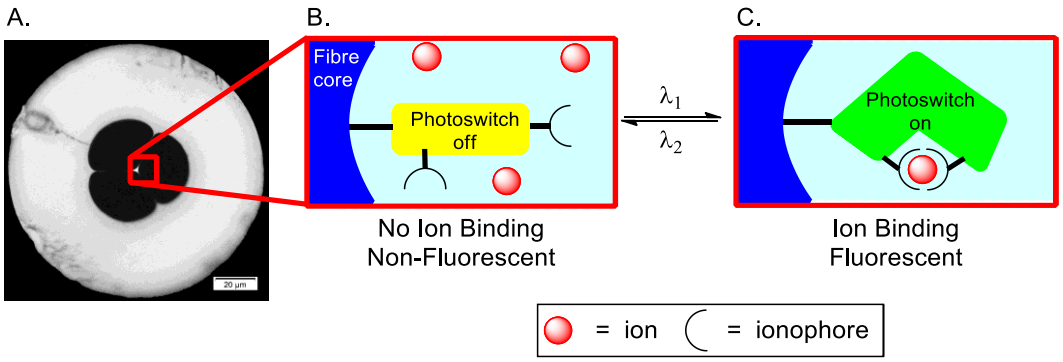

FIGURE 1-1: Basic schematic of the design of the photoswitchable microstructure optical fibre sensor targeted in this thesis. A) cross-section of the MOF showing the three sample voids around a central core; B) the photoswitch attached to the surface in the 'off' conformation unable to bind ions; C) the conformation of the photoswitch is changed by light induced photoswitching to give the 'on' state, in which the ionophore is able to bind ions and give a detectable signal.

1.2 THE MICROSTRUCTURED OPTICAL FIBRE COMPONENT

The work outlined in this thesis builds on previous work at The University of Adelaide regarding sensing with microstructured optical fibres (MOFs).[68, 70-75] The following section provides background into the fundamentals and literature in this area.

A microstructured optical fibre (MOF) is a special type of optical fibre that consists of a light guiding microfibre core suspended in a greater protecting structure. The MOF combines the tight mode confinement of microfibres with the strength and durability of larger sized fibres.

Microstructured optical fibres are made from a fibre drawing process, which is described by Ebendorff-Heidepriem *et al*.[76] This process can form fibres from a wide variety of types of glasses such as silica, lead silicate, tellurite and bismuth,[70, 77, 78] in a variety of different architectures.[76, 77, 79-84] The primary fibre used in this work was a 3-hole wagon-wheel suspended core fibre (SCF) (Figure 1-2) prepared by Dr. Heike Ebendorff-Heidepriem and Dr. Erik Schartner on a 6 metre drawing tower.[77] This fibre was made from high purity F300 silica manufactured by Heraeus Quartzglas and features a core with a diameter of 1.5 μm, holes with a diameter of approximately 28 μm, and an external polymer coating.[76, 85]

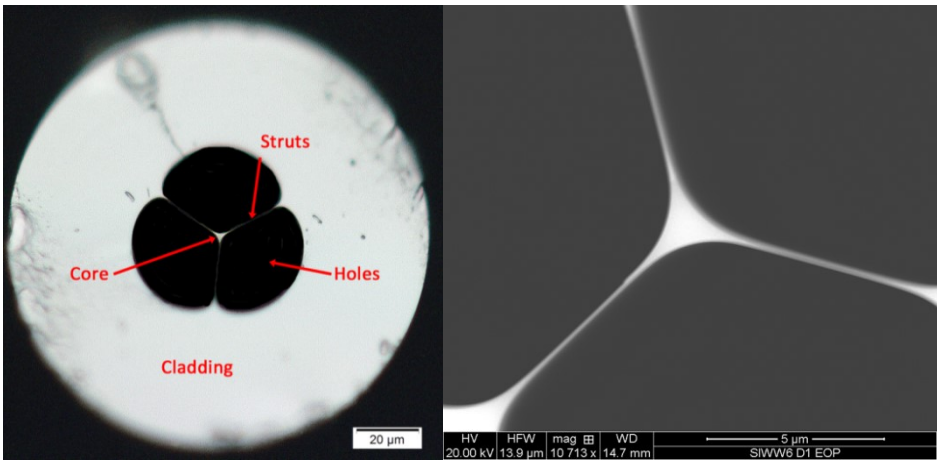

FIGURE 1-2: Cross section of the suspended core MOF (SC-MOF) used. Left) light microscope image showing the micro-architecture of the fibre. Right) SEM image of the 1.5 µm waveguide core (provided by Roman Kostecki).

Fibres were made from high purity, low OH, fused silica glass due to their attractive properties over other glass materials.[86] Silica has better mechanical and thermal properties (due to its high melting point), this enables its use in a wider range of environments.[87] It also has low loss, with an optical range within the UV region (0.24 – 2 µm). Silica nanofibres have a large evanescence field-matter overlap compared to bismuth, and a larger fluorescence capture fraction (FCF) at larger core diameters (d = 1 µm).[85] Also, the reduced amount of impurities of F300 is possibly advantageous for modification of the surface chemistry; as the pure silica surface possibly creates a more uniform silica surface, providing a more uniform functionalisation layer, thereby eliminating possible variables in the surface chemistry.[88]

1.2.1 OPTICAL FIBRES AS SENSORS

Optical fibres generally have two modes of function when used as sensors. These are generally classified as intrinsic and extrinsic. In extrinsic fibres, the fibre is used mainly as a method of transportation of light/data from the source to the detector. This mechanism is generally the main use of optical fibres, e.g., telecommunications. In sensing applications this includes fibre tip sensing, where there is a light emitting sensor on the tip of the fibre and the fibre is a signal capture device (Figure 1-3a). Intrinsic sensors use changes in light properties while within the fibre to sense

(Figure 1-3b). Examples include: changes in the reflection from Bragg gratings due to heat or physical stress;[67, 89, 90] Rayleigh scattering;[87, 91] Raman scattering;[67, 69, 91] Brillouin scattering;[69, 91] as well as the principal applied throughout this work, evanescence field sensing[75, 80, 82, 92, 93] (described below). MOFs are capable of both extrinsic and intrinsic types of sensing, however, fibres with small core sizes are less suitable for extrinsic sensing.

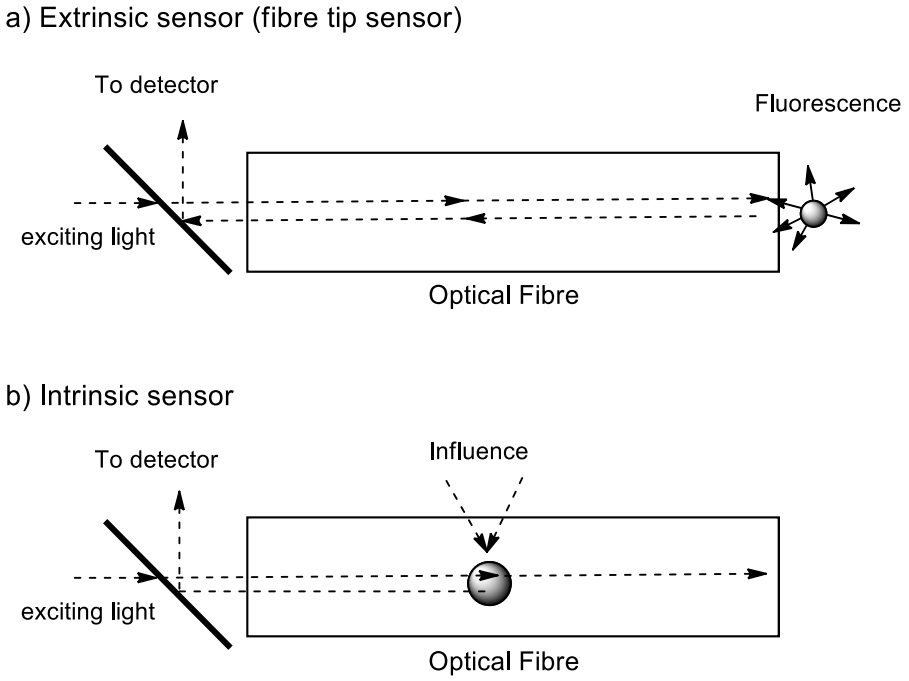

FIGURE 1-3: Diagram of a) extrinsic and b) intrinsic fibre optic sensors.

1.2.2 THE PRINCIPLES OF MOFS AS FLUORESCENCE SENSORS

Optical fibres provide a means for the guided transportation of light between two points. The light is confined within the high refractive index fibre core, which is surrounded by lower refractive index medium, for SCFs this consists of the air holes.[94] As the modes of light propagate along the fibre a proportion of the light's electric field extends beyond the surface into the lower refractive index medium to the extent of less than one wavelength.[95] This is known as the evanescent field. The intensity of this evanescent field is enlarged when the fibre waveguide size is decreased to near/sub wavelength proportions (Figure 1-4).[76, 85]

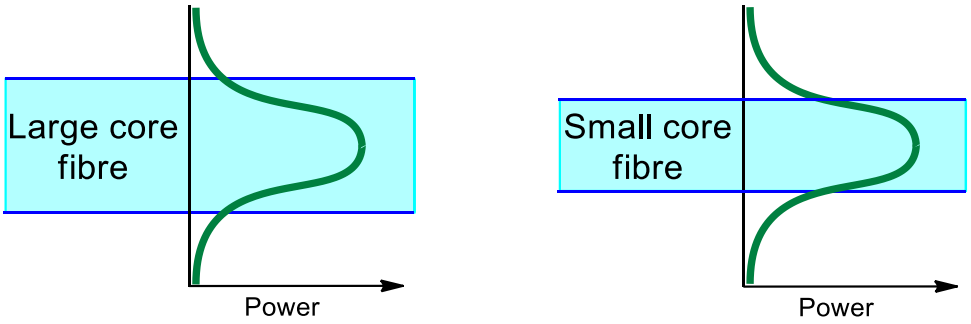

FIGURE 1-4: Evanescent field strength of different sized fibres. Horizontal axis (green) - optical power, Vertical axis – cross sectional coordinate.

In a MOF the evanescent field perturbs into the voids around the fibre core and is able to interact with the analyte in the voids that is in close proximity to the light guiding surface (approx. within 100 nm).[85] Therefore, the evanescent field can be used to sense changes in the analyte.[96] When a fluorophore is located in the voids and an appropriate wavelength of light is propagated along the fibre core, the fluorophore can interact with, absorb the photon from the evanescent field, and enter an excited state. To return to the ground state the fluorophore can undergo radiative emission of a photon, as described by a Jablonski diagram of its electronic states (Figure 1-5).

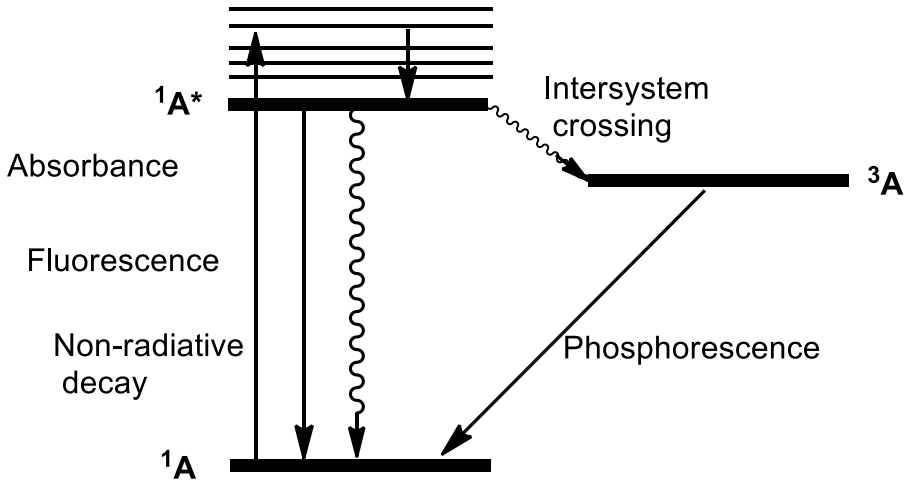

FIGURE 1-5: A generalised Jablonski diagram showing the internal energy transmissions from the absorption of a photon. After absorption, the molecule is transferred from a singlet ground state to an excited singlet state. From this state the molecule can thermally return to the ground state, or undergo two radiative processes, fluorescence ($^1A^* \rightarrow {}^1A$) or phosphorescence ($^3A \rightarrow {}^1A$).

As the orientation of fluorophore in solution is random, the average directionality of the emission is random,[97] the possibility exists for some of the radiated light from the fluorophore to enter the fibre core at an appropriate angle to be recaptured by the fibre and transmitted along the length of the fibre to a fibre tip (Figure 1-6). The proportion of emitted light captured by the fibre is known as the fluorescence capture fraction.[85, 96] By monitoring the intensity of the emitted light at the fibre tip, the fluorescence of the particles in the holes can be observed. As the directionality is random, light can be transmitted forwards or backwards to either end of the fibre (where the forwards direction is the same direction as the excitation light, and the backwards direction is back towards the light source). Afshar *et al.*[96] found that the backwards fluorescence was best for MOF fluorescence sensing due to higher efficiency and lower loss, as well as providing the option to be used as a dip sensor. A dip sensor is advantageous as it allows for all the optics required to excite and measure the signal to be assembled at one end of the fibre and frees the other end for interaction with the analyte of interest at a distance from the detector.

Interaction with an analyte solution is performed by immersing the tip in a solution. The solution can then enter and fill the three holes by capillary action, or forced

through with a pressure differential. Two of the main advantages of MOFs as fluorescence detecting devices over standard cuvette measurements are that: 1) a much greater path length is possible. Theoretically, the path length is dependent of the length of the fibre filled with analyte and not the size of the cuvette (usually 10 mm); this makes the fibres a lot more sensitive. Also, 2) it is acting as a nanolitre size cuvette. As the irradiation area is small and controlled, only a small amount of analyte is required. A fibre with three 30 µm sized holes only requires approx. 180 nL per 100 mm path length. Therefore, MOFs are a versatile new sensing platform highly suitable for biological fluorescence sensing, application of MOFs for fluorescence based detection has been published.[68, 71-73, 75, 82, 85, 96]

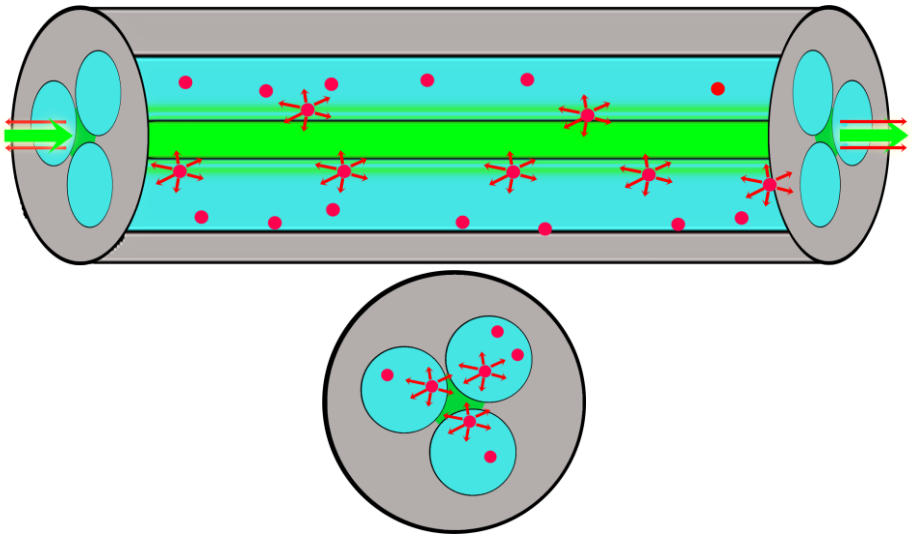

FIGURE 1-6: MOF filled with fluorophore containing solution. The green excitation light enters the fibre through the left end, where the light is guided along the length of the core. The fluorophore (red) in the evanescent field absorbs the green light and emits red fluorescence, some of which is captured by the fibre and transmitted to either end.

1.3 SURFACE CHEMISTRY

To improve the sensitivity and versatility of MOF sensors the fluorophore can be localised within the evanescent field via attachment to the surface of the fibre core. Attachment of the fluorophore to the fibre surface has several advantages: Firstly, it avoids the requirement to pre-treat the analyte with the fluorophore, thereby, reducing sample preparation; and secondly, it enables the fibre to perform sensing in locations where the introduction of an external fluorophore is not possible, such as in a living sample or other sensitive situations where the fluorophore could be toxic or destructive. Surface chemistry is a broad field as there are many different methods to achieve a functionalised surface. The method used greatly depends on the type of surface to be functionalised. As silica optical fibres are the target surface for this thesis, only functionalisation of silica glass will be discussed.

1.3.1 CHEMICAL PROPERTIES OF SILICA GLASS

Silica glass is an amorphous solid lattice of silicon dioxide. The surface of bulk silica consists of three chemical domains, Si-O-Si, Si-O^-, and Si-OH as well as any species arising from impurities (Figure 1-7).[98] The glass used to make the MOFs in this thesis was of high purity silica (F300) with trace impurities below the detection limit of ICP-MS (Heraeus Quarzglas). Other common glasses, such as lead silicate (F2), and standard laboratory glassware (borosilicates) contain a mixture of silica and other elements, which give those glasses differing physical and optical properties, and may also alter the surface chemistry; e.g., borosilicate is composed of a varying mixture of silicon oxide (80.6 %), aluminium oxide (2.3 %), boric oxide (13 %), sodium oxide (4 %).[99] The surface allows for attachment of organic molecules via covalent reactions (silanization), electrostatic interaction (charged polymer, lipid membrane) or by physical adsorption.[100, 101]

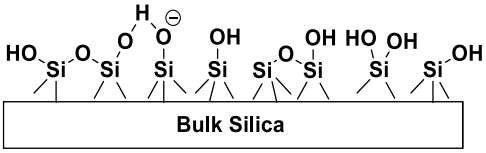

FIGURE 1-7: The structure of the silica surface.

1.3.2 SILANIZATION: BASIC OVERVIEW OF THE CHEMISTRY AND PROTOCOLS

Silanization is the process of attaching a silane reagent to the silica surface by a covalent coupling reaction to form a self-assembled monolayer (SAM). Generally, the silane reagent contains a central silicon atom connected to three leaving groups (either three methyl esters, ethyl esters or chlorines) as well as an alkyl chain with some chemical functionality which can be modified at a later time.[102] Common silane reagents with useful functionality are aminopropyl triethoxysilane (APTES),[103-107] carboxy triethoxysilane (CTES),[108] 3-(triethoxysilyl)propylsuccinic anhydride (TESPSA),[109, 110] alkenes/alkynes (ATES),[111] methacryloxypropyltrimethoxysilane (MAPTMS), 3-mercaptopropyltriethoxysilane (MPTES)[112-114] and 3-chloropropyltrimethoxysilane, and others shown in Figure 1-8.[115]

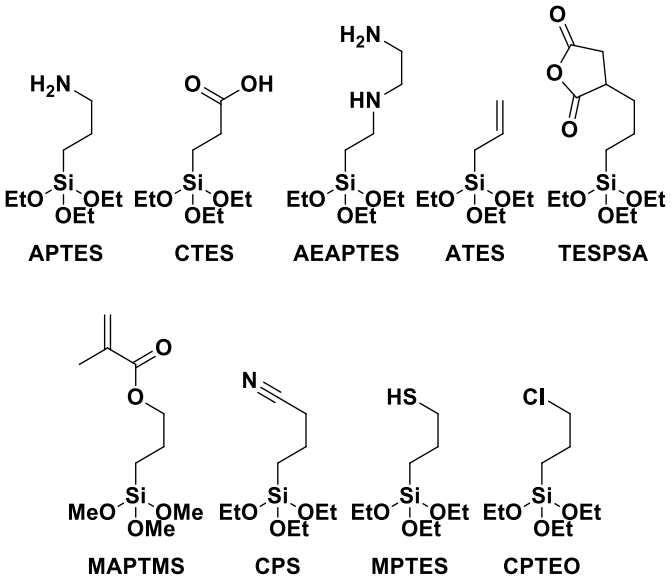

FIGURE 1-8: Different silane reagents impose various functionality to a silanized material.

The mechanism of coupling of ethoxy silanes to a surface is shown in Figure 1-9. The process involves two steps, the rates of which contribute to successful formation of a uniform SAM.[116] Firstly, there is a solution phase hydrolysis of the ethoxy to a silanol. This can be acid or base catalysed; the rate that this step is dependent on the pH of the solution, as well as the leaving group on the silicon, and the concentration of water. The second step involves a hydrogen bond formation between the silanol

and the silica surface, followed by a condensation reaction. Achieving a balance between the rates of hydrolysis and condensation is important in forming a uniform surface, as the reactive silanol intermediate is able to react with other silanes in the solution to form dimers and polymers. These can block the surface, or form structures protruding from the surface. This is an important factor in the silanization reaction involving APTES, which is discussed further in Chapter 4.

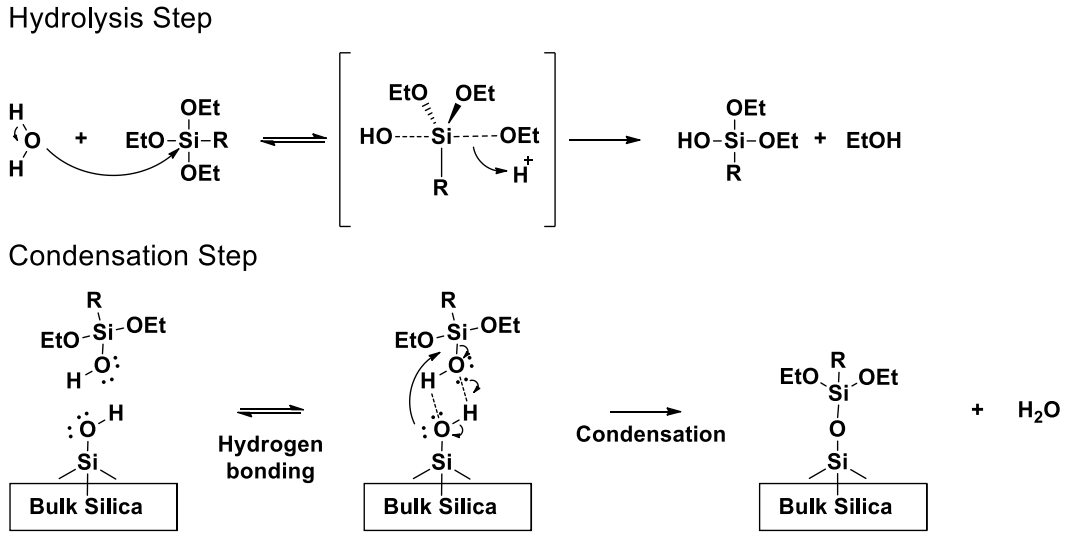

FIGURE 1-9: The general two step mechanism for the silanization of a triethoxysilane to a surface.

1.4 THE PHOTOSWITCHABLE COMPONENT

Molecular switches are a class of molecules with an ability to reversibly change molecular properties/structure when exposed to different stimuli.[117] This differs from a conventional irreversible reaction where, once the product is formed, it is difficult to return to the reagents. Possible stimuli for molecular switching are reductive/oxidative environments, acid/base, heat, or light. When the reversible change occurs due to a photoreaction this is known as photochromism; as there is a change in the colour between each conformation.[118] Photochromic compounds can be classified into two different types, P-Type and T-Type (Figure 1-10).[119] T-Type molecules have an unstable photoswitched state, which thermally switches back to the more stable unswitched state (e.g., azobenzenes and spiropyrans). P-Type molecules are thermally stable and require another photon to cause a competing photochemical process to return to the initial molecule (e.g., fulgides, diarylalkenes). Because of the greater control of switching and increased stability of the switched state, P-type photoswitchable molecules will have greater potential for precision materials, such as for data storage.

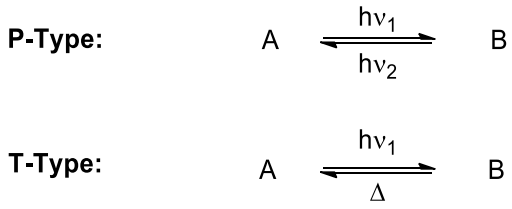

FIGURE 1-10: The isomerisation process of P-type and T-type photoswitches.

The use of photochromic molecular switches for switchable devices has been gathering growing attention over the last 60 years, especially the last 30-40 years, as new physical technologies have emerged and new chemistries developed.[118] There is a broad range of practical applications for organic photoswitches, such as, in data storage,[120, 121] switchable materials (e.g., polymers,[122-124] molecular organic frameworks,[125] and functionalised surfaces[90, 123, 126-129]), sensors,[130-134] biological agents,[135-139] as well as use in colour pigments.[140, 141] Such molecules are already in common use in photochromic sunglasses.[142, 143]

There are many different classes of organic photoswitches in which the method of switching varies from changes in steric hindrance (atropoisomerisation), *cis*/*trans* isomerisation, reversible bond cleaving or electrocyclization/ring opening. Some common photoswitches are azobenzenes, stilbenes, diarylalkenes, fulgides, dihydroazulene, spiropyran, spironaphthoxazine, naphthopyran, DASAs,[144] and HBDI[145, 146].[140] Further discussion of these photoswitches can be found in Chapter 2.

1.5 OUTLINE OF THESIS

This thesis describes the methodological development towards a photoswitchable metal ion sensor as described above. The chapter-by-chapter outline of the content of the thesis is described below.

1.5.1 CHAPTER 2

This chapter describes an investigation into photoswitchable molecules to determine which of the common organic photoswitches are best for use in a biological optical sensor device. The chapter is divided into two key sections: the first is a comparative investigation of photoswitches in MOFs. This investigation fills a gap in knowledge where the relative photostability, in particular for use as evanescent field fluorophores in MOFs, is largely unknown. This work is presented as a published article (PAPER 1). The second section is composed of a literature review comparing the most common classes of organic photoswitches, and is an extension of the brief introduction of photoswitches given above. The classes are introduced and properties examined and compared regarding their suitability for use in the creation of a microstructured optical fibre metal ion sensor. This chapter therefore determines the preferred photoswitch class to carry forward in further investigations to create photoswitchable molecular sensors and reusable fibre optic sensors.

1.5.2 CHAPTER 3

This chapter presents a published report (PAPER 2) on the design, synthesis and alkali metal ion selectivity of a series of three aza-crowncrown ether functionalised spiropyran photoswitches **SP-1**, **SP-2**, and **SP-3**.

1.5.3 CHAPTER 4

This chapter continues from the investigation presented in Chapter 3. The versatility of the design of these types of spiropyran photoswitches is described further in the design of a different sensor **SP-4**, which contains an alternate ethoxy moiety attached at the indoline nitrogen. Here the metal ion selectivity of **SP-1**, **SP-3**, and **SP-4** towards biologically relevant divalent metal ions is investigated and compared. The absorbance and fluorescence response to 15 metal cations is compared, along with a further investigation into the stoichiometry of chelation (via a Job's analysis), and the

spectral changes produced by photoswitching of the spiropyrans in the presence of metals. Finally, the ability of **SP-4** to sense and photoswitch in calcium rich cells is examined (PAPER 5).

1.5.4 CHAPTER 5

This chapter investigates the surface chemistry component of the photoswitchable sensor to create a fibre sensor. The activation of glass surfaces with an APTES monolayer is investigated first on glass slides as a model system before being transferred to MOFs. Photoswitchable surfaces are created with model photoswitch systems consisting of a spiropyran (**SP-5**) and azobenzene (**Azo1**) fluorophore. The sensing capacity of MOFs for Ca^{2+} is then investigated using the **SP-3** photoswitchable spiropyran system, both in solution and covalently attached to the MOF core. Finally, two more MOF photoswitchable sensing systems are presented (PAPER 3 and 4), which investigate the sensing of Ca^{2+} and Cd^{2+} as well as Zn^{2+}.

1.5.5 APPENDICES

This chapter presents additional work and information relating to previous sections of this thesis.

Appendix A presents the synthesis, characterisation, and an investigation into the photoswitching of the fulgide photoswitch, **CF_3-fulgide**, which was used for the investigation in PAPER 1.

Appendix B continues on from the glass slide experiments in Chapter 5 and looks at the feasibility of the use of the Malvern Zetasizer to determine the zeta potential of quartz glass slides. This was done with the aim to perform a preliminary investigation looking at changes in surface potential during slide cleaning, functionalisation and those induced by photoswitching of a spiropyran fluorophore attached to a silica surface.

Appendix C presents images of the computational models of spiropyran **SP-1** bound to Li^{+}, and **SP-3** and **SP-4** in both photoswitched states and with the metal ions Mg^{2+}, Ca^{2+}, Sr^{2+}, and Ba^{2+}.

Appendix D presents the full re-formatted versions of PAPERS 3, 4 and 5.

1.6 REFERENCES FOR CHAPTER 1

1. Long, G. J. Cadmium perturbs calcium homeostasis in rat osteosarcoma (ROS 17/2.8) cells; A possible role for protein kinase C. *Toxicology Letters* 1997, *91* (2), 91-97.
2. Weber, J. T. Altered calcium signaling following traumatic brain injury. *Frontiers in Pharmacology* 2012, *3*.
3. Pors Nielsen, S. The biological role of strontium. *Bone* 2004, *35* (3), 583-588.
4. Nordberg, G. F.; Fowler, B. A.; nordberg, M. *Handbook on the Toxicity of Metals*. 4th ed.; Elsevier: Europe, 2015.
5. Zalups, R. K.; Koropatnik, J. *Molecular Biology and Toxicology of Metals*. Taylor & Francis Group: 2000; 608.
6. Que, E. L.; Domaille, D. W.; Chang, C. J. Metals in Neurobiology: Probing Their Chemistry and Biology with Molecular Imaging. *Chemical Reviews* 2008, *108* (5), 1517-1549.
7. Lee, H. J.; Korshavn, K. J.; Kochi, A.; Derrick, J. S.; Lim, M. H. Cholesterol and metal ions in Alzheimer's disease. *Chemical Society Reviews* 2014, *43* (19), 6672-6682.
8. Needleman, H. Lead Poisoning. *Annual Review of Medicine* 2004, *55* (1), 209-222.
9. B L Vallee, a.; Ulmer, D. D. Biochemical Effects of Mercury, Cadmium, and Lead. *Annual Review of Biochemistry* 1972, *41* (1), 91-128.
10. Vinceti, M.; Guidetti, D.; Bergomi, M.; Caselgrandi, E.; Vivoli, R.; Olmi, M.; Rinaldi, L.; Rovesti, S.; Solime, F. Lead, cadmium, and selenium in the blood of patients with sporadic amyotrophic lateral sclerosis. *Italian Journal of Neurological Sciences* 1997, *18* (2), 87-92.
11. Nordberg, G. F. Index. In *Handbook on the Toxicology of Metals (Third Edition)*, Nordberg, G. F.; Fowler, B. A.; Nordberg, M.; Friberg, L. T., Eds. Academic Press: Burlington, 2007; 949-975.
12. Berlin, M.; Zalups, R. K.; Fowler, B. A. Chapter 33 - Mercury. In *Handbook on the Toxicology of Metals (Third Edition)*, Nordberg, G. F.; Fowler, B. A.; Nordberg, M.; Friberg, L. T., Eds. Academic Press: Burlington, 2007; 675-729.
13. Skerfving, S.; Bergdahl, I. A. Chapter 31 - Lead. In *Handbook on the Toxicology of Metals (Third Edition)*, Nordberg, G. F.; Fowler, B. A.; Nordberg, M.; Friberg, L. T., Eds. Academic Press: Burlington, 2007; 599-643.
14. Nordberg, G. F.; Nogawa, K.; Nordberg, M.; Friberg, L. T. Chapter 23 - Cadmium. In *Handbook on the Toxicology of Metals (Third Edition)*, Nordberg, G. F.; Fowler, B. A.; Nordberg, M.; Friberg, L. T., Eds. Academic Press: Burlington, 2007; 445-486.
15. Fowler, B. A.; Selene, C. H.; Chou, J.; Jones, R. L.; Chen, C. J. Chapter 19 - Arsenic. In *Handbook on the Toxicology of Metals (Third Edition)*, Nordberg, G. F.; Fowler, B. A.; Nordberg, M.; Friberg, L. T., Eds. Academic Press: Burlington, 2007; 367-406.
16. Maynard, C. J.; Bush, A. I.; Masters, C. L.; Cappai, R.; Li, Q. X. Metals and amyloid-beta in Alzheimer's disease. *International Journal of Experimental Pathology* 2005, *86* (3), 147-159.

17. Carter, K. P.; Young, A. M.; Palmer, A. E. Fluorescent Sensors for Measuring Metal Ions in Living Systems. *Chemical Reviews* 2014, *114* (8), 4564-4601.
18. Kim, A. M.; Bernhardt, M. L.; Kong, B. Y.; Ahn, R. W.; Vogt, S.; Woodruff, T. K.; O'Halloran, T. V. Zinc Sparks Are Triggered by Fertilization and Facilitate Cell Cycle Resumption in Mammalian Eggs. *Acs Chemical Biology* 2011, *6* (7), 716-723.
19. Wang, C.-Y.; Wang, T.; Zheng, W.; Zhao, B.-L.; Danscher, G.; Chen, Y.-H.; Wang, Z.-Y. Zinc Overload Enhances APP Cleavage and A beta Deposition in the Alzheimer Mouse Brain. *Plos One* 2010, *5* (12).
20. Long, A. E.; Gillespie, K. M.; Aitken, R. J.; Goode, J. C.; Bingley, P. J.; Williams, A. J. K. Humoral Responses to Islet Antigen-2 and Zinc Transporter 8 Are Attenuated in Patients Carrying HLA-A*24 Alleles at the Onset of Type 1 Diabetes. *Diabetes* 2013, *62* (6), 2067-2071.
21. VanLandingham, J. W.; Fitch, C. A.; Levenson, C. W. Zinc inhibits the nuclear translocation of the tumor suppressor protein p53 and protects cultured human neurons from copper-induced neurotoxicity. *Neuromolecular Medicine* 2002, *1* (3), 171-182.
22. Formigari, A.; Gregianin, E.; Irato, P. The effect of zinc and the role of p53 in copper-induced cellular stress responses. *Journal of Applied Toxicology* 2013, *33* (7), 527-536.
23. McDevitt, C. A.; Ogunniyi, A. D.; Valkov, E.; Lawrence, M. C.; Kobe, B.; McEwan, A. G.; Paton, J. C. A Molecular Mechanism for Bacterial Susceptibility to Zinc. *Plos Pathogens* 2011, *7* (11).
24. Youness, E. R.; Mohammed, N. A.; Morsy, F. A. Cadmium impact and osteoporosis: mechanism of action. *Toxicology Mechanisms and Methods* 2012, *22* (7), 560-567.
25. Okuda, B.; Iwamoto, Y.; Tachibana, H.; Sugita, M. Parkinsonism after acute cadmium poisoning. *Clinical Neurology and Neurosurgery* 1997, *99* (4), 263-265.
26. Bonner, F. W.; King, L. J.; Parke, D. V. The acute and sub-acute effects of cadmium on calcium homeostasis and bone trace-metals in the rat. *Journal of Inorganic Biochemistry* 1981, *14* (2), 107-114.
27. Basun, H.; Lind, B.; Nordberg, M.; Nordstrom, M.; Bjorksten, K. S.; Winblad, B. Cadmium in blood in alzheimers-disease and nondemented subjects - results from a population based study. *Biometals* 1994, *7* (2), 130-134.
28. Wier, P. J.; Miller, R. K.; Maulik, D.; Disantagnese, P. A. Toxicity of cadmum in the perfused human placenta. *Toxicology and Applied Pharmacology* 1990, *105* (1), 156-171.
29. Godt, J.; Scheidig, F.; Grosse-Siestrup, C.; Esche, V.; Brandenburg, P.; Reich, A.; Groneberg, D. A. The toxicity of cadmium and resulting hazards for human health. *Journal of occupational medicine and toxicology (London, England)* 2006, *1*, 22-22.
30. Brzoska, M. M.; Moniuszko-Jakoniuk, J. Low-level exposure to cadmium during the lifetime increases the risk of osteoporosis and fractures of the lumbar spine in the elderly: Studies on a rat model of human environmental exposure. *Toxicological Sciences* 2004, *82* (2), 468-477.
31. Asara, Y.; Marchal, J. A.; Carrasco, E.; Boulaiz, H.; Solinas, G.; Bandiera, P.; Garcia, M. A.; Farace, C.; Montella, A.; Madeddu, R. Cadmium

Modifies the Cell Cycle and Apoptotic Profiles of Human Breast Cancer Cells Treated with 5-Fluorouracil. *International Journal of Molecular Sciences* 2013, *14* (8), 16600-16616.

32. Adams, S. V.; Passarelli, M. N.; Newcomb, P. A. Cadmium exposure and cancer mortality in the Third National Health and Nutrition Examination Survey cohort. *Occupational and Environmental Medicine* 2012, *69* (2), 153-156.
33. Beveridge, R.; Pintos, J.; Parent, M.-E.; Asselin, J.; Siemiatycki, J. Lung Cancer Risk Associated With Occupational Exposure to Nickel, Chromium VI, and Cadmium in Two Population-Based Case-Control Studies in Montreal. *American Journal of Industrial Medicine* 2010, *53* (5), 476-485.
34. Panayi, A. E.; Spyrou, N. M.; Iversen, B. S.; White, M. A.; Part, P. Determination of cadmium and zinc in Alzheimer's brain tissue using inductively coupled plasma mass spectrometry. *Journal of the Neurological Sciences* 2002, *195* (1), 1-10.
35. Xu, B.; Chen, S.; Luo, Y.; Chen, Z.; Liu, L.; Zhou, H.; Chen, W.; Shen, T.; Han, X.; Chen, L.; Huang, S. Calcium Signaling Is Involved in Cadmium-Induced Neuronal Apoptosis via Induction of Reactive Oxygen Species and Activation of MAPK/mTOR Network. *Plos One* 2011, *6* (4).
36. Montell, C. The latest waves in calcium signaling. *Cell* 2005, *122* (2), 157-63.
37. Clapham, D. E. Calcium Signalling. *Cell* 1995, *80* (2), 259-268.
38. Kazantzis, G. Cadmium, osteoporosis and calcium metabolism. *Biometals* 2004, *17* (5), 493-498.
39. Stricker, S. A. Comparative Biology of Calcium Signaling during Fertilization and Egg Activation in Animals. *Developmental Biology* 1999, *211* (2), 157-176.
40. Whitaker, M. Calcium signalling in early embryos. Philosophical Transactions of the Royal Society of London B: Biological Sciences 2008, 363 (1495), 1401-1418.
41. Homa, S. T.; Carroll, J.; Swann, K. Fertilization and early embryology: The role of calcium in mammalian oocyte maturation and egg activation. *Human Reproduction* 1993, *8* (8), 1274-1281.
42. Whitaker, M. Calcium at fertilization and in early development. *Physiological Reviews* 2006, *86* (1), 25-88.
43. Jope, R. S. Anti-bipolar therapy: mechanism of action of lithium. *Molecular Psychiatry* 1999, *4* (2), 117-128.
44. Klemfuss, H. Rhythms and the pharmacology of lithium. *Pharmacology & Therapeutics* 1992, *56* (1), 53-78.
45. Citterio, D.; Takeda, J.; Kosugi, M.; Hisamoto, H.; Sasaki, S.; Komatsu, H.; Suzuki, K. pH-Independent Fluorescent Chemosensor for Highly Selective Lithium Ion Sensing. *Analytical Chemistry* 2007, *79* (3), 1237-1242.
46. Ando, Y.; Hiruta, Y.; Citterio, D.; Suzuki, K. A highly Li+-selective glass optode based on fluorescence ratiometry. *Analyst* 2009, *134* (11), 2314-2319.
47. Sidaginamale, R. P.; Joyce, T. J.; Lord, J. K.; Jefferson, R.; Blain, P. G.; Nargol, A. V. F.; Langton, D. J. Blood metal ion testing is an effective screening tool to identify poorly performing metal-on-metal bearing surfaces. *Bone & Joint Research* 2013, *2* (5), 84-95.

48. WHO. Brief guide to analytical methods for measuring lead in blood. www.who.int/ipcs/assessment/public_health/lead_blood.pdf (accessed 06/02/2016).
49. FDA. Information about Soft Tissue Imaging and Metal Ion Testing. http://www.fda.gov/MedicalDevices/ProductsandMedicalProcedures/ImplantsandProsthetics/MetalonMetalHipImplants/ucm331971.htm (accessed 06/02/2016).
50. Yin, J.; Hu, Y.; Yoon, J. Fluorescent probes and bioimaging: alkali metals, alkaline earth metals and pH. *Chemical Society Reviews* 2015.
51. Dean, K. M.; Qin, Y.; Palmer, A. E. Visualizing metal ions in cells: an overview of analytical techniques, approaches, and probes. *Biochimica et biophysica acta* 2012, *1823* (9), 1406-1415.
52. Domaille, D. W.; Que, E. L.; Chang, C. J. Synthetic fluorescent sensors for studying the cell biology of metals. *Nature Chemical Biology* 2008, *4* (3), 168-175.
53. Richards, E. A. Limitations in Optical Imaging Devices at Low Light Levels. *Applied Optics* 1969, *8* (10), 1999-2005.
54. Török, P.; Kao, F. J. Optical Imaging and Microscopy: Techniques and Advanced Systems. Springer: 2003.
55. Gibson, A. P.; Hebden, J. C.; Arridge, S. R. Recent advances in diffuse optical imaging. *Physics in Medicine and Biology* 2005, *50* (4), R1.
56. Diaspro, A. Nanoscopy and Multidimensional Optical Fluorescence Microscopy. CRC Press: 2010.
57. Seefeldt, B.; Kasper, R.; Beining, M.; Mattay, J.; Arden-Jacob, J.; Kemnitzer, N.; Drexhage, K. H.; Heilemann, M.; Sauer, M. Spiropyrans as molecular optical switches. *Photochemical & Photobiological Sciences* 2010, *9* (2), 213-220.
58. Rust, M. J.; Bates, M.; Zhuang, X. Sub-diffraction-limit imaging by stochastic optical reconstruction microscopy (STORM). *Nature Methods* 2006, *3* (10), 793-796.
59. Folling, J.; Bossi, M.; Bock, H.; Medda, R.; Wurm, C. A.; Hein, B.; Jakobs, S.; Eggeling, C.; Hell, S. W. Fluorescence nanoscopy by ground-state depletion and single-molecule return. *Nature Methods* 2008, *5* (11), 943-945.
60. Heilemann, M.; van de Linde, S.; Schüttpelz, M.; Kasper, R.; Seefeldt, B.; Mukherjee, A.; Tinnefeld, P.; Sauer, M. Subdiffraction-Resolution Fluorescence Imaging with Conventional Fluorescent Probes. *Angewandte Chemie International Edition* 2008, *47* (33), 6172-6176.
61. Betzig, E.; Patterson, G. H.; Sougrat, R.; Lindwasser, O. W.; Olenych, S.; Bonifacino, J. S.; Davidson, M. W.; Lippincott-Schwartz, J.; Hess, H. F. Imaging Intracellular Fluorescent Proteins at Nanometer Resolution. *Science* 2006, *313* (5793), 1642-1645.
62. Manley, S.; Gillette, J. M.; Patterson, G. H.; Shroff, H.; Hess, H. F.; Betzig, E.; Lippincott-Schwartz, J. High-density mapping of single-molecule trajectories with photoactivated localization microscopy. *Nature Methods* 2008, *5* (2), 155-157.
63. Giannone, G.; Hosy, E.; Levet, F.; Constals, A.; Schulze, K.; Sobolevsky, Alexander I.; Rosconi, M. P.; Gouaux, E.; Tampé, R.; Choquet, D.; Cognet, L. Dynamic Superresolution Imaging of Endogenous Proteins on Living Cells at Ultra-High Density. *Biophysical Journal* 2010, *99* (4), 1303-1310.

64. Sharonov, A.; Hochstrasser, R. M. Wide-field subdiffraction imaging by accumulated binding of diffusing probes. *Proceedings of the National Academy of Sciences* 2006, *103* (50), 18911-18916.
65. Winckler, P.; Lartigue, L.; Giannone, G.; De Giorgi, F.; Ichas, F.; Sibarita, J.-B.; Lounis, B.; Cognet, L. Identification and super-resolution imaging of ligand-activated receptor dimers in live cells. *Scientific Reports* 2013, *3*, 2387.
66. Ma, Q.-J.; Zhang, X.-B.; Zhao, X.-H.; Gong, Y.-J.; Tang, J.; Shen, G.-L.; Yu, R.-Q. A ratiometric fluorescent sensor for zinc ions based on covalently immobilized derivative of benzoxazole. *Spectrochimica Acta Part A: Molecular and Biomolecular Spectroscopy* 2009, *73* (4), 687-693.
67. Mescia, L.; Prudenzano, F. Advances on Optical Fiber Sensors. *Fibers* 2013, *2* (1), 1-23.
68. Monro, T. M.; Warren-Smith, S.; Schartner, E. P.; Francois, A.; Heng, S.; Ebendorff-Heidepriem, H.; Afshar, S. Sensing with suspended-core optical fibers. *Optical Fiber Technology* 2010, *16* (6), 343-356.
69. Grattan, K. T. V.; Sun, T. Fiber optic sensor technology: an overview. *Sensors and Actuators A: Physical* 2000, *82* (1–3), 40-61.
70. Foo, H. T. C.; Ebendorff-Heidepriem, H.; Sumby, C. J.; Monro, T. M. Towards microstructured optical fibre sensors: surface analysis of silanised lead silicate glass. *Journal of Materials Chemistry C* 2013, *1* (41), 6782-6789.
71. Englich, F. V.; Foo, T. C.; Richardson, A. C.; Ebendorff-Heidepriem, H.; Sumby, C. J.; Monro, T. M. Photoinduced Electron Transfer Based Ion Sensing within an Optical Fiber. *Sensors* 2011, *11* (10), 9560-9572.
72. Richardson, A. C.; Foo, T. C.; Englich, F. V.; Ebendorff-Heidepriem, H.; Sumby, C. J.; Monro, T. M. A Microstructured Optical Fiber Sensor for Ion-Sensing Based on the Photoinduced Electron Transfer Effect. In *Third Asia Pacific Optical Sensors Conference*, Canning, J.; Peng, G. D., Eds. Spie-Int Soc Optical Engineering: Bellingham, 2012; Vol. 8351.
73. Warren-Smith, S. C.; Ebendorff-Heidepriem, H.; Foo, T. C.; Moore, R.; Davis, C.; Monro, T. M. Exposed-core microstructured optical fibers for real-time fluorescence sensing. *Optics Express* 2009, *17* (21), 18533-18542.
74. Heng, S.; Nguyen, M.-C.; Kostecki, R.; Monro, T. M.; Abell, A. D. Nanoliter-scale, regenerable ion sensor: sensing with a surface functionalized microstructured optical fibre. *RSC Advances* 2013, *3* (22), 8308-8317.
75. Warren-Smith, S. C.; Heng, S.; Ebendorff-Heidepriem, H.; Abell, A. D.; Monro, T. M. Fluorescence-based aluminum ion sensing using a surface-functionalized microstructured optical fiber. *Langmuir* 2011, *27* (9), 5680-5.
76. Ebendorff-Heidepriem, H.; Warren-Smith, S. C.; Monro, T. M. Suspended nanowires: fabrication, design and characterization of fibers with nanoscale cores. *Optics Express* 2009, *17* (4), 2646-2657.
77. Kostecki, R.; Ebendorff-Heidepriem, H.; Davis, C.; McAdam, G.; Warren-Smith, S. C.; Monro, T. M. Silica exposed-core microstructured optical fibers. *Optical Materials Express* 2012, *2* (11), 1538-1547.
78. Schartner, E. P.; Ebendorff-Heidepriem, H.; Warren-Smith, S. C.; White, R. T.; Monro, T. M. Driving down the Detection Limit in Microstructured Fiber-Based Chemical Dip Sensors. *Sensors* 2011, *11* (3), 2961-2971.

79. Jensen, J. B.; Pedersen, L. H.; Hoiby, P. E.; Nielsen, L. B.; Hansen, T. P.; Folkenberg, J. R.; Riishede, J.; Noordegraaf, D.; Nielsen, K.; Carlsen, A.; Bjarklev, A. Photonic crystal fiber based evanescent-wave sensor for detection ofbiomolecules in aqueous solutions. *Optics Letters* 2004, *29* (17), 1974-1976.
80. Webb, A. S.; Poletti, F.; Richardson, D. J.; Sahu, J. K. Suspended-core holey fiber for evanescent-field sensing. *Optical Engineering* 2007, *46* (1), 010503.
81. Ebendorff-Heidepriem, H.; Foo, T. C.; Moore, R. C.; Zhang, W. Q.; Li, Y. H.; Monro, T. M.; Hemming, A.; Lancaster, D. G. Fluoride glass microstructured optical fiber with large mode area and mid-infrared transmission. *Optics Letters* 2008, *33* (23), 2861-2863.
82. Cubillas, A. M.; Unterkofler, S.; Euser, T. G.; Etzold, B. J.; Jones, A. C.; Sadler, P. J.; Wasserscheid, P.; Russell, P. S. Photonic crystal fibres for chemical sensing and photochemistry. *Chemical Society Review* 2013, *42* (22), 8629-48.
83. Stepien, R.; Cimek, J.; Pysz, D.; Kujawa, I.; Klimczak, M.; Buczynski, R. Soft glasses for photonic crystal fibers and microstructured optical components. *Optical Engineering* 2014, *53* (7), 071815-071815.
84. Ebendorff-Heidepriem, H.; Moore, R. C.; Monro, T. M. Progress in the Fabrication of the Next-Generation Soft Glass Microstructured Optical Fibers. *AIP Conference Proceedings* 2008, *1055* (1), 95-98.
85. Afshar V, S.; Warren-Smith, S. C.; Monro, T. M. Enhancement of fluorescence-based sensing using microstructured optical fibres. *Optics. Express* 2007, *15* (26), 17891-17901.
86. Richardson, K.; Krol, D.; Hirao, K. Glasses for Photonic Applications. *International Journal of Applied Glass Science* 2010, *1* (1), 74-86.
87. Kostecki, R.; Ebendorff-Heidepriem, H.; Afshar V, S.; McAdam, G.; Davis, C.; Monro, T. M. Novel polymer functionalization method for exposed-core optical fiber. *Opt. Materials. Express* 2014, *4* (8), 1515-1525.
88. Metwalli, E.; Haines, D.; Becker, O.; Conzone, S.; Pantano, C. G. Surface characterizations of mono-, di-, and tri-aminosilane treated glass substrates. *Journal of Colloid and Interface Science* 2006, *298* (2), 825-831.
89. Warren-Smith, S. C.; Monro, T. M. Exposed core microstructured optical fiber Bragg gratings: refractive index sensing. *Optics Express* 2014, *22* (2), 1480-1489.
90. Bianco, A.; Perissinotto, S.; Garbugli, M.; Lanzani, G.; Bertarelli, C. Control of optical properties through photochromism: a promising approach to photonics. *Laser & Photonics Reviews* 2011, *5* (6), 711-736.
91. Bao, X.; Chen, L. Recent Progress in Distributed Fiber Optic Sensors. *Sensors* 2012, *12* (7), 8601.
92. Williams, G. O.; Chen, J. S.; Euser, T. G.; Russell, P. S.; Jones, A. C. Photonic crystal fibre as an optofluidic reactor for the measurement of photochemical kinetics with sub-picomole sensitivity. *Lab Chip* 2012, *12* (18), 3356-61.
93. Warren-Smith, S.; Ebendorff-Heidepriem, H.; Afshar, S.; McAdam, G.; Davis, C.; Monro, T. M. Corrosion sensing of aluminium alloys using exposed core microstructured optical fibres. *Materials Forum* 2009, *33*.
94. Ajoy Ghatak, K. T. *SPIE: Fundamentals of Photonics: Module 1.7 optical waveguides and fibers* [Online]; University of Conneticut, 2000.

http://spie.org/Documents/Publications/00 %20STEP %20Module %2007.pdf.
95. Lambeck, P. V. Integrated opto-chemical sensors. *Sensors and Actuators B: Chemical* 1992, *8* (1), 103-116.
96. Afshar V, S.; Ruan, Y.; Warren-Smith, S. C.; Monro, T. M. Enhanced fluorescence sensing using microstructured optical fibers: a comparison of forward and backward collection modes. *Optics Letters.* 2008, *33* (13), 1473-1475.
97. Rohatgi-Mukherjee, K. K. *Fundamentals of Photochemistry*. Wiley: 1978.
98. McDonald, R. S. Surface Functionality of Amorphous Silica by Infrared Spectroscopy. *The Journal of Physical Chemistry* 1958, *62* (10), 1168-1178.
99. Fluegel, A. Glass Composition, Glass Types. http://glassproperties.com/glasses/ (accessed 16/02/2016).
100. Ulman, A. Formation and Structure of Self-Assembled Monolayers. *Chemical Reviews* 1996, *96* (4), 1533-1554.
101. Parida, S. K.; Dash, S.; Patel, S.; Mishra, B. K. Adsorption of organic molecules on silica surface. *Advances in Colloid and Interface Science* 2006, *121* (1–3), 77-110.
102. Nicosia, C.; Huskens, J. Reactive self-assembled monolayers: from surface functionalization to gradient formation. *Materials Horizons* 2014, *1* (1), 32-45.
103. Flink, S.; van Veggel, F. C. J. M.; Reinhoudt, D. N. Functionalization of self-assembled monolayers on glass and oxidized silicon wafers by surface reactions. *Journal of Physical Organic Chemistry* 2001, *14* (7), 407-415.
104. Karrasch, S.; Dolder, M.; Schabert, F.; Ramsden, J.; Engel, A. Covalent binding of biological samples to solid supports for scanning probe microscopy in buffer solution. *Biophysical Journal* 1993, *65* (6), 2437-2446.
105. Howarter, J. A.; Youngblood, J. P. Optimization of Silica Silanization by 3-Aminopropyltriethoxysilane. *Langmuir* 2006, *22* (26), 11142-11147.
106. Wang, W.; Vaughn, M. W. Morphology and Amine Accessibility of (3-Aminopropyl) Triethoxysilane Films on Glass Surfaces. *Scanning* 2008, *30* (2), 65-77.
107. Zeng, X.; Xu, G.; Gao, Y.; An, Y. Surface Wettability of (3-Aminopropyl)triethoxysilane Self-Assembled Monolayers. *The Journal of Physical Chemistry B* 2010, *115* (3), 450-454.
108. González-Guerrero, A. B.; Alvarez, M.; Castaño, A. G.; Domínguez, C.; Lechuga, L. M. A comparative study of in-flow and micro-patterning biofunctionalization protocols for nanophotonic silicon-based biosensors. *Journal of Colloid and Interface Science* 2013, *393* (0), 402-410.
109. Barabanova, A. I.; Pryakhina, T. A.; Afanas'ev, E. S.; Zavin, B. G.; Vygodskii, Y. S.; Askadskii, A. A.; Philippova, O. E.; Khokhlov, A. R. Anhydride modified silica nanoparticles: Preparation and characterization. *Applied Surface Science* 2012, *258* (7), 3168-3172.
110. Gang, A.; Gabernet, G.; Renner, L. D.; Baraban, L.; Cuniberti, G. A simple two-step silane-based (bio-) receptor molecule immobilization without additional binding site passivation. *RSC Advances* 2015, *5* (45), 35631-35634.
111. Rosario, R.; Gust, D.; Hayes, M.; Jahnke, F.; Springer, J.; Garcia, A. A. Photon-Modulated Wettability Changes on Spiropyran-Coated Surfaces. *Langmuir* 2002, *18* (21), 8062-8069.

112. Gooding, J. J.; Ciampi, S. The molecular level modification of surfaces: from self-assembled monolayers to complex molecular assemblies. *Chemical Society Reviews* 2011, *40* (5), 2704-2718.
113. Vistas, C. R.; Águas, A. C. P.; Ferreira, G. N. M. Silanization of glass chips—A factorial approach for optimization. *Applied Surface Science* 2013, *286* (0), 314-318.
114. Kurth, D. G.; Bein, T. Surface reactions on thin layers of silane coupling agents. *Langmuir* 1993, *9* (11), 2965-2973.
115. Mittal, K. L. *Silanes and Other Coupling Agents*. Taylor & Francis: 2007.
116. Halliwell, C. M.; Cass, A. E. G. A Factorial Analysis of Silanization Conditions for the Immobilization of Oligonucleotides on Glass Surfaces. *Analytical Chemistry* 2001, *73* (11), 2476-2483.
117. Feringa, B. L.; Browne, W. R. *Molecular Switches*. Wiley: 2011.
118. Bouas-Laurent, H.; Durr, H. Organic photochromism. *Pure Appl. Chem.* 2001, *Vol. 73* (No. 4), 639-665.
119. Durr, H. *Photochromism - Molecules and systems - General introduction*. Elsevier Science Bv: Amsterdam, 2003; 1-14.
120. Lee, H. W.; Kim, Y. M.; Jeon, D. J.; Kim, E.; Kim, J.; Park, K. Rewritable organic films for near-field recording. *Optical Materials* 2003, *21* (1–3), 289-293.
121. Guo, X.; Zhang, D.; Yu, G.; Wan, M.; Li, J.; Liu, Y.; Zhu, D. Reversible Photoregulation of the Electrical Conductivity of Spiropyran-Doped Polyaniline for Information Recording and Nondestructive Processing. *Advanced Materials* 2004, *16* (7), 636-640.
122. Osakada, Y.; Hanson, L.; Cui, B. Diarylethene doped biocompatible polymer dots for fluorescence switching. *Chemical Communications* 2012, *48* (27), 3285-3287.
123. Florea, L.; Diamond, D.; Benito-Lopez, F. Photo-Responsive Polymeric Structures Based on Spiropyran. *Macromolecular Materials and Engineering* 2012, *297* (12), 1148-1159.
124. Yagai, S.; Kitamura, A. Recent advances in photoresponsive supramolecular self-assemblies. *Chemical Society Reviews* 2008, *37* (8), 1520-1529.
125. Lyndon, R.; Konstas, K.; Ladewig, B. P.; Southon, P. D.; Kepert, P. C.; Hill, M. R. Dynamic photo-switching in metal-organic frameworks as a route to low-energy carbon dioxide capture and release. *Angewandte Chemie* 2013, *52* (13), 3695-8.
126. Klajn, R. Immobilized azobenzenes for the construction of photoresponsive materials. *Pure and Applied Chemistry* 2010, *82* (12), 2247.
127. Bossi, M. L.; Aramendía, P. F. Photomodulation of macroscopic properties. *Journal of Photochemistry and Photobiology C: Photochemistry Reviews* 2011, *12* (3), 154-166.
128. Browne, W. R.; Feringa, B. L. Light Switching of Molecules on Surfaces. *Annual Review of Physical Chemistry* 2009, *60* (1), 407-428.
129. Katsonis, N.; Lubomska, M.; Pollard, M. M.; Feringa, B. L.; Rudolf, P. Synthetic light-activated molecular switches and motors on surfaces. *Progress in Surface Science* 2007, *82* (7-8), 407-434.
130. Bianchi, A.; Delgado-Pinar, E.; García-España, E.; Giorgi, C.; Pina, F. Highlights of metal ion-based photochemical switches. *Coordination Chemistry Reviews* 2014, *260* (0), 156-215.

131. Liu, W.; Pu, S.; Jiang, D.; Cui, S.; Liu, G.; Fan, C. Fluorescent probes for Al(III) and Cr(III) based on a photochromic diarylethene bearing a fluorescent rhodamine unit. *Microchimica Acta* 2011, *174* (3), 329-336.
132. Natali, M.; Soldi, L.; Giordani, S. A photoswitchable Zn (II) selective spiropyran-based sensor. *Tetrahedron* 2010, *66* (38), 7612-7617.
133. Alfimov, M. V.; Fedorova, O. A.; Gromov, S. P. Photoswitchable molecular receptors. *Journal of Photochemistry and Photobiology A: Chemistry* 2003, *158* (2-3), 183-198.
134. Blank, M.; Soo, L. M.; Wassermann, N. H.; Erlanger, B. F. Photoregulated Ion Binding. *Science* 1981, *214* (4516), 70-72.
135. Lerch, M. M.; Hansen, M. J.; van Dam, G. M.; Szymanski, W.; Feringa, B. L. Emerging Targets in Photopharmacology. *Angewandte Chemie International Edition* 2016, n/a-n/a.
136. Dong, S.-L.; Löweneck, M.; Schrader, T. E.; Schreier, W. J.; Zinth, W.; Moroder, L.; Renner, C. A Photocontrolled β-Hairpin Peptide. *Chemistry – A European Journal* 2006, *12* (4), 1114-1120.
137. Ciardelli, F.; Pieroni, O.; Fissi, A.; Houben, J. L. Azobenzene-containing polypeptides - photoregulation of conformation in solution. *Biopolymers* 1984, *23* (7), 1423-1437.
138. Sadovski, O.; Beharry, A. A.; Zhang, F.; Woolley, G. A. Spectral Tuning of Azobenzene Photoswitches for Biological Applications. *Angewandte Chemie International Edition* 2009, *48* (8), 1484-1486.
139. Park, S. B.; Standaert, R. F. A photoregulated ligand for the nuclear import receptor karyopherin α. *Bioorganic and Medicinal Chemistry* 2001, *9* (12), 3215-3223.
140. Kobatake, S.; Irie, M. 8 Photochromism. *Annual Reports Section "C" (Physical Chemistry)* 2003, *99* (0), 277-313.
141. Klajn, R. Spiropyran-based dynamic materials. *Chemical Society Review* 2014, *43* (1), 148-84.
142. Organic Photochromic and Thermochromic Compounds, Volume 2: Physicochemical Studies, Biological Applications, and Thermochromism. Kluwer Academic Publishers: Hingham, MA, USA, 1999.
143. Lukyanov, B. S.; Lukyanova, M. B. Spiropyrans: Synthesis, Properties, and Application. (Review). *Chemistry of Heterocyclic Compounds* 2005, *41* (3), 281-311.
144. Helmy, S.; Leibfarth, F. A.; Oh, S.; Poelma, J. E.; Hawker, C. J.; Read de Alaniz, J. Photoswitching Using Visible Light: A New Class of Organic Photochromic Molecules. *Journal of the American Chemical Society* 2014, *136* (23), 8169-8172.
145. Altoe, P.; Bernardi, F.; Conti, I.; Garavelli, M.; Negri, F.; Orlandi, G. Light driven molecular switches: exploring and tuning their photophysical and photochemical properties. *Theoretical Chemistry Accounts* 2007, *117* (5-6), 1041-1059.
146. Abbandonato, G.; Signore, G.; Nifosì, R.; Voliani, V.; Bizzarri, R.; Beltram, F. Cis–trans photoisomerization properties of GFP chromophore analogs. *European Biophysics Journal* 2011, *40* (11), 1205-1214.

CHAPTER 2

SUITABILITY OF PHOTOSWITCHES FOR MOF DEVICES

2.1 OVERVIEW OF CHAPTER

The choice of organic photoswitch to use as the core of a photoswitchable sensing device, as described in Chapter 1, is central to the design and creation of an effective sensor. The choice of photoswitch for incorporation into photochromic materials is generally made based on researcher preference, availability, or convenience rather than systematic design towards the most suitable switch for the desired purpose. There are however, many different classes of photoswitches that are available for use, each with wide potential for further modification. This chapter investigates and compares the properties of four of the more common photoswitches (diarylalkenes, azobenzenes, fulgides and spiropyrans), in order to select the most suitable photoswitch to use as the core photoswitchable moiety for our microstructured optical fibre (MOF) sensor. Section 2.2 presents a published (PAPER 1) comparison of these photoswitches in MOFs comparing the in-fibre photodecay rates to determine the most photostable photoswitches. Section 2.3 then presents a literature review of these photoswitches, comparing the other key properties which need to be considered; such as, their photochromic properties, biologically relevant absorption/emission wavelengths, and ease of synthesis/structural diversity etc.

2.2 PAPER 1: A COMPARATIVE STUDY OF THE FLUORESCENCE AND PHOTOSTABILITY OF COMMON PHOTOSWITCHES IN MICROSTRUCTURED OPTICAL FIBRE

Statement of Authorship

Title of Paper	Fluorescence and Photostability of Organic Photoswitches on Microstructured Optical Fibre
Publication Status	☑ Published ☐ Accepted for Publication ☐ Submitted for Publication ☐ Publication Style
Publication Details	Stubing, D. B.; Heng, S.; Monro, T. M.; Abell, A. D. "A comparative study of the fluorescence and photostability of common photoswitches in microstructured optical fibre". *Sensors and Actuators B: Chemical* **2017,** *239*, 474-480.

Principal Author

Name of Principal Author (Candidate)	Daniel B. Stubing		
Contribution to the Paper	Synthesis of **CF_3-fulgide** (see Appendix A for details). All solution and fibre fluorescence experiments and data analysis. Writing of manuscript		
Overall percentage (%)	75		
Signature		Date	08/09/2016

Co-Author Contributions

By signing the Statement of Authorship, each author certifies that:

i. the candidate's stated contribution to the publication is accurate (as detailed above);

ii. permission is granted for the candidate in include the publication in the thesis;

iii. the sum of all co-author contributions is equal to 100 % less the candidate's stated contribution.

Name of Co-Author	Sabrina Heng		
Contribution to the Paper	Synthesis of **Azo1**[1] and **SP1**[2]. Project direction and significant editing of manuscript.		
Signature		Date	06.10.16

Name of Co-Author	Tanya M. Monro		
Contribution to the Paper	Project direction and editing of manuscript.		
Signature		Date	21/9/16

Name of Co-Author	Andrew D. Abell		
Contribution to the Paper	Project direction and significant editing of manuscript.		
Signature		Date	13/09/2016

A COMPARATIVE STUDY OF THE FLUORESCENCE AND PHOTOSTABILITY OF COMMON PHOTOSWITCHES IN MICROSTRUCTURED OPTICAL FIBRE[3]

Daniel B. Stubing [a], Sabrina Heng [a,*], Tanya M. Monro [a,b], and Andrew D. Abell [a]

[a] ARC Centre of Excellence for Nanoscale BioPhotonics, Institute for Photonics & Advanced Sensing and School of Physical Sciences, The University of Adelaide, South Australia, Australia 5005;

[b] University of South Australia, South Australia, 5000;

2.2.1 ABSTRACT

The fluorescence spectra and photostability under 532 nm laser excitation of four different common photoswitches (an azobenzene, spiropyran, indolylfulgide, and a diarylperfluorocyclopentene) were investigated in a silica microstructured optical fibre. An example of each photoswitch was examined in solution and physically adsorbed to the silica fibre surface. This comparison was made to define fluorescence behaviour in these two states and to determine which photoswitch has the best performance in this light intense microenvironment. The azobenzene and the spiropyran switches demonstrated the strongest fluorescence response and the least degradation of the fluorescence signal.

2.2.2 INTRODUCTION

The study and development of smart materials and sensors that can be switched on and off or modulated in some way, is an important area of current endeavour.[4-7] These materials must possess at least two functional states that can be interconverted by an external stimulus such as heat, electric potential or light. Of particular interest in this context is the use of an organic photochromic dye that can be attached to a solid support such as polymer, nanoparticles, or bulk surfaces; providing materials where surface properties such as hydrophobicity, charge, conductivity, colour, molecular recognition, and material size can be easily controlled. Such photoswitchable materials have been proposed for many applications; for example in

data storage,[8] nanoelectronics,[9, 10] switchable polymers,[11, 12] nanomachines,[13, 14] gas storage,[15] drugs,[16, 17] and sensor devices[18-20].

Microstructured Optical Fibres (MOFs) show particular promise as a new material for smart sensor devices.[21] The holes surrounding the micron sized waveguide core in wagon-wheel MOFs (Supporting Information Figure 2-8) allow interaction between an analyte within the holes and the evanescent field of guided light to allow the absorbance and fluorescence (through light recapture) of the analyte to be detected.[22] A MOF provides a very sensitive sensing platform due to its large light interaction path length and ability to sample nanolitre quantities; and combined with its small size, biocompatibility and ability to sense remotely allows for use within an *in vivo* environment.[23] Chemical detection at picomolar sensitivity has previously been demonstrated in such systems.[24, 25] However, a major limitation of such optical sensing devices is that the sample can be exposed to high intensity light, which can result in bleaching. As such, the organic sensing molecule needs to be photostable, especially if required over extended periods and repeated use, and particularly if fixed to the photon rich waveguide surface.[23, 26]

MOFs are particularly promising for fluorescence-based applications, rather than absorbance, as the fluorescence spectrum is measurable at either end of the fibre. Therefore, all instrumentation required for analyte excitation and detection can be located at one end of the fibre; freeing the other end for sample interaction, such as for fibre tip based sensing.[27] However, while the absorption and photoswitching properties of common photoswitches for use in such devices are well studied and reported, the associated fluorescence spectra are typically not, possibly due to a tendency to have poor fluorescence yields.[28] However, this is of lesser importance for MOF sensors due to enhanced sensitivity. This paper addresses this shortfall by comparing and contrasting the fluorescence and photostability of four common photoswitches within a common MOF sensing system under high intensity light conditions broadly associated with fibre sensors. Conclusions are drawn regarding the suitability of each photoswitch for use in MOF based sensors, and potentially other devices that utilize high intensity light.

Four examples of photoswitches, each representing a different class of organic photoswitch was chosen for study, i.e. an azobenzene, spiropyran, indolylfulgide, and diarylalkene (Figure 2-1). Members of these classes are known to have high fatigue resistance, an ability to operate at biologically compatible wavelengths, and well-defined switching states that exhibit large conformational differences; making them suitable for applications in devices. Azobenzenes and spiropyrans have already found use in MOF devices,[1, 2, 29-31] while the indolylfulgide (**CF_3-fulgide**) and diarylalkene (**DA1**) show promising properties in terms of high photoswitching fatigue resistance, a large spectroscopic change upon photoswitching, and tunable absorption profiles within the biologically viable visible-red region.[32-34] The photochemical properties of unsubstituted spiropyrans[35] and azobenzenes[36] on optical fibre have been reported. In addition, we have found little spectral differences between substituted and non-substituted azobenzenes (Supporting Information Figure 2-11) and spiropyrans[2, 25, 31, 37, 38] particularly in the absence of ion binding. Therefore, for this study, we focused on the characterization of 3-carboxy-5,2',4'-trimethoxy azobenzene (**Azo1**)[1, 23] and spiropyran **SP1**.[2] These compounds have been reported in applications for sensing of aluminium ions with respect to corrosion detection and sensing of zinc ions in biology. Importantly, **Azo1** and **SP1** can be attached to a surface, which makes them ideal candidates for this study in the context of sensor development. The trifluorinated indolylfulgide (**CF_3-fulgide**), first reported by Yokoyama,[32] has high fatigue resistance, high thermal stability (no thermo-isomerisation) and large separation between ring opening and closing photoisomerisation wavelengths, and as such shows much promise for applications in data storage.[39-41] However, 3-indolylfulgides, such as **CF_3-fulgide**, do not have a strong fluorescence, which limits their readout capacity.[42] Diarylalkene, 1,2-bis(2,4-dimethyl-5-phenylthiophen-3-yl)-perfluorocyclopentene (**DA1**),[33, 43] has high thermal stability and high photofatigue resistance (>850 cycles) in hexane, demonstrating the potential of diarylalkenes for devices applications.

The absorbance and fluorescence spectra of each of the four photoswitches (**Azo1**, **SP1**, **CF_3-fulgide** and **DA1** (Figure 2-1)) were determined in both DMSO and acetonitrile (polar aprotic solvents) and also within a MOF. The effect of solvent, irradiation brightness and surface proximity on the emission spectra and the stability

of the respective photoswitches on repeated exposure to the excitation light source was then defined. These two solvents were chosen for comparison as they provided sufficient solubility for all photoswitches, while also being biologically relevant; the photoswitches were found to have poor solubility in water or mixed acetonitrile:water (1:9) solutions. Finally, the fluorescence, photostability and photoswitchability of each photoswitch was investigated in the solid state, by physically adsorbing them onto the fibre surface, in order to compare to the solvated systems and to approximate surface functionalized behaviour.

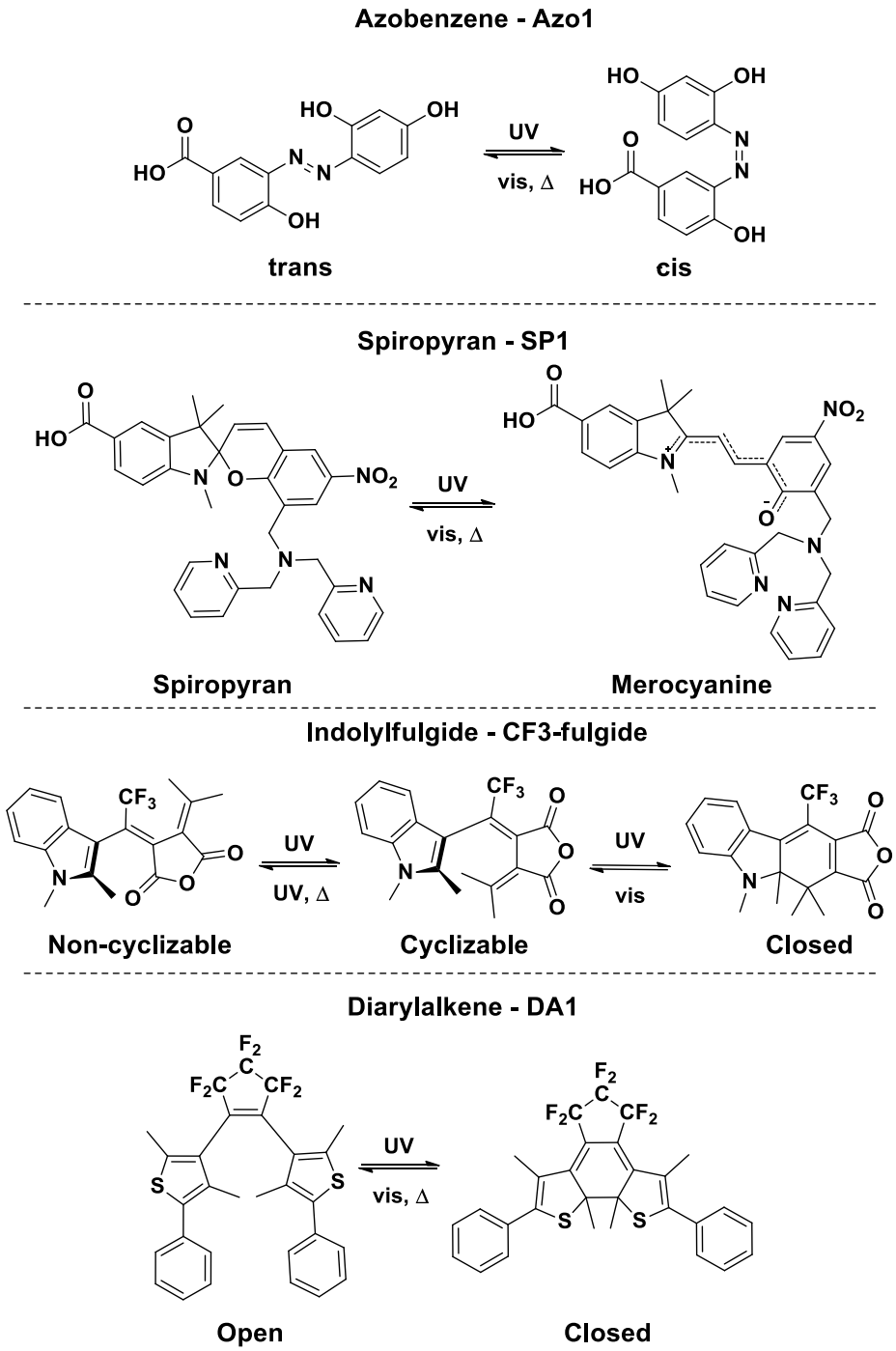

FIGURE 2-1: Structures of the photoswitches **Azo1**, **SP1**, **CF_3-fulgide** and **DA1**.

2.2.3 RESULTS AND DISCUSSION

2.2.3.1 Azobenzene Fluorescence in Solution

The fluorescence spectra of solutions of **Azo1** (Figure 2-1) in DMSO and acetonitrile showed a weak fluorescence signal in cuvette, with an emission max at 595 nm in DMSO and 572 nm in acetonitrile (Figure 2-2A, red and blue). The DMSO fluorescence signal intensity was four times more intense. Irradiation of **Azo1** with 352 nm light from a UV black light, to promote *trans* to *cis* photoisomerisation, did not change either the fluorescence or absorbance (Supporting Information Figure 2-9). This may be due to the poor absorption and photoswitching yield at 352 nm, or possibly fast thermal isomerisation back to the initial *trans* isomer on the experiment timescale.[44] The weak signal observed for **Azo1** is consistent with the general observation that azobenzenes have poor fluorescence yields.[28, 45] However, the fluorescence and photostability are still relevant properties of some azobenzenes; i.e. as some azobenzenes, such as **Azo1**, are used as fluorescence based sensors due to a fluorescence turn-on upon ligand interaction, also, as photoswitchable compounds azobenzenes are routinely exposed to light.

The fluorescence signal of **Azo1** in a MOF and the fluorescence decay over 50 x 8 ms pulses was obtained after filling a fibre with a 1 mM solution of **Azo1** in DMSO or acetonitrile (Figure 2-2A). The fluorescence of **Azo1** in the MOF is broader and bathochromically shifted compared to that determined in the cuvette spectrometer, with emission maximum around 630 nm and 600 nm in DMSO and acetonitrile, respectively (Figure 2-2A, pink and cyan). This fluorescence was similar to that previously reported for **Azo1** in water and on poly(allylamine hydrochloride) coated fibre surfaces.[1, 24]

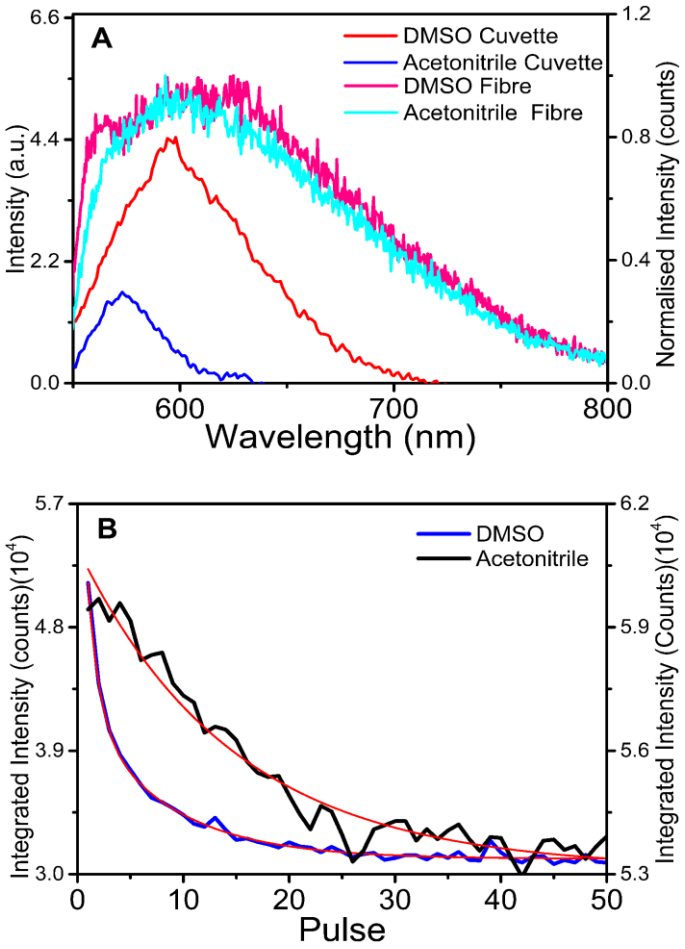

FIGURE 2-2: (A) Fluorescence spectra of **Azo1** in cuvette (10 µM) in DMSO and acetonitrile; and normalized fluorescence within a MOF in DMSO and acetonitrile. (B) Integrated fluorescence signal of **Azo1** in a MOF during pulsing with 532 nm light in DMSO (left axis) and acetonitrile (right axis) (1 mM), fitted with a second order exponential decay model (red).

The photodecay study showed that in DMSO solution the fluorescence intensity of **Azo1** decreased by 33 % over the first ten pulses relative to the initial intensity (Figure 2-2B). This rapid decrease in fluorescence is likely due to photobleaching rather than from *trans* to *cis* photoisomerisation, as the original fluorescence spectrum was unable to be regenerated thermo- or photochemically after prolonged exposure with white or UV light; as would be expected if photochromism was occurring. The fluorescence signal degrades at 0.05 % per pulse after the initial rapid decrease. Interestingly the decrease in fluorescence trended to a non-zero value, possibly due to diffusion within the fibre, as only the photoswitch close to the fibre core will undergo photoexcitation and bleaching. The photobleaching rate of

Azo1 in acetonitrile is lower than in DMSO, here the signal decayed by 12 % of the initial intensity over the whole 50 pulses (0.24 % per pulse). It is thus clear that the excitation laser light used to provide the fluorescence signal promotes photodegradation of **Azo1.** The extent of degradation is solvent dependent, with acetonitrile giving a reduced rate of decay compared to DMSO.

2.2.3.2 Spiropyran Fluorescence in Solution

The DMSO and acetonitrile samples of **SP1** in MOF have maximum fluorescence observed at 640 nm in both solvents, with only a small difference in emission spectra (Figure 2-3A, pink and cyan). This is bathochromically shifted from the 620 nm fluorescence peak observed in cuvette using the benchtop spectrometer (Figure 2-3A, red and blue). The filled MOFs were exposed repeatedly to the excitation light source in order to determine photostability over time. For DMSO this produced a 30 % decrease and blue shift in the emission peak over the first ten pulses, after the initial intensity decrease an increase in the integrated intensity was observed due to a continued blue peak shift (Figure 2-3B, blue). In acetonitrile an initial decrease of 13 % was observed followed by a linear decrease of 0.15 % per pulse (Figure 2-3B black). Photoswitching of **SP1** to **MC1** was induced on exposing the filled fibre to UV black light (observed as a colouration at 562 nm in cuvette (Supporting Information Figure 2-9B)). The **MC1** photostationary state gave a significant increase in the emission intensity at 650 nm, as would be expected from its more fluorescent cyanine structure;[46] in MOF the UV light also produced a side peak at approx. 740 nm in both solvents which was not photochromic on exposure to UV or white light and it is likely due to a product of photodegradation. Pulsing of the **MC1** state with the excitation light source led to a rapid decrease in the 650 nm merocyanine peak and the appearance of the **SP1** derived 640 nm emission peak within four pulses (Figure 2-3B, insert). Irradiation of this 'bleached' solution with UV light caused an increase in the fluorescence due to regeneration of **MC1**. This suggests that the 532 nm excitation light induced rapid reverse photoswitching of **MC1** to **SP1**. This is not ideal for continuous and repetitive measurements involving a photoswitchable state, highlighting the requirement to have a non-destructive readout capability for use in optical devices.

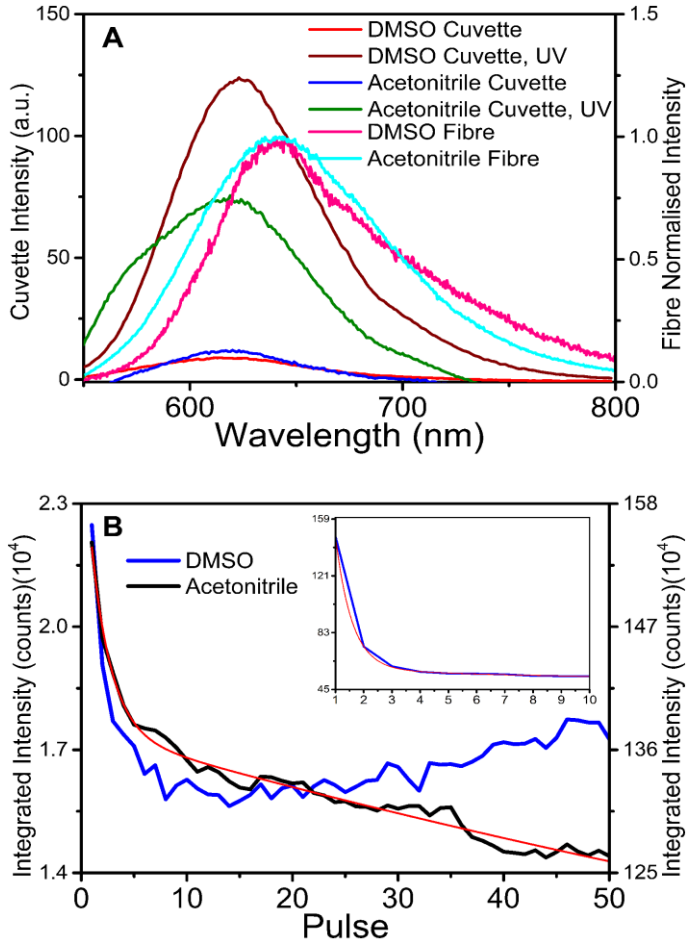

FIGURE 2-3: (A) Fluorescence spectra of **SP1** and **MC1** 100 μM in cuvette before and after irradiation with 352 nm UV light in DMSO and acetonitrile; and normalised fluorescence spectra within a MOF in DMSO and acetonitrile. (B) Integrated fluorescence signal of **SP1** in a MOF during pulsing with 532 nm light in DMSO (left axis), acetonitrile (right axis), and after 5 min UV photoswitching to the **MC1** isomer in DMSO (insert) (1 mM), fitted with a second order exponential decay model (red).

Both **Azo1** and **SP1** showed similar trends on exposure to repeated excitation light; that is, both had increased stability in acetonitrile compared to in DMSO, observed as a decreased rate of fluorescence signal loss and reduced formation of fluorescent side products.

2.2.3.3 Indolylfulgide Fluorescence in Solution

To the best of our knowledge, there are currently no reports on the fluorescence of an 3-indolylfulgide, such as **CF_3-fulgide**, possibly due to a low quantum yield of

fluorescence. This therefore limits the application of fulgides within devices with fluorescence readout capabilities. However, this limitation can be overcome by using a MOF as discussed earlier. This then provides an opportunity to use fulgides, and potentially other weak fluorophores in sensing applications. The fluorescence of **CF_3-fulgide** in either DMSO and acetonitrile (1 mM) in cuvette revealed a weak signal, at this high concentration, with a peak at 580 nm and 600 nm, respectively (Figure 2-4, blue and red). Interestingly, the emission of the **CF_3-fulgide** solution in DMSO in the MOF differed, with a 600 nm peak and a broad 650 nm emission peak (Figure 2-4, pink). Irradiation of this sample with either UV light or white light, to switch the molecule to the photocyclised closed state (Figure 2-1) (Supporting Information Figure 2-9C)), did not produce a change in the emission spectra. Solutions of **CF_3-fulgide** in acetonitrile and DMSO gave different fluorescence spectra within the MOF; with multiple peaks at 600 nm, 630 nm and a broad peak around 770 nm (Figure 2-4, cyan). The longer wavelength peaks are the result of degradation of the **CF_3-fulgide**, possibly due to hydrolysis, as revealed by comparing to samples known to have decomposed over time.[40] Therefore, a comparison of photobleaching of the **CF_3-fulgide** sample with 532 nm light was not possible due to contamination by emissions from its degradation products.

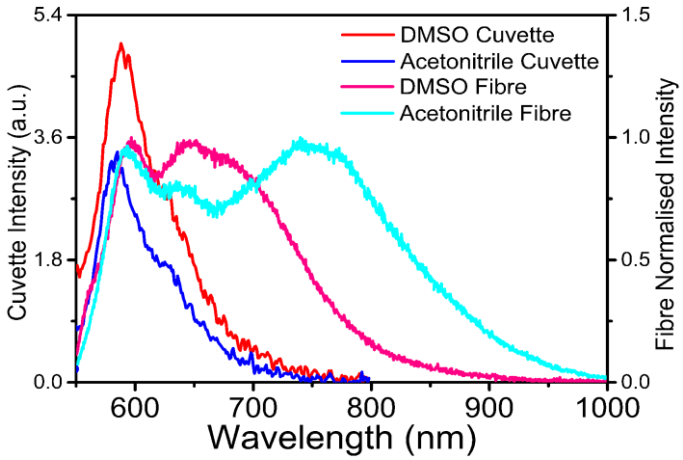

FIGURE 2-4: Fluorescence of **CF_3-fulgide** (1 mM) in cuvette in DMSO and acetonitrile; and within a MOF in DMSO and acetonitrile (1 mM).

2.2.3.4 Diarylalkene Fluorescence in Solution

In both DMSO and acetonitrile **DA1** showed a low fluorescence in cuvette in the uncyclised state (Figure 2-5, red and blue). Photoswitching of **DA1** from the uncyclised uncoloured state to the cyclised coloured state (Figure 2-1) with irradiation with 256 nm UV lamp produced no change to the fluorescence emission. This was expected as the uncyclised form does not absorb at the 532 nm excitation wavelength (Figure 2-9D), and other diarylalkenes which have only thiophene substituents are not known to be fluorescent.[33, 47] However, as shown earlier for **CF_3-fulgide**, that even with very low fluorescence quantum yields a measureable signal can be detected with suspended core MOFs. Initially the **DA1** solutions in the uncyclised form gave a weak broad fluorescence signal around 590 nm (Figure 2-5, orange/cyan), with a feature at 655 nm (as also observed in cuvette). Photoswitching to the cyclised coloured state by exposing the filled fibre to 254 nm UV light in DMSO resulted in a broad fluorescence signal with an increase in the 655 nm feature, in acetonitrile the maximum at 590 nm decreased with the formation of a broad emission peak around 640 nm. These emissions were not photo-reversible on exposure to photoswitching white light, and the 634 nm peak increased in a time dependent manner when within the fibre. Therefore, these signals are believed to be due to the products of either oxidative degradation or photodegradgation.[48, 49] A relative photodegradation rate, for comparison to the other photoswitches, was not obtained due to the lack of significant fluorescence signal.

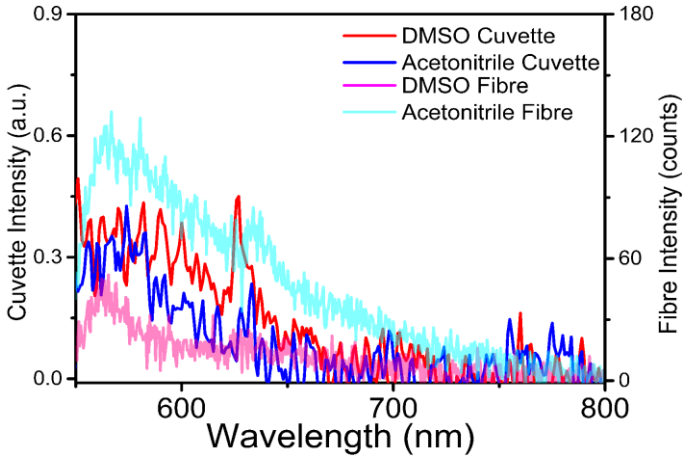

FIGURE 2-5: Fluorescence of **DA1** in cuvette (100 µM) in DMSO and acetonitrile; and within a MOF in DMSO and acetonitrile (1 mM).

This investigation into the fulgide **CF_3-fulgide** and diarylalkene **DA1** highlights that while some fluorophores may be suitable for a variety of applications their use can be limited in situations involving biological samples or high intensity optical devices, due to enhanced degradation.

2.2.3.5 Solid State Fibre Fluorescence

The environment of a photoswitch (*e.g.,* dissolved in solution, dried to a powder or crystalline state, covalently attached to a surface, suspended in a matrix, or physically adsorbed to a material) can influence its ability to interact with light and its associated spectral and photochemical properties. In this section, the fluorescence of the photoswitches **Azo1**, **SP1**, **CF_3-fulgide** and **DA1** physically adsorbed to the core of a MOF, is investigated and the results compared to the solution observations discussed above.

Microstructured optical fibres were internally coated separately with each photoswitch using a modified "drip method"[35, 50] (Section 2.2.5.4) prior to coupling to the optics setup; fluorescence and photostability measurements were then performed as described in Section 2.2.5.4. This method of surface deposition was chosen over other methods, such as sublimation or salinization, due to the mild deposition conditions and the general availability of photoswitchable compounds with appropriate chemical functionality, respectively. It was not determined whether the deposition from solution provides layers of individual compounds or clusters on the surface, because the enclosed structure of the MOF restricts the use of conventional surface characterization techniques. MOFs with coated surfaces were observed to have an increased amount of loss in transmittance, due to increased absorption and scattering of the guided light. The optical alignment of the coated fibre to the optics setup (Figure 2-7) presented an increased risk of pre-exposing the photoswitch to the alignment/excitation light, which could cause undesirable photobleaching. Therefore, the photoswitch coated fibres were roughly coupled to the laser setup as quickly as possible using filtered laser light and the relative optical power and photobleaching rates of the samples were compared based on relative changes in fluorescence intensities. The initial fluorescence spectra and integrated

signal decay due to photobleaching from each of the four photoswitches prior to prolonged exposure to 532 nm light is shown in Figure 2-6A.

The azobenzene, **Azo1**, showed a broad peak with a maximum around 600 nm (Figure 2-6B, black), similar to that observed in the solution-based fibre experiment described in Section 2.2.3.1. Pulsing with the 532 nm laser caused a reduction in the signal intensity by 30 % over the 50 pulses (Figure 2-6A). This decrease is similar to when in DMSO and is twice as much as that observed when **Azo1** was dissolved in acetonitrile. Fluorescence from the dried **Azo1** continued to decrease after the monitored 50 pulses, unlike the DMSO and acetonitrile dissolved sample which plateaued within 50 pulses. This, further suggests that plateauing of signal intensity in solution is due to diffusion of the fluorophore solution near the light exposed surface mixing within the MOF; no such equilibrium can be formed with a fixed fluorophore. Subsequent UV exposure, to induce photoswitching from the native *trans* isomer to the *cis* isomer, gave no change in the fluorescence peak shape, however, a small recovery of the signal intensity was observed.

The adsorbed spiropyran, **SP1**, showed a broad emission with peak maxima at 580 nm and 620 nm (Figure 2-6B, red), similar to that in observed in DMSO and acetonitrile solutions (Section 2.2.3.2). Bleaching of 30 % of the initial intensity over the 50 pulses was apparent (Figure 2-6A, red). Irradiation of the fibre with UV 352 nm light for 10 min to switch **SP1** to **MC1** resulted in an increase in the fluorescence, with a new emission at 647 nm (Figure 2-6B, green). Pulsing of the **MC1** with the 532 nm excitation light quickly bleached this new peak, with a return to the original spectrum within ten pulses. Photobleaching then continued at the same rate as was observed with the unswitched **SP1** (Figure 2-6A, green). Photoswitching between the different **SP1** and **MC1** states with UV 352 nm and green 532 nm light was reproducible over at least three cycles, with a gradual decrease in the intensity, presumably due to photodegradation (Figure 2-10). The fluorescence spectra of **SP1** in the solid state did not develop a new emission peak at 740 nm like what was observed when dissolved in solution in fibre. This suggests that degradation in the solid state is occurring by a different pathway to that in solution.

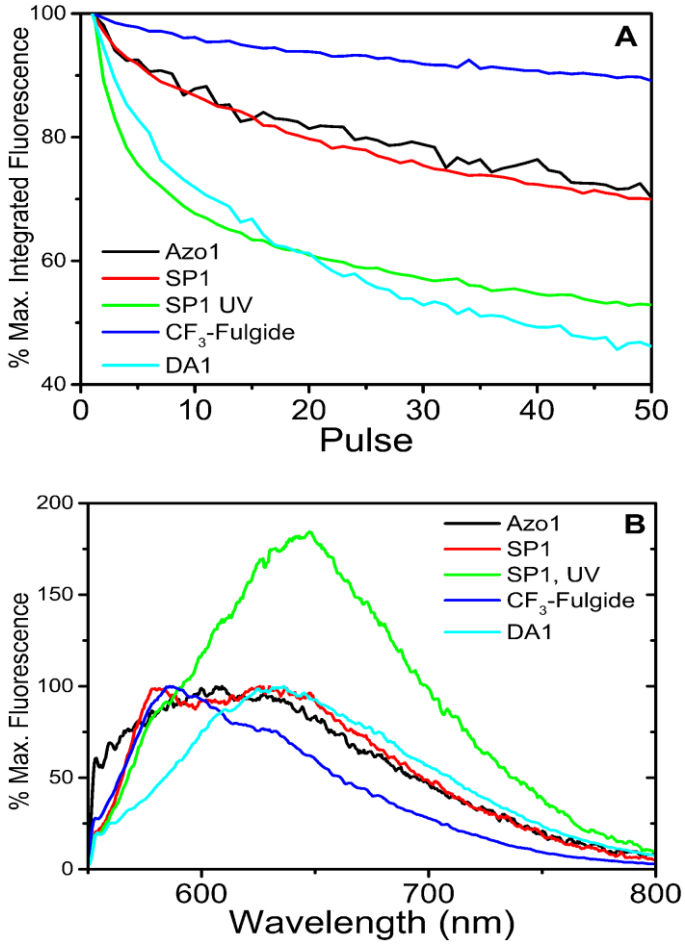

FIGURE 2-6: (A) The integrated fluorescence of each photoswitch (**Azo1**, **SP1**, **SP1** after subsequent 10 min 352 nm UV irradiation, **CF_3-fulgide**, and **DA1**) coated onto the inner surface of a MOF during irradiation with 532 nm light; and (B) initial fluorescence spectra of photoswitches adsorbed to the fibre surface.

As observed in cuvette, **CF_3-fulgide** adsorbed to the fibre core gave a main emission peak at 590 nm and a shoulder peak at 630 nm (Figure 2-6B, blue). The other emissions above 650 nm from the solution based decomposition of **CF_3-fulgide**, as observed when in solution in fibre were not observed. A 10 % decrease in signal intensity was apparent over the 50 pulses (Figure 2-6A). Irradiation of **CF_3-fulgide** in the fibre using UV light or halogen white light to induce photoswitching, again, gave no change in the fluorescence spectrum. Meaning that either photoswitching was not occurring in the adsorbed state or, as the same observation was made in solution, the closed fulgide is not fluorescent from excitation at 532 nm.

The emission spectra of diarylalkene **DA1**, absorbed on the MOF was different to when dissolved in DMSO and acetonitrile solutions, with a broad fluorescence maximum at 627 nm (Figure 2-6B, cyan). This signal decreased by 54 % and broadened after exposure to pulsing of the 532 nm excitation light (Figure 2-6A). Exposure to UV light in order to photoswitch to the cyclised state resulted in an increase in the peak intensity at 627 nm. A new peak was apparent at 660 nm after repeated exposure to the 532 nm excitation light. This new peak at approx. 660 nm did not appear to change with UV, or white light irradiation, suggesting that this was not photochromic and possibly due to a photodecay product.

The above investigation shows that the fluorescence of each of the four photoswitches was observable in the solid state, with the fluorescence spectral features were comparable to in solution; apart from for **DA1**, which did not show fluorescence in solution. Solid state photoswitching was observed for **SP1**. Photodegradation is more prominent on the surface; possibly due to proportionally higher intensity light due to the fluorophore concentrated within the evanescent field, as well as the absence of diffusion of the fluorophores away from the surface.

2.2.4 CONCLUSIONS/OUTLOOK

The stability and photostability of organic photoswitches must be defined if they are to be incorporated into functional switchable smart materials for optical systems. The fluorescence and photostability of four distinct types of photochromic molecules (**Azo1**, **SP1**, **CF_3-fulgide** and **DA1**) was investigated in DMSO and acetonitrile solution, and also adsorbed to a MOF silica surface. **Azo1** and **SP1** gave stronger fluorescence in solution compared to **CF_3-fulgide** and **DA1**. **Azo1** and **SP1** were observed to photobleach 2-3 fold slower in acetonitrile compared to DMSO. Despite being soluble in these polar solvents many photoswitches still lack sufficient aqueous solubility to be applicable in biological systems. An alternative approach is to attach the compounds to surfaces; thereby, eliminating the need to dissolve the compounds before testing. In this context, surface functionalization of photoswitchable biosensors is currently being pursued in our lab. As an analogous method to surface attachment, photoswitches were adsorbed to the silica surface and resultant fluorescence was characterized. Photodegradation was faster than in solution,

possibly a result of the concentration of the photoswitch on the light intense fibre surface as well as a lack of diffusion within the fibre air-holes. The azobenzene, **Azo1**, and spiropyran, **SP1** are clearly the most suitable for fibre device applications due to their higher fluorescence yield, and solution stability**.**

2.2.5 MATERIALS AND METHODS

2.2.5.1 Materials

All solvents used were HPLC grade obtained from Sigma-Aldrich and were used as supplied. The diarylalkene, **DA1**, was obtained from TCI co. (Tokyo). The purity of this compound was confirmed by ^{1}H NMR spectroscopy and was used as supplied. All other photoswitches were synthesized following published methods; **Azo1**,[1] **CF_3-fulgide**[*],[51, 52] and **SP1**[2].

The wagon wheel suspended core optical fibres (MOF) (Figure 2-8) used in these experiments were made from high purity silica F300 glass by the fibre drawing technique, and fabricated in-house.[53] The fibres have hole diameters of 27.7 μm, providing a total fill volume of 18 nL/cm. The core size is 1.5 μm.

2.2.5.2 Apparatus

Cuvette Measurements

Bulk solution absorbance and fluorescence measurements of the photoswitches in acetonitrile and DMSO (10 μM – 1 mM) were obtained using a CARY 5000 UV-Vis spectrometer and a CARY Eclipse fluorometer respectively. Measurements were conducted in a quartz cuvette, path length 10 mm, volume 700 μL. Fluorescence emission measurements were obtained after excitation at 532 nm, emission slit width 5 mm, excitation slit width 10 mm, and at 20 ^{o}C. Switching experiments were performed in the cuvette using a mercury lamp (UVP, 8 W, 352 nm (filtered BLB) or 254 nm (shortwave) tube) or with a halogen white light.

[*] The detailed synthesis and characterisation of **CF_3**-fulgide is presented in Appendix A.

Fibre Fluorescence Optics Setup

The optics setup for determining the fluorescence of fluorophores within a MOF is shown in Figure 2-7. An attenuated 25 mW fibre coupled laser light source (CrystaLaser) with an excitation wavelength of 532 nm was coupled into the core of the MOF. Optimal alignment and calibration of the MOF to the optics setup was achieved by monitoring the optical power transmitted by the fibre at the 'fill' end using a power meter (Thorlabs). The fluorophores fluorescence emission is captured by the fibre and its propagation in the backward direction[22] was recorded with a Horiba iHR550 spectrometer with Synapse CCD detector (100 g/mm grating, 0.5 mm entrance slit width). Photoswitching was performed by externally irradiating (Figure 2-7, blue box) the filled MOF with a mercury lamp (UVP, 8 W, 352 nm (filtered BLB) or 254 nm (shortwave) tube).

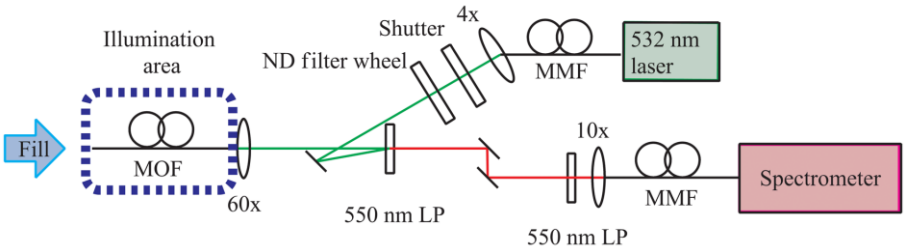

FIGURE 2-7: Optical set-up for measuring the fluorescence with a Microstructured Optical Fibre.

2.2.5.3 Fibre Fluorescence and Photostability

Solutions containing each photoswitch (**Azo1**, **SP1**, **CF_3-fulgide** or **DA1**, Figure 2-1) in DMSO or acetonitrile (1 mM) were drawn into separate 20 cm lengths of MOF fibre by capillary action over a 1 min period (filled length of approx. 14 cm). The sample was then exposed to 50 x 8 ms pulses of 532 nm light of either approx. 0.017 mW for the **SP1** or 0.17 mW for the other photoswitches (**Azo1**, **CF_3-fulgide** or **DA1**) (determined by the optical power transmitted by the empty fibre) and the resulting fluorescence was measured after each pulse. This excitation power provided a significant fluorescence signal for detection and analysis. The change in integrated peak intensity over the 50 pulses was calculated to compare the relative rates of photobleaching.

2.2.5.4 Solid State Fluorescence Measurements

Solutions of photoswitches **Azo1**, **SP1**, **CF_3-fulgide** or **DA1** in acetonitrile (1 mL, 1 mM) were each separately flowed through 40 cm lengths of MOF by external positive pressure supplied by a nitrogen source. Each fibre was then cleared of solution and dried by flowing nitrogen though the holes overnight. A 3 cm length was removed from each end of each fibre to remove possible end-facet damage that may have occurred during the filling process and the remaining fibre was split into two 15 cm sections for analysis. Each fibre was visually inspected under an Olympus BX51 optical microscope with a 20x objective to check for obstructions in the fibre holes, fluorophore precipitation, and complete drying. For analysis, each 15 cm section was coupled to the optical setup in Figure 2-7 and fluorescence signal was measured as described in Section 2.2.5.3.

2.2.6 SUPPORTING INFORMATION

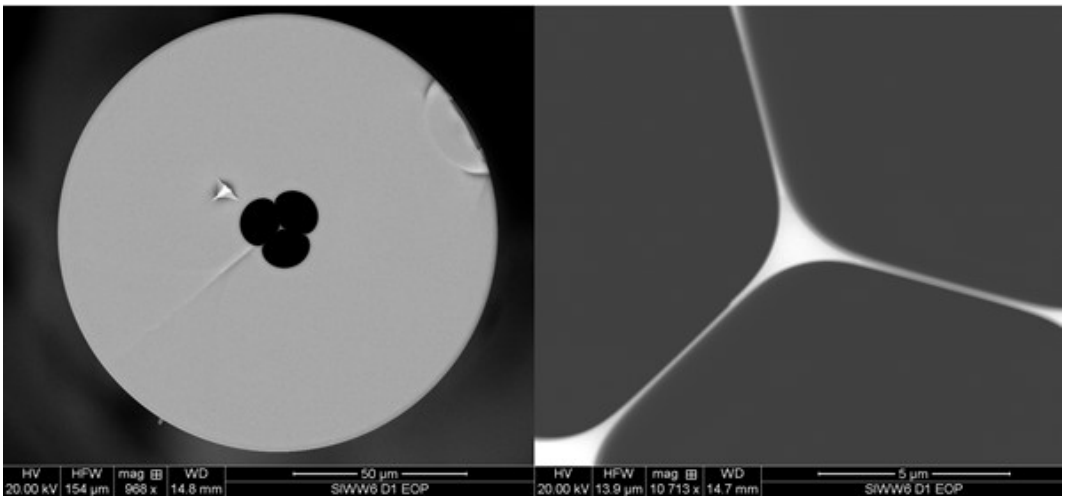

FIGURE 2-8: SEM image of the cross section of the F300 silica MOF used for photoswitch fluorescence experiments. The entire MOF is shown on the left showing the three central holes, scale 50 µm. On the right, zoomed in image of the light guiding core, scale 5 µm, core size 1.5 µm.

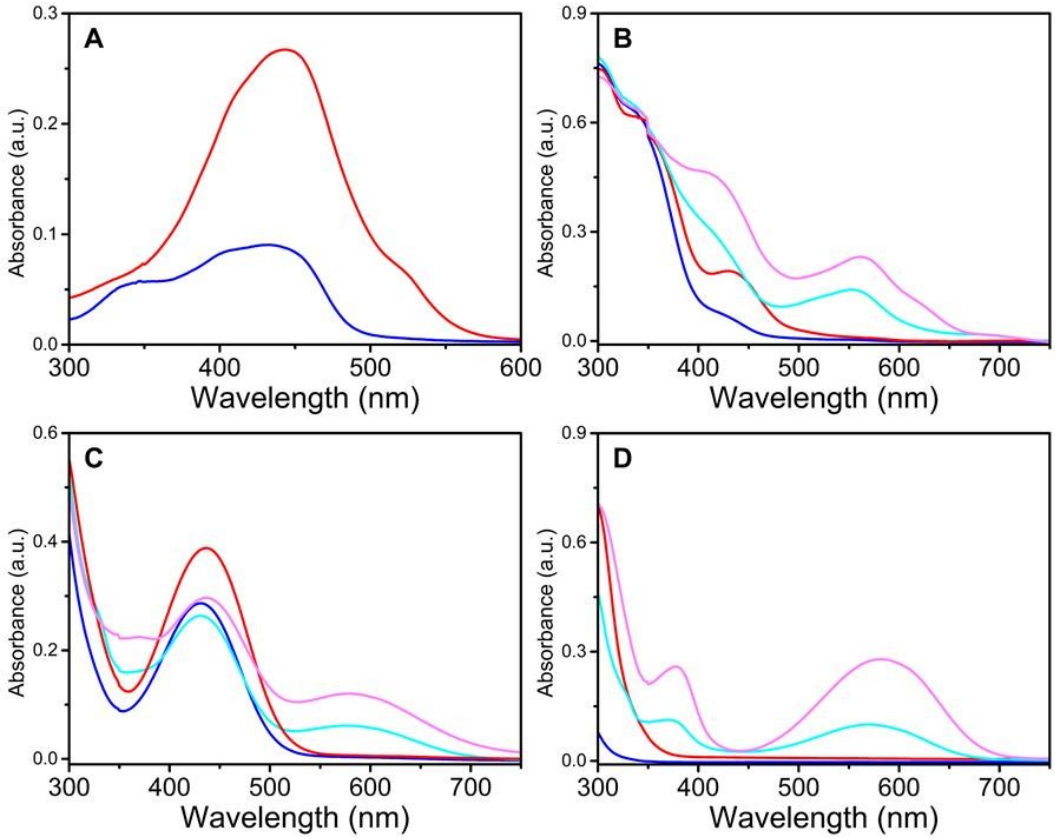

FIGURE 2-9: UV-vis absorption spectra of all four photoswitches before and after irradiation with UV light in acetonitrile (blue/cyan) and DMSO (red/pink) at $1x10^{-4}$ M: A) Azo1 ($1x10^{-3}$ M for in acetonitrile); B) SP1; C) CF_3-fulgide; D) DA1.

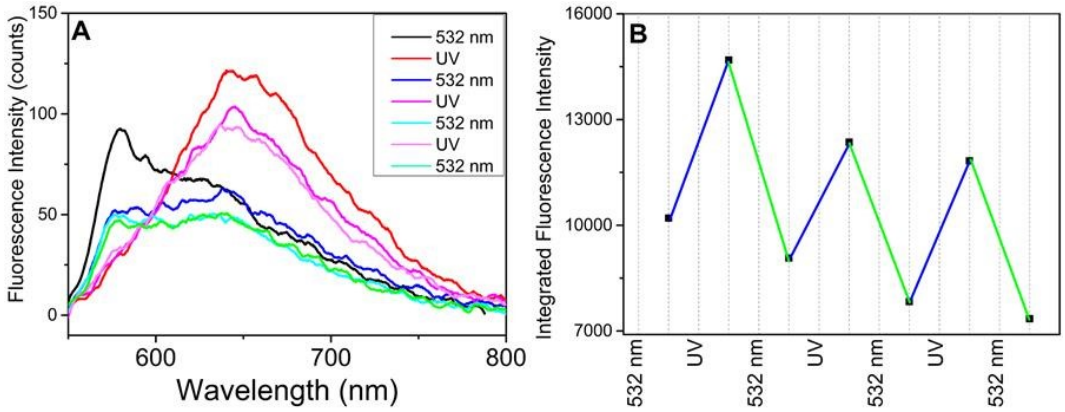

FIGURE 2-10: Photoswitching of **SP1** when adsorbed to the surface. The fluorescence spectral changes (A) and the integrated intensity (B) with each photoswitching cycle from irradiation with green 532 nm laser light (50 x 8 ms pulses) and 352 nm UV lamp for 10 min.

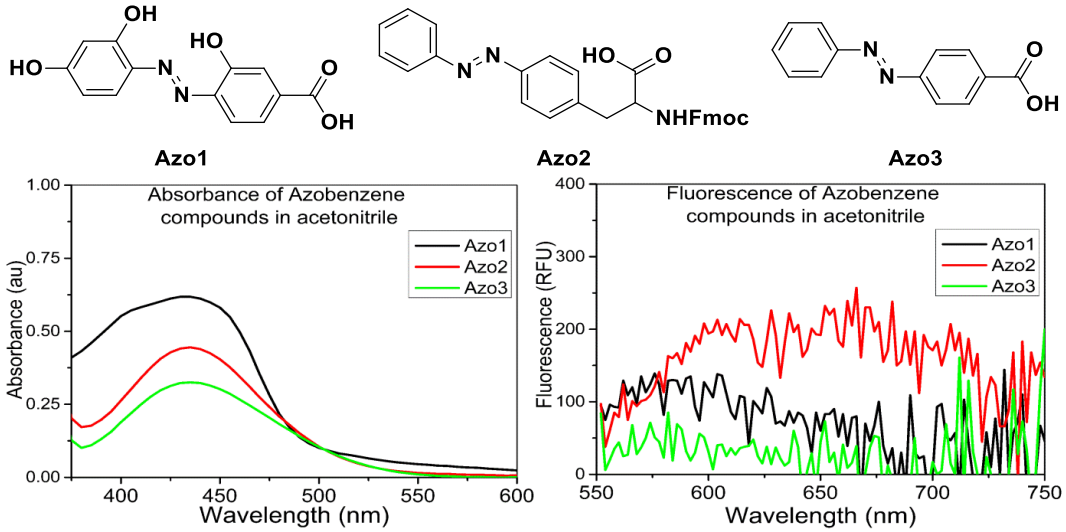

FIGURE 2-11: Comparison of the absorbance and fluorescence spectra of a series of azobenzene derivatives. Comparing the less modified **Azo2** and **Azo3** to **Azo1**. Absorbance and fluorescence spectra acquired using a BioTek Synergy H4 Hybrid Multi-Mode Microplate Reader at 1 mM in acetonitrile (200 µL).

2.3 DISCUSSION OF PHOTOSWITCH PROPERTIES FOR USE AS SENSORS.

The above published work (PAPER 1) introduced and compared the performance of four photoswitches in optical fibres with regards to fluorescence and photostability. However, other properties are also vital for creating an effective photoswitchable biosensor. A photoswitch for use in optical sensor devices requires the following key properties: a significant difference in the structures of the two switched states leading to a change in analyte binding affinity; an ability to photoswitch under exposure to light that is compatible with both biology and the optical device; high yields of photoswitching, to allow rapid cycling and reusability; two well-defined photostationary states with high yields of photoswitching in each direction, such that the system can be completely switched to an 'off' state; high switching fatigue resistance; a chemically simple and cost-effective synthesis, with the ability to customise to a specific purpose; and a high photostability for light intense environments. The following section provides a short review of these properties for the four classes of photoswitches investigated in PAPER 1 (azobenzenes, spiropyrans, diarylalkenes and fulgides) for the determination of the optimal class of photoswitchable ionophore to target for a photoswitchable MOF biosensor.

2.3.1 STRUCTURAL PROPERTIES OF THE PHOTOSWITCHES: USEABLE CHANGES UPON PHOTOSWITCHING

The structures of five of the most common photoswitches and the changes induced by photoswitching are shown in Figure 2-12, Figure 2-14 and Figure 2-15. For a photoswitch to function as a reversible sensor there needs to be a change in ion affinity between the two photoswitch isomers. This change in affinity is produced by a change in either the structure of, or electronic properties of an ion binding site.

Stilbenes,[10, 11] diarylalkenes,[33] and azobenzenes all give rise to a large change in conformation (between an elongated planar state to a bent shape) on switching, which allows for the binding of a metal ion via a tweezer-like mechanism[54, 55] (Figure 2-13). For stilbenes and azobenzenes, this change arises from a *trans* to *cis* isomerisation of a central alkene or azo group, respectively. Diarylalkenes, which were designed based on the stilbene degradation pathway,[33] undergo a UV induced 4

+ 2π cycloaddition, which rigidifies the molecule to form an elongated structure with an extended π orbital system.

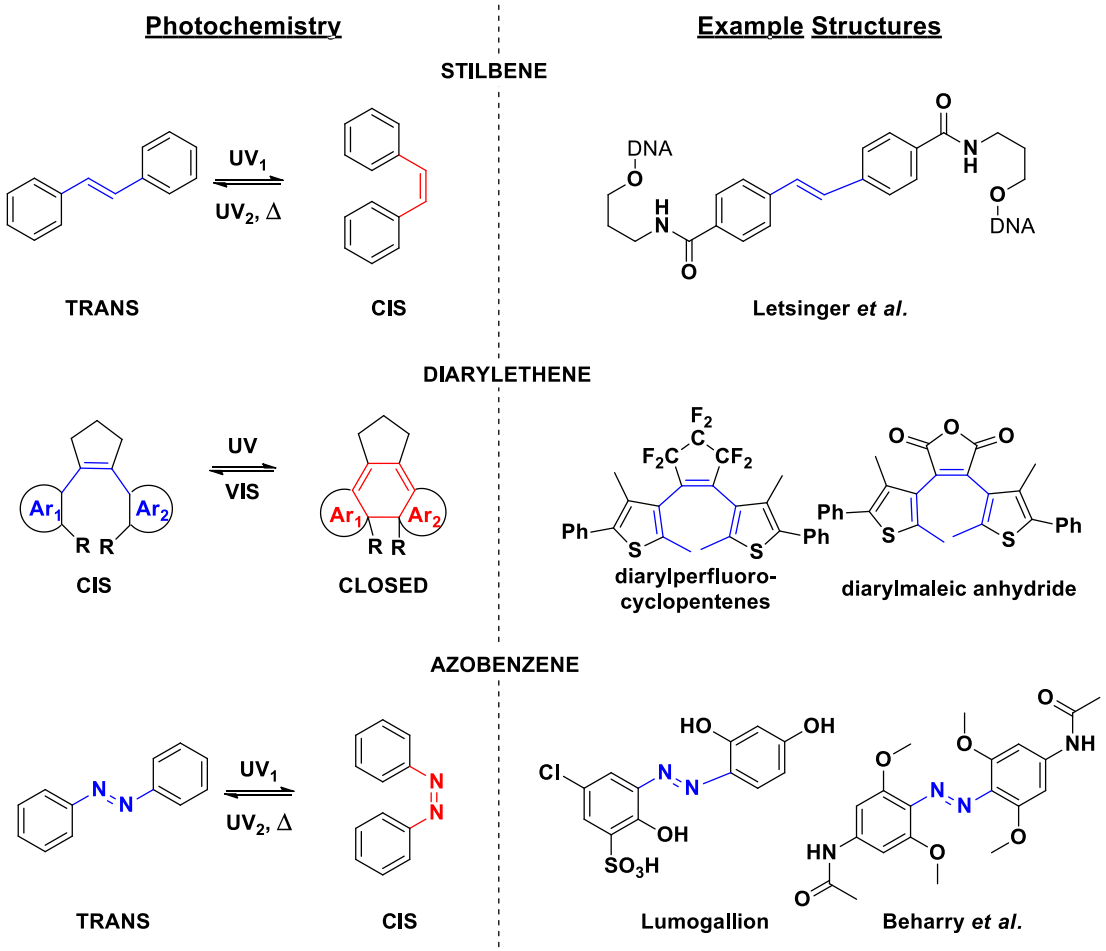

FIGURE 2-12: Photoswitching reactions of stilbenes, diarylethenes, and azobenzenes, with examples of structures demonstrating the structural diversity.[33, 56, 57]

There are many examples in recent literature of these photochromic molecules that have incorporated a metal ion binding domain (such as a crown ether). [54, 55, 58-61] In theory it is quite simple to modify photoswitches with an ion binding domain; however, being able to utilise the photochromism to modulate the ion binding while also providing a fluorescence change is not always a trivial task. The most common photoswitches that have been used to moderate ion binding are stilbenes, azobenzene, diarylalkenes and spiropyrans; examples of structures that exhibit

photocontrolable ion binding are shown in Figure 2-13.[62, 63] In most cases, photo-control of ion binding has simply been used for ion extraction and transportation, with detection of the ion binding arising from changes in the absorbance spectra, and are not used for ion sensing, or more specifically, fluorescence based sensing. This may be because these photochromic systems have very low, or have no intrinsic fluorescence. Therefore, to create a fluorescent metal ion sensor from these photoswitches may require extra complexity in which the photochromic ion binding is separated from the fluorophore (*i.e.* in a FRET sensor).[52] To the best of our knowledge such a system has not been reported, and is of current interest within our research group. With azobenzenes, it is possible to utilise the central azo bond as a metal chelator, which induces a switchable binding signal, such as with lumogallion.[1, 20, 28, 64-66]

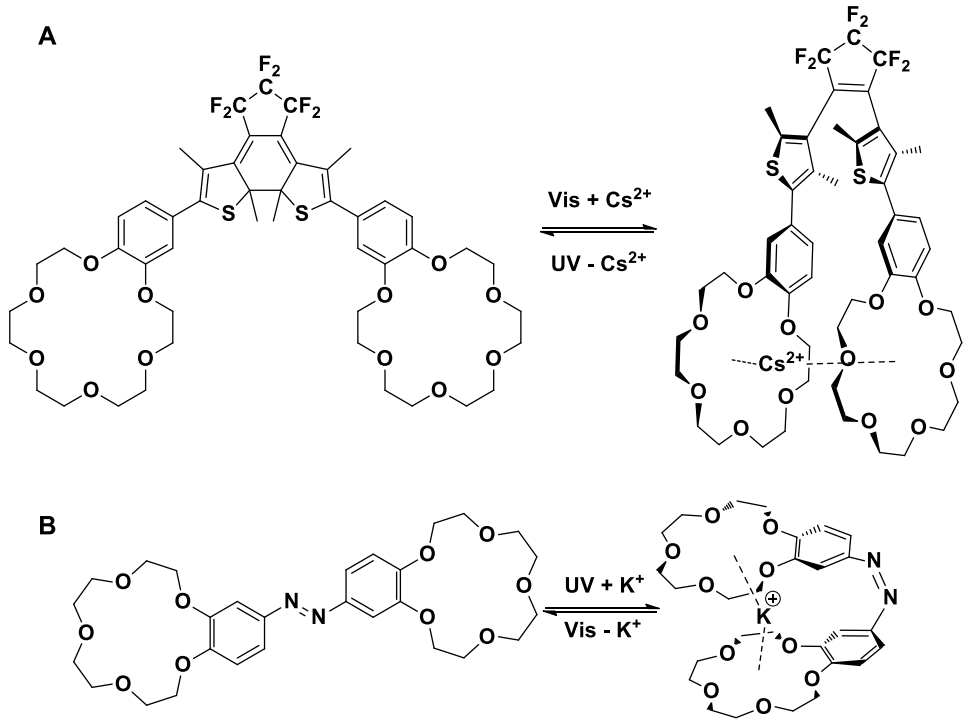

FIGURE 2-13: Two examples of photoswitchable metal ion chelators. A) Cs^{2+} diarylalkene tweezers by Takeshita *et al.*[67] and B) azobenzene ion transporter by Shinkai *et al.*[68]

The difficulty in utilising a photo-induced structural change towards a measurable ion binding response is more evident for fulgides as sensors. Fulgides are di-diisopropylidene succinic acid anhydride derivatives containing at least one aromatic

group connected by a double bond to the succinic anhydride (Figure 2-14).[41] Fulgides undergo two competing photoswitching processes, a *trans* to *cis* isomerisation, and a 6π-electrocyclization reaction; the latter providing the greatest and most controllable photochromic change. Although, in fulgides there is a distinct electronic and structural change upon photoswitching, the structural region around the photoswitching site is difficult to synthetically modify to contain an ionophore. The easiest locations for modification of fulgides are at the distal ends (the anhydride or aromatic regions), and therefore are not sterically influenced by the photoswitching. It may be possible to modulate ion binding by the electronic changes in the anhydride region, for example utilising fulgenates[69-71] or fulgimides[72, 73], however more investigation of this is needed.

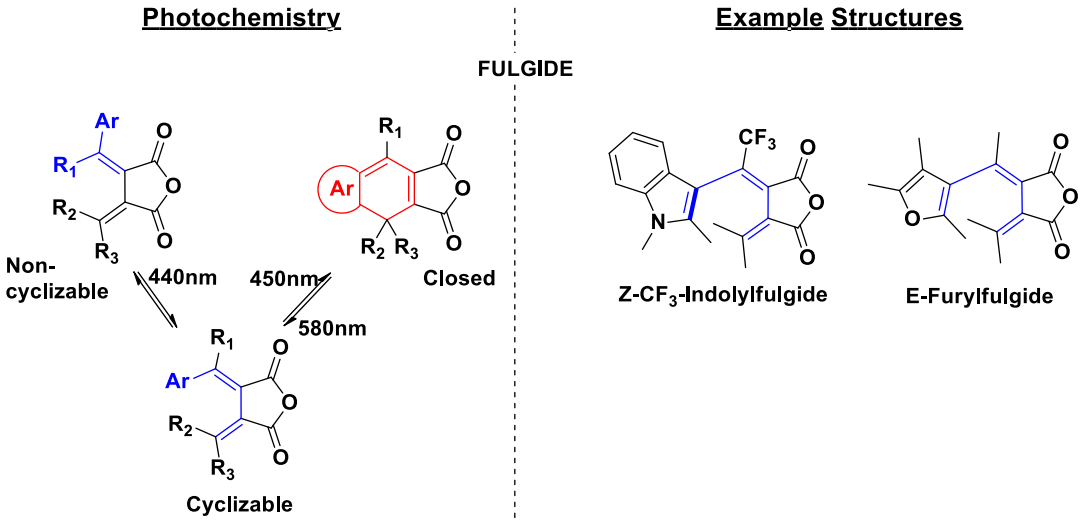

FIGURE 2-14: Photoswitching reactions of fulgides, with examples of structures demonstrating the structural diversity.

The combination of photo-controllable metal ion binding and dose responsive fluorescence can be achieved with spiropyran type photo-ionophores. The structure of spiropyran consists of a central spiro carbon bridging an indole and a pyran with an extended aromatic region (Figure 2-15). Upon photoswitching with near-UV light to its coloured form the central spiro C-O bond of the pyran breaks producing a zwitterionic merocyanine molecule. This greatly changes the shape of the molecule from a compact three-dimensional structure to an open, planar structure (as illustrated in the *in silico* models in Appendix C). This charged delocalised

merocyanine state is advantageous in metal ion sensing, as the negatively charged phenolate oxygen is able to strongly coordinate a cation; and, as it is electronically connected to the fluorescent cyanine like structure, the fluorescence is modulated by ion interactions.[74-76] Examples of this being used in ion binding has been investigated by Chibisov and others.[77] Further selectivity for ion sensing can be obtained by designing-in specific ion chelators adjacent (-ortho) to the phenolate, which can capture specific metal ions and take advantage of the phenolate as a lariat chelator, or just provide bulk to hinder the binding of certain metals. This technique has been used in the sensing of Li^{+},[29, 78] Zn^{2+},[2, 79, 80] Ca^{2+},[81] Cu^{2+},[82] and others[63, 83-87]. Photoswitching also induces two other major changes: firstly, the conductance across the molecule changes, allowing it to be an electrical switch;[74] and secondly, the polarity changes from non-polar to polar, affecting its solubility, affinity to organic systems, and its fluorescence.[7, 18, 74, 88]

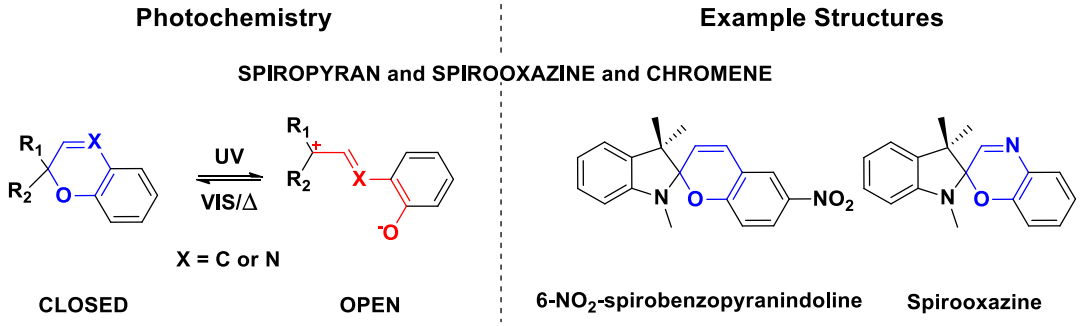

FIGURE 2-15: Photoswitching reactions of spiropyrans, spirooxazines and chromenes, with examples of structures demonstrating the structural diversity.

Therefore, spiropyran photoswitches provide the best properties regarding the ability to controllably bind and detect metal ions. However, due to the occurrence of a large structural change, azobenzenes and diarylalkenes are possibly also useful switches for sensing applications.

2.3.2 WAVELENGTHS OF PHOTOSWITCHING

The energy/wavelength of light required to cause photoswitching of a photoswitch can substantially limit its applications. The material in which the photoswitching is required may only have a 'window' of optical transparency, therefore limiting access

of the light to the photoswitch. For example in glass waveguides, the optical transparency, and therefore the ability to guide light, is dependent on the wavelength of light; with the higher energy UV light unable to be guided.[89] Ultraviolet light is also an issue in biological samples as it is readily absorbed by many organic materials and can lead to damaging excited states. The optical window of living tissue is approximately 600 nm to 1000 nm,[90-92] any light outside this window will have poor penetration into tissue; therefore, ideally any biological photoswitch or sensing fluorophore will have switching wavelengths within this region.

Azobenzenes generally have switching wavelengths between 320 nm and 440 nm (from an n → π* transition).[4, 54] This is bathochromically shifted compared to the UV wavelength required for the closely related stilbenes, making use of these photoswitches more appealing in biological environments compared to stilbenes.[93] However, by modifying the substituents on the two aromatic rings, azobenzene systems have been designed in which switching can be performed at wavelengths up to 550 nm.[12a, 27] Spiropyrans generally have switching wavelengths in the near UV (330-380 nm)[94] for the ring opening reaction, and in the visible region (around 550 nm) for ring closing. Diarylalkenes require UV light for the 4 + 2π photocyclisation reaction (<350 nm[95, 96]), although depending on the structure (the choice of aromatic substituents, and substitution) photoswitching can be achieved at longer wavelengths.[97] In the cyclised form, due to the larger area of electron π delocalisation there is a large bathochromic shift in the absorption spectra; as such, reverse switching wavelengths are generally in the visible range, from around 500 nm to 800 nm.[33] Finally, fulgides also require near-UV light (300-400 nm) for the photocyclisation reaction and visible (500-650 nm) for the ring opening process.[40, 52, 69]

None of the photoswitches undergo initial photoswitching within the biological window; however, the reverse photoswitching wavelengths, especially in fulgide and diarylalkene systems, do overlap in this region, thereby providing the ability to photoswitch in tissue. For use with waveguides, *i.e.* MOFs, azobenzenes and fulgides, which switch with lower energy visible light, may be the most viable photoswitches.

2.3.3 YIELDS OF PHOTOSWITCHING

The ability to completely turn 'off' (or 'on') a photoswitchable sensor is necessary to fully regenerate the sensing system and avoid signal contamination and background. This ability to completely turn "off" the sensor requires the photoswitch to be able to exist in a photo-stationary state (PSS) which is composed of only a single isomeric state. This is generally achieved in systems that have a large separation in photoswitching wavelengths; in which, there is no competing reverse photoswitching, creating an equilibrium of photochemical processes. Of the four photoswitches being discussed the spiropyran, diarylalkene and fulgide all have this large separation with a UV or UV-vis absorbance of the 'off' state compared to the visible absorbance of the 'on' state. This therefore enables the complete reversal of photoswitching with visible light; however, due to an overlap in the UV absorption region full conversion to the 'on' state is generally not possible. Azobenzene (and stilbenes) have, in most incidents,[98, 99] poor separation between switching wavelengths and generally exists in mixed PSS's; this is due to its similar *cis*- and *trans*- isomers. However, thermoswitching from the *cis*- form to the more energetically stable *trans*- form can provide complete 'off' switching; the thermal lifetimes of *cis*-azobenzenes are highly dependent on aromatic substitutions, and can range from milliseconds to days.[100, 101]

2.3.4 HIGH SWITCHING FATIGUE RESISTANCE

The ability to reuse a photoswitch and repetitively cycle between 'on' and 'off' states is a property routinely investigated in photoswitches, this is known as fatigue resistance and is generally defined as "number of photochromic cycles at which the absorbance of the coloured isomers decrease to 80 % of the first cycle".[33] The fatigue resistance is similar to the photostability investigated in PAPER 1, however, the photostability was determined based on continuous high intensity exposure, whereas, fatigue is from minimal alternating light exposure. Both processes restrict the lifetime of any device utilising photoswitchable molecules, as such, molecules with the greatest fatigue resistance is preferred such that the desired purpose can be fulfilled without a detrimental decrease in signal and photocontrol. Like all photochemical processes the amount of fatigue depends greatly on the conditions used (e.g., temperature, solvent, solvent purity, light intensity/irradiation time),

which makes it difficult to give an accurate comparison between literature reported samples. Azobenzenes have excellent fatigue resistance, and are probably the best performing photoswitch in this regard, with most reports claiming no apparent fatigue.[98, 99, 102-104] The merocyanine form of spiropyran is known to give photodegradation due to reactions with singlet and triplet oxygen.[105, 106] Radu *et* al.[105] found that in solution their spiropyran degraded to 43 % in a solution after only 12 cycles, however incorporation into a PMMA matrix, which reduces exposure to oxygen, was able to decrease this effect. Diarylalkenes can be very resistant to photochemical fatigue, with 100s-1000s of switching cycles possible in hexane and toluene solvents with little loss in signal.[33] However, this is greatly reduced in non-deaerated solvents due to oxidative degradation.[34] Some fulgides are also known to show very good fatigue resistance,[107] in particular the furylfulgides and the indolylfulgides.[41, 108, 109] For example, **CF_3-fulgide** has been shown to undergo over 1000 cycles without any change.[32]

2.3.5 EASE OF SYNTHESIS AND VERSATILITY IN STRUCTURE DIVERSIFICATION

An important consideration in choosing an appropriate photoswitch is ease of synthesis and ability to generate a range of related structures. These two factors influence the cost, and therefore commercialisation, of the sensor, as well as the ability to easily tailor the photoswitch to match any desired application.

There are a number of methods for the synthesis of azobenzenes and these have been thoroughly reviewed by Merino.[110] The two most common methods are the azo coupling reaction[110] and the Mills reaction, which involves a condensation between a nitrosobenzene and an aniline[111-113]. Therefore, wide varieties of different structures are available.

Spiropyrans are prepared by condensation reaction between an o-hydroxy-aromatic aldehyde and a methylene base (as performed in Chapter 3 and 4) or activated heteroaromatic methylene salt and proceeds in good yields (generally > 50 %).[60, 114, 115] This combination of two different halves of the switch allows for the incorporation of a large range of structural variation early in the synthesis.

Methods for the preparation of diarylalkenes have been reviewed elesewhere.[3, 116-119] In general, synthesis of the diarylalkene photochromic unit is short (1-2 steps from a halogenated heterocycle); however, it is achieved in moderate to low yields. In addition, the availability and synthesis of the staring materials, and in particular octafluorocyclopentene and each aryl group, respectively, has a major impact on structural variation, yields and costs.[3, 116-119]

Fulgides, such as the indolylfulgide **CF_3-fulgide**, are synthesised by a Stobbe condensation reaction between an acylindolyl and an isopropyl succinate,[41, 120] which is low yielding (usually between 5 % and 30 %).[51] A detailed experimental for the synthesis of **CF_3-fulgide** used in Paper 1 is presented in Appendix A.

2.4 CONCLUSIONS TO CHAPTER 2

This chapter introduces and compares four types of photoswitches, azobenzenes, spiropyrans, diarylalkenes and fulgides. Firstly, an investigation into the fluorescence and photobleaching resistance of four photoswitches using microstructured optical fibre in acetonitrile and DMSO solutions as well as deposited onto the fibre core revealed that azobenzenes and spiropyrans showed the most promising fluorescence and photostability for MOF based applications. Then secondly, a literature review into the other key properties of a photoswitchable sensor was performed; a summary of this discussion is illustrated in Table 2-1. From this detailed analysis it was determined that, of the photoswitches investigated, azobenzene and spiropyran were the most suited to further study towards a MOF photoswitchable ion sensor.

TABLE 2-1: Summary on the discussion on the properties of the families of photoswitches azobenzene, spiropyran, diarylalkene, and fulgide. Green, favourable; yellow, moderately favourable; orange, moderately unfavourable; red, unfavourable.

	Absorbance (switching) Wavelengths	Fluorescence	Yields of photo-switching	Conformational change or usable structural difference	Switching fatigue	Ease of synthesis /versatility in structure diversification	Photo-bleaching in fibre
Azobenzene	440 and 480	Weak	Moderate to high T-type	cis to trans	High	Short reaction pathway Wide structure diversification	Good
Spiropyran	UV and vis 330-400 and >530	Strong in switched state	Moderate to High T-type	Change in polarity	Moderate-high	Simple conditions Moderate yields	Good
Diarylalkene	UV and vis 250-400 and 500-800	Only in limited structures	High P-type	Flexible to elongated linear	High (environ-ment dependent)	Costly materials Moderate yields	Poor
Fulgide	Visible 440 and 580	Not for 3' indolylfulgides	Moderate to High P-type	Uncyclised to cyclised	High	Difficult synthesis Low yielding	Poor

2.5 REFERENCES CHAPTER 2

1. Warren-Smith, S. C.; Heng, S.; Ebendorff-Heidepriem, H.; Abell, A. D.; Monro, T. M. Fluorescence-based aluminum ion sensing using a surface-functionalized microstructured optical fiber. *Langmuir* 2011, *27* (9), 5680-5.
2. Heng, S.; McDevitt, C. A.; Stubing, D. B.; Whittall, J. J.; Thompson, J. G.; Engler, T. K.; Abell, A. D.; Monro, T. M. Microstructured optical fibers and live cells: a water-soluble, photochromic zinc sensor. *Biomacromolecules* 2013, *14* (10), 3376-9.
3. Stubing, D. B.; Heng, S.; Monro, T. M.; Abell, A. D. A comparative study of the fluorescence and photostability of common photoswitches in microstructured optical fibre. *Sensors and Actuators B: Chemical* 2017, *239*, 474-480.
4. Klajn, R. Immobilized azobenzenes for the construction of photoresponsive materials. *Pure and Applied Chemistry* 2010, *82* (12), 2247.
5. Bianco, A.; Perissinotto, S.; Garbugli, M.; Lanzani, G.; Bertarelli, C. Control of optical properties through photochromism: a promising approach to photonics. *Laser & Photonics Reviews* 2011, *5* (6), 711-736.
6. Bossi, M. L.; Aramendía, P. F. Photomodulation of macroscopic properties. *Journal of Photochemistry and Photobiology C: Photochemistry Reviews* 2011, *12* (3), 154-166.
7. Florea, L.; Diamond, D.; Benito-Lopez, F. Photo-Responsive Polymeric Structures Based on Spiropyran. *Macromolecular Materials and Engineering* 2012, *297* (12), 1148-1159.
8. Sun, X.; Park, S.; Shin, D. S.; Dong, W.; Zhao, B.; Jang, K. Multi-level recording of photochromic indolylfulgide. *Optical Materials* 2007, *30* (4), 652-656.
9. Guo, X.; Zhang, D.; Yu, G.; Wan, M.; Li, J.; Liu, Y.; Zhu, D. Reversible Photoregulation of the Electrical Conductivity of Spiropyran-Doped Polyaniline for Information Recording and Nondestructive Processing. *Advanced Materials* 2004, *16* (7), 636-640.
10. Sysoiev, D.; Fedoseev, A.; Kim, Y.; Exner, T. E.; Boneberg, J.; Huhn, T.; Leiderer, P.; Scheer, E.; Groth, U.; Steiner, U. E. Synthesis and Photoswitching Studies of Difurylperfluorocyclopentenes with Extended π-Systems. *Chemistry – A European Journal* 2011, *17* (24), 6663-6672.
11. Luo, Q.; Cheng, H.; Tian, H. Recent progress on photochromic diarylethene polymers. *Polymer Chemistry* 2011, *2* (11), 2435-2443.
12. Nishi, H.; Namari, T.; Kobatake, S. Photochromic polymers bearing various diarylethene chromophores as the pendant: synthesis, optical properties, and multicolor photochromism. *Journal of Materials Chemistry* 2011, *21* (43), 17249-17258.
13. Balzani, V.; Bergamini, G.; Ceroni, P. Light-powered Molecular Devices and Machines. In *Nanoparticles and Nanodevices in Biological Applications - the Infn Lectures - Vol I*, Bellucci, S., Ed. Springer-Verlag Berlin: Berlin, 2009; Vol. 4, 131-158.
14. Vives, G.; Tour, J. M. Synthesis of Single-Molecule Nanocars. *Accounts of Chemical Research* 2009, *42* (3), 473-487.
15. Lyndon, R.; Konstas, K.; Ladewig, B. P.; Southon, P. D.; Kepert, P. C.; Hill, M. R. Dynamic photo-switching in metal-organic frameworks as a route to

low-energy carbon dioxide capture and release. *Angewandte Chemie* 2013, *52* (13), 3695-8.
16. Tochitsky, I.; Polosukhina, A.; Degtyar, V. E.; Gallerani, N.; Smith, C. M.; Friedman, A.; Van Gelder, R. N.; Trauner, D.; Kaufer, D.; Kramer, R. H. Restoring visual function to blind mice with a photoswitch that exploits electrophysiological remodeling of retinal ganglion cells. *Neuron* 2014, *81* (4), 800-13.
17. Willner, I.; Rubin, S. Control of the Structure and Functions of Biomaterials by Light. *Angewandte Chemie International Edition in English* 1996, *35* (4), 367-385.
18. Florea, L.; Hennart, A.; Diamond, D.; Benito-Lopez, F. Synthesis and characterisation of spiropyran-polymer brushes in micro-capillaries: Towards an integrated optical sensor for continuous flow analysis. *Sensors and Actuators B: Chemical* 2012, *175* (0), 92-99.
19. Zou, Q.; Jin, J.; Xu, B.; Ding, L.; Tian, H. New photochromic chemosensors for Hg2+ and F−. *Tetrahedron* 2011, *67* (5), 915-921.
20. Wang, J.; Ha, C.-S. A colorimetric and fluorescent turn-on chemosensor for Zn2+ based on an azobenzene-containing compound. *Tetrahedron* 2009, *65* (34), 6959-6964.
21. Cubillas, A. M.; Unterkofler, S.; Euser, T. G.; Etzold, B. J.; Jones, A. C.; Sadler, P. J.; Wasserscheid, P.; Russell, P. S. Photonic crystal fibres for chemical sensing and photochemistry. *Chemical Society Review* 2013, *42* (22), 8629-48.
22. Afshar V, S.; Ruan, Y.; Warren-Smith, S. C.; Monro, T. M. Enhanced fluorescence sensing using microstructured optical fibers: a comparison of forward and backward collection modes. *Optics Letters.* 2008, *33* (13), 1473-1475.
23. Monro, T. M.; Warren-Smith, S.; Schartner, E. P.; Francois, A.; Heng, S.; Ebendorff-Heidepriem, H.; Afshar, S. Sensing with suspended-core optical fibers. *Optical Fiber Technology* 2010, *16* (6), 343-356.
24. Schartner, E. P.; Ebendorff-Heidepriem, H.; Warren-Smith, S. C.; White, R. T.; Monro, T. M. Driving down the Detection Limit in Microstructured Fiber-Based Chemical Dip Sensors. *Sensors* 2011, *11* (3), 2961-2971.
25. Heng, S.; Mak, A. M.; Stubing, D. B.; Monro, T. M.; Abell, A. D. Dual Sensor for Cd(II) and Ca(II): Selective Nanoliter-Scale Sensing of Metal Ions. *Analytical Chemistry* 2014, *86* (7), 3268-3272.
26. Afshar V, S.; Warren-Smith, S. C.; Monro, T. M. Enhancement of fluorescence-based sensing using microstructured optical fibres. *Optics Express* 2007, *15* (26), 17891-17901.
27. Valeur, B.; Leray, I. Design principles of fluorescent molecular sensors for cation recognition. *Coordination Chemistry Reviews* 2000, *205* (1), 3-40.
28. Wagner-Wysiecka, E.; Rzymowski, T.; Szarmach, M.; Fonari, M. S.; Luboch, E. Functionalized azobenzocrown ethers as sensor materials—The synthesis and ion binding properties. *Sensors and Actuators B: Chemical* 2013, *177* (0), 913-923.
29. Heng, S.; Nguyen, M.-C.; Kostecki, R.; Monro, T. M.; Abell, A. D. Nanoliter-scale, regenerable ion sensor: sensing with a surface functionalized microstructured optical fibre. *RSC Advances* 2013, *3* (22), 8308-8317.

30. Williams, G. O.; Chen, J. S.; Euser, T. G.; Russell, P. S.; Jones, A. C. Photonic crystal fibre as an optofluidic reactor for the measurement of photochemical kinetics with sub-picomole sensitivity. *Lab Chip* 2012, *12* (18), 3356-61.
31. Zhang, X.; Heng, S.; Abell, A. D. Photoregulation of alpha-Chymotrypsin Activity by Spiropyran-Based Inhibitors in Solution and Attached to an Optical Fiber. *Chemistry* 2015, *21* (30), 10703-13.
32. Yokoyama, Y.; Takahashi, K. Trifluoromethyl-substituted photochromic indolylfulgide. A remarkably durable fulgide towards photochemical and thermal treatments. *Chemistry Letters* 1996, (12), 1037-1038.
33. Irie, M. Diarylethenes for Memories and Switches. *Chemical Reviews* 2000, *100* (5), 1685-1716.
34. Irie, M.; Lifka, T.; Uchida, K.; Kobatake, S.; Shindo, Y. Fatigue resistant properties of photochromic dithienylethenes: by-product formation. *Chemical Communications* 1999, *0* (8), 747-750.
35. Wiedemann, U.; Alt, W.; Meschede, D. Switching photochromic molecules adsorbed on optical microfibres. *Optics Express* 2012, *20* (12), 12710-20.
36. Brzozowski, L.; Sargent, E. H. Azobenzenes for photonic network applications: Third-order nonlinear optical properties. *Journal of Materials Science: Materials in Electronics* 2001, *12* (9), 483-489.
37. Stubing, D. B.; Heng, S.; Abell, A. D. Crowned spiropyran fluoroionophores with a carboxyl moiety for the selective detection of lithium ions. *Organic & Biomolecular Chemistry* 2016, 14 (15), 3752-7.
38. Warken, F.; Vetsch, E.; Meschede, D.; Sokolowski, M.; Rauschenbeutel, A. Ultra-sensitive surface absorption spectroscopy using sub-wavelength diameter optical fibers. *Optics Express* 2007, *15* (19), 11952-11958.
39. Wolak, M. A.; Gillespie, N. B.; Thomas, C. J.; Birge, R. R.; Lees, W. J. Optical properties of photochromic fluorinated indolylfulgides. *Journal of Photochemistry and Photobiology A: Chemistry* 2001, *144* (2-3), 83-91.
40. Wolak, M. A.; Thomas, C. J.; Gillespie, N. B.; Birge, R. R.; Lees, W. J. Tuning the Optical Properties of Fluorinated Indolylfulgimides. *The Journal of Organic Chemistry* 2002, *68* (2), 319-326.
41. Yokoyama, Y. Fulgides for Memories and Switches. *Chemical Reviews* 2000, *100* (5), 1717-1740.
42. Liang, Y. C.; Dvornikov, A. S.; Rentzepis, P. M. Fluorescent photochromic fulgides. *Research on Chemical Intermediates* 1998, *24* (9), 905-914.
43. Irie, M.; Sakemura, K.; Okinaka, M.; Uchida, K. Photochromism of Dithienylethenes with Electron-Donating Substituents. *The Journal of Organic Chemistry* 1995, *60* (25), 8305-8309.
44. Garcia-Amoros, J.; Sanchez-Ferrer, A.; Massad, W. A.; Nonell, S.; Velasco, D. Kinetic study of the fast thermal cis-to-trans isomerisation of para-, ortho- and polyhydroxyazobenzenes. *Phys Chem Chem Phys* 2010, *12* (40), 13238-42.
45. Tsai, B.-K.; Chen, C.-H.; Hung, C.-H.; Hsiao, V. K. S.; Chu, C.-C. Photoswitchable fluorescence on/off behavior between cis- and trans-rich azobenzenes. *Journal of Materials Chemistry* 2012, *22* (39), 20874-20877.
46. Seefeldt, B.; Kasper, R.; Beining, M.; Mattay, J.; Arden-Jacob, J.; Kemnitzer, N.; Drexhage, K. H.; Heilemann, M.; Sauer, M. Spiropyrans as

molecular optical switches. *Photochemical & Photobiological Sciences* 2010, *9* (2), 213-220.
47. Matsuda, K.; Irie, M. Diarylethene as a photoswitching unit. *Journal of Photochemistry and Photobiology C: Photochemistry Reviews* 2004, *5* (2), 169-182.
48. Taniguchi, H.; Shinpo, A.; Okazaki, T.; Matsui, F.; Irie, M. Photodegradation Mechanism of Photochromic Diarylethene Derivatives. *Nippon Kagaku Kaishi* 1992, *1992* (10), 1138-1140.
49. Bonacchi, S.; El Garah, M.; Ciesielski, A.; Herder, M.; Conti, S.; Cecchini, M.; Hecht, S.; Samori, P. Surface-induced selection during in situ photoswitching at the solid/liquid interface. *Angewandte Chemie* 2015, *54* (16), 4865-9.
50. Garcia-Fernandez, R.; Alt, W.; Bruse, F.; Dan, C.; Karapetyan, K.; Rehband, O.; Stiebeiner, A.; Wiedemann, U.; Meschede, D.; Rauschenbeutel, A. Optical nanofibers and spectroscopy. *Applied Physics B* 2011, *105* (1), 3-15.
51. Thomas, C. J.; Wolak, M. A.; Birge, R. R.; Lees, W. J. Improved Synthesis of Indolyl Fulgides. *The Journal of Organic Chemistry* 2001, *66* (5), 1914-1918.
52. Strübe, F.; Rath, S.; Mattay, J. Functionalized Fulgides and Fluorophore-Photoswitch Conjugates. *European Journal of Organic Chemistry* 2011, *2011* (24), 4645-4653.
53. Webb, A. S.; Poletti, F.; Richardson, D. J.; Sahu, J. K. Suspended-core holey fiber for evanescent-field sensing. *Optical Engineering* 2007, *46* (1), 010503.
54. Takahashi, I.; Honda, Y.; Hirota, S. Regulating Copper-Binding Affinity with Photoisomerizable Azobenzene Ligand by Construction of a Self-Assembled Monolayer. *Angewandte Chemie International Edition* 2009, *48* (33), 6065-6068.
55. Shinkai, S. Switch-functionalized systems in biomimetic chemistry. *Pure and Applied Chemistry* 1987, *59* (3), 425-430.
56. Letsinger, R. L.; Wu, T. Use of a Stilbenedicarboxamide Bridge in Stabilizing, Monitoring, and Photochemically Altering Folded Conformations of Oligonucleotides. *Journal of the American Chemical Society* 1995, *117* (28), 7323-7328.
57. Beharry, A. A.; Sadovski, O.; Woolley, G. A. Azobenzene Photoswitching without Ultraviolet Light. *Journal of the American Chemical Society* 2011, *133* (49), 19684-19687.
58. Ducrot, A.; Verwilst, P.; Scarpantonio, L.; Goudet, S.; Kauffmann, B.; Denisov, S.; Jonusauskas, G.; McClenaghan, N. D. Photolariats: synthesis, metal ion complexation and photochromism. In *Supramolecular Chemistry*, Taylor & Francis Ltd.: 2012;
59. Blank, M.; Soo, L. M.; Wassermann, N. H.; Erlanger, B. F. Photoregulated Ion Binding. *Science* 1981, *214* (4516), 70-72.
60. Lukyanov, B. S.; Lukyanova, M. B. Spiropyrans: Synthesis, Properties, and Application. (Review). *Chemistry of Heterocyclic Compounds* 2005, *41* (3), 281-311.
61. Natali, M.; Giordani, S. Molecular switches as photocontrollable "smart" receptors. *Chemical Society Reviews* 2012, *41* (10), 4010-4029.

62. Shinkai, S.; Manabe, O. Photocontrol of ion extraction and ion transport by photofunctional crown ethers. In *Host Guest Complex Chemistry III*, Vögtle, F.; Weber, E., Eds. Springer Berlin / Heidelberg: 1984; Vol. 121, 67-104.
63. Bianchi, A.; Delgado-Pinar, E.; García-España, E.; Giorgi, C.; Pina, F. Highlights of metal ion-based photochemical switches. *Coordination Chemistry Reviews* 2014, *260* (0), 156-215.
64. Wang, Z.; Cook, M. J.; Nygård, A.-M.; Russell, D. A. Metal-Ion Chelation and Sensing Using a Self-Assembled Molecular Photoswitch. *Langmuir* 2003, *19* (9), 3779-3784.
65. Tria, J.; Butler, E. C. V.; Haddad, P. R.; Bowie, A. R. Determination of aluminium in natural water samples. *Analytica Chimica Acta* 2007, *588* (2), 153-165.
66. Luboch, E.; Wagner-Wysiecka, E.; Biernat, J. F. Chromogenic azocrown ethers with peripheral alkyl, alkoxy, hydroxy or dimethylamino group. *Journal of Supramolecular Chemistry* 2002, *2* (1–3), 279-291.
67. Takeshita, M.; Irie, M. Photoresponsive Tweezers for Alkali Metal Ions. Photochromic Diarylethenes Having Two Crown Ether Moieties. *The Journal of Organic Chemistry* 1998, *63* (19), 6643-6649.
68. Shinkai, S.; Honda, Y.; Ueda, K.; Manabe, O. Photorespnsive crown ethers 2. Azobenzene-pillared cylindrical macrocycle as a photoresponsive receptor. *Israel Journal of Chemistry* 1984, *24* (4), 302-306.
69. Yokoyama, Y.; Miyasaka, M.; Uchida, S. Cyclic fulgentes - enlargement of quantum yield of coloring reaction of photochromic fulgenates. *Chemistry Letters* 1995, (6), 479-480.
70. Yokoyama, Y.; Sugiyama, K.; Yamada, S.; Takimoto, H.; Kurita, Y. Fulgenates - A new class of fulgide-related thermally irreversible photochromic system. *Chemistry Letters* 1994, (4), 749-752.
71. Yokoyama, Y.; Ohmori, T.; Okuyama, T.; Yokoyama, Y.; Uchida, S. Photochromism of Fulgenates Possessing Crown-Ether Moiety. *Molecular Crystals and Liquid Crystals Science and Technology. Section A. Molecular Crystals and Liquid Crystals* 2000, *344*, 265 - 270.
72. Chen, X.; Islamova, N. I.; Garcia, S. P.; DiGirolamo, J. A.; Lees, W. J. Synthesis and Optical Properties of Aqueous Soluble Indolylfulgimides. *The Journal of Organic Chemistry* 2009, *74* (17), 6777-6783.
73. Karabaeva, L.; Platonova, I.; Zavarzin, I.; Luiksaar, S.; Yarovenko, V.; Nabatov, B.; Krayushkin, M.; Barachevski, V. Synthesis, photochromic and fluorescent properties of hybrid compounds of fulgimides and benzothiazolylthienothiophene. *Chemistry of Heterocyclic Compounds* 2011, *47* (2), 229-236.
74. Klajn, R. Spiropyran-based dynamic materials. *Chemical Society Reviews* 2014, *43* (1), 148-84.
75. Kubinyi, M.; Varga, O.; Baranyai, P.; Kállay, M.; Mizsei, R.; Tárkányi, G.; Vidóczy, T. Metal complexes of the merocyanine form of nitrobenzospyran: Structure, optical spectra, stability. *Journal of Molecular Structure* 2011, *1000* (1-3), 77-84.
76. Kimura, K.; Kaneshige, M.; Yamashita, T.; Yokoyama, M. Cation Complexation, Photochromism, and Reversible Ion-Conducting Control of Crowned Spironaphthoxazine. *The Journal of Organic Chemistry* 1994, *59* (6), 1251-1256.

77. Chibisov, A. K.; Görner, H. Complexes of spiropyran-derived merocyanines with metal ions: relaxation kinetics, photochemistry and solvent effects. *Chemical Physics* 1998, *237* (3), 425-442.
78. Sakamoto, H.; Yamamura, T.; Takumi, K.; Kimura, K. Absorption- and fluorescence-spectral sensing of alkali metal ions in anionic micelle solutions containing crowned spirobenzopyrans. *Journal of Physical Organic Chemistry* 2007, *20* (11), 900-907.
79. Natali, M.; Soldi, L.; Giordani, S. A photoswitchable Zn (II) selective spiropyran-based sensor. *Tetrahedron* 2010, *66* (38), 7612-7617.
80. Natali, M.; Aakeroy, C.; Desper, J.; Giordani, S. The role of metal ions and counterions in the switching behavior of a carboxylic acid functionalized spiropyran. *Dalton Transactions* 2010, *39* (35), 8269-8277.
81. Yagi, S.; Nakamura, S.; Watanabe, D.; Nakazumi, H. Colorimetric sensing of metal ions by bis(spiropyran) podands: Towards naked-eye detection of alkaline earth metal ions. *Dyes and Pigments* 2009, *80* (1), 98-105.
82. Shao, N.; Zhang, Y.; Cheung, S.; Yang, R.; Chan, W.; Mo, T.; Li, K.; Liu, F. Copper Ion-Selective Fluorescent Sensor Based on the Inner Filter Effect Using a Spiropyran Derivative. *Analytical Chemistry* 2005, *77* (22), 7294-7303.
83. Tsukanov, A.; Dubonosov, A.; Bren, V.; Minkin, V. Organic chemosensors with crown-ether groups (review). *Chemistry of Heterocyclic Compounds* 2008, *44* (8), 899-923.
84. Chernyshev, A. V.; Metelitsa, A. V.; Gaeva, E. B.; Voloshin, N. A.; Borodkin, G. S.; Minkin, V. I. Photo- and thermochromic cation sensitive spiro indoline-pyridobenzopyrans. *Journal of Physical Organic Chemistry* 2007, *20* (11), 908-916.
85. Kimura, K.; Sakamoto, H.; Kado, S.; Arakawa, R.; Yokoyama, M. Studies on metal-ion complex formation of crown ether derivatives incorporating a photoionizable spirobenzopyran moiety by electrospray ionization mass spectrometry. *Analyst* 2000, *125* (6), 1091-1095.
86. Winkler, J. D.; Bowen, C. M.; Michelet, V. Photodynamic Fluorescent Metal Ion Sensors with Parts per Billion Sensitivity. *Journal of the American Chemical Society* 1998, *120* (13), 3237-3242.
87. Paramonov, S. V.; Lokshin, V.; Fedorova, O. A. Spiropyran, chromene or spirooxazine ligands: Insights into mutual relations between complexing and photochromic properties. *Journal of Photochemistry and Photobiology C: Photochemistry Reviews* 2011, *12* (3), 209-236.
88. Florea, L.; Benito-Lopez, F.; Hennart, A.; Diamond, D. Photo-Detection of Solvent Polarities using Non-Invasive Coatings in Capillaries. *Procedia Engineering* 2011, *25* (0), 1545-1548.
89. Kostecki, R.; Ebendorff-Heidepriem, H.; Davis, C.; McAdam, G.; Warren-Smith, S. C.; Monro, T. M. Silica exposed-core microstructured optical fibers. *Optical Materials Express* 2012, *2* (11), 1538-1547.
90. Que, E. L.; Domaille, D. W.; Chang, C. J. Metals in Neurobiology: Probing Their Chemistry and Biology with Molecular Imaging. *Chemical Reviews* 2008, *108* (5), 1517-1549.
91. Zaera, F. Probing Liquid/Solid Interfaces at the Molecular Level. *Chemical Reviews* 2012, *112* (5), 2920-2986.

92. Steven, L. J. Optical properties of biological tissues: a review. *Physics in Medicine and Biology* 2013, *58* (11), R37.
93. Rau, H. Chapter 4 - Azo Compounds. In *Photochromism*, Bouas-Laurent, H. D., Ed. Elsevier Science: Amsterdam, 2003; 165-192.
94. Kholmanskii, A. S.; Zubkov, A. V.; Kirill, M. D. The Nature of the Primary Photochemical Step in Spiropyrans. *Russian Chemical Reviews* 1981, *50* (4), 305.
95. Hamano, M.; Irie, M. Rewritable Near-Field Optical Recording on Photochromic Thin Films. *Japanese Journal of Applied Physics* 1996, *35* (3R), 1764.
96. Tsivgoulis, G. M.; Lehn, J.-M. Photonic Molecular Devices: Reversibly Photoswitchable Fluorophores for Nondestructive Readout for Optical Memory. *Angewandte Chemie International Edition in English* 1995, *34* (10), 1119-1122.
97. Yamaguchi, T.; Uchida, K.; Irie, M. Asymmetric Photocyclization of Diarylethene Derivatives. *Journal of the American Chemical Society* 1997, *119* (26), 6066-6071.
98. Bléger, D.; Schwarz, J.; Brouwer, A. M.; Hecht, S. o-Fluoroazobenzenes as Readily Synthesized Photoswitches Offering Nearly Quantitative Two-Way Isomerization with Visible Light. *Journal of the American Chemical Society* 2012, *134* (51), 20597-20600.
99. Siewertsen, R.; Neumann, H.; Buchheim-Stehn, B.; Herges, R.; Näther, C.; Renth, F.; Temps, F. Highly Efficient Reversible Z−E Photoisomerization of a Bridged Azobenzene with Visible Light through Resolved S1(nπ*) Absorption Bands. *Journal of the American Chemical Society* 2009, *131* (43), 15594-15595.
100. Weston, C. E.; Richardson, R. D.; Haycock, P. R.; White, A. J. P.; Fuchter, M. J. Arylazopyrazoles: Azoheteroarene Photoswitches Offering Quantitative Isomerization and Long Thermal Half-Lives. *Journal of the American Chemical Society* 2014, *136* (34), 11878-11881.
101. Samanta, S.; Babalhavaeji, A.; Dong, M. X.; Woolley, G. A. Photoswitching of ortho-substituted azonium ions by red light in whole blood. *Angewandte Chemie* 2013, *52* (52), 14127-30.
102. Gilat, S. L.; Kawai, S. H.; Lehn, J.-M. Light-Triggered Molecular Devices: Photochemical Switching Of optical and Electrochemical Properties in Molecular Wire Type Diarylethene Species. *Chemistry – A European Journal* 1995, *1* (5), 275-284.
103. Abellán, G.; García, H.; Gómez-García, C. J.; Ribera, A. Photochemical behavior in azobenzene having acidic groups. Preparation of magnetic photoresponsive gels. *Journal of Photochemistry and Photobiology A: Chemistry* 2011, *217* (1), 157-163.
104. Bandara, H. M. D.; Burdette, S. C. Photoisomerization in different classes of azobenzene. *Chemical Society Reviews* 2012, *41* (5), 1809-1825.
105. Radu, A.; Byrne, R.; Alhashimy, N.; Fusaro, M.; Scarmagnani, S.; Diamond, D. Spiropyran-based reversible, light-modulated sensing with reduced photofatigue. *Journal of Photochemistry and Photobiology A: Chemistry* 2009, *206* (2–3), 109-115.

106. Arai, K.; Shitara, Y.; Ohyama, T. Preparation of photochromic spiropyrans linked to methyl cellulose and photoregulation of their properties. *Journal of Materials Chemistry.* 1996, *6* (1), 11-14.
107. Matsushima, R.; Sakaguchi, H. Comparison of the photochromic properties of fulgides and fulgimides. *Journal of Photochemistry and Photobiology A: Chemistry* 1997, *108* (2-3), 239-245.
108. Whittal, J. Chapter 9 - 4n+2 Systems: Fulgides. In *Photochromism*, Bouas-Laurent, H. D., Ed. Elsevier Science: Amsterdam, 2003; pp 467-492.
109. Kaneko, A.; Tomoda, A.; Ishizuka, M.; Suzuki, H.; Matsushima, R. Photochemical fatigue resistance and thermal stabilities of heterocyclic fulgides in PMMA film. *Bulletin of the Chemical Society of Japan* 1988, *61* (10), 3569-3573.
110. Merino, E. Synthesis of azobenzenes: the coloured pieces of molecular materials. *Chemical Society Reviews* 2011, *40* (7), 3835-3853.
111. Davey, M. H.; Lee, V. Y.; Miller, R. D.; Marks, T. J. Synthesis of Aryl Nitroso Derivatives by tert-Butyl Hypochlorite Oxidation in Homogeneous Media. Intermediates for the Preparation of High-Hyperpolarizability Chromophore Skeletons. *The Journal of Organic Chemistry* 1999, *64* (13), 4976-4979.
112. *Nitro and Nitroso Groups*. Wiley: 1970; Vol. 2.
113. Hamon, F.; Djedaini-Pilard, F.; Barbot, F.; Len, C. Azobenzenes—synthesis and carbohydrate applications. *Tetrahedron* 2009, *65* (49), 10105-10123.
114. Bergmann, E. D.; Weizmann, A.; Fischer, E. Structure and Polarity of Some Polycyclic Spirans. *Journal of the American Chemical Society* 1950, *72* (11), 5009-5012.
115. Laptev, A. V.; Lukin, A. Y.; Belikov, N. E.; Zvezdin, K. V.; Demina, O. V.; Barachevsky, V. A.; Varfolomeev, S. D.; Khodonov, A. A.; Shvets, V. I. Synthesis and studies of photochromic properties of spirobenzopyran carboxy derivatives and their model compounds as potential markers. *Russian Chemical Bulletin* 2015, *63* (9), 2026-2035.
116. Polyakova, S. Fluorescent and photochromic fluorescent Compounds for Applications in Optical Nanoscopy. Georg-August-Universität zu Göttingen, 2009.
117. Hecht, S. Introduction Introduction to the Synthesis of Synthesis of Photochromes Photochromes: Spiropyrans Spiropyrans & Diarylethenes. http://www.physik.fu-berlin.de/einrichtungen/sfb/sfb658/tutorials/dokumente/Tutorial_Hecht_2011-06.pdf (accessed 22/02/2016).
118. Krayushkin, M. M.; Barachevsky, V. A.; Irie, M. Synthesis of thienyl-containing photochromes (dithienylethenes, fulgides, fulgimides, and spirocompounds). *Heteroatom Chemistry* 2007, *18* (5), 557-567.
119. Krayushkin, M. M. Synthesis of Photochromic Dihetarylethenes. (Review). *Chemistry of Heterocyclic Compounds* 2001, *37* (1), 15-36.
120. Stobbe, H. The colour of the 'fulgenic acid' and 'fulgide'. *Berichte Der Deutschen Chemischen Gesellschaft* 1905, *38*, 3673-3682.

CHAPTER 3

PHOTOSWITCHABLE SPIROPYRAN SENSORS FOR LITHIUM METAL IONS

3.1 OVERVIEW OF CHAPTER

This chapter presents a reformatted version of the published paper "Crowned spiropyran fluoroionophores with a carboxyl moiety for the selective detection of lithium ions" (PAPER 2). This publication presents the synthesis, as well as the absorbance and fluorescence of a series of spiropyran based photoswitchable ionophores in the presence of alkali metals Li^+, Na^+, K^+, and Cs^+ in 1:100 and 1:1 concentration ratios. This series of carboxylated spiropyrans (**SP-1**, **SP-2** and **SP-3**) contain aza-crown ether rings of increasing size (methyl-1-aza-12-crown-4, methyl-1-aza-15-crown-5, methyl-1-aza-18-crown-6, respectively), and the influence on the ring size on binding affinity and fluorescence spectra was compared. This was performed to determine which sensor exhibits the strongest and most selective response towards these metal ions, in order to achieve a selective photoreversible sensor for biological applications.

3.2 PAPER 2: CROWNED SPIROPYRAN FLUOROIONOPHORES WITH A CARBOXYL MOIETY FOR THE SELECTIVE DETECTION OF LITHIUM IONS[1]

Statement of Authorship

Title of Paper	Crowned spiropyran fluoroionophores with a carboxyl moiety for the selective detection of lithium ions
Publication Status	☑ Published ☐ Accepted for Publication ☐ Submitted for Publication ☐ Publication Style
Publication Details	Stubing, D. B.; Heng, S.; Abell, A. D., Crowned spiropyran fluoroionophores with a carboxyl moiety for the selective detection of lithium ions. *Organic Biomolecular Chemistry* 2016, 14 (15), 3752-7.

Principal Author

Name of Principal Author (Candidate)	Daniel B. Stubing		
Contribution to the Paper	Synthesis of spiropyrans **SP-1** and **SP-3**. All absorbance and fluorescence assays and data analysis. Writing of manuscript		
Overall percentage (%)	75		
Signature		Date	08/09/2016

Co-Author Contributions

By signing the Statement of Authorship, each author certifies that:

i. the candidate's stated contribution to the publication is accurate (as detailed above);
ii. permission is granted for the candidate in include the publication in the thesis;
iii. the sum of all co-author contributions is equal to 100 % less the candidate's stated contribution.

Name of Co-Author	Sabrina Heng		
Contribution to the Paper	Synthesis of **SP-2**. Project direction and significant editing of manuscript.		
Signature		Date	06. 10. 16

Name of Co-Author	Andrew D. Abell		
Contribution to the Paper	Project direction and significant editing of manuscript.		
Signature		Date	13/09/2016

CROWNED SPIROPYRAN FLUOROIONOPHORES WITH A CARBOXYL MOIETY FOR THE SELECTIVE DETECTION OF LITHIUM IONS.

D. B. Stubing,[a] S. Heng,[a] and A. D. Abell[a]

[a] ARC Centre of Excellence for Nanoscale BioPhotonics, Institute of Photonics and Advanced Sensing, Department of Chemistry, The University of Adelaide, South Australia, 5005

3.2.1 ABSTRACT

The absorbance and fluorescence spectra of carboxylated spiropyrans containing methyl-1-aza-12-crown-4, methyl-1-aza-15-crown-5, methyl-1-aza-18-crown-6 moieties are compared. Characteristic changes in spectra after addition of the alkali metal salts of Li^+, Na^+, K^+, and Cs^+ were observed. Chromism induced by the binding of the metal cations was observed as an increase in absorbance and fluorescence. Of these metal cations, the Li^+ ion produced the largest change in all three spiropyran systems. Reversible photoswitching of the spiropyran-metal complexes was observed on irradiation with alternating 352 nm UV and white light. This results in reversible fluorescence based sensing of lithium ions with potential for use in a biological sensor device.

3.2.2 INTRODUCTION

An ability to selectively detect metal ions in biological samples is an important area of current biosensor research.[2] This is especially true of lithium cation (Li^+), a trace metal of unknown biological function found in mammalian tissues at levels of 0.001-0.01 mM.[3-6] Li^+ is also of interest as a therapeutic to treat neurological diseases such as manic-depressive illness. However, dosage is critical, as Li^+ is only effective within a narrow therapeutic window (0.6-1.2 mM); too lower a dose has no effect while too higher a dose (>2 mM) is toxic and lethal.[2-4, 7]

Despite the importance of Li^+ in biology there are only a few reports of fluorescence-based sensors for its detection.[2, 7-12] Most of these are either non-functional at relevant biological concentrations, or they do not display sufficient selectivity over

other metal cations, in particular Na^+. New biologically compatible fluorescent sensors and sensing devices that are selective for Li^+ are needed to provide a greater understanding of the biological role of Li^+. Spiropyran-based photoswitchable sensors offer some potential in this area. These structures reversibly switch between a non-fluorescent spiropyran form (SP) and a charge delocalized fluorescent merocyanine isomer (MC) when exposed to a stimulus; such as UV light, change in local environment (polarity), or when interacting with a charged metal ion (Scheme 3-1). The charged MC state can be exploited to provide a strong ion interaction site.[13-15] For example, incorporating a cation binding domain at the 8 position of the spiropyran *ortho*- to the phenolate group (Scheme 3-1), is known to enhance ion affinity and selectivity of the ion binding domain.[16-18]

We have previously reported a methyl-1-aza-15-crown-5 modified spiropyran (Scheme 3-1, compound **2**) attached to a microstructured optical fibre surface via a 5'-carboxyl group for fluorescence based detection of Li^+.[12] Here we compare the influence on the fluorescence spectra produced by the photoswitching and binding of a range of biologically relevant alkali metal ions to spiropyrans containing differing sized aza-crown ether rings. This then provides a fluorescence based structure affinity profile with potential to develop a more selective regenerable sensor for Li^+ that will have applications as a dye in fluorescence microscopy, for example.[19] Three carboxylated spiropyrans, each with a different aza-crown at the 8-position were prepared; methyl-1-aza-12-crown-4 (**SP-1**), methyl-1-aza-15-crown-5 (**SP-2**) and methyl-1-aza-18-crown-6 (**SP-3**). The incorporation of a 5'-carboxyl group to the spiropyran sensor provides increased aqueous solubility for biological based studies as well as a site for potential functionalization.[20] Previous studies have modified this 5' site with electron withdrawing CF_3 or NO_2 groups to enhance the control of reverse photoswitching by stabilising the spiropyran isomer, the more weakly electron withdrawing CO_2H is expected to have a similar effect, whilst providing the added before mentioned benefits.[21, 22]

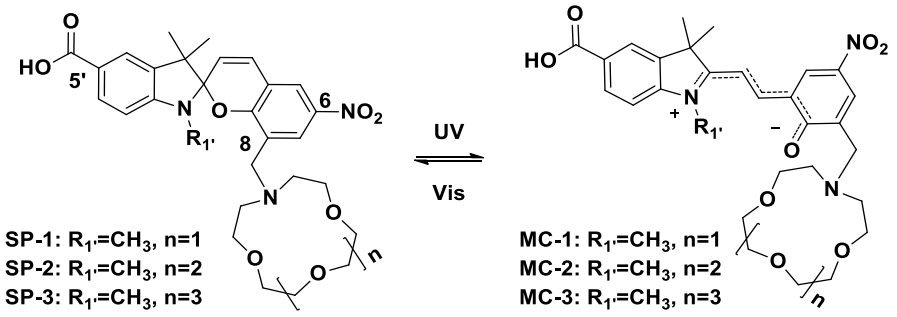

SCHEME 3-1: Structures of the crowned spiropyrans, **SP-1**, **-2**, and **-3** and the corresponding photoswitched merocyanine isomers, **MC-1**, **-2**, and **-3** respectively.

3.2.3 RESULTS AND DISCUSSION

Compounds **SP-1**, **SP-2**, and **SP-3** were prepared using methodology previously reported for **2**, see Scheme 3-2.[12] 4-Hydrazinobenzoic acid **4** was reacted with 2-methyl-2-butanone (Fischer indole reaction)[23, 24] to give indoline **5**, which was alkylated with iodomethane to give the methylindole **6**. The aza-1-crown ethers **7-9** were separately alkylated with the chloride **10** to give 3-methyl(aza-crown ether)-2-hydroxy-5-nitrobenzaldehydes **11-13**. A condensation reaction between these benzylaldehydes and the methylindole **6** in refluxing ethanol, followed by purification by reverse-phase liquid chromatography gave the desired spiropyrans **1-3**.

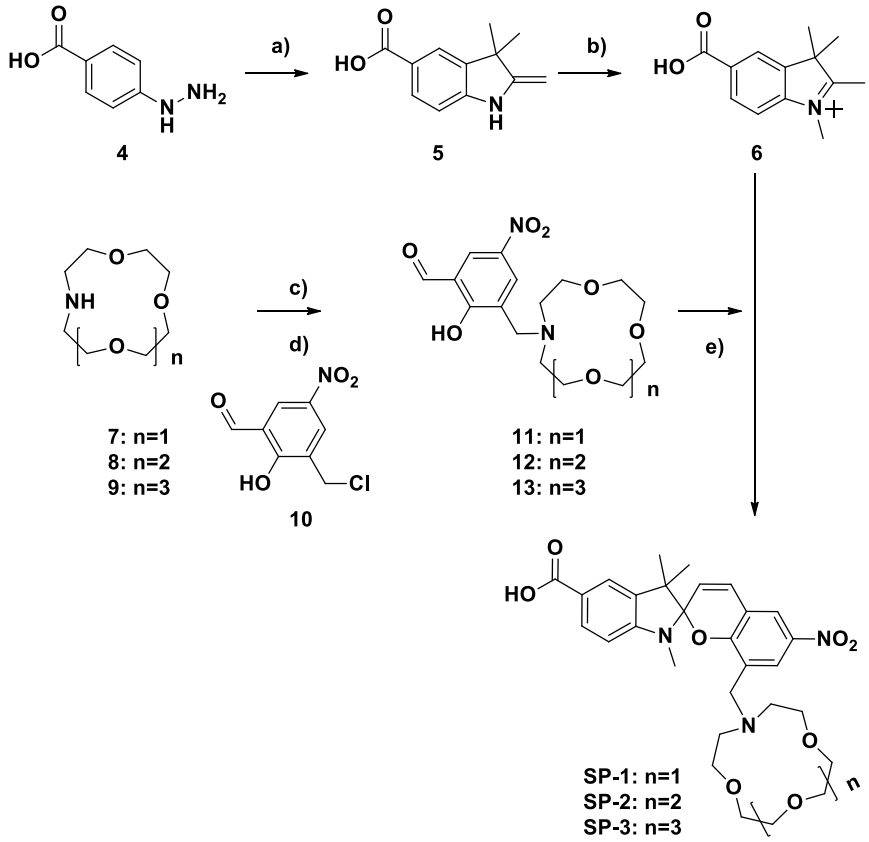

SCHEME 3-2: Synthesis of spiropyrans **SP-1**, **SP-2** and **SP-3**. a) 2-methyl-butanone, sulphuric acid, EtOH, 85 °C, 18 h, 73 %; b) iodomethane, 2:1 toluene:MeCN, 95 °C, 24 h, 72 %; c) triethyl amine, THF, 0 °C, 1h; d) THF, 75 °C, 17 h; e) EtOH, 85 °C, 3 h, 18-20 % (3 steps).

3.2.3.1 Influence of the Aza-1-crown ether Group On Absorbance and Fluorescence of the Spiropyran Base-unit.

The effect that the size of the aza-1-crown ether ring has on absorbance and fluorescence spectra of **SP-1**, **SP-2**, and **SP-3** and the corresponding UV photoswitched **MC** states was investigated. Specifically, **SP-1**, **SP-2**, and **SP-3** were separately dissolved in acetonitrile (50 μM) and the respective UV-vis absorbance and fluorescence (λ_{ex} = 532 nm) spectra were recorded using a Synergy H4 Hybrid Microplate Reader. Acetonitrile was used as solvent since it is known to give rise to slow thermal switching of a spiropyran providing a reduced background signal,[25] and we have shown that it gives comparable fluorescence in the presence of Li^+ in H_2O:acetonitrile solutions.[12] **SP-1**, **SP-2** and **SP-3** gave a common absorbance in the UV region at 360 nm, with **SP-1** and **SP-2** giving an additional peak at 400 nm. All

three solutions showed a weak absorbance peak at 545 nm (Figure 3-1, black) possibly due to the presence of small amounts of the **MC** isomer. Irradiation of these three solutions, with a filtered UV black lamp (352 nm) for 10 min, induced photoswitching to give the **MC** enriched photostationary state. This resulted in an increase in the absorbance at 545 nm in each case. Photoswitching caused an increase in the intensity of the fluorescence of **MC-1** and **MC-2** with a maximum intensity observed around 627 nm, and for **MC-3** with a slight bathochromically shifted peak at around 632 nm (Figure 3-3, black). **MC-1** and **MC-3** had comparable emission intensities; however, **MC-2** showed a 3-4 fold higher emission intensity. Irradiation of the solutions with white light resulted in reversal of the absorbance and fluorescence spectra associated with the ring closed spiropyran isomer (Figure 3-3B, black). Thus, the ring size of the aza-crowncrown ether rings does not appear to have a significant effect on the peak absorption/emission and ability to photoswitch in these spiropyrans.

3.2.3.2 Absorbance Changes Upon Binding Alkali Metal Ions

The absorbance spectra of compounds **SP-1**, **SP-2**, and **SP-3** in the presence of 100 fold excess of perchlorate salts of Li^+, Na^+ and K^+ and Cs_2SO_4 in acetonitrile (as per literature on similar sensing systems)[12, 21, 25, 26] were next measured to investigate spectral changes induced by ion binding, as well as the influence of the 5'-carboxylic acid group on the observed spectra. An excess of metal ions was used in order to give the maximum signal from the spiropyran complexes, despite the optimal binding stoichiometry of 1:1 spiropyran to metal ion (as determined by a Job's plot, Figure 3-7). **SP-1** showed a 2 fold greater absorbance in the visible region in the presence of Li^+ and Na^+ compared to K^+ and Cs^+ (Figure 3-1A). This increase in absorbance is the result of metal ion induced thermal switching to the more coloured merocyanine state, see Scheme 3-3.[25] Binding of **SP-1** to Li^+ (**SP-1-Li$^+$**) caused a blue shift compared to the unbound form, with a peak maximum at 530 nm (Figure 3-1A, red). Interestingly this peak is bathochromically shifted compared to a structurally similar crowned spiropyran lacking a carboxylic acid group, which is reported to have a peak at 514 nm with Li^+.[25] **SP-1-Na$^+$** gave a similar absorbance intensity compared to **SP-1-Li$^+$**, however it was significantly bathochromically shifted to 550 nm. UV induced photoswitching to the **MC-1** isomer caused a further

3-4 fold increase in the absorbance of the resulting **MC-1-Li**$^+$ and **MC-1-Na**$^+$. **MC-1-K**$^+$ and **MC-1-Cs**$^+$ showed only a small increase, giving an absorbance spectrum similar to **MC-1** without metal ions (Figure 3-4).

SP-2 showed a 4 fold greater increase in absorbance at 550 nm in the presence of Li^+ compared to Na^+, Cs^+, and K^+ (Figure 3-1B). Again, this **SP-2-Li**$^+$ absorbance peak is bathochromically shifted compared to the 533 nm peak reported for a structurally similar crowned spiropyran lacking a carboxylic acid group at 5'.[25] Photoswitching on irradiation with 352 nm UV light caused a 2 fold increase in the signal intensity for **MC-2-Li**$^+$, and a 3 fold increase for **MC-2-Na**$^+$. The absorbance intensity of **MC-2-K**$^+$ and **MC-2-Cs**$^+$ underwent only a small increase at 550 nm, to give a signal similar to **MC-2** in the absence of metal ions.

SP-3 displayed an increase in absorbance at 540 nm in the presence of Li+ (Figure 3-1C). **SP-3** with K^+ and Na^+ underwent a smaller increase in absorbance, with peaks at 550 nm and 565 nm respectively. After UV induced photoswitching to give the **MC-3** metal complexes the **MC-3-Li**$^+$ system underwent a 4.5 fold increase in absorbance, much greater than the 2-3 fold increase observed in the **MC-3-Na**$^+$ and **MC-3-K**$^+$ solutions. Therefore, unlike for the **SP-3** isomeric form in which there was only a small difference between its absorbance with Li^+ and K^+, **MC-3** showed an improved selectivity profile with a much larger, 3 fold greater, absorption intensity in the presence of Li^+ compared to the other metal ions (Figure 3-4iii). Reverse photoswitching with visible light reduced the absorbance intensity of each system to near that of the non-irradiated system, demonstrating reversibility of the photoswitch (Figure 3-4B). This shows, however, that the carbonyl at the 5' position does not sufficiently stabilise the spiropyran form to shift the spiropyran:merocyanine equilibrium towards the spiropyran under visible irradiation, unlike previously observed for the CF_3 group.[21, 22] However, formation of the spiropyran-metal complex had sufficient time to reequilibrate between irradiation and spectral measurements.

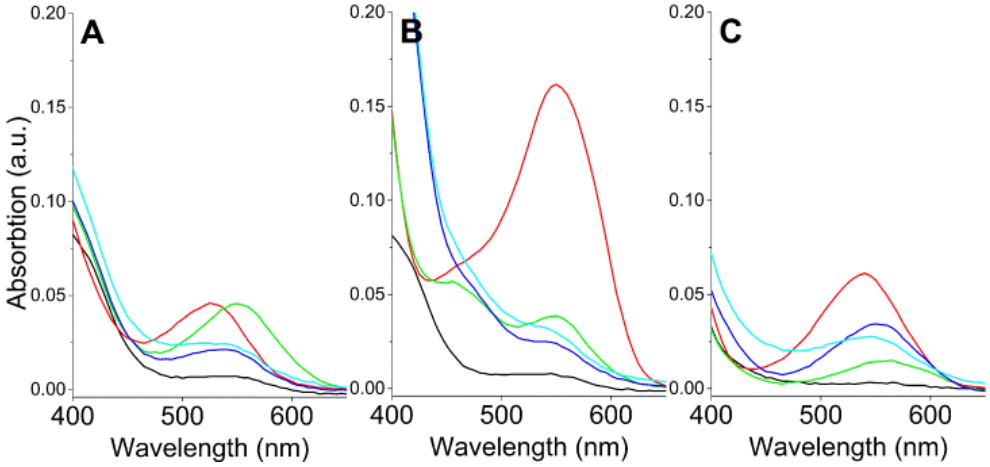

FIGURE 3-1: Absorption spectra of crowned spiropyrans in acetonitrile A) **SP-1**, B) **SP-2**, C) **SP-3** in the presence of no ions (black), 100x excess of lithium perchlorate (red), sodium perchlorate (green), potassium perchlorate (navy), caesium sulphate (cyan).

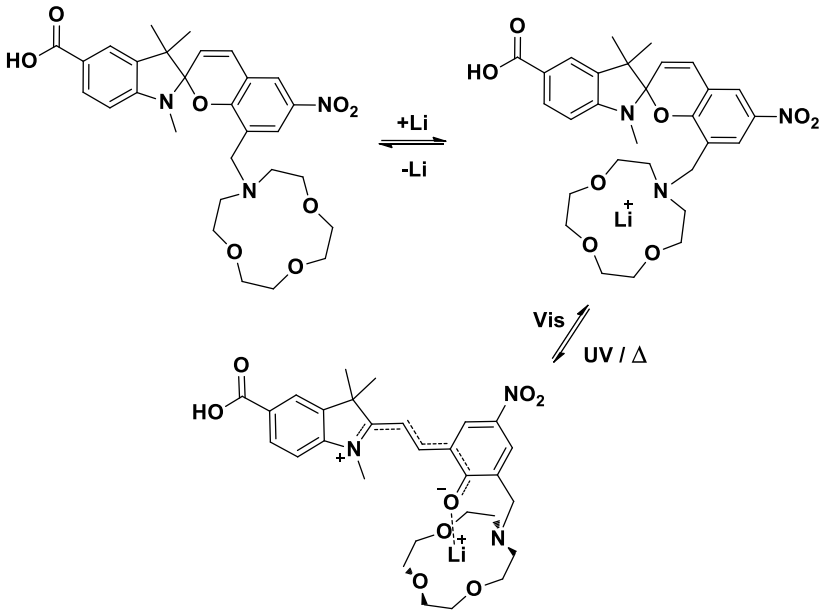

SCHEME 3-3: Model of lithium ion binding and ion induced switching of **SP-1**.

These absorbance profiles indicate that, regardless of the ring size, all compounds (**1**, **2**, and **3**) undergo metal ion induced chromism in the presence of lithium perchlorate in acetonitrile; with the largest and most selective change observed for **2-Li**$^{+}$. Binding of the different metal cations produced varying shifts in the maximum absorbance wavelength dependent on the size of the ring and the metal cation species. Importantly, this difference was significant enough for **SP-1** to distinguish

between Li^+ and Na^+. This observation may reflect the exact nature of the interactions between the metal ion and the phenolate of the merocyanine. The crown ether ring size also influences selectivity of binding to the other alkali metal ions. The smaller rings of **1** and **2** show some selectivity for Na^+ over K^+ while the larger ring in **SP-3** showed increased selectivity for K^+. However, selectivity of binding is also dependent on the photoswitched state, with **SP-2** only showing a strong response to Na^+ in the **MC-2** isomeric form.

The absorption spectra of **1-3** with Li^+, Na^+, and K^+ in a 1:1 mixture reveal similar absorption profiles compared to other related spiropyrans.[25, 27, 28] Thus the 5' carboxyl substituent does not interfere with ion binding and sensing (Figure 3-5). This group does, however, cause an approximate 15 nm bathochromic shift in the merocyanine absorbance peak. This needs to be considered in the design of other spiropyran sensors that employ such modification.

3.2.3.3 Fluorescence Detection of Alkali Metal Ion Binding

The fluorescence emissions of the three crowned spiropyrans **1**, **2**, and **3**, in the presence of perchlorate salts of Li^+, Na^+ and K^+ and Cs_2SO_4, were observed (Figure 3-3). Binding to Li^+ ions caused the largest increase in the fluorescence for all three spiropyrans, producing emission maxima at 627, 647, and 637 nm for **1**, **2** and **3** respectively (Figure 3-3A red). A 15 fold increase in fluorescence intensity was observed for **SP-1** (Figure 3-3i) bound with Li^+ (**SP-1-Li$^+$**) compared to **SP-1** alone, a change significantly greater than the 6 fold increase observed in the absorbance. **SP-1-Na$^+$** and **SP-1-K$^+$** had a similar fluorescence of half the intensity of **SP-1-Li$^+$**, despite **SP-1-Na$^+$** having a similar absorbance intensity to **SP-1-Li$^+$**. **SP-1-Na$^+$** and **SP-1-K$^+$** have emission maximum at around 642 and 632 nm, respectively, bathochromically shifted compared to the peaks of **SP-1**, **SP-1-Li$^+$**, and **SP-1-Cs$^+$** at 627 nm. Irradiation with UV black light for 10 min, to promote photoswitching to **MC-1**, caused a large increase in emission intensity of **MC-1-Li$^+$**, compared to the smaller increases in intensity when in the presence of Na^+, K^+, Cs^+, or just **MC-1** alone (Figure 2Bi). Irradiation with white light, to photoswitch back to the **SP-1** isomer, resulted in a decrease in fluorescence back to the non-photoswitched intensities, demonstrating photo-reversibility of the systems. **SP-2-Li$^+$** produced, a 3

fold greater fluorescence signal compared to **SP-2** alone, which in turn was slightly greater than that in the presence of Na^+, Cs^+, and K+ (Figure 3-3ii). This contrasts the greater absorbance observed for **SP-2-Na**$^+$, **SP-2-K**$^+$, and **SP-2-Cs**$^+$ compared to **SP-2**. UV induced photoswitching of all the **SP-2** complexes caused only a small fluorescence increase (Figure 3-3Bii) compared to the 2-3 fold increase observed in the absorbance spectra of **MC-2-Li**$^+$ and **MC-2-Na**$^+$. Surprisingly, the presence of Na^+, Cs^+ and K^+ resulted in a weaker fluorescence compared to that in the absence of metal ions. **SP-3-K**$^+$ and **SP-3-Cs**$^+$ gave a similar fluorescence intensity with emission maxima at 652 nm and 647 nm, respectively, and with an intensity approximately one third to that of **SP-3-Li**+, (Figure 3-3Aiii). **SP-3-Na**$^+$ had a low intensity emission around 655 nm. Interestingly photoswitching with UV light caused a large increase in emission from **MC-3-Na**$^+$ with a hypsochromically shifted peak at 605 nm (Figure 2Biii green, for spectrum see Supplementary Information Figure 3-6). This contrasts the small increase in a hypsochromically shifted absorbance spectrum (Figure 3-4Aiii)).

Exposure of **MC-3-Na**$^+$ to white light for 10 min, to induce photoswitching back to **SP-3**, gave no change in the fluorescence signal. This lack of photoswitching for **MC-3-Na**$^+$ suggests a strong binding affinity for the Na^+ ion which stabilises the merocyanine complex, therefore reducing the ability for **MC-3** to isomerise to **SP-3**.

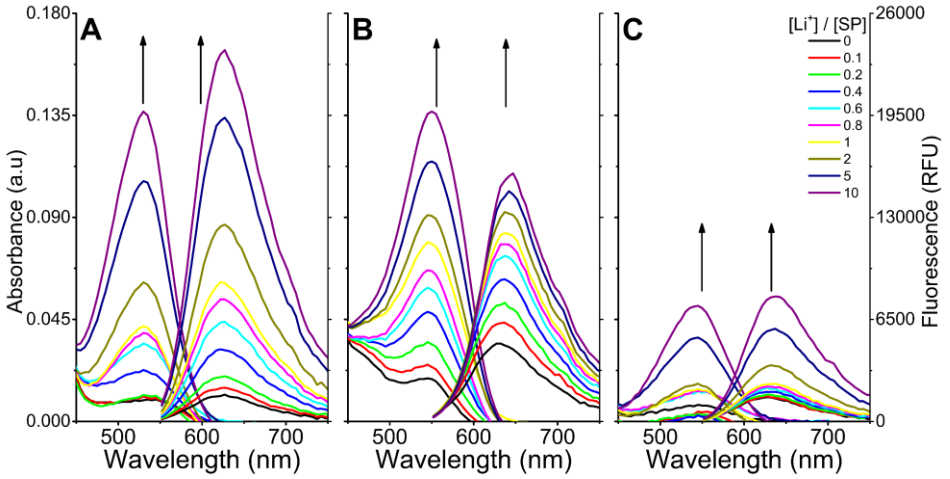

FIGURE 3-2: The absorbance and fluorescence spectra of crowned spiropyrans A) **SP-1**, B) **SP-2**, C) **SP-3** 50 μM in the presence of increasing concentrations of $LiClO_4$ 0, 10, 20, 30, 40, 50, 100, 250, 500 μM in acetonitrile.

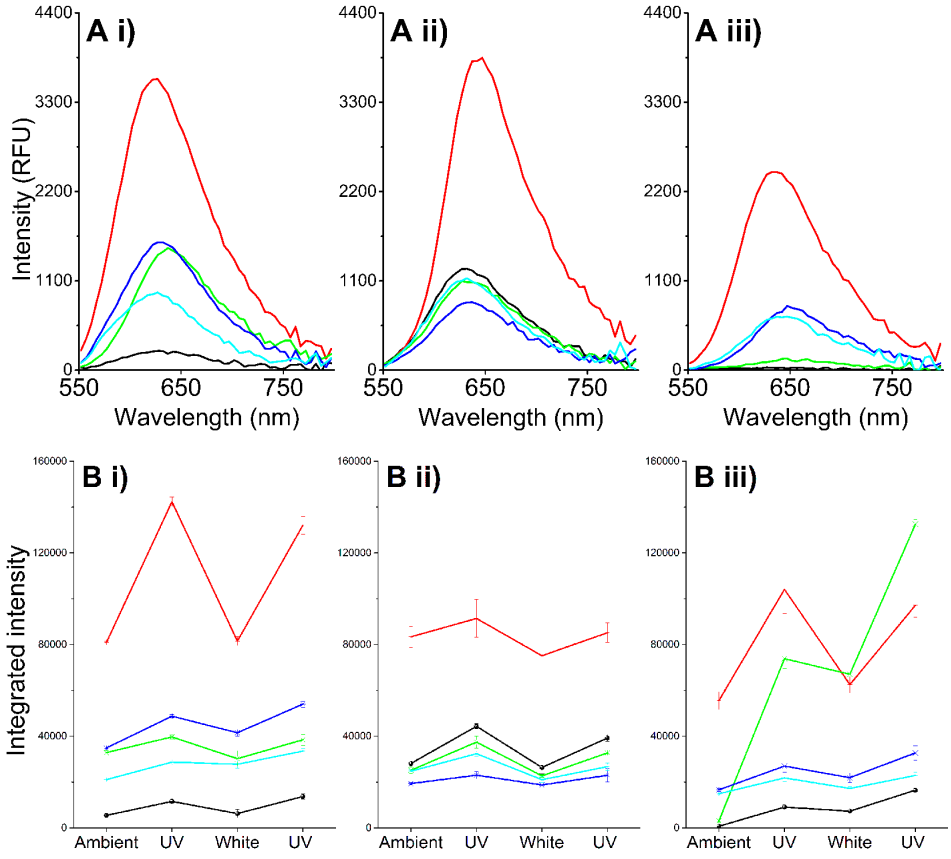

FIGURE 3-3: A) The fluorescence spectra of crowned spiropyrans i) **1**, ii) **2**, iii) **3** in the presence of no ions (black), and 100x excess of lithium perchlorate (red), sodium perchlorate (green), potassium perchlorate (navy), and caesium sulphate (cyan). B) Integrated fluorescence intensities in the presence of metals during photocycling with UV black light and white light.

These results demonstrate that, although ion induced switching from the spiropyran to merocyanine isomers in **1-3** can be observed as an increase in the absorbance spectra, the same relative increase in signal intensity is not observed in the fluorescence spectra. That is, the binding of the different metal ions appears to alter the fluorescence yields of each spiropyran. Regardless, based on fluorescence spectroscopy all three crowned spiropyran complexes (**1-3**) were able to selectively detect Li^+ over the other alkali metal ions investigated. **SP-2** appeared to show the greatest difference in fluorescence intensity between the binding to Li^+ and the other metal ions, hence demonstrating the best selectivity for Li^+.

Finally the concentration dependence of Li^+ on the absorbance and fluorescence was investigated. Figure 3-2 shows the increase in absorbance and fluorescence signal of spiropyrans **1-3** on increasing Li^+ concentrations. In these conditions an increase in the **SP-2** spectrum was observed for Li^+ at 0.1 molar equivalents, the lowest concentration ratio investigated. Spiropyrans **SP-1** and **SP-3** likewise showed a typical concentration dependant sigmoidal increase between 0.1 and 1 molar equivalents.

3.2.4 CONCLUSIONS

Three photoswitchable spiropyrans **SP-1**, **SP-2**, and **SP-3** were synthesized, each with a different sized aza-crown ether attached at the 8-position. Absorbance and fluorescence responses to binding of alkali metal cations Li^+, Na^+, K^+, and Cs^+ in acetonitrile were determined. Each spiropyran gave a strong absorbance and fluorescence response in the presence of Li^+, irrespective of the size of the crown ether ring. A weaker response was observed in the binding of all spiropyrans to the other alkali metal ions, with the selectivity of ion binding defined by the size of the crown ether ring. As such the 1-aza-15-crown-5 containing spiropyran (**SP-2**) showed the most selective response to Li^+ over the other metal ions, exhibiting a stronger relative absorbance and fluorescence spectra. Therefore in conclusion, these aza-crowncrown ether spiropyrans have potential as new reversible fluorescent probes for investigating the concentration of Li^+ in biological systems, which will lead to a greater understanding of Li^+'s role in diseases such as manic-depressive illness.

3.2.5 EXPERIMENTAL

3.2.5.1 Materials and Methods

All ^{13}C NMR and ^{1}H NMR spectra were recorded on an Agilent Technologies 500 MHz NMR with DD2 console in $CDCl_3$ or DMSO-d_6 (Cambridge Isotope Laboratories, Cambridge, MA). Chemical shifts (δ) are reported in ppm, with $CDCl_3$ (δ_C = 77.1 ppm), DMSO-d_6 (δ_C = 39.52 ppm) or TMS (δ_H= 0.0 ppm) used as internal standards. High resolution mass spectrometry was performed on the Agilent 6230 TOF LC-MS. All commercially available chemicals were reagent grade and used without further purification.

3.2.5.2 Synthesis of Aza-crowncrown ether Spiropyrans

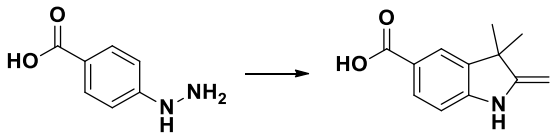

3,3-Dimethyl-2-methyleneindoline-5-carboxylic acid (5)

4-Hydrazinobenzoic acid (**4**) (5.0 g, 33 mmol) was suspended in ethanol (20 mL) and to this was added 2-methyl-2-butanone (4 mL, 37 mmol) followed by conc. sulphuric acid (1 mL). The mixture was stirred at reflux for 18 h. After cooling to r.t. the precipitate was removed by filtration and washed with acetonitrile. The filtrate was quenched with saturated sodium bicarbonate solution and washed with DCM 2x 60 mL. The aqueous layer was carefully acidified to pH 5 (universal indicator paper) with 2 M aqueous hydrochloric acid solution and red product was extracted with DCM (3x 60 mL), dried with $MgSO_4$ and solvent removed *in vacuo* to give **5** as a dark red solid (4.8 g) in 73 % yield. mp. 198-202 ^{o}C, ^{1}H NMR (500 MHz, $CDCl_3$) δ 8.16 (d, J = 8.1 Hz, ^{1}H), 8.07 (s, 1H), 7.67 (d, J = 8.1 Hz, 1H), 2.38 (s, 3H), 1.38 (s, 6H); ^{13}C NMR (126 MHz, $CDCl_3$) δ 192.4 (s), 171.3 (s), 157.6 (s), 145.6 (s), 130.9 (s), 126.6 (s), 123.2 (s), 119.7 (s), 53.9 (s), 22.9 (s), 15.6 (s). HRMS (m/z) for $C_{12}H_{13}NO_2$ + H ($[M+H^+]^+$) calcd 204.1025; found 204.1025.

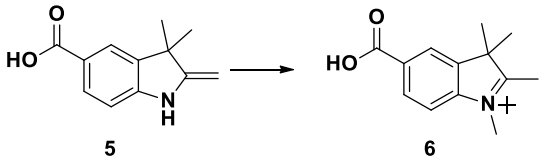

1,3,3-Trimethyl-2-methyleneindoline-5-carboxylic acid (6)

3,3-Dimethyl-2-methyleneindoline-5-carboxylic acid (**5**) (3.9 g, 19 mmol) was dissolved in a solution of 2:1 toluene:acetonitrile (100 mL). To this was added iodomethane (1.3 mL, 21 mmol) and the solution was stirred at 95 ^{o}C for 24 h. The solution was cooled to r.t. and the precipitate was collected by filtration and washed with acetonitrile to give **6** (3.0 g) in 72 % yield. mp. 154-157 ^{o}C, ^{1}H NMR (500 MHz, DMSO-d_6) δ 8.36 (s, 1H), 8.17 (d, J = 8.1 Hz, 1H), 8.02 (d, J = 8.2 Hz, 1H), 4.00 (s, 3H), 2.82 (s, 3H), 1.57 (s, 6H); ^{13}C NMR (126 MHz, DMSO-d_6) δ 199.0 (s), 166.5 (s), 145.2 (s), 141.9 (s), 131. 6 (s), 130. 3 (s), 124.2 (s), 115.4 (s), 54.3 (s), 35.2 (s), 21.5 (s), 14.8 (s). HRMS (m/z) for $C_{13}H_{16}NO_2$ ($[M]^+$) calcd 218.1181; found 218.1184.

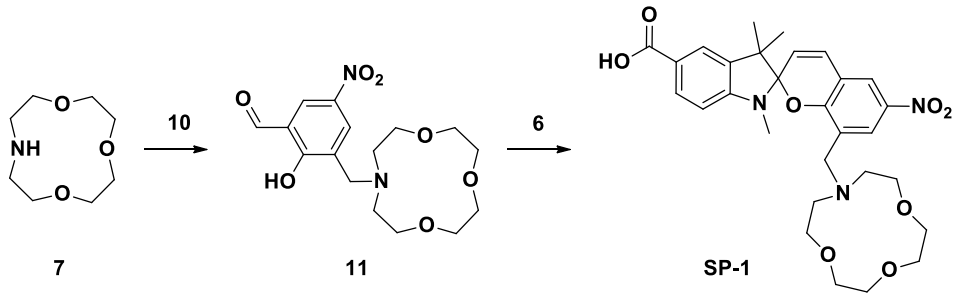

Aza-12-crown-4-ether spiropyran (SP-1)

To a solution of 1-aza-12-crown-4-ether (**7**) (90 mg, 0.51 mmol) in dry THF (3 mL) was added triethylamine (80 µL, 1.1 mmol) and the solution cooled in an ice bath. To this mixture was added a solution of 3-(chloromethyl)-2-hydroxy-5-nitrobenzaldehyde (**10**) (0.11 g, 0.51 mmol) in dry THF (5 mL). The solution was allowed to warm to r.t. over 1 h followed by reflux for 17 h. The precipitate was removed by filtration and the solvent was removed *in vacuo* to give **11** as a yellow solid (0.19 g). ^{1}H NMR (500 MHz, DMSO-d_6) δ 10.19 (d, J = 0.6 Hz, 1H), 8.27 (dd, J = 0.5, 3.0 Hz, 1H), 8.09 (d, J = 3.0 Hz, 1H), 4.28 (s, 2H), 3.83 – 3.75 (m, 5H), 3.68 – 3.51 (m, 11H); ^{13}C NMR (126 MHz, DMSO-d_6) δ 190.1 (s), 178.9 (s), 130.7 (s),

129.9 (s), 126.4 (s), 123.7 (s), 122.3 (s), 70.1 (s), 69.8 (s), 64.6 (s), 56.5 (s), 54.3 (s). HRMS (*m/z*) for $C_{16}H_{22}N_2O_7$ + H ($[M+H^+]^+$) calcd 355.1505; found 355.1507. A sample of **11** (0.18 g) and **6** (0.18 g, 0.51 mmol) were dissolved in ethanol (10 mL) and the solution refluxed for 3 h. The solvent was removed *in vacuo* and the resulting purple solid (0.36 g) was purified twice by C18 reverse phase silica chromatography eluting with a gradient of acetonitrile in water to give **SP-1** (50 mg) in a yield of 18 % (based on **7**). mp. 118-121 ^oC, ^1H NMR (500 MHz, DMSO-d_6) δ 12.31 (s, 1H), 8.35 (d, J = 2.6 Hz, 1H), 8.13 (d, J = 2.6 Hz, 1H), 7.81 (d, J = 8.2 Hz, 1H), 7.69 (s, 1H), 7.25 (d, J = 10.4 Hz, 1H), 6.70 (d, J = 8.2 Hz, 1H), 6.01 (d, J = 10.4 Hz, 1H), 3.58 – 3.36 (m, 18H), 2.73 (s, 3H), 1.25 (s, 3H), 1.14 (s, 3H); ^{13}C NMR (126 MHz, DMSO-d_6) δ 167.4 (s), 156.5 (s), 151.2 (s), 140.3 (s), 135.9 (s), 130.8 (s), 128.7 (s), 127.1 (s), 125.9 (s), 122.9 (s), 121.5 (s), 121.3 (s), 120.3 (s), 118.4 (s), 106.3 (s), 105.8 (s), 70.9 (s), 69.5 (s), 69.3 (s), 54.4 (s), 52.4(s), 51.3 (s), 28.4 (s), 25.5 (s), 19.5 (s). HRMS (*m/z*) for $C_{29}H_{35}N_3O_8$ + H ($[M+H^+]^+$) calcd 554.2502; found 554.2517

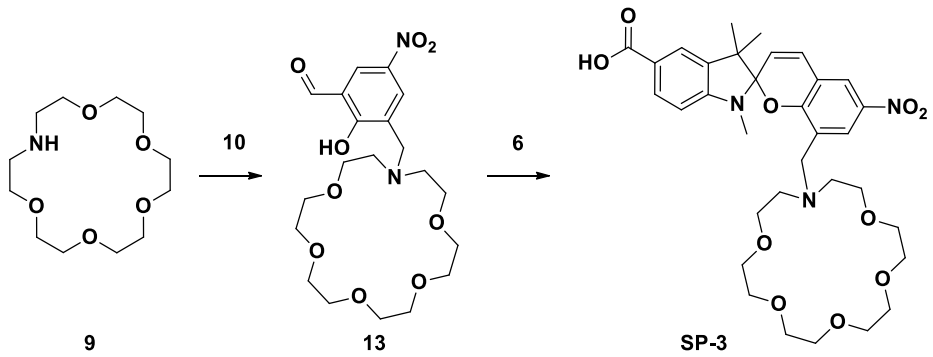

Aza-18-crown-6-ether spiropyran (SP-3)

To a solution of 1-aza-18-crown-6-ether (**9**) (0.25 g, 0.95 mmol) in dry THF (5 mL) was added triethylamine (0.16 mL, 2.2 mmol). The solution was cooled in an ice bath and to this was added dropwise a solution of 3-(chloromethyl)-2-hydroxy-5-nitrobenzaldehyde (**10**) (0.21 g, 0.97 mmol) in dry THF (7 mL). The solution was allowed to warm to r.t. over 1 h followed by reflux for 17 h. The precipitate was removed by filtration and the solvent was removed *in vacuo* to give **13** as a thick orange oil (0.48 g). ^1H NMR (500 MHz, DMSO-d_6) δ 10.23 (s, 1H), 8.27 (d, J = 3.1 Hz, 1H), 8.13 (d, J = 3.1 Hz, 1H), 4.38 (s, 2H), 3.84 – 3.79 (m, 4H), 3.56 (s, 8H),

3.53 (s, 8H), 3.33 – 3.27 (m, 5H); ^{13}C NMR (126 MHz, DMSO-d_6) δ 189.9 (s), 178.6 (s), 130.7 (s), 130.6 (s), 126.0 (s), 123.8 (s), 122.2 (s), 69.9 (s), 69.8 (s), 69.7 (s), 69.4 (s), 64.6 (s), 56.0 (s), 52.0 (s). HRMS (*m/z*) for $C_{20}H_{30}N_2O_9$ + H ([M+H$^+$]$^+$) calcd 443.2030; found 443.2009. A sample of **13** (0.47 g) and **6** (0.24 g, 1.1 mmol) were dissolved in ethanol (15 mL), and the solution refluxed for 18 h. Solvent was removed *in vacuo* to give purple crude solid (0.68 g, 1.1 mmol) of which 0.34 g was purified by C18 reverse phase silica chromatography eluting with a gradient of acetonitrile in water to give **SP-3** (120 mg) in a yield of 20 % (Based on **10**). mp. 95-99 ^{o}C, ^{1}H NMR (500 MHz, DMSO-d_6) δ 12.30 (s, 1H), 8.15 – 8.11 (m, 2H), 7.81 (d, J = 8.2 Hz, 1H), 7.68 (s, 1H), 7.24 (d, J = 10.3 Hz, 1H), 6.69 (d, J = 8.2 Hz, 1H), 6.00 (d, J = 10.3 Hz, 1H), 3.57 – 3.46 (m, 12H), 3.46 – 3.42 (m, 5H), 3.41 (s, 2H), 3.37 – 3.33 (m, 2H), 3.29 – 3.26 (m, 5H), 2.71 (s, 3H), 1.26 (s, 3H), 1.14 (s, 3H); ^{13}C NMR (126 MHz, DMSO-d_6) δ 167.9 (s), 157.1 (s), 151.6 (s), 140.6 (s), 136.4 (s), 131.2 (s), 129.2 (s), 127.4 (s), 126.4 (s), 123.3 (s), 122.1 (s), 121.9 (s), 120.8 (s), 118.9 (s), 106.8 (s), 106.2 (s), 70.4 (s), 70.4 (s), 70.3 (s), 70.0 (s), 69.3 (s), 53.7 (s), 52.1 (s), 51.7 (s), 28.8 (s), 26.1 (s), 19.8 (s). HRMS (*m/z*) for $C_{33}H_{43}N_3O_{10}$ + Na ([M+Na$^+$]$^+$) calcd 664.2846; found 664.2868.

3.2.5.3 Comparative Assay Procedure

Stock solutions of spiropyran **1-3** (100 μM) and metal ion salts (100 μM and 10 mM) were prepared in HPLC grade acetonitrile. Salt solutions were prepared from dried $LiClO_4$, $NaClO_4$, $KClO_4$ and Cs_2SO_4. On the same microplate tray, each spiropyran 100 μL was mixed separately with each of the metal solutions 100 μL (1:1 or 1:100 ratio spiropyran:metal ion) in triplicate. The absorbance and fluorescence spectra were recorded between 300 and 800 nm, and 552 and 802 nm, respectively, at 25 ^{o}C using a BioTek Synergy H4 Hybrid Multi-Mode Microplate Reader scanning with a resolution of 5 nm. Fluorescence excitation was at 532 nm with bandgap of 9 nm. The assay tray was then removed and repetitive photoswitching was performed by exposing to 352 nm UV light from a filtered 8 W Hg lamp (UVP), or halogen white lamp for 10 min each, with the absorbance and fluorescence spectra obtained after each irradiation.

3.2.5.4 Li^+ Concentration Dependence Assay Procedure

Stock solutions of spiropyran **1-3** (100 μM) and $LiClO_4$ (100 μM and 1 mM) were prepared in HPLC grade acetonitrile. On the same microplate tray in triplicate each spiropyran 100 μL was mixed separately with the $LiClO_4$ solutions and acetonitrile to make a total volume of 200 μL per well with spiropyran 50 μM and Li^+ 0, 5, 10, 20, 30, 40, 50, 100, 250, 500 μM. The solutions were left in the dark for 30 min. The absorbance and fluorescence spectra were recorded between 300 and 800 nm, and 552 and 802 nm, respectively, at 25 ^oC using a BioTek Synergy H4 Hybrid Multi-Mode Microplate Reader scanning with a resolution of 5 nm. Fluorescence excitation was at 532 nm with bandgap of 9 nm and gain of 100.

3.2.5.5 Job's Plot

Stock solutions of spiropyran **SP-1** (100 μM) and $LiClO_4$ (100 μM) were prepared in HPLC grade acetonitrile. On the same microplate tray in triplicate the **SP-1** and $LiClO_4$ solutions (combined total 100 μL) and acetonitrile (100 μL) were combined such that the total concentration was constant ([M] + [SP-1] = 50 μM) [SP-1]= 0, 5, 10, 15, 20, 25, 30, 35, 40, 45, and 50 μM. The absorbance and fluorescence spectra were recorded between 300 and 700 nm, and 552 and 697 nm, respectively, at 25 ^oC using a BioTek Synergy H4 Hybrid Multi-Mode Microplate Reader scanning with a resolution of 5 nm. Fluorescence excitation was at 532 nm with bandgap of 9 nm.

3.2.6 SUPPLEMENTARY INFORMATION

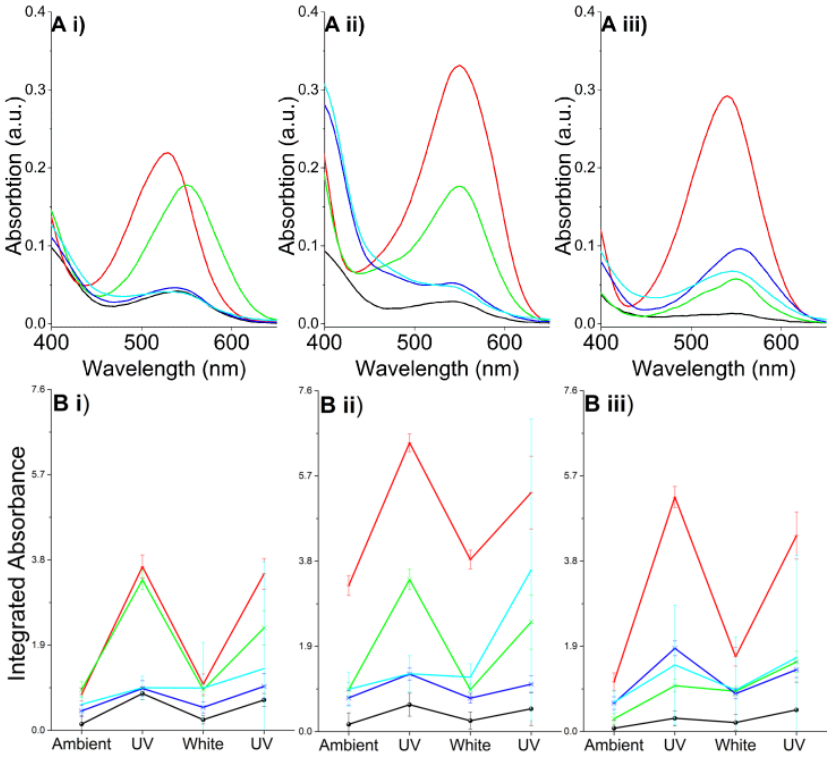

FIGURE 3-4: A) the absorbance spectra of crowned spiropyrans i) **1**, ii) **2**, iii) **3** after 10 min of UV black light irradiation in the presence of no ions (black), and 100x excess of lithium perchlorate (red), sodium perchlorate (green), potassium perchlorate (navy), and caesium sulphate (cyan). B) Integrated absorbance intensities (between 470 and 650 nm) of crowned spiropyrans in the presence of metal salts during photocycling with UV black light and white light 10 min each.

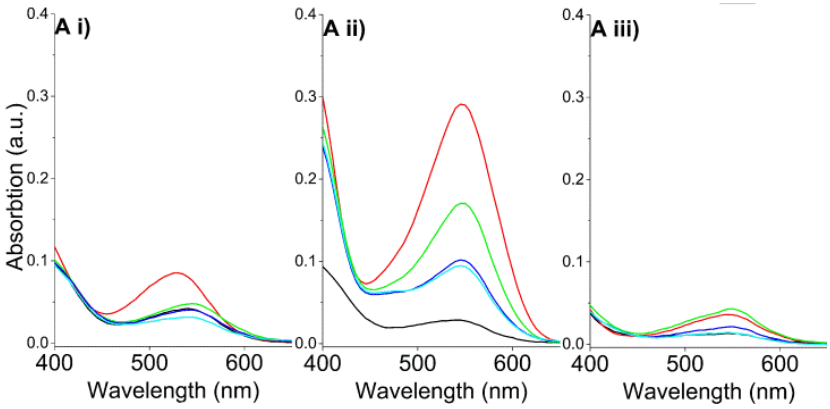

FIGURE 3-5: A) the absorbance spectra of crowned spiropyrans i) **1**, ii) **2**, iii) **3** after 10 min of UV black light irradiation in the presence of no ions (black), and equimolar quantities of lithium perchlorate (red), sodium perchlorate (green), potassium perchlorate (navy), and caesium sulphate (cyan).

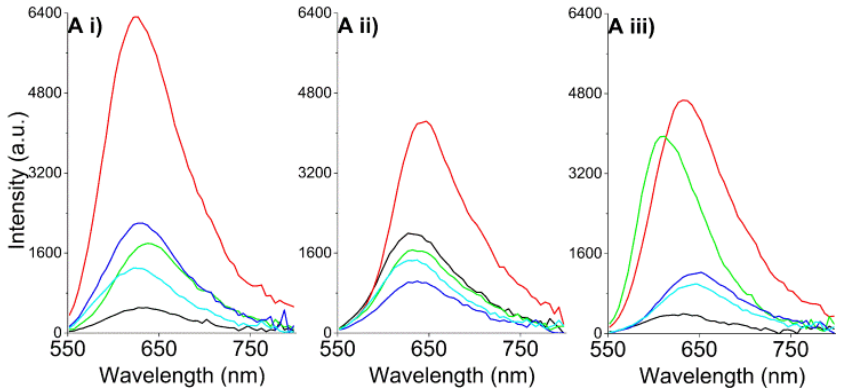

FIGURE 3-6: A) the fluorescence spectra of crowned spiropyrans i) **1**, ii) **2**, iii) **3** after 10 min of UV black light irradiation in the presence of no ions (black), and 100x excess of lithium perchlorate (red), sodium perchlorate (green), potassium perchlorate (navy), and caesium sulphate (cyan).

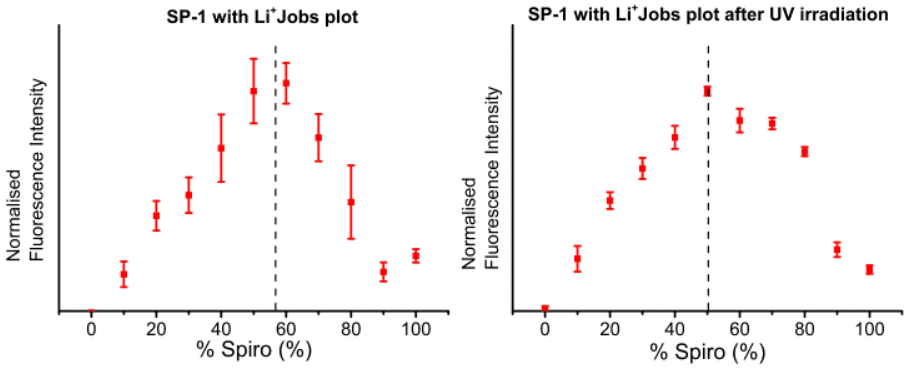

FIGURE 3-7: Job's plot of the fluorescence of **SP-1** with $LiClO_4$ in the dark (left) and after UV_{352} irradiation for 10 min (right).

NMR spectra of spiropyrans and intermediates

^{1}H and ^{13}C NMR spectra of synthesised compounds (**5, 6, 11, 13**, **SP-1** and **SP-3**) can be found in Supplementary Information file online at http://dx.doi.org/10.1039/C6OB00468G.

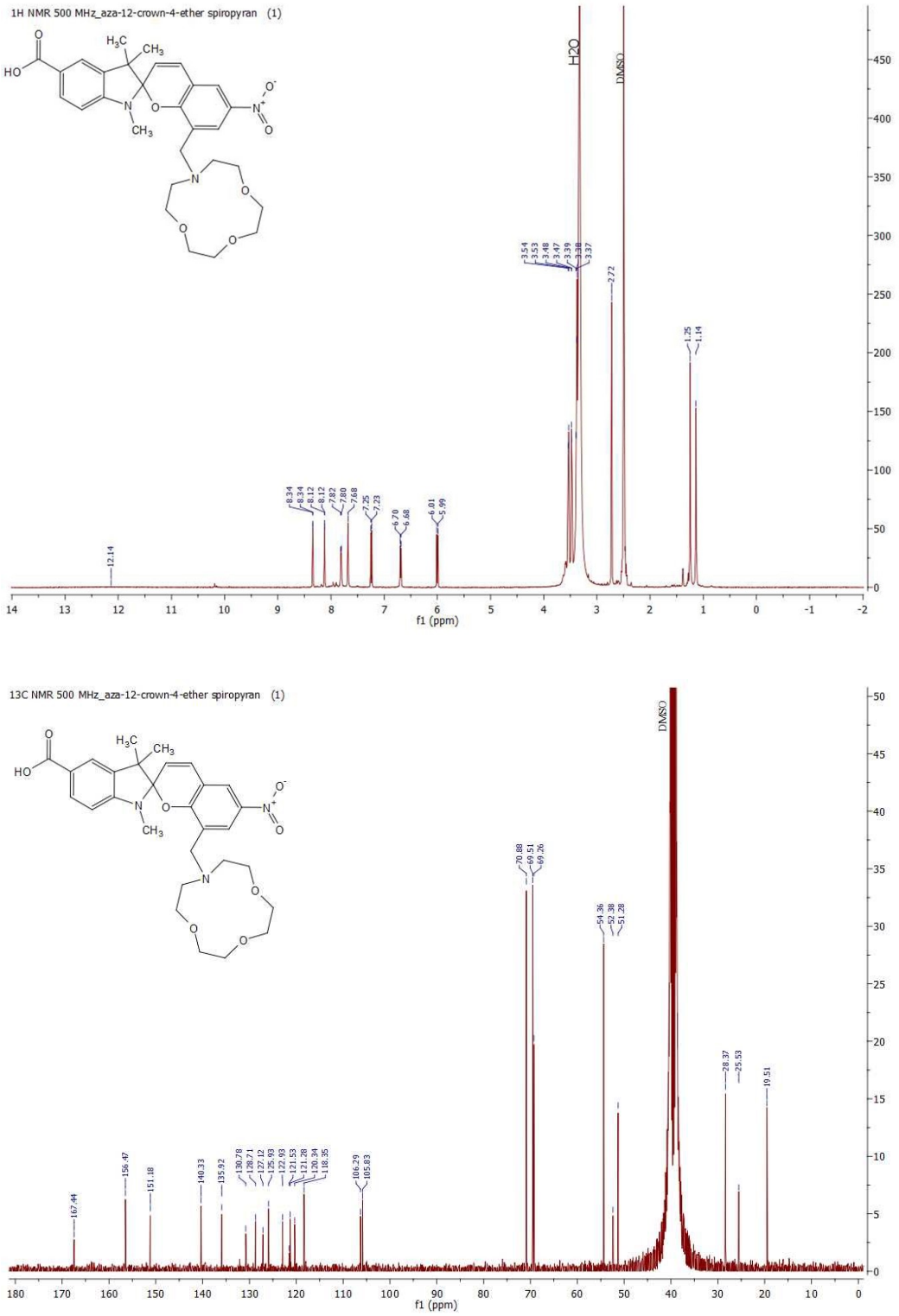

FIGURE 3-8: 1H and 13C NMR spectrum of **SP-1** recorded in DMSO-d_6

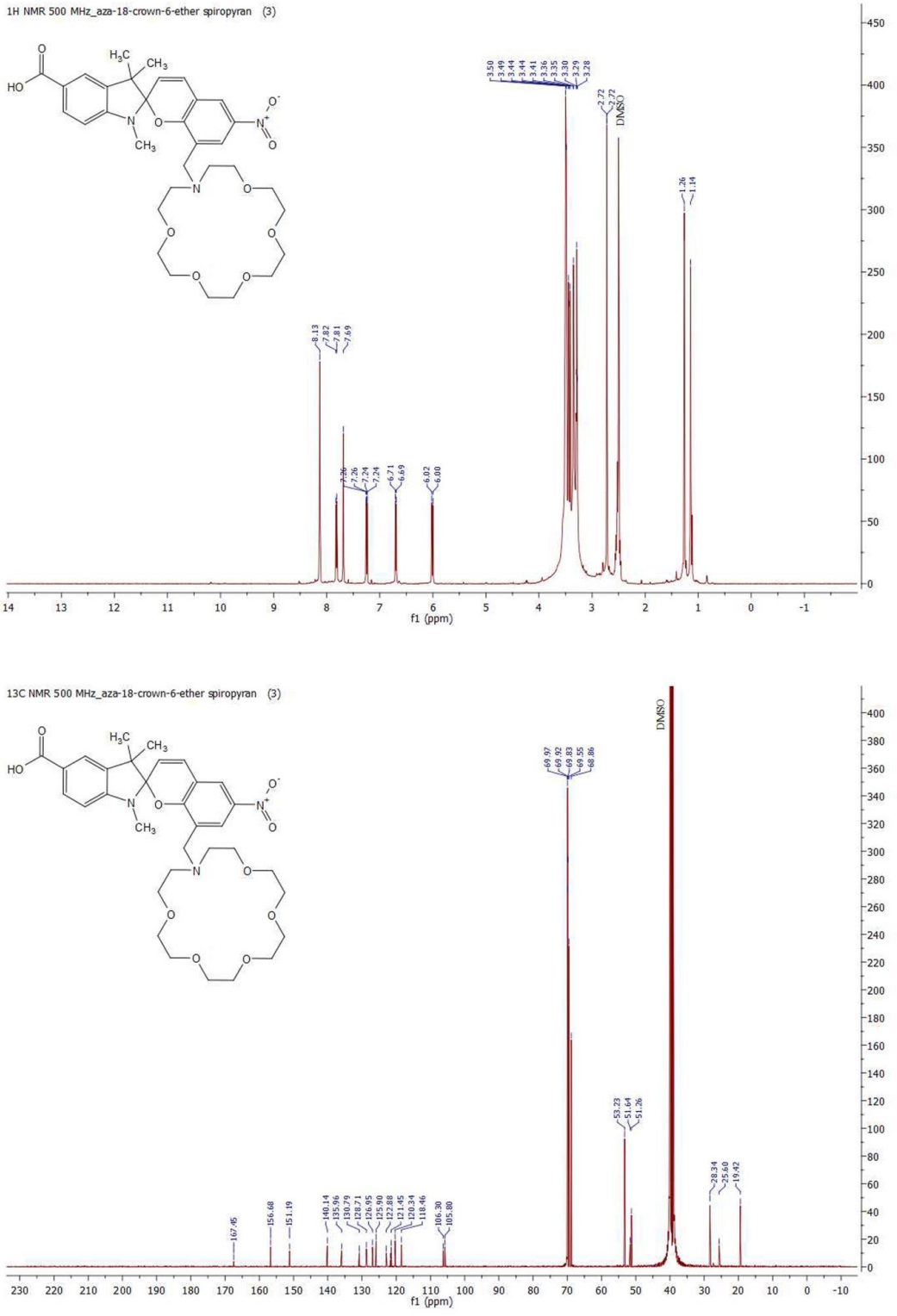

FIGURE 3-9: 1H and 13C NMR spectrum of **SP-3** recorded in DMSO-d_6

3.3 REFERENCES FOR CHAPTER 3

1. Stubing, D. B.; Heng, S.; Abell, A. D. Crowned spiropyran fluoroionophores with a carboxyl moiety for the selective detection of lithium ions. *Organic & Biomolecular Chemistry* 2016, 14 (15), 3752-7.
2. Yin, J.; Hu, Y.; Yoon, J. Fluorescent probes and bioimaging: alkali metals, alkaline earth metals and pH. *Chemical Society Reviews* 2015.
3. Klemfuss, H. Rhythms and the pharmacology of lithium. *Pharmacology & Therapeutics* 1992, *56* (1), 53-78.
4. Alda, M. Lithium in the treatment of bipolar disorder: pharmacology and pharmacogenetics. *Molecular Psychiatry* 2015, *20* (6), 661-670.
5. Manji, H. K.; Potter, W. Z.; Lenox, R. H. Signal transduction pathways. Molecular targets for lithium's actions. *Archives of General Psychiatry* 1995, *52* (7), 531-43.
6. Jope, R. S. Anti-bipolar therapy: mechanism of action of lithium. *Molecular Psychiatry* 1999, *4* (2), 117-128.
7. Ando, Y.; Hiruta, Y.; Citterio, D.; Suzuki, K. A highly Li+-selective glass optode based on fluorescence ratiometry. *Analyst* 2009, *134* (11), 2314-2319.
8. Gulino, A.; Lupo, F.; Cristaldi, D. A.; Pappalardo, S.; Capici, C.; Gattuso, G.; Notti, A.; Parisi, M. F. A Viable Route for Lithium Ion Detection. *European Journal of Inorganic Chemistry* 2014, *2014* (3), 442-449.
9. Obare, S. O.; Murphy, C. J. A Two-Color Fluorescent Lithium Ion Sensor. *Inorganic Chemistry* 2001, *40* (23), 6080-6082.
10. Citterio, D.; Takeda, J.; Kosugi, M.; Hisamoto, H.; Sasaki, S.-i.; Komatsu, H.; Suzuki, K. pH-Independent Fluorescent Chemosensor for Highly Selective Lithium Ion Sensing. *Analytical Chemistry* 2007, *79* (3), 1237-1242.
11. Sakamoto, H.; Yamamura, T.; Takumi, K.; Kimura, K. Absorption- and fluorescence-spectral sensing of alkali metal ions in anionic micelle solutions containing crowned spirobenzopyrans. *Journal of Physical Organic Chemistry* 2007, *20* (11), 900-907.
12. Heng, S.; Nguyen, M.-C.; Kostecki, R.; Monro, T. M.; Abell, A. D. Nanoliter-scale, regenerable ion sensor: sensing with a surface functionalized microstructured optical fibre. *RSC Advances* 2013, *3* (22), 8308-8317.
13. Shao, N.; Zhang, Y.; Cheung, S.; Yang, R.; Chan, W.; Mo, T.; Li, K.; Liu, F. Copper Ion-Selective Fluorescent Sensor Based on the Inner Filter Effect Using a Spiropyran Derivative. *Analytical Chemistry* 2005, *77* (22), 7294-7303.
14. Chibisov, A. K.; Görner, H. Complexes of spiropyran-derived merocyanines with metal ions: relaxation kinetics, photochemistry and solvent effects. *Chemical Physics* 1998, *237* (3), 425-442.
15. Winkler, J. D.; Bowen, C. M.; Michelet, V. Photodynamic Fluorescent Metal Ion Sensors with Parts per Billion Sensitivity. *Journal of the American Chemical Society* 1998, *120* (13), 3237-3242.
16. Kimura, K.; Teranishi, T.; Yokoyama, M.; Yajima, S.; Miyake, S.; Sakamoto, H.; Tanaka, M. Cation complexation, isomerization, and photoresponsive ionic conduction of a crown ether derivative carrying two

spirobenzopyran units. *Journal of the Chemical Society, Perkin Transactions 2* 1999, (2), 199-204.

17. Tanaka, M.; Nakamura, M.; Salhin, M. A. A.; Ikeda, T.; Kamada, K.; Ando, H.; Shibutani, Y.; Kimura, K. Synthesis and photochromism of spirobenzopyran derivatives bearing an oxymethylcrown ether moiety: Metal ion-induced switching between positive and negative photochromisms. *Journal of Organic Chemistry* 2001, *66* (5), 1533-1537.
18. Heng, S.; McDevitt, C. A.; Stubing, D. B.; Whittall, J. J.; Thompson, J. G.; Engler, T. K.; Abell, A. D.; Monro, T. M. Microstructured optical fibers and live cells: a water-soluble, photochromic zinc sensor. *Biomacromolecules* 2013, *14* (10), 3376-9.
19. Ueno, T.; Nagano, T. Fluorescent probes for sensing and imaging. *Nature Methods* 2011, *8* (8), 642-645.
20. Zhang, P.; Meng, J.; Li, X.; Wang, Y.; Matsuura, T. Synthesis and photochromism of photochromic spiro compounds having a reactive pendant group. *Journal of Heterocyclic Chemistry* 2002, *39* (1), 179-184.
21. Abdullah, A.; Roxburgh, C. J.; Sammes, P. G. Photochromic crowned spirobenzopyrans: Quantitative metal-ion chelation by UV, competitive selective ion-extraction and metal-ion transportation demonstration studies. *Dyes and Pigments* 2008, *76* (2), 319-326.
22. Roxburgh, C. J.; Sammes, P. G. Substituent tuning of photoreversible lithium chelating agents. *Dyes and Pigments* 1995, *28* (4), 317-325.
23. Fischer, E.; Hess, O. Synthese von Indolderivaten. *Berichte der deutschen chemischen Gesellschaft* 1884, *17* (1), 559-568.
24. Fischer, E.; Jourdan, F. Ueber die Hydrazine der Brenztraubensäure. *Berichte der deutschen chemischen Gesellschaft* 1883, *16* (2), 2241-2245.
25. Kimura, K.; Yamashita, T.; Yokoyama, M. Synthesis, cation complexation, isomerization and photochemical cation-binding control of spirobenzopyrans carrying a monoaza-crown moiety at the 8-position. *Journal of the Chemical Society-Perkin Transactions 2* 1992, (4), 613-619.
26. Salhin, Abdussalam M. A.; Tanaka, M.; Kamada, K.; Ando, H.; Ikeda, T.; Shibutani, Y.; Yajima, S.; Nakamura, M.; Kimura, K. Decisive Factors in the Photoisomerization Behavior of Crowned Spirobenzopyrans: Metal Ion Interaction with Crown Ether and Phenolate Anion Moieties. *European Journal of Organic Chemistry* 2002, *2002* (4), 655-662.
27. Kimura, K.; Yamashita, T.; Yokoyama, M. Photochemical switching of ionic-conductivity in composite films containing a crowned spirobenopyran. *Journal of Physical Chemistry* 1992, *96* (13), 5614-5617.
28. Kimura, K.; Yamashita, T.; Yokoyama, M. Cation-specific isomerization of crowned spirobenzopyrans. *Journal of the Chemical Society, Chemical Communications* 1991, (3), 147-148.

CHAPTER 4

PHOTOSWITCHABLE SPIROPYRAN SENSORS FOR THE DETECTION OF CALCIUM IONS

4.1 INTRODUCTION

4.1.1 THE DESIGN OF A SPIROPYRAN METAL ION SENSOR

In Chapter 2 it was determined that the most promising photoswitches for use in optical fibres were azobenzenes and spiropyrans. As spiropyrans have intrinsic metal ion affinity and fluorescence, which azobenzenes lack, photoswitchable ion sensors designed based on the benzospiropyran core (Figure 4-1) were further investigated, as previously presented in Chapter 3. This core can be modified and tailored for targeted sensing at several positions around the structure. The spiropyran sensors were designed with four different modifiable moieties that are critical for tailoring the ability for the switch to reversibly bind ions and be attached to a surface. These are a -NO_2 at the 6-position, a -CO_2H at the 5' position, as well as changeable ion chelators R_8 and $R_{1'}$ at the 8- and 1'-position, respectively (Figure 4-1).

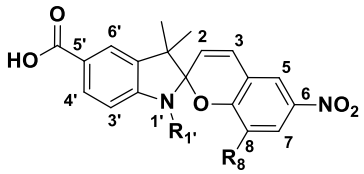

FIGURE 4-1: Positions of modification on a 5'-carboxylic acid, 6-NO_2-spiropyran.

A nitro group has long been recognised to promote photochromism of spiropyrans, increasing the thermal stability of the switched isomer; by relaxing through an alternate mechanism which involves an excited triplet state.[1] The NO_2 group modifies the solubility, absorbance and fluorescence properties, photochromic properties, and withdraws electron density from the phenolate oxygen promoting reversible binding.[2] Therefore, the presence of the NO_2 is critical for the sensor.

The 5'-carboxyl group allows attachment of the spiropyran to other structural units, such as an aminated surface, as discussed further in Chapter 5. The position of this surface attachable group was chosen due to its spatial remoteness from the ion binding region; therefore, possibly minimising the influence of the surface on the photoswitching and ion binding properties of the sensor.

Ion binding specificity is provided by incorporating ion chelating domains at R_8 and/or $R_{1'}$. The R_8 and $R_{1'}$ position are adjacent to the photochromic core of the spiropyran, therefore are strongly affected by the spatial and electronic changes induced by photoswitching. The versatility of this sensor design allows for the incorporation of a wide variety of tailored ion binding groups at these locations;[3] as already demonstrated in the three spiropyrans **SP-1** to **SP-3** (Chapter 3) (Scheme 4-1) which contained aza-crown ethers[4-7] of increasing size at the R_8 position.

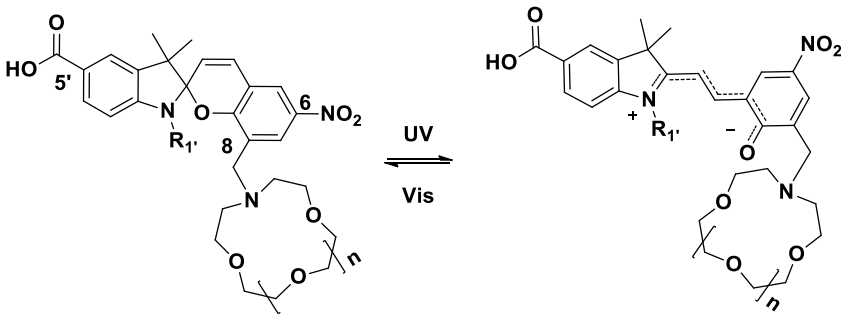

SP-1: $R_{1'}$=CH_3, n=1
SP-2: $R_{1'}$=CH_3, n=2
SP-3: $R_{1'}$=CH_3, n=3
SP-4: $R_{1'}$=CH_2CH_2OH, n=3

MC-1: $R_{1'}$=CH_3, n=1
MC-2: $R_{1'}$=CH_3, n=2
MC-3: $R_{1'}$=CH_3, n=3
MC-4: $R_{1'}$=CH_2CH_2OH, n=3

SCHEME 4-1: Spiropyrans **SP-1**, **SP-2**, **SP-3**, and **SP-4** showing key locations of functionalisation from a standard spiropyran core structure.

The spiropyrans **SP-1** to **SP-3** contained a methyl group on the indoline nitrogen ($R_{1'}$) which does not contribute to the ion binding. Further modification of this group provides an opportunity to alter the ion specificity of these sensors by either creating more ion binding sites or sterically restricting the ion binding region. Specifically, replacement of the methyl group of **SP-3** with an ethoxy moiety (**SP-4**) is expected to provide additional interaction between the positive metal ions and the hydroxyl group, altering the ion selectivity/affinity.

This chapter further investigates the metal ion binding properties of the spiropyran ionofluorophores **SP-1** and **SP-3** towards multivalent metal ions. The chapter is composed of two sections. In Section 4.2 the investigation of the ion binding and sensing of **SP-1** is presented with the aim to determine its sensitivity to a broader range of biological relevant ions than investigated in Chapter 3 and to look at the mechanism of binding. Section 2.3 then further investigates the sensing capabilities

of **SP-3**, providing comparisons to **SP-1** and to an N-ethoxy variant **SP-4,** in order to determine the best biological sensor for metal ions, in particular the calcium ion.

4.2 EXTENDED COMPARISON OF THE SELECTIVITY OF 1-AZA-12-CROWN-4 SPIROPYRAN (SP-1) TO DIVALENT METAL IONS

The metal ion sensing capacity of **SP-1**[†] toward a broader range of biologically relevant divalent cations was investigated in acetonitrile. The selectivity of this sensor was determined by comparing the ion induced absorbance and fluorescence response, then binding was further examined by investigating the dose specific response, ion binding ratio (by a Job's plot), as well as the photoswitchability in the presence of metal ions in order to better understand the ion sensing capabilities of this photoswitchable sensor.

4.2.1 RESULTS AND DISCUSSION

4.2.1.1 Absorbance, Fluorescence, and Metal Ion Selectivity of SP-1

The sensing selectivity of the spiropyran, **SP-1**, towards metal ions was investigated in acetonitrile by mixing the spiropyran with a selection of biologically relevant and other available metal salts, as described in Experimental Section 4.5.2. Acetonitrile was used as the solvent as it is able to dissolve the spiropyran and the perchlorate salts, and is a common solvent used within literature for the investigation of spiropyrans due to the increased stability of the mero-form.[8-13] Stock solutions containing vacuum dried (to remove H_2O contamination, which may influence photochromism) perchlorate salts of the alkali metals: lithium, sodium, potassium, caesium; alkaline earth metals: magnesium, calcium, strontium, barium; and transition metals: manganese, iron(II), cobalt, nickel, zinc, cadmium, and copper(II); and lead were prepared in acetonitrile. These ion solutions were separately mixed with the crowned spiropyran **SP-1** in an 100 fold excess of metal ions; this ensured saturation of **SP-1** with the metal ions.

The presence of the metal salts, in most incidents, produced an increase in absorbance in the visible region (Figure 4-2). This change in spectrum is an indicator of binding between the metal ion and **SP-1** and is associated with a metal

[†] Please note spiropyran **SP-1** (PAPER 2 (Chapters 3 and 4)) is not the same as spiropyran **SP1** (PAPER 1, PAPER 4 (Chapters 2, and 5)

ion induced thermal isomerisation from the spiropyran state to the merocyanine state.[14-16] More specifically, in the presence of the alkaline earth metals Ca^{2+}, Sr^{2+}, and Ba^{2+} there was an strong increase in the absorbance at around 365 nm and 395 nm for each complex, as well as the formation of a new ion dependent visible peak at around 520 nm, 525 nm and 535 nm, respectively, with intensities of around 0.41 a.u., 0.33 a.u., and 0.40 a.u. (Figure 4-2B). Mg^{2+} produced a much smaller and broader peak than Ca^{2+}, Sr^{2+}, and Ba^{2+} at around 510 nm with an intensity of 0.14 au.

In the presence of the transition and other metal ions, there was a large variation in the peak maximum and the peak shape depending on the metal ion. Pb^{2+} produced the largest increase in visible absorbance with a maximum absorbance hypsochromically shifted to around 495 nm (0.27 au) (Figure 4-2C). Ni^{2+}, Cd^{2+}, and Co^{2+} (as well as the already mentioned Mg^{2+}) showed broad spectra which indicated the presence of two peaks, suggesting that there could possibly be two different binding states within the system. Fe^{2+} and Cu^{2+} showed no change in absorbance in the visible region; however, both metals produced a difference in the UV absorbance with a slight increase observed at 400 nm for Fe^{2+}, and a decrease of the 365 nm and 400 nm peaks for Cu^{2+}.

The fluorescence (λ_{ex} = 532 nm) of each spiropyran complex showed a large increase in intensity in the **SP-1** complexes with Ca^{2+}, Sr^{2+}, and Ba^{2+} with maximums at around 625 nm, 625 nm and 630 nm, respectively, and similar intensities around 2700 RFU (Figure 4-3). A gradual increase in intensity as well as a bathochromic shift can be observed as metal size increased ($Ca^{2+} < Sr^{2+} < Ba^{2+}$). **SP-1-$Mg^{2+}$**, **SP-1-$Cd^{2+}$**, **SP-1-$Pb^{2+}$** all coincidently produced similar fluorescence spectra with a peak maximum at around 620 nm and intensity of 1300 RFU, approximately half as intense as the signal from the Ca^{2+}, Sr^{2+}, and Ba^{2+} complexes. Interestingly the other metal ion complexes (of Mn^{2+}, Co^{2+}, Ni^{2+} and Zn^{2+}) that showed similar overall absorbance intensity did not show a corresponding increase in fluorescence. Binding of the other metal ions produced a much lower fluorescence with the greatest being **SP-1-Li^{+}** (λ_{max} = 625 nm, 500 RFU), **SP-1-Zn^{2+}** (λ_{max} = 610 nm, 400 RFU) and **SP-1-Na^{+}** (λ_{max} = 645 nm, 300 RFU). These fluorescence results indicate that this spiropyran will be best used as a sensor for the divalent, alkaline earth metal ions Ca^{2+}, Sr^{2+}, and Ba^{2+} when in acetonitrile solutions. As the **SP-1** was designed

with a small crown ether ring this was not expected; as literature regarding similar spiropyrans only investigated/reported the binding of the spiropyrans to alkali metals, with this sized ring having a strong preference to Li^{+}.[14] Therefore it was reasoned that, either the binding of 2+ charged alkaline earth metals was either overlooked in these studies and **SP-1** prefers the more charge dense larger ions, or that perhaps these metals were binding to the spiropyran and triggering photoswitching differently, perhaps in a 2:1 spiropyran to metal complex (such as in Scheme 4-2 below). Therefore, the binding of these metals was further investigated with a Job's plot.

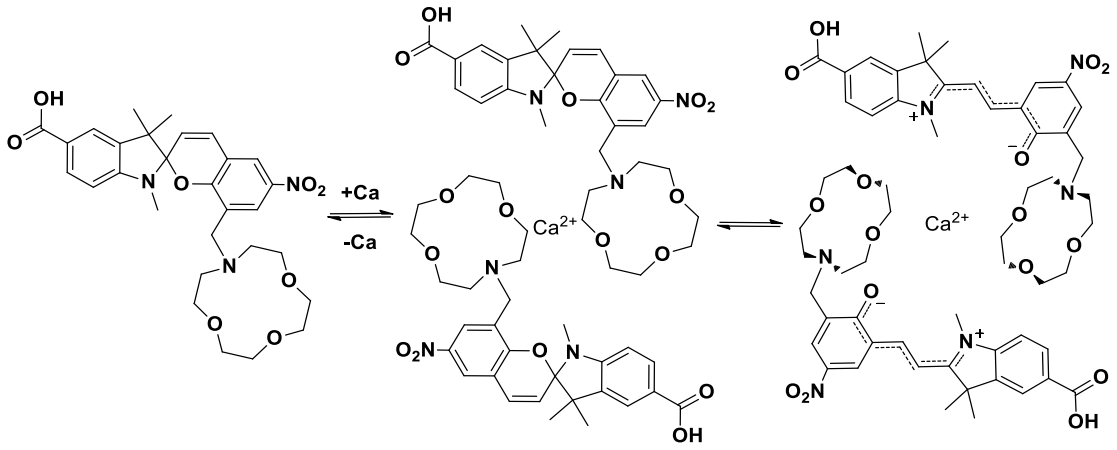

SCHEME 4-2: Possible binding of two **SP-1** molecules to Ca^{2+}.

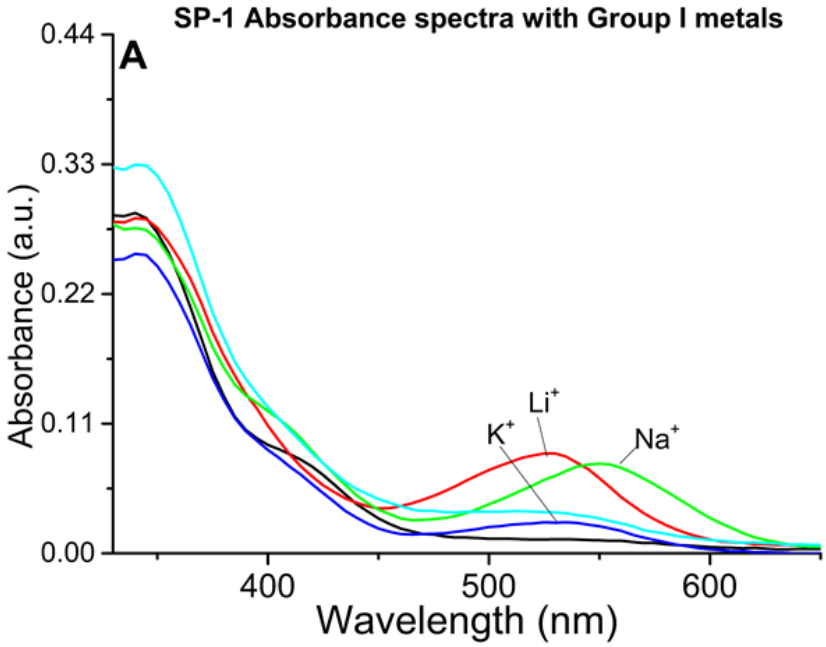
SP-1 Absorbance spectra with Group I metals
A
0.44
0.33
0.22
0.11
0.00
Absorbance (a.u.)
400
500
600
Wavelength (nm)
Li+
K+
Na+

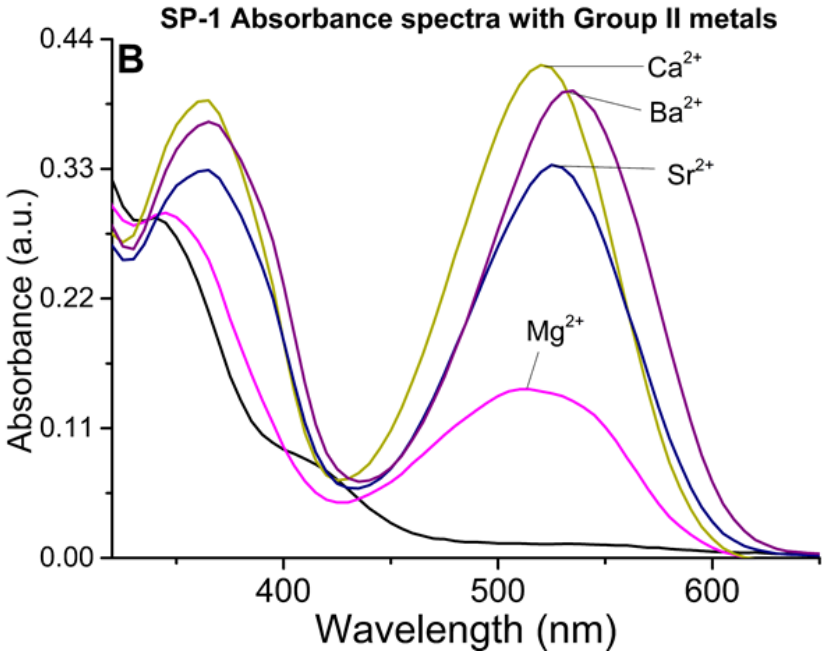
SP-1 Absorbance spectra with Group II metals
B
0.44
0.33
0.22
0.11
0.00
Absorbance (a.u.)
400
500
600
Wavelength (nm)
Ca2+
Ba2+
Sr2+
Mg2+

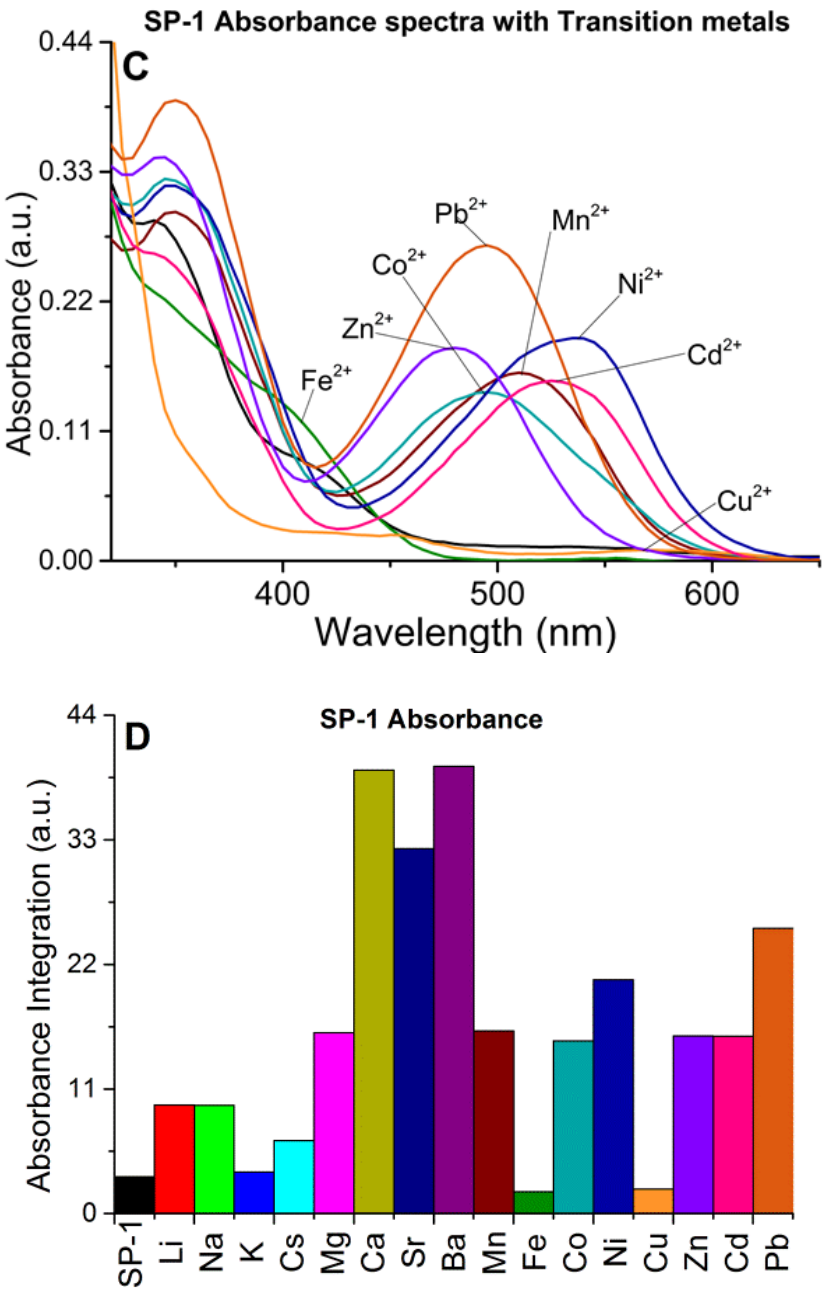

FIGURE 4-2: The absorbance spectra of **SP-1** (black) and in the presence of 100x excess metal perchlorates. A) alkali metals; B) alkaline earth metals; C) other metals; D) comparison absorbance integration between 425 and 650 nm.

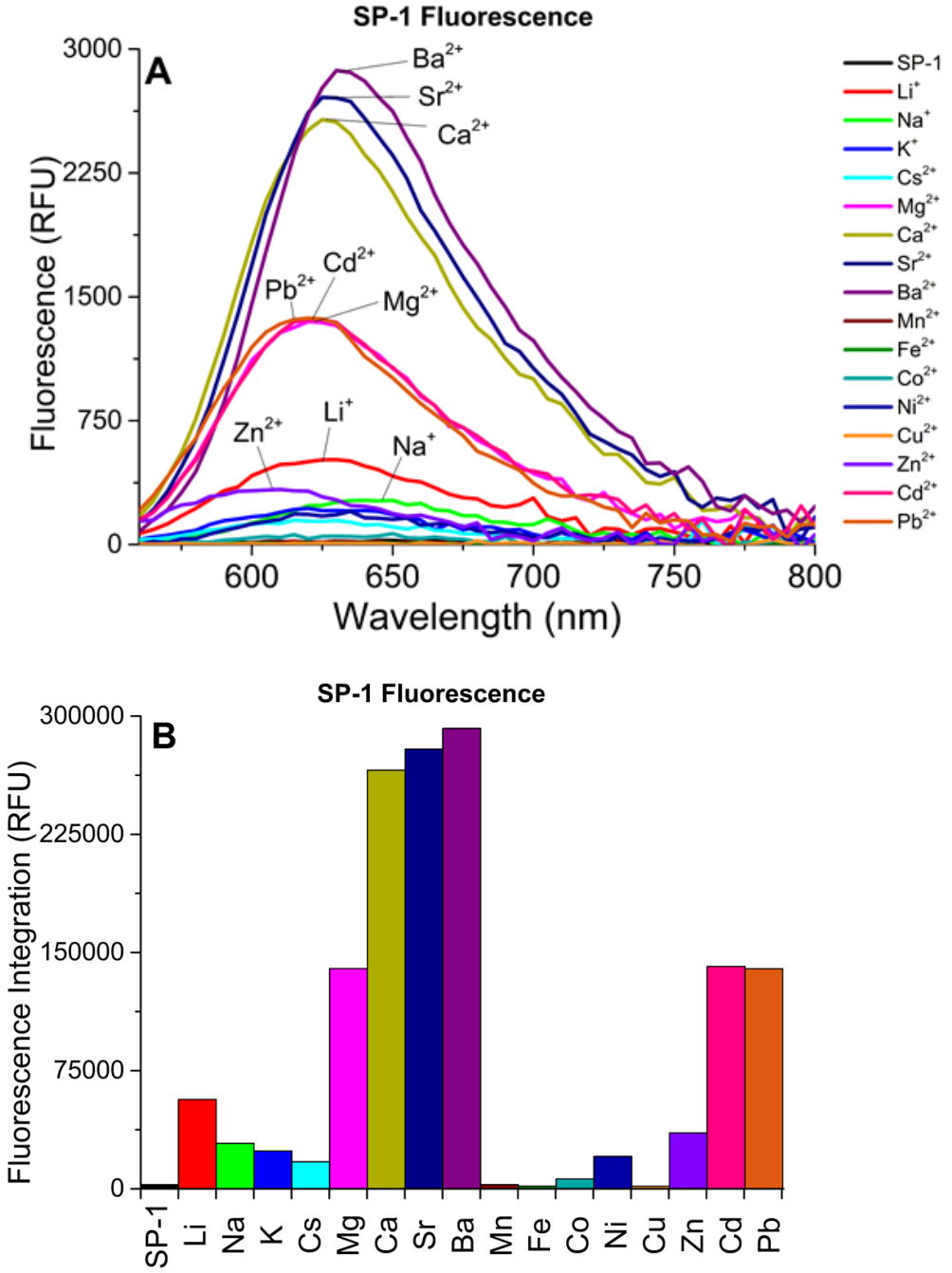

FIGURE 4-3: A) The fluorescence spectra of **SP-1** in the presence of 100x excess metal perchlorates. B) Comparison of the integrated fluorescence intensities.

4.2.1.2 Job's Plot

As mentioned, this small crown ether ring was expected to bind more dominantly to small monovalent metal ions, such as Li^{+}.[5, 14, 17-23] Therefore, we were interested in studying this binding interaction further to try and determine its mode of binding and ion induced thermoswitching. It was hypothesised that in the presence of the larger

metal ions, such as the alkaline earth metals and the transition metals (such as cadmium), the spiropyran would bind to the metal ion in a 2:1 ratio of spiropyran to metal ion. Whereas for the small metal ions, like lithium, the desired 1:1 binding will dominate. To test this, a Job's plot was performed of the systems of **SP-1** with Li^{+}, Ca^{2+}, and Cd^{2+}.

A Job's plot is a method of continuous variation to determine the binding stoichiometry between a host (H) and guest (G). That is, it is used to determine the ratio n:m for the reaction $n[H] + m[G] \rightarrow [H_nG_m]$. The assay is performed by maintaining a constant concentration (C) of host and guest while varying the relative concentrations of host and guest; *i.e.* [H] + [G] = C. It assumes that the host or the guest do not contribute to the absorbance or fluorescence signal. The absorbance or fluorescence of the solutions are then measured for a series of concentration ratios, and the signal intensity is plotted against the ratio of host to guest. By finding the ratio in which the maximum signal intensity is observed, the ideal ratio of host to guest is determined.

The stoichiometry of the reaction $n\mathbf{SP\text{-}1} + m\mathbf{M}^{+} \rightarrow \mathbf{SP\text{-}1}_n\mathbf{M}^{+}_m$ was determined by mixing **SP-1** in a 96 well plate with varying ratios of the metal ions Li^{+}, Ca^{2+}, and Cd^{2+}, as described experimental Section 4.5.2.2. Calcium and cadmium ions were selected for this investigation from the other metal ions that gave a fluorescent response because: they are both biologically relevant metals; calcium was the smallest of the three alkaline earth metals that gave the intense fluorescence response; and cadmium being the only transition metal to show a significant fluorescence response. The Job's plots showing the absorbance of the complexes with Ca^{2+} and Cd^{2+} is shown below in Figure 4-4; both the metal ion induced Job's plot and the Job's plot after forced photoswitching with 352 nm UV light is shown. In both cases the maximum absorbance occurs with solutions of between 60 % and 70 % **SP-1**, showing a clear 2:1 [**SP-1**] to [M^{2+}] ratio. Indicating that as hypothesised in the case of the divalent metals each metal ion is coordinating to two spiropyrans. Interestingly, for the solutions that were not exposed to UV light there appeared to be a lag period at very high spiropyran ratios; in which very little absorbance/fluorescence was observed in the sample with 9:1 spiropyran to metal ion. This lag was not observed after UV irradiation of the sample.

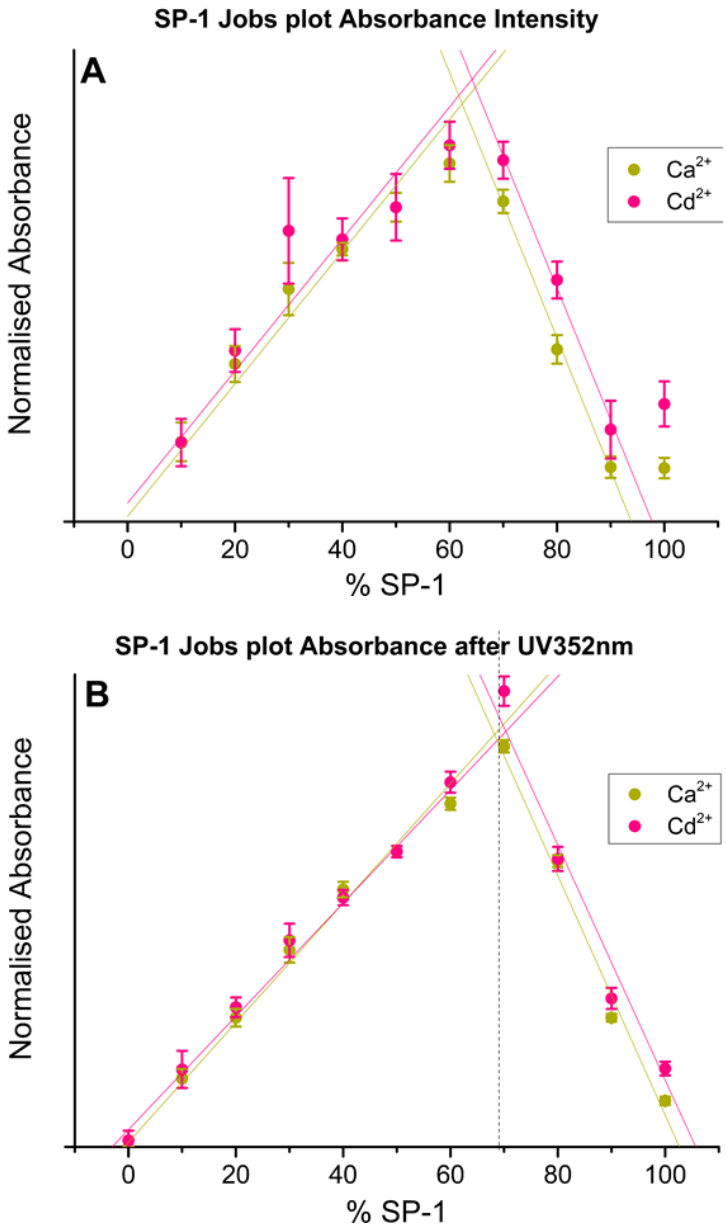

FIGURE 4-4: Job's plot showing the normalised absorbance intensity of the binding of **SP-1** to calcium (gold) and cadmium (pink): A) after mixing in the dark; B) after UV irradiation to the merocyanine state.

The fluorescence Job's plot of **SP-1** the presence of Li^+ (Shown previously in Figure 3-7) indicates that the binding ratio is closer to a 1:1 ratio than a 2:1 ratio, which matches the hypothesis that due to the size of the Li^+ it should bind well to 1-aza-12-crown-4 ring of **SP-1**. The lag at high **SP-1** to Li^+ ratios was also observed in this system.

These Job's plots confirm that there is a difference in the binding mechanism between Li^+ and the divalent metals Ca^{2+} and Cd^{2+}. This binding difference could be

utilised to change the selectivity of the **SP-1** system by changing its ability to coordinate metal ions in a 2:1 ratio. It has been shown that attaching fluorophores to a solid support greatly restricts its free movement, making it impossible/difficult to form multi-ligand complexes.[24] Therefore, by attaching **SP-1** to a solid MOF sensing platform its selectivity profile may be altered to favour Li^+ over other metal ions.

4.2.1.3 Concentration Dependence

The metal ion concentration dependent response of **SP-1** towards Li^+, Ca^{2+}, and Cd^{2+} ions was determined using the microplate reader; as described in Experimental Section 4.5.2.4. The experimental and results for the Li^+ response is discussed in Chapter 3,[25] the concentration dependent response with Ca^{2+} and Cd^{2+} is shown in Figure 4-5. The absorbance spectra showed a sigmoidal type increase with increasing metal ion concentrations up to 1-2 molar equivalents, then a reduced increase up to 10 equivalents (the maximum concentration investigated). The fluorescence intensities showed a similar response; however, the intensity for **SP-1** with the Cd^{2+} ion showed a reduced signal despite a similar absorption.

4.2.1.4 Photoswitching in the Presence of Metal Ions

To investigate and compare the photoswitchability of **SP-1** alone and in the presence of metal ions the photoswitch complexes were repetitively exposed to alternating UV or white light (Experimental Section 4.5.2.6). The assay was performed with **SP-1** (50 μM) with each of the metal ions Li^+, Na^+, K^+, Ba^{2+}, Sr^{2+}, Ca^{2+}, Mg^{2+}, Cd^{2+}, and Pb^{2+} at 50 μM and 5 mM to make a 1:1 or 1:100 ratio of **SP-1** to metal ion, respectively; the 1:1 ratio was used to determine if there was a greater turn-off in a less saturated system. Only one solution of each mixture was measured, rather than in triplet, to limit the time required to measure all solutions, thereby, reducing the influence of thermoswitching; as such, no errors could be determined. Five and a half complete switching cycles were observed with only a small decrease in well solution volume observed due to evaporation.

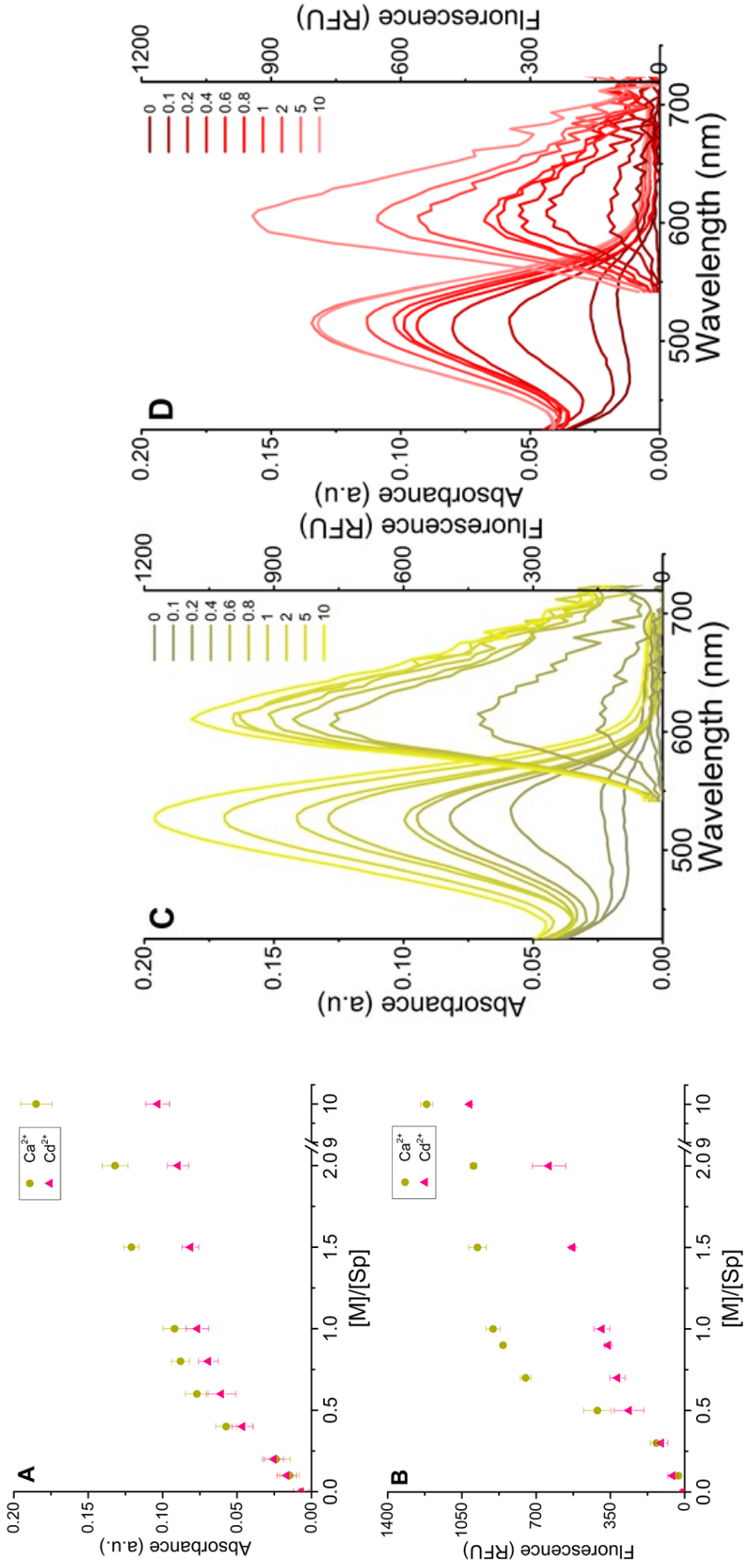

FIGURE 4-5: Concentration dependent signal response for **SP-1** with Ca^{2+} or Cd^{2+}. A) Comparative changes in absorbance (λmax = 540 nm); B) Comparative changes in Fluorescence (λmax = 627 nm); C) Spectral changes with increasing Ca^{2+} concentration (legend: equivalents Ca^{2+}); D) Spectral changes with increasing Cd^{2+} concentration.

Figure 4-6 shows the absorbance intensity (λ = 540 nm) after either 5 min UV352nm irradiation (ring opening) or 10 min white light irradiation (cyclisation) at each concentration ratio. The solutions of the 1:1 concentration ratio (Figure 4-6A) showed very different photoswitching profile compared to the 1:100 solutions (Figure 4-6B). At the 1:1 ratio **SP-1** with Mg^{2+}, Ca^{2+}, Sr^{2+}, and Ba^{2+} , (which showed the greatest absorbance intensity) showed similar changes in absorbance intensity due to photoswitching, with consistent and repeatable absorbance changes over the 5.5 cycles. In the presence of the other metal ions a reduced change in signal between each photocycle was observed.

In the 1:100 system there was a greater variation between the signal from the Mg^{2+}, Ca^{2+}, Sr^{2+}, and Ba^{2+} complexes, compared to the tight grouping of the signal intensities in the 1:1 system. As expected, due to the higher metal ion concentration, the starting intensities were higher in the 1:100 solutions; however, the changes associated with photoswitching were much smaller and the maximum intensities were similar to the UV switched 1:1 system (0.2 – 0.25 a.u.). This suggests that, due to the high concentration of metal ions, a greater proportion of **SP-1** is switched to the open form via a metal ion induced switching process. Therefore, upon UV switching (which forces the **SP-1** to the **MC-1** isomer) there is less photoswitching occurring and hence the smaller change in absorbance. This however, was not observed for the Li^{+} and Na^{+} system which still observed a large change in the signal in the 1:100 system, possibly suggesting a weaker metal ion induced switching effect in these monovalent systems. Another interesting observation in the 1:100 system is that the systems with Ca^{2+}, Sr^{2+}, Ba^{2+}, and Pb^{2+} initially showed negative chromism; where a decrease in the absorbance was observed after the first UV irradiation. For Sr^{2+} and Ba^{2+} this only occurred during the first cycle and for Ca^{2+} and Pb^{2+} lasted until the 4^{th} cycle when the expected normal photoswitching, of turn-on with UV and turn-off with white light, continued.

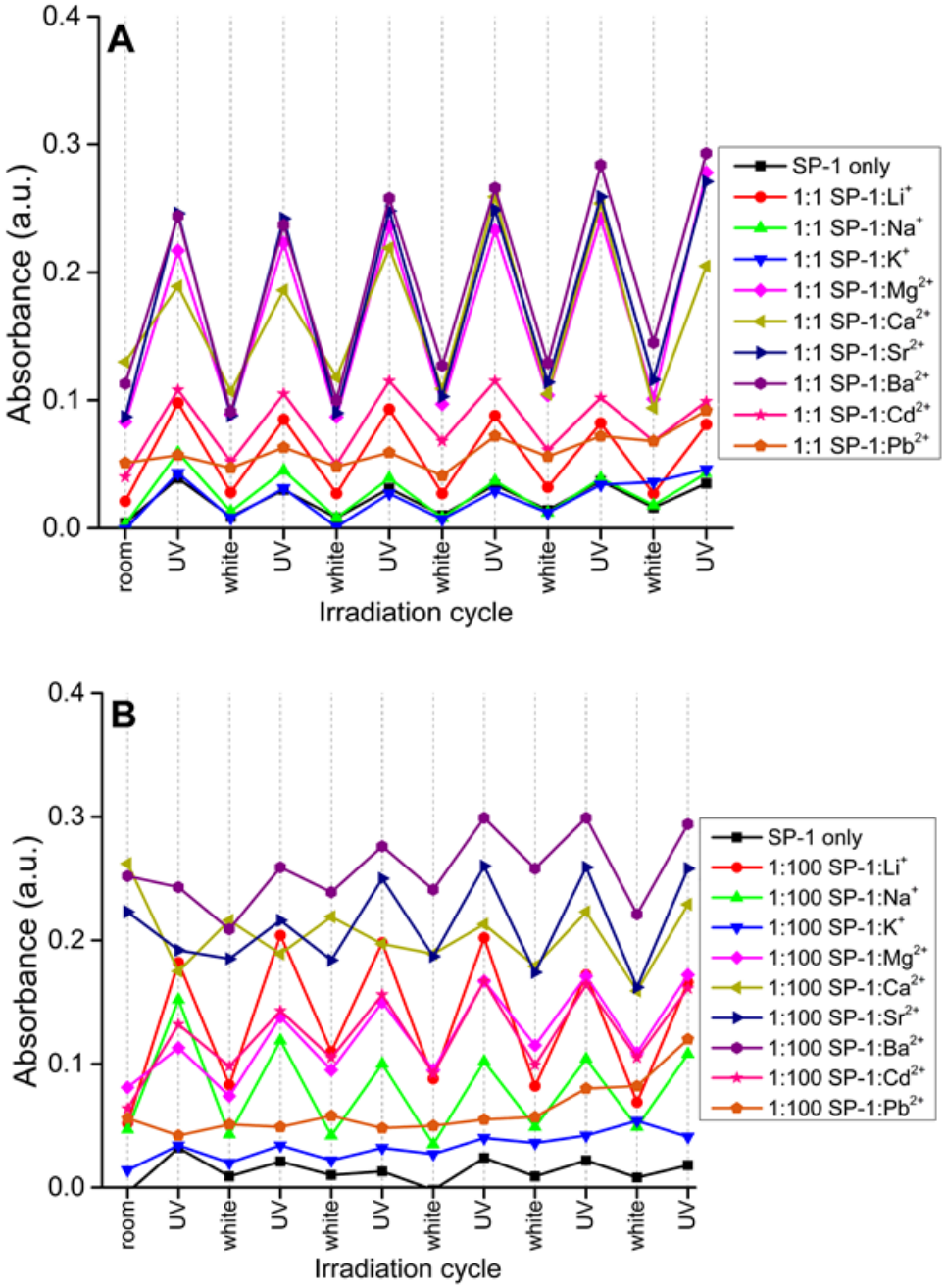

FIGURE 4-6: Photoswitching assay showing the absorbance of **SP-1** (black) and in A) equimolar (1:1) and B) excess (1:100) metal perchlorate salts of Li^{+}, Na^{+}, K^{+}, Ba^{2+}, Sr^{2+}, Ca^{2+}, Mg^{2+}, Cd^{2+}, and Pb^{2+}.

The fluorescence intensity (λ_{ex} = 532 nm, λ_{em} = 627 nm) changes upon photoswitching are shown in Figure 4-7. This was collected on the same plate as the absorbance data shortly after the absorbance was recorded; yet interestingly, exhibited several differences compared to the absorbance changes. Firstly, in the 1:1

system (Figure 4-7A), the alkaline earth metals (Mg^{2+}, Ca^{2+}, Sr^{2+}, and Ba^{2+}) showed the expected largest initial fluorescence intensity; however, unlike in the absorbance data, the intensity of fluorescence was not as tightly grouped, demonstrating that quantum yield of florescence is dependent on the **SP-1-M^{n+}** complex. Secondly, over the first 5.5 cycles the magnitude of the fluorescence intensity as well as the magnitude of the change due to switching decreased, where in the absorbance it increased. This decrease in signal was not observed in the presence of the other metal ions. This may have occurred due to either: solvent loss causing in increase in the concentration of the fluorophore, causing self-quenching of the fluorescence; or more likely, an artefact of the 2:1 binding stoichiometry affecting photoswitchability. Where initially there is a greater proportion of 2:1 complexes, but over time due to the forced switching with light, free merocyanine is able to trap/be trapped by the free ions in a 1:1 binding ratio, increasing the relative proportion of fluorophore bound in a 1:1 ratio and, due to a different quantum yield of fluorescence in the different binding state, producing a decrease in fluorescence while maintaining a high absorbance. This is possibly supported in the spectral changes observed in subsequent photocycling that was performed after an addition of more acetonitrile, where the intensity of the fluorescence is near identical to the other metal systems with 1:1 binding (not shown). To test this, a Job's plot after many switching cycles would need to be produced; which was not performed as part of this study.

In the 1:100 solutions (Figure 4-7B), the Ca^{2+}, Sr^{2+}, and Ba^{2+} solutions started saturated with a high fluorescence and, like the absorption spectra, little fluctuation was observed with photoswitching. The negative chromism for the first 1-3 cycles with Ca^{2+}, Sr^{2+}, Ba^{2+}, and Pb^{2+} was observed, as in the absorbance spectra.

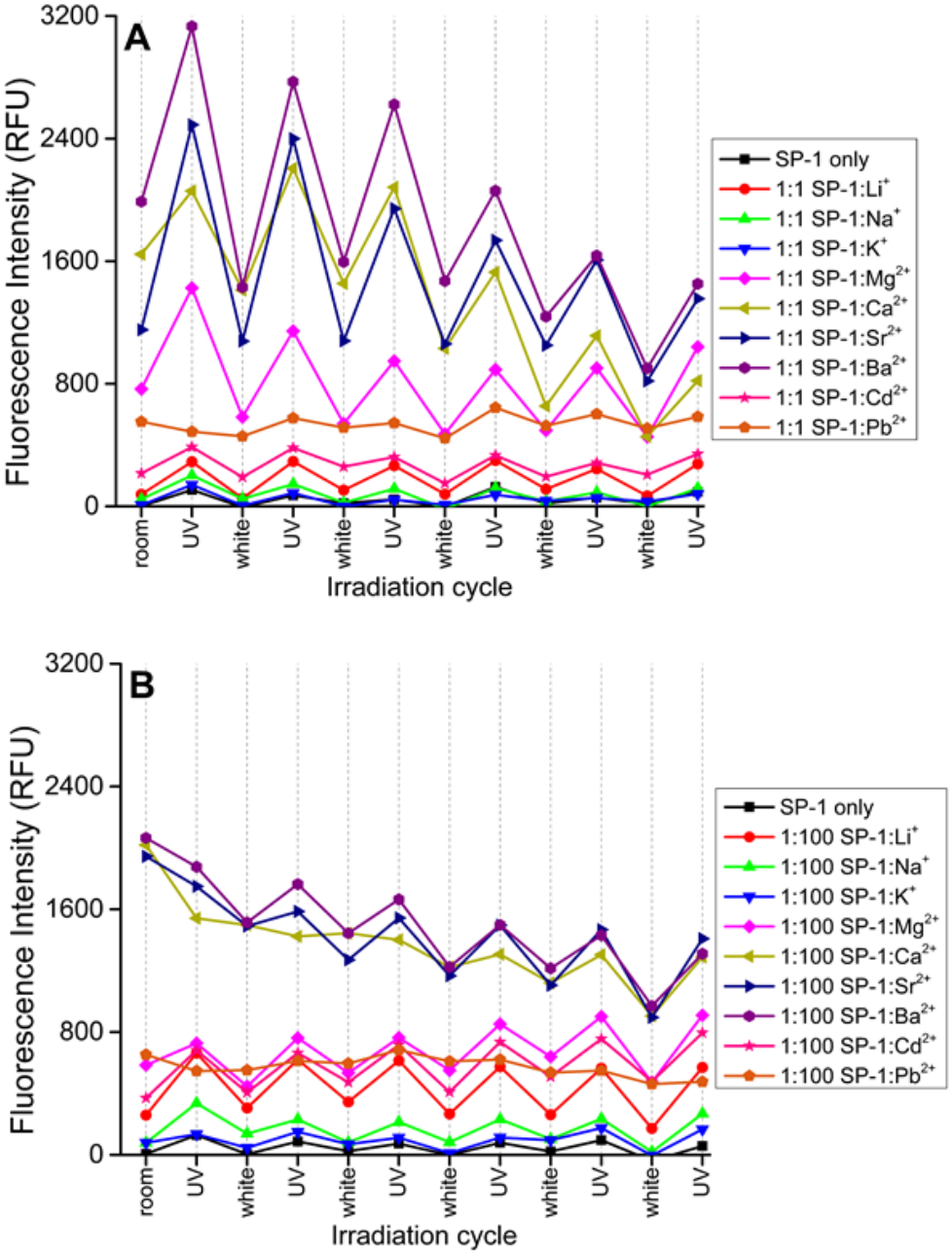

FIGURE 4-7: Photoswitching assay showing the Fluorescence of **SP-1** (black) and in equimolar (1:1) and excess (1:100) metal perchlorate salts of Li^{+}, Na^{+}, K^{+}, Ba^{2+}, Sr^{2+}, Ca^{2+}, Mg^{2+}, Cd^{2+} and Pb^{2+}.

4.2.2 CONCLUSIONS TO SECTION 4.2

A carboxylic acid functionalised 1-aza-12-crown-4 spiropyran (**SP-1**) was synthesised and its photoswitching in the presence of metal ion perchlorates in acetonitrile was investigated by observing changes in the absorbance and fluorescence properties. This spiropyran showed a strong binding response to the

divalent metal ions, in particular Ca^{2+}, Sr^{2+}, and Ba^{2+}. It was found that this was caused by a 2:1 spiropyran to metal ion binding mechanism, whereas Li^{+} bound in a 1:1 ratio. This 2:1 binding stoichiometry possibly has an influence on the ability to repeatedly switch these systems and get a repeatable signal for sensing. Ideally, for a fluorophore attached to a solid support, as would be desired for a MOF photoswitchable sensor, binding to the analyte would occur in a 1:1 ratio (due to the limited mobility of the fluorophore on the surface). Therefore, **SP-1** is not that suitable as a sensor for Ca^{2+} or other divalent metal ions. An alternate sensor design would be needed to provide improved selectivity for binding and sensing.

4.3 COMPARISON OF THE INFLUENCE OF A N-INDOLINE ETHOXY MOIETY ON SENSING METAL IONS BETWEEN SP-3 AND SP-4

Following on from the investigation of **SP-1** in Section 4.2 the larger crown ether spiropyran **SP-3** was similarly investigated regarding its selectivity to a series of biologically relevant metal ions. **SP-3** has a larger crown ether ring, and therefore it was hypothesised that **SP-3** will bind to divalent metals stronger than **SP-1**, possibly in the desired 1:1 binding ratio. The absorbance and fluorescence of **SP-3** was compared when in the presence of the alkali earth metal ions Mg^{2+}, Ca^{2+}, Sr^{2+}, and Ba^{2+}, as well as ions Mn^{2+}, Co^{2+}, Fe^{2+}, Ni^{2+}, Cu^{2+}, Zn^{2+}, Cd^{2+}, and Pb^{2+} in acetonitrile. The selectivity of this spiropyran was compared to a modified spiropyran fluorophore (**SP-4**) (Scheme 4-1), which was designed with an ethoxy substitution on the indoline nitrogen to further restrict and specialise the metal ion binding site. This modification may contribute to selectivity by either blocking the binding site, or by providing a lariat-type interaction (

Scheme 4-3). Therefore, two similar spiropyrans systems were designed based on the spiropyran aza-18-crown-6 scaffold with different indoline nitrogen functionalization in order to perform a structural affinity analysis comparing the two structures in order determine if the structural difference alters and improves selectivity between metal ions.

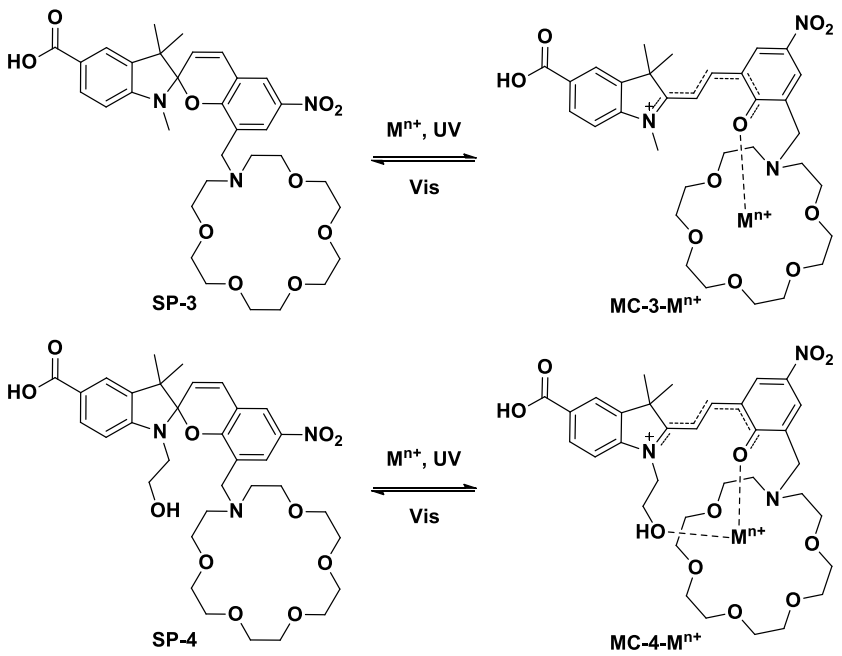

SCHEME 4-3: Proposed photoswitching and ion binding of **SP-3** and **SP-4**.

4.3.1 RESULTS AND DISCUSSION

4.3.1.1 Discussion of the Synthesis

The synthesis of **SP-3** was completed following a previously reported procedure for **SP-2** with the only modification being the usage of a larger aza-crowncrown ether ring. The synthesis for **SP-3** is presented in PAPER 2 (Section 3.2.5.2).[25] The synthesis for **SP-4** was performed based on this procedure and the reaction scheme is shown in Scheme 4-4. 4-Hydrazinobenzoic acid **4** was reacted with 2-methyl-2-butanone to give indoline **5**, which was alkylated with bromoethanol to give the ethoxyindole **14**. The aza-1-crown ether **9** was separately alkylated with the chloride **10** to give 3-methyl(aza-crown ether)-2-hydroxy-5-nitrobenzaldehyde **13**. A condensation reaction between the benzylaldehyde and the ethoxyindole **14** in refluxing ethanol, followed by purification by reverse-phase liquid chromatography gave the desired spiropyran **SP-4** in 25 % total yield. This low yield could be attributed to loss associated with two runs through reverse-phase chromatography. The purity of **SP-4** was confirmed by analytical RP-HPLC (Agilent Technologies 1260 Infinity system fitted with a Gemini-NX C18 110A 250 x 4.6mm column,

eluting at 10 % acetonitrile for 4 min followed by a gradient of 10-70 % acetonitrile in water with 0.1 % TFA over 15 min) with a single peak observed at 15.5 min (56 % acetonitrile).

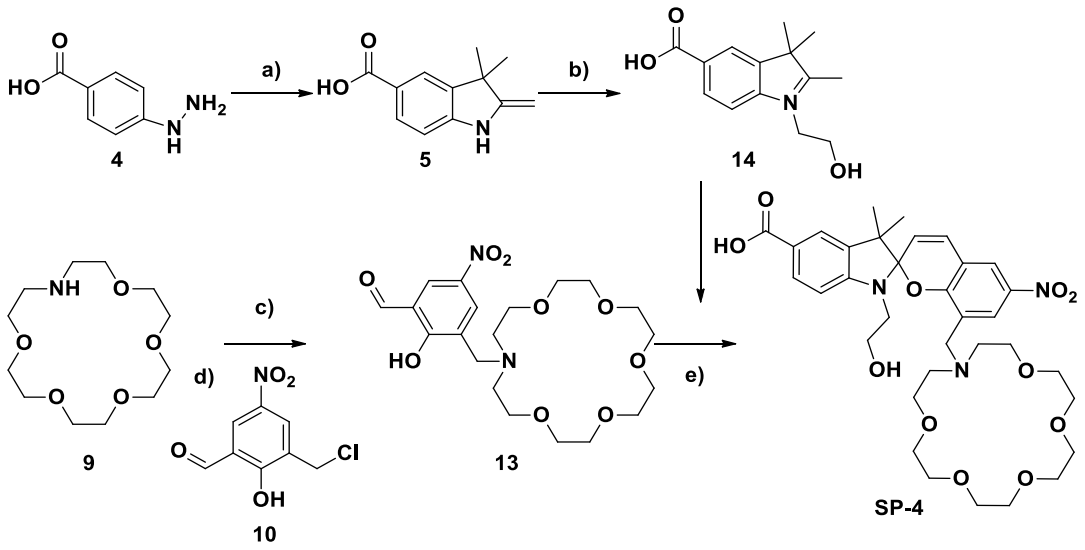

SCHEME 4-4: The reaction scheme for the synthesis of **SP-4**. a) 2-methyl-butanone, sulphuric acid, EtOH, 85 °C, 18 h, 73 %; b) bromoethanol, MeCN, 95 °C, 48 h; c) triethyl amine, THF, 0 °C, 1h; d) THF, 75 °C, 17 h; e) EtOH, 85 °C, 3 h, 25 % (from 5).‡

The structure was confirmed by HRMS and with ^{1}H and ^{13}C NMR. The ^{1}H NMR confirmed the high purity and showed the characteristic spiropyran alkene doublets at 7.21 ppm and 6.02 ppm, as well as the crown ether O-CH_2- protons between 3.18 and 3.66 ppm masking the N-ethoxy signals (Figure 4-8).

‡ Compound numbers are continued from PAPER 2 for clarity between the same compounds

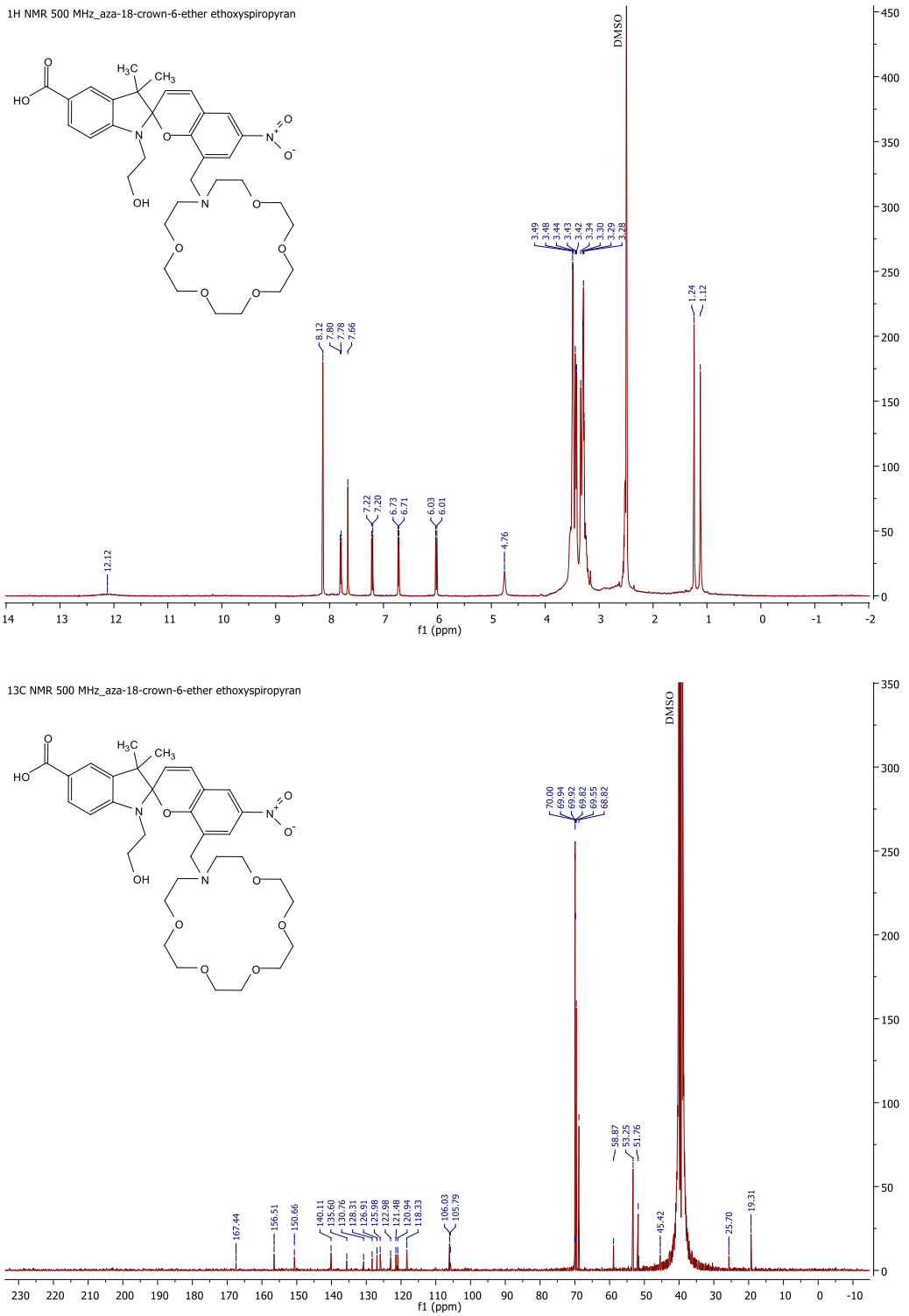

FIGURE 4-8: ^{1}H and ^{13}C NMR spectra of **SP-4**

4.3.1.2 Metal Ion Specificity Assay of Spiropyrans SP-3 and SP-4

To determine and compare the absorbance and fluorescence responses of the photoswitches **SP-3** and **SP-4** in the presence of biologically relevant metal ions, **SP-**

3 and **SP-4** were incubated in a series of salt solutions. Fifteen different perchlorate salts of different metals were first dried under reduced pressure to remove excess adsorbed water, which would alter the calculated concentration of the stock solutions as well as possibly influencing the photoswitching process. Metal salts to be investigated were selected based on their periodic group and biological relevance. They included Group 1 alkali metals: lithium, sodium and potassium; Group 2 alkaline earth metals: magnesium, calcium, strontium and barium; first row transition metals: manganese, iron, cobalt, nickel, copper, zinc; and other metals: cadmium and lead.

SP-3 was incubated with 100-fold excess metal perchlorates in HPLC grade acetonitrile (Section 4.5.2.1), and the UV-vis absorbance (Figure 4-9) and the fluorescence (λ_{ex} = 532 nm) spectra (Figure 4-10) were observed. There was a metal ion dependent spectral response to all the metals tested. The alkali metals showed a smaller response compared to the alkaline earth metals, with the strongest change associated with the lithium cation (as discussed in Chapter 3). The relatively large turn on of Li^+ over Na^+ is interesting because the lithium ion is not expected to have a strong interaction with the crown ether due to its relatively smaller size, and therefore ion binding and chromism may be occurring via another mechanism (possibly direct interaction with the spiropyran core).

The largest absorbance spectral increase occurred with the alkaline earth metals; with the largest turn-on observed for the **SP-3-Ca^{2+}** complex (λ_{max} = 535 nm, 0.7 au), then **SP-3-Sr^{2+}** (λ_{max} = 550 nm, 0.53 au) and **SP-3-Ba^{2+}** (λ_{max} = 545 nm, 0.33 au). As well as an increase in this major visible peak there was an increase in absorbance around 370 nm with a shoulder at 390 nm; this increase was observed previously for **SP-1** systems. **SP-3** complexes **SP-3-Mn^{2+}**, **SP-3-Co^{2+}**, and **SP-3-Ni^{2+}** all had a similar strength response of around 2.2 au, and **SP-3-Zn^{2+}** showed a weaker absorbance of 0.15 au. Interestingly, **SP-3-Fe^{2+}** and **SP-3-Cu^{2+}** and **SP-3-Cd^{2+}** showed very different spectra to the other complexes with no signal turn-on at 540 nm, and a new peak at 400 nm; this Cd^{2+} response is vastly different to the moderate-to-strong signal observed with **SP-1**. This clear difference between the sensing selectivity between Ca^{2+} and Cd^{2+} of **SP-3** and **SP-1** is interesting due to the similar biological

modes of action with these ions which leads to Cd^{2+} toxicity, as discussed in Appendix D, PAPER 3.

Of the other metals tested Pb^{2+} produced the largest absorbance change, with an increase in absorbance in the visible region around 490 nm, hypsochromically shifted compared to the group 2 metal complexes, and of intensity similar to **SP-3-Sr^{2+}**. The large shift for **SP-3-Pb^{2+}**, which was also observed in the **SP-1** and **SP-4** system, could be used in the targeted sensing of Pb^{2+} using these fluoroionophores; the selectivity for Pb^{2+} over other transition metal ions is greater in the **SP-3** system, and even greater in the **SP-4** system compared to with **SP-1**.

The fluorescence of the **SP-3** and **SP-4** metal complexes is shown in Figure 4-10. Compared to the absorbance signal, the increase in the fluorescence of **SP-3-Ca^{2+}** and **SP-3-Sr^{2+}** was much greater than the other ion complexes; both complexes showed a large fluorescence signal with peaks at 625 nm and 635 nm, respectively, and at the same intensity of around 5000 RFU. **SP-3-Mg^{2+}** and **SP-3-Ba^{2+}** both showed a reduced signal with intensities around 1500 RFU and peak emissions at 620 nm and 645 nm, respectively, and therefore are very distinguishable. This similar intensity for the **SP-3-Mg^{2+}** and **SP-3-Ba^{2+}** complexes contrasts the absorbance spectra in which the absorbance with Ba^{2+} was twice as intense as with Mg^{2+}. **SP-3-Pb^{2+}** also produced a moderate fluorescence increase with a peak at 520 nm; however, due to the shifted absorbance transition, **SP-3-Pb^{2+}** was not excited at the optimal wavelength. A comparatively much smaller fluorescence signal was observed for the **SP-3** complexes with Li^{+}, Na^{+}, Mn^{2+}, Ni^{2+} and Zn^{2+}, and no signal for the other metal complexes of K^{+}, Fe^{2+}, Co^{2+}, Cu^{2+}, and Cd^{2+}.

SP-4, with the N-ethoxy structural difference, produced a very similar response to that of **SP-3** with the absorbance spectra being almost identical for the alkali earth metals and Pb^{2+}. The main difference was observed in the spectra of **SP-4** with Fe^{2+}, Cu^{2+}, and Cd^{2+}, as well as an apparent reduced affinity towards the transition metal ions. Fe^{2+} and Cd^{2+} caused no increase in absorbance, and Cu^{2+} produced a broad peak with local maximums around 500 nm, 400 nm and 360 nm. The integrated fluorescence intensity of the **SP-4-Ba^{2+}** complex was twice as bright as that of **SP-4-Mg^{2+}**, despite the very similar absorbance intensity. This selectivity data implies that

the extra hydroxyl group could be helping to exclude all the metals with weak binding. However, the increase in the **SP-4-Ba^{2+}** fluorescence could be because the Ba^{2+}, which would normally be too big to fit in the crown properly, is being held there by the extra hydroxyl group. Mg^{2+} Ca^{2+} and Sr^{2+} possibly remain unaffected because they have strong bonding, but are too small to be effected by the hydroxyl group.

Computational modelling of the binding of the metal ions to **SP-4** in a 1:1 ratio show that the proton on the ethoxy -OH hydrogen bonds to the merocyanine phenolate. Also, that the ethyl hydroxy is possibly too far away to have any interaction with most metals within the crown ether ring (Appendix C, Figure C-2). However, for the larger metal ions (Ba^{2+} and Sr^{2+}) the hydroxyl is close to the metal centre, therefore could contribute to the increased binding affinity (fluorescence signal) of barium over the methyl derivative. By altering the length of the alkyl chain, and therefore the proximity of the hydroxyl group to the ion binding site, the hydroxyl group may have a greater impact on ion binding ability and produce a more favourable spiropyran photoswitchable sensor.

4.3.1.3 Ion Affinity Assays

The spiropyrans **SP-3** and **SP-4** were then further investigated in the presence of the alkaline earth metals ions, calcium, strontium, and barium (which showed the greatest binding response). The concentration dependent responses (obtained as described above in Section 4.5.2.5) of the absorbance and fluorescence was obtained, and the spectra and changes in peak signal intensity for each system is compared in Figure 4-11 and Figure 4-12, respectively. These assays show a sigmoidal increase in the absorbance and fluorescence signal of **SP-3** and **SP-4** with increasing metal ion concentration. Maximum signal intensities were achieved at approximately a 1:1 ratio of spiropyran to metal ion. **SP-3** appears to have a stronger binding affinity than **SP-4**, reflected in a stronger signal turn-on at lower metal ion concentrations.

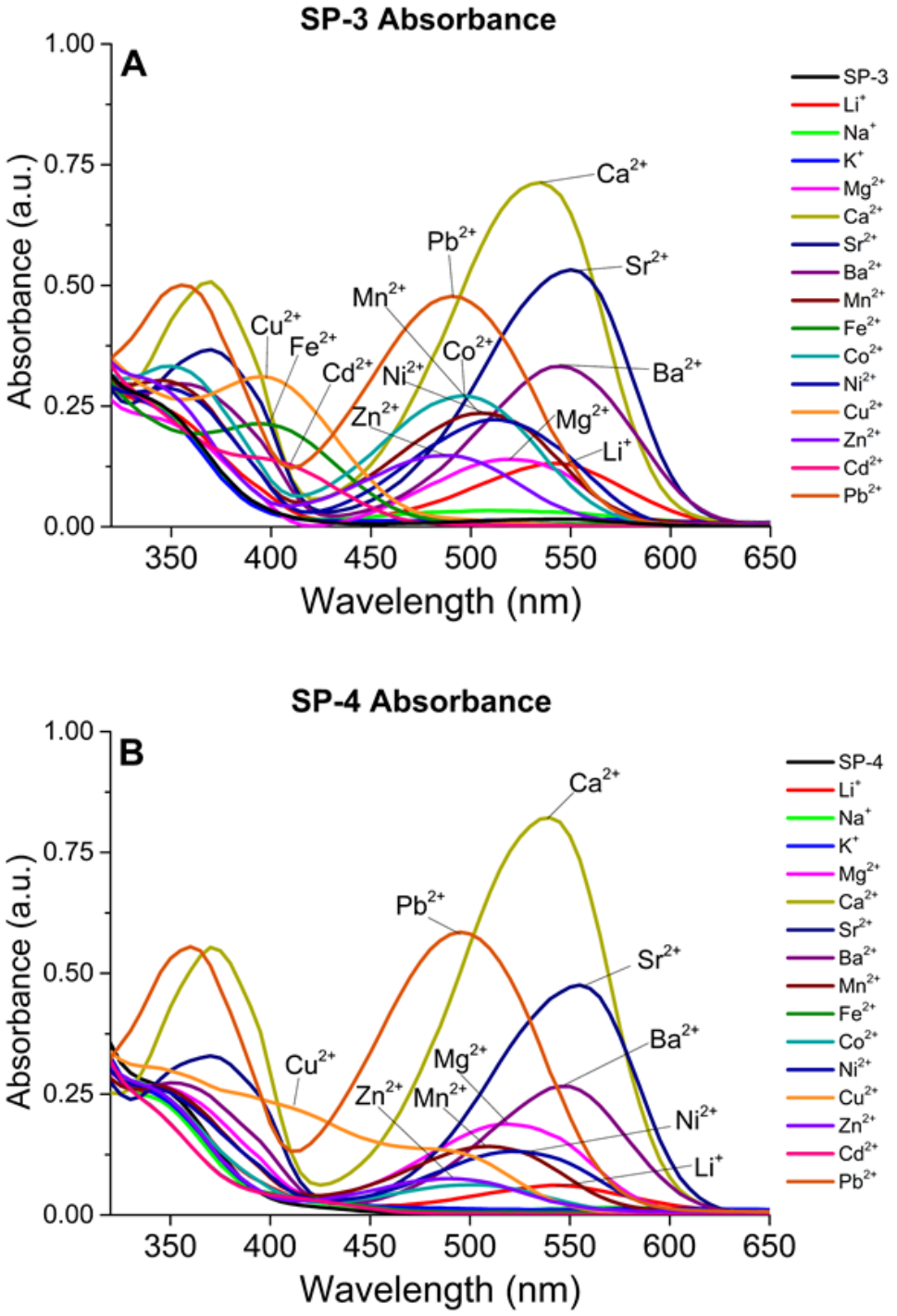
SP-3 Absorbance
A
Absorbance (a.u.)
Wavelength (nm)
1.00
0.75
0.50
0.25
0.00
350
400
450
500
550
600
650
SP-3
Li+
Na+
K+
Mg2+
Ca2+
Sr2+
Ba2+
Mn2+
Fe2+
Co2+
Ni2+
Cu2+
Zn2+
Cd2+
Pb2+
Ca2+
Pb2+
Sr2+
Mn2+
Cu2+
Fe2+
Cd2+
Co2+
Ni2+
Ba2+
Zn2+
Mg2+
Li+

SP-4 Absorbance
B
Absorbance (a.u.)
Wavelength (nm)
1.00
0.75
0.50
0.25
0.00
350
400
450
500
550
600
650
SP-4
Li+
Na+
K+
Mg2+
Ca2+
Sr2+
Ba2+
Mn2+
Fe2+
Co2+
Ni2+
Cu2+
Zn2+
Cd2+
Pb2+
Ca2+
Pb2+
Sr2+
Ba2+
Cu2+
Mg2+
Zn2+
Mn2+
Ni2+
Li+

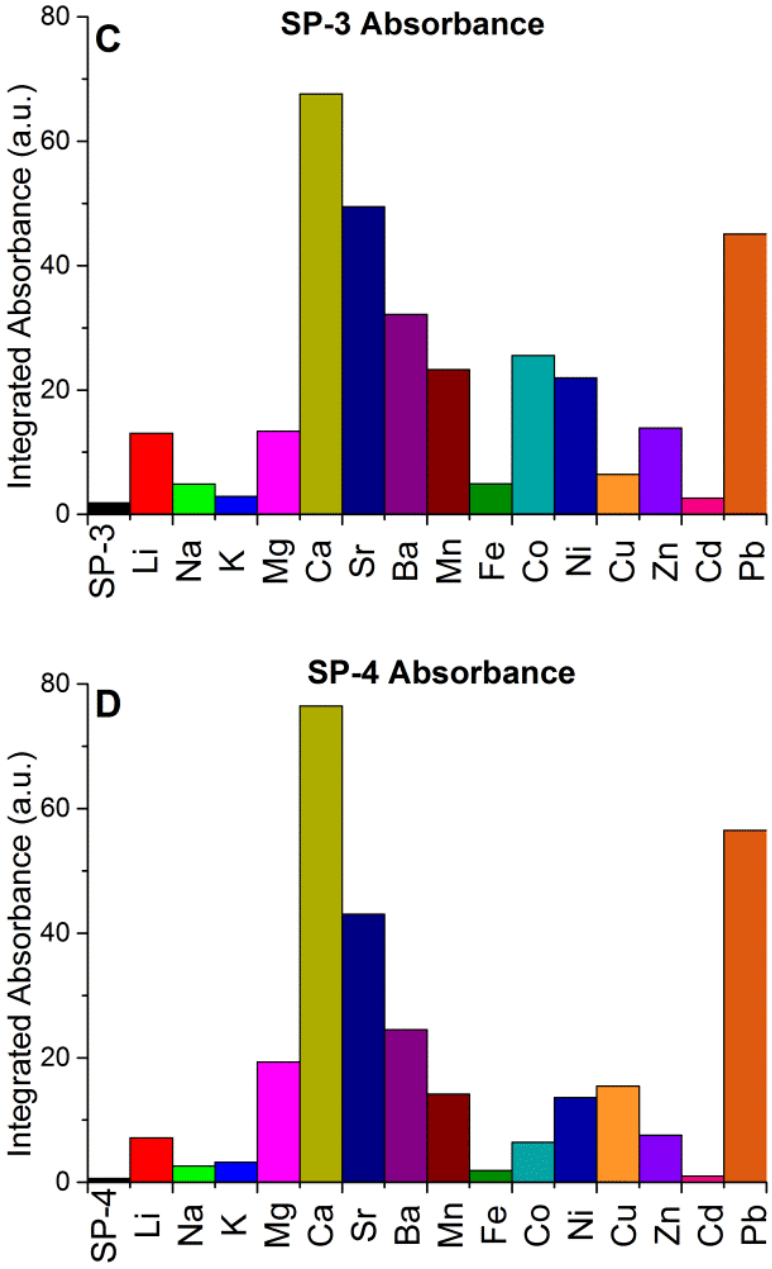

FIGURE 4-9: Absorbance spectra of **SP-3** and **SP-4** in the presence of metal ions in acetonitrile. A) **SP-3** spectra; B) **SP-4** spectra; C) **SP-3** integrated absorption between 425 and 650 nm; D) **SP-4** integrated absorption between 425 and 650 nm.

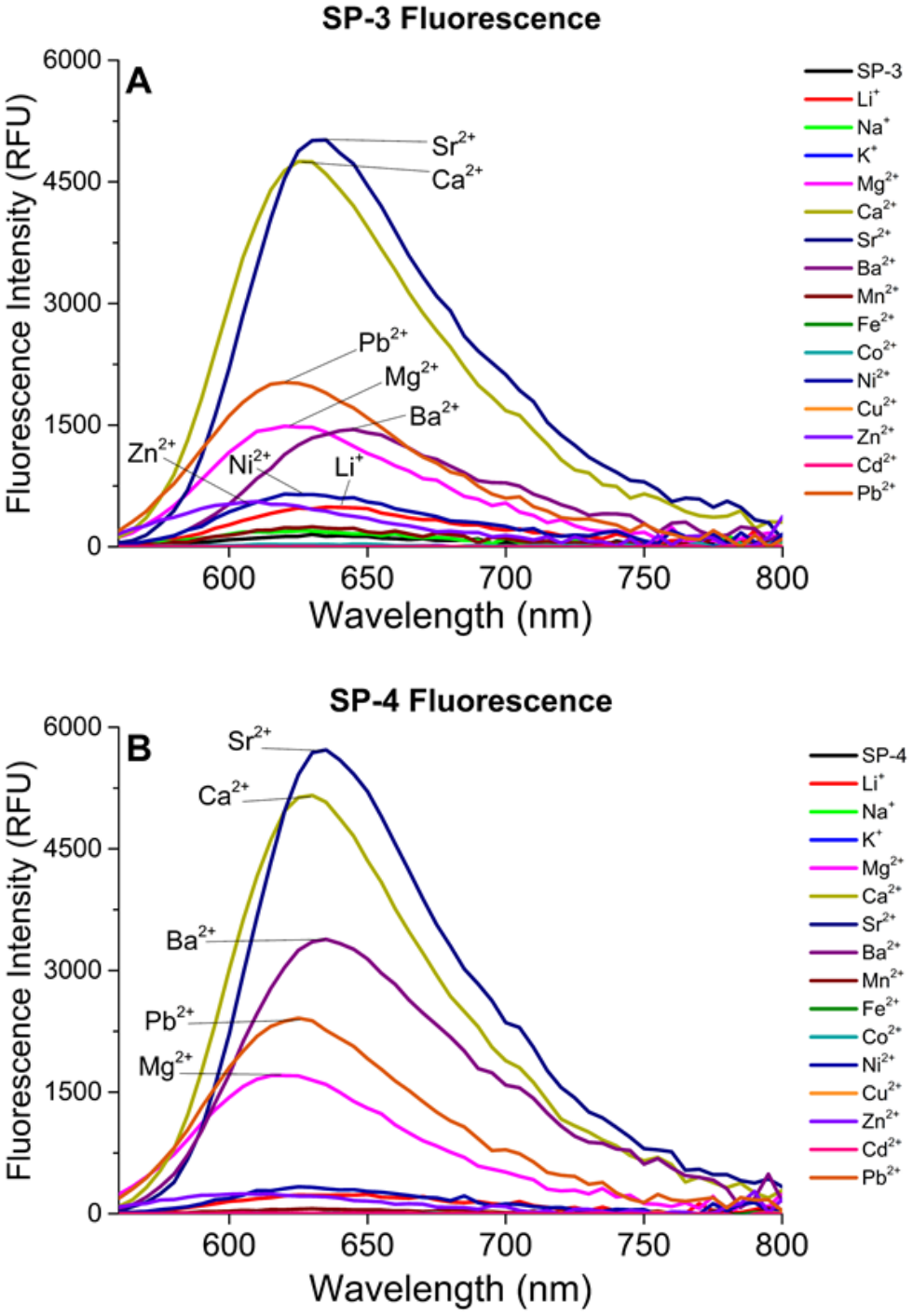
SP-3 Fluorescence
A
Fluorescence Intensity (RFU)
Wavelength (nm)
Sr2+
Ca2+
Pb2+
Mg2+
Ba2+
Zn2+
Ni2+
Li+
SP-3
Li+
Na+
K+
Mg2+
Ca2+
Sr2+
Ba2+
Mn2+
Fe2+
Co2+
Ni2+
Cu2+
Zn2+
Cd2+
Pb2+
SP-4 Fluorescence
B
Fluorescence Intensity (RFU)
Wavelength (nm)
Sr2+
Ca2+
Ba2+
Pb2+
Mg2+
SP-4
Li+
Na+
K+
Mg2+
Ca2+
Sr2+
Ba2+
Mn2+
Fe2+
Co2+
Ni2+
Cu2+
Zn2+
Cd2+
Pb2+

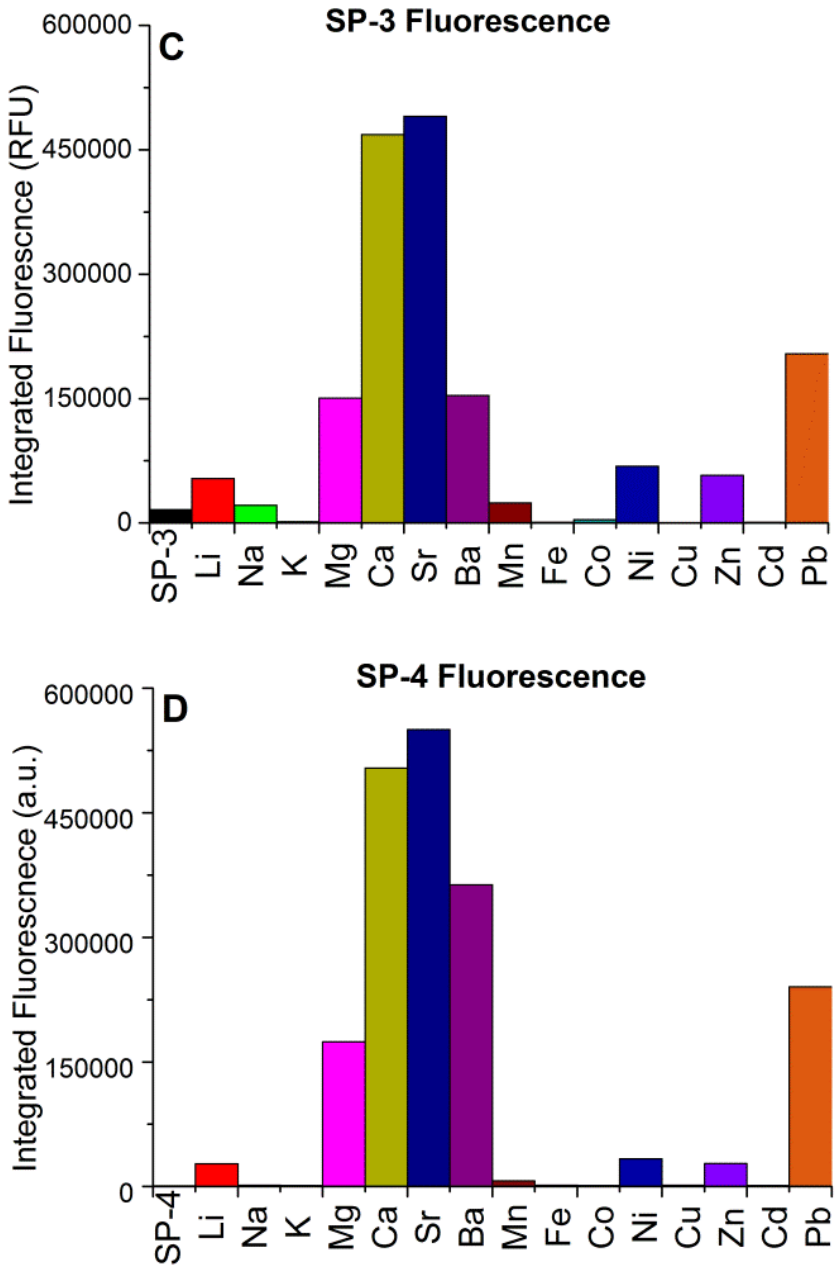

FIGURE 4-10: Fluorescence spectra of **SP-3** and **SP-4** after excitation with 532 nm: A) **SP-3** spectra; B) **SP-4** spectra; C) **SP-3** integrated intensity; D) **SP-4** integrated intensity.

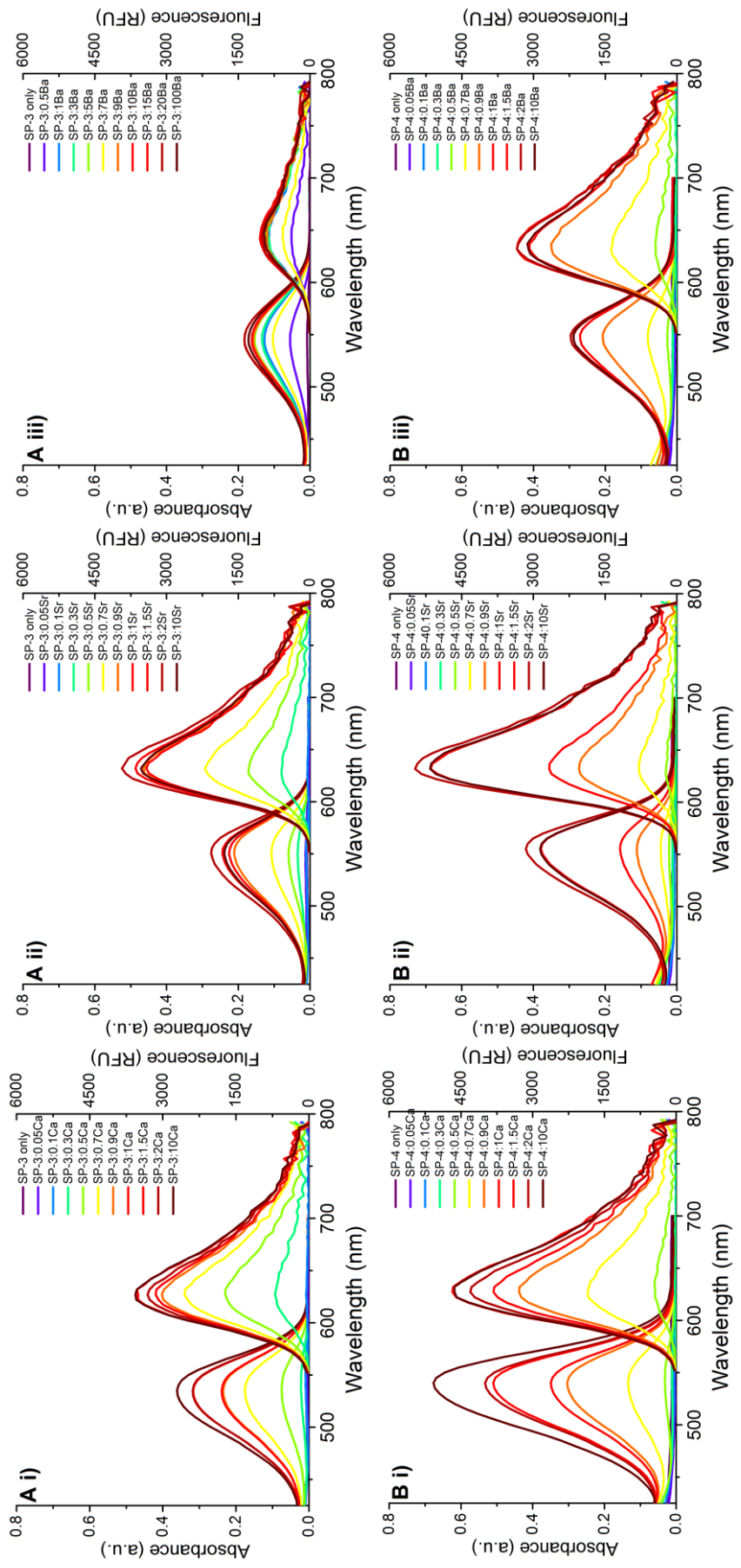

FIGURE 4-11: Concentration dependent spectral changes for A) **SP-3** and B) **SP-4** (50 μM) mixed with increasing concentrations of metal ions i) Ca^{2+}, ii) Sr^{2+}, iii) Ba^{2+} in acetonitrile at 25 °C in ambient conditions.

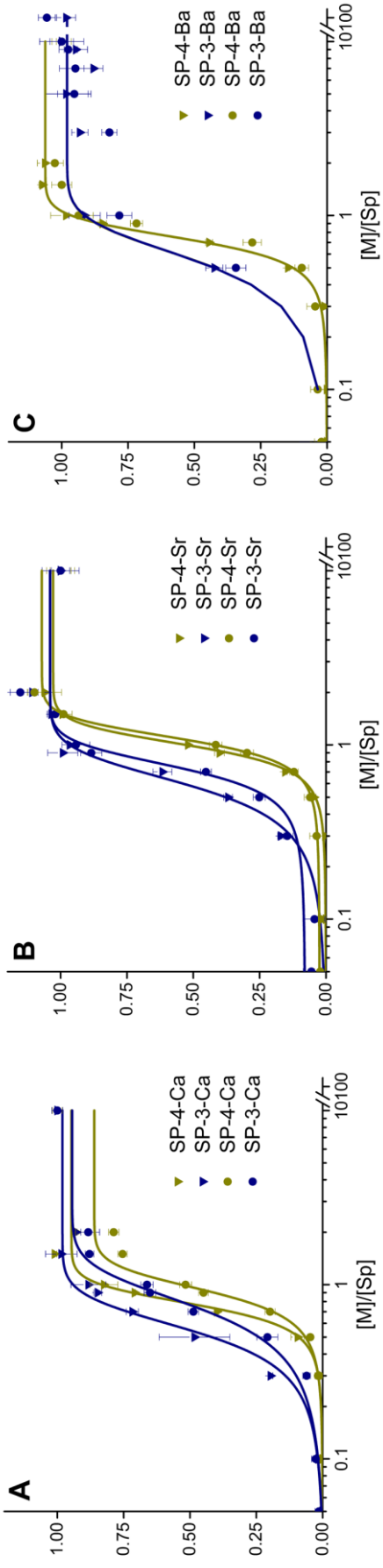

FIGURE 4-12: Relative peak absorption (circle) and fluorescence (triangle) intensity of **SP-3** (blue) and **SP-4** (gold) at different concentrations of metal ions A) Ca^{2+}, B) Sr^{2+}, and C) Ba^{2+} in acetonitrile at 25 °C in ambient conditions. The fitted lines were calculated from a Boltzmann distribution function.

4.3.1.4 Job's Plot

A Job's plot was performed for the **SP-3** and **SP-4** systems with calcium, strontium and barium ions to determine the binding ratio of photoswitch to metal ion, and to determine if the metal ions bind to each of the photoswitches in the same ratio (and therefore by a similar mechanism). The resulting Job's plots of the fluorescence before and after exposure to UV352nm light is shown in Figure 4-13.

The Job's plots for these systems gave an unusual profile as to what is usually observed for Job's plots;[27] the possible reasons for this are discussed later below. At low spiropyran to metal ion ratios (*i.e.* in excess metal ion) a standard linear increase in the absorbance and fluorescence intensities is observed. However, at high spiropyran to metal ion ratios (mole fraction greater than 0.5) a single linear decrease was not observed, instead there appeared to be two different rates of signal decrease; this was more obvious in the absorbance Job's plots (not shown). In both the **SP-3** and **SP-4** systems a 1:1 binding stoichiometry was observed with the maximum signal occurring at mole fraction of 0.5. This is different to the 2:1 binding observed in the **SP-1** system (Section 4.2.1.2), confirming a difference in the metal complexation between the smaller crown ether spiropyran system and the larger crown ether spiropyrans.

After UV irradiation to shift the equilibrium to the open merocyanine state (**MC-3** and **MC-4**), the **SP-3** systems showed a different behaviour. The **MC-3** Job's plot indicated a change in the binding ratio to a 2:1 binding stoichiometry, which was maintained after subsequent white light irradiation. Whereas, the Ca^{2+}, Ba^{2+}, and Sr^{2+} metal ion binding stoichiometry to **SP-4** remained unchanged after UV irradiation and subsequent white light irradiation. This suggests that the spiropyran isomer may be only able to bind to free metal ions; however, under UV light the unbound **SP-3** is able to photoswitch to the merocyanine isomer, which is able to bind to the existing **MC-3-M^{2+}** complex. The ethoxy substitution in **SP-4** disrupts the 2:1 binding, thereby making it less favourable.

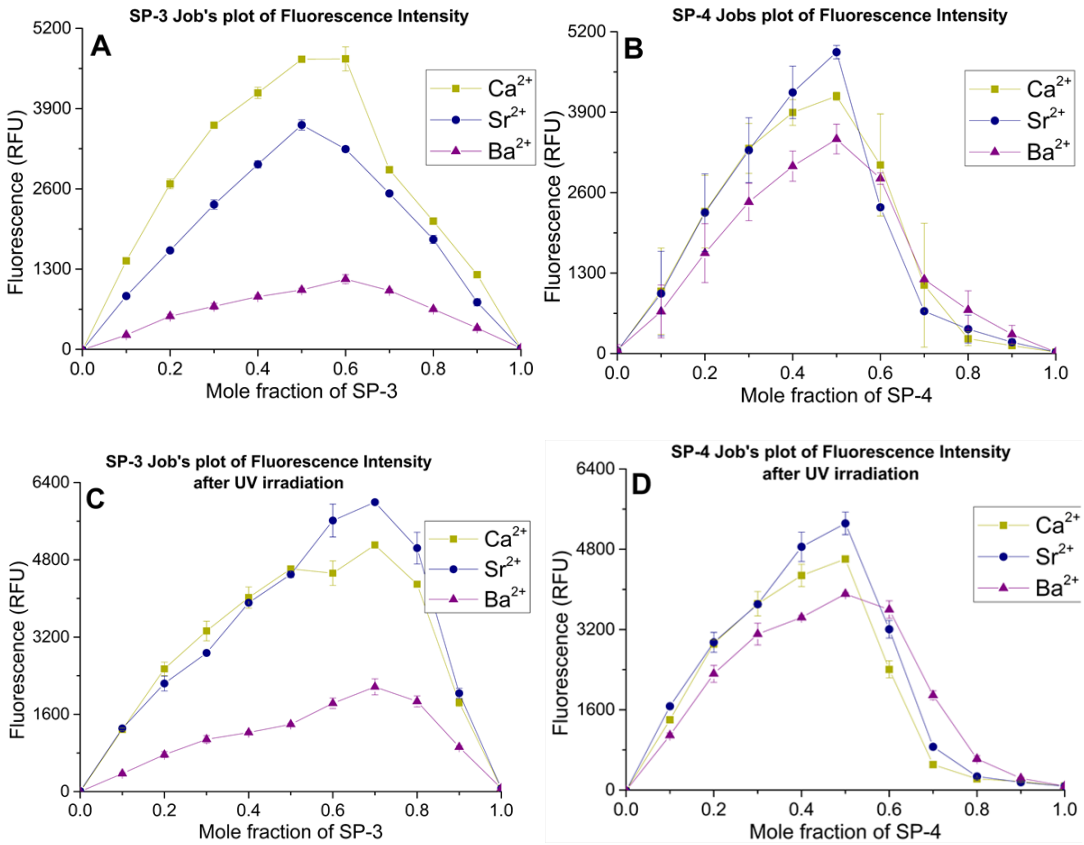

FIGURE 4-13: Job's plots of spiropyrans **SP-3** (left) and **SP-4** (right) with Ca^{2+} (gold), Sr^{2+} (navy), and Ba^{2+} (purple) showing both before (top) and after (bottom) irradiation with UV light for 10 min.

The unusual Job's plots obtained in this system is possibly due to the complex binding kinetics that can occur with spiropyran sensors, which are not generally observed with conventional metal ion chelators. The reaction scheme of a spiropyran capable of binding in a 1:1 and 2:1 stoichiometry with a metal ion is shown in Scheme 4-5. Unlike conventional binding systems, in which the observed signal arises purely from the desired binding interaction, the presence of the absorbing/fluorescing merocyanine isomer can arise from light and thermal processes, and therefore, there is always some population of the merocyanine form present. Scheme 4-5 shows that in a 2:1 binding system that there are conceivably seven different spiropyran/merocyanine species present, four of which contain the fluorescent merocyanine species; and, as the ion interactions are different in each of these states the influence on fluorescence is likely to differ, creating different fluorescence spectra and yields.

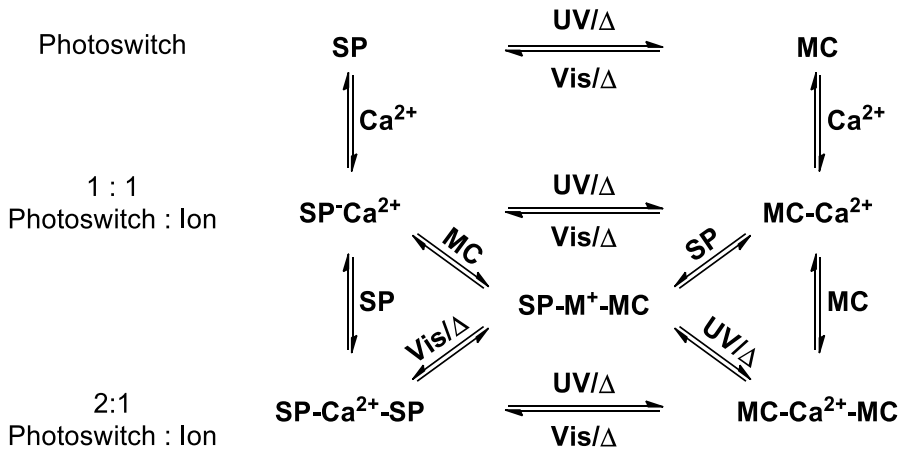

SCHEME 4-5: All of the possible equilibrium process that can occur with a spiropyran system that can interact with Ca^{2+} metal ions in a 2:1 binding ratio.

This highlights one of the main problems with using spiropyrans as photoswitchable metal ion sensors. In the ideal sensing scenario, the photochromic system is always in a known conformational state that is modulated by only one input, light. However, with spiropyran photoswitches other factors influence the state of photochromism; such as, temperature influencing rates of conversion to the lowest energy conformation; or solvent polarity influencing the energy barriers between conformations and which conformation is more thermally stable; or ion binding itself having an influence on photochromism, with the binding of a metal ion to spiropyran causing thermal switching to the merocyanine form. This dictates that for some spiropyran systems the sensing ability of the molecule isn't 'turned-on' by photoswitching but by metal ion induced thermoswitching. This can still be advantageous in photoreversible metal ion sensing, as it may be still possible to force the complex back into the unbound, 'off', spiropyran form with the appropriate white light. This will still enable the photoswitch to be actively reset, which is what is desired in a reversible ion sensor. This is also advantageous for biological sensing due to elimination of the need for hazardous UV light. As such, the photoreversibility of these systems needs to be examined.

4.3.1.5 Photoswitching Assays

In this section the spectral changes associated with photoswitching and the repeatability of the photoswitching of the spiropyrans **SP-3** and **SP-4** in the presence

of excess of metal ions is investigated. Irradiation with UV light is expected to promote ring opening to the coloured fluorescent merocyanine isomer, increasing ion affinity and spectral response, and white light is expected to promote ring closing, reducing the ion affinity and absorbance and fluorescence intensity. As already evident in the previously discussed assays the presence of metal ion alone causes switching to the coloured merocyanine. For use as a photochromic sensor, control of this ion binding process with light is required.

Photoswitching was performed on two occasions using two different UV light wavelengths; from a 352 nm black light (UV352nm) or a 254 nm germicidal lamp (UV254nm). This was done to investigate the difference between the two light sources, as the photoswitch-ion complexes have an absorbance peak at 350 nm which could competitively absorb the UV352nm light, possibly altering the influence of the UV light on the photostationary state. Ultraviolet irradiation was performed in the assay tray with the plastic cover slip removed to reduce scattering and absorption of the UV light by the plastic, this however allowed for evaporation of the solution. For full experimental see Section 4.5.2 below.

UV352nm photoswitching assay

In the absence of metal ions exposure of solutions of **SP-3** and **SP-4** to UV352nm light caused the formation of an absorbance peak at around 550 nm as well as an increase in fluorescence (Figure 4-14A), as expected for the photoswitching from the spiropyran isomer to the merocyanine isomer. Subsequent white light irradiation reversed this signal back to nearly zero. It may have been possible to fully reverse photoswitch the molecule and reproduce the original spectra with extended duration of exposure to the white light; however, investigations comparing the exposure time to photoswitching yield, in order to determine the optimal light exposure time, were not performed. The photoswitching was able to be consistently reproduced over the 8 photocycles (after the second UV exposure the **SP-3** sample (Figure 4-15A, black) showed a large increase in signal, this was likely due to contamination with an unknown metal ion). Comparison of the absorbance spectra of the white and UV exposed photo-stationary states highlight several differences between the two spiropyrans (Figure 4-14A). Firstly, the **MC-3** absorbance peak around 545 nm is

bathochromically shifted in **MC-4** (575 nm). Also **MC-4** has a more pronounced feature at 420 nm which does not exist in **MC-3**. Both of these differences could be due to the different electronic environment of the spiropyran nitrogen caused by the change from the methyl to ethoxy moiety.

As mentioned above, binding of metal ions induces a switching process which produces the merocyanine isomer and the change in spectra. Ideally this binding process can be reversed with exposure of the complex to white light, thereby displacing the metal ion. Upon exposure of the spiropyran-metal ion complexes to white light there was only a minor decrease in absorbance and fluorescence intensities (Figure 4-15), and the samples were not able to be photoswitched to provide a signal below this in subsequent photoswitching cycles. This suggests displacement of the metal ion does occur, which is desired for a reversible sensor; however, there is a strong ion induced thermal equilibrium formed within the measurement timescale. This equilibrium could potentially be shifted to favour the photochromism process in less saturated samples, however this was not investigated. The **SP-4-**metal ion complexes produced a greater decrease in fluorescence upon the initial white light exposure than the **SP-3**-metal ion complexes; suggesting weaker binding and greater photocontrol of binding in the **SP-4** system.

For the spiropyran complexes with the ions Sr^{2+}, Ba^{2+}, and Mg^{2+} (Figure 4-15 navy, purple, and pink, respectively) exposure to UV352nm light produced an increase in signal greater than the original thermal equilibrium. The Sr^{2+}, Ca^{2+} and Ba^{2+} solutions showed an approximate 30 % decrease in signal over the 8 cycles, whereas complexes with Mg^{2+} and Pb^{2+} showed very little decay in signal. Complexes with Ca^{2+} and Pb^{2+} also exhibited reverse photoswitching; where UV352nm light caused a decrease in the signal and white light caused an increase. This can possibly be explained by the UV-vis spectrum as the UV light used to irradiate the solutions has a wavelength of 352 nm, both spiropyrans with these metals produce a pronounced peak at this wavelength, therefore irradiation at this wavelength could potentially also cause a competing merocyanine to spiropyran isomerisation, therefore decreasing the observed fluorescence signal. This was tested further by trying photoswitching with a different UV wavelength from a germicidal 254 nm source (discussed below).

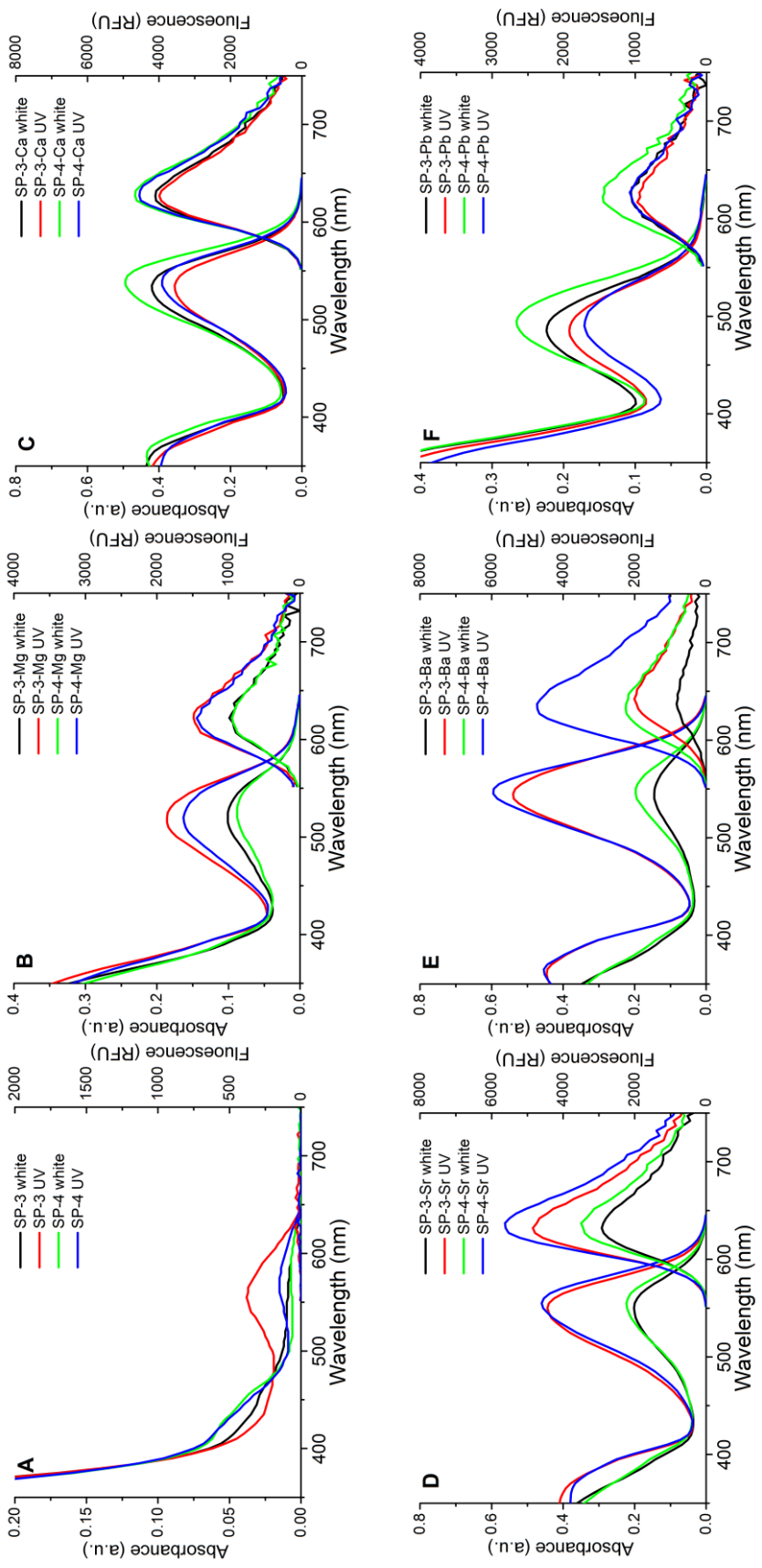

FIGURE 4-14: Absorbance and fluorescence (λ_{532}) spectral changes upon photoswitching for **SP-3** and **SP-4**, spectra shown is after the first white and UV irradiation. (A) with no metal ions; and in the presence of metal ions (B) Mg^{2+}; (C) Ca^{2+}; (D) Sr^{2+}; (E) Ba^{2+}; and (F) Pb^{2+}. After irradiation with: **SP-3** white light (black); **SP-3** UV352nm light (red); **SP-4** white light (green); **SP-4** UV352nm light (blue).

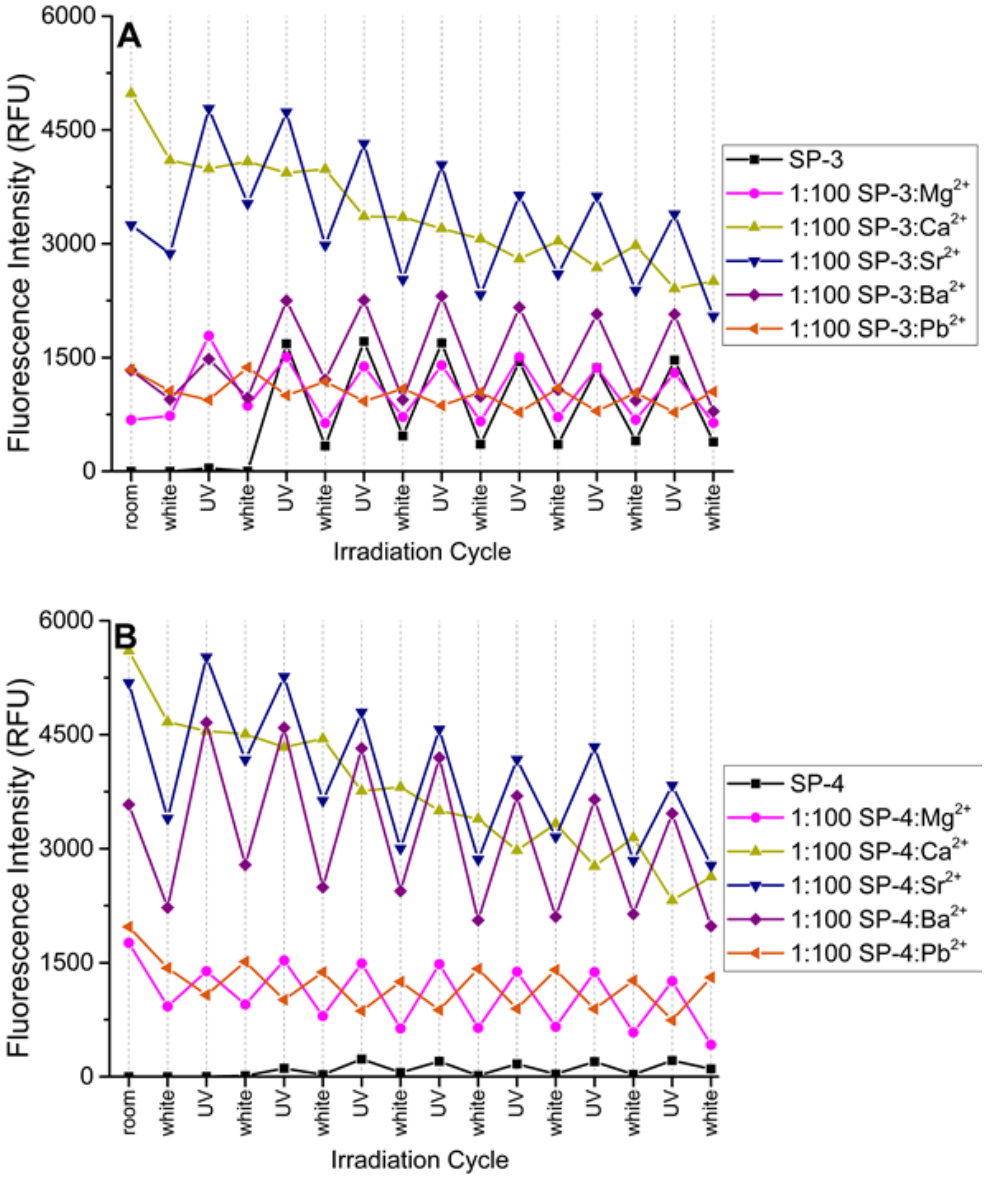

FIGURE 4-15: Changes in peak fluorescence intensity (λ_{ex} = 532 nm) with photoswitching (with UV352nm (UV), or Halogen (white)) of A) **SP-3** and B) **SP-4** in the presence of excess metal salts in acetonitrile.

UV254nm photoswitching assay

The photoswitching of the spiropyran metal ion complexes was then investigated under irradiation from a 254 nm lamp to determine any differences due to a different wavelength exciting different absorption transitions. The changes in peak intensity during photo-cycling and changes in spectra are shown in Figure 4-16 and Figure 4-17, respectively. There were several observations in the comparison between these photoswitching experiments and the previous photoswitching under 352 nm light.

Firstly, it was observed that the metals Sr^{2+}, Ba^{2+}, and Mg^{2+} behaved very similarly to when exposure to the 352 nm light. Each showed strong UV-on and white-off signal with less variation between the different metal ions and a gradual decrease in the signal over time due to fatigue. In the absence of metal ions **SP-3** had greater absorbance increase with UV254nm light than **SP-4**, both exhibiting a gradual increase in signal over time. The main difference between the photoswitching assays was in the Ca^{2+} and Pb^{2+} samples. In the presence of Ca^{2+} both spiropyrans showed a large absorbance turn-on after the initial exposure to white light (not shown), but very little change in the fluorescence spectra (Figure 4-17, gold). Then for the first few UV exposures (2 for **SP-3**, 5 for **SP-4**) negative photochromism was observed in the absorbance spectra (not shown) (similarly to **SP-1-Ca^{2+}**, Section 4.2.1.4); however, this was not observed in the fluorescence spectra, where normal photochromism of UV-on white-off photocycling was observed (Figure 4-17, gold).

The complexes with Pb^{2+} produced a very different photoswitching profile compared to the UV352nm experiment. With only very small changes or no changes in the spectra observed during photoswitching for **SP-3-Pb^{2+}** and **SP-4-Pb^{2+}**, respectively (Figure 4-16F, Figure 4-17, orange); indicating that 254 nm light does not induce photoswitching for this spiropyran complex.

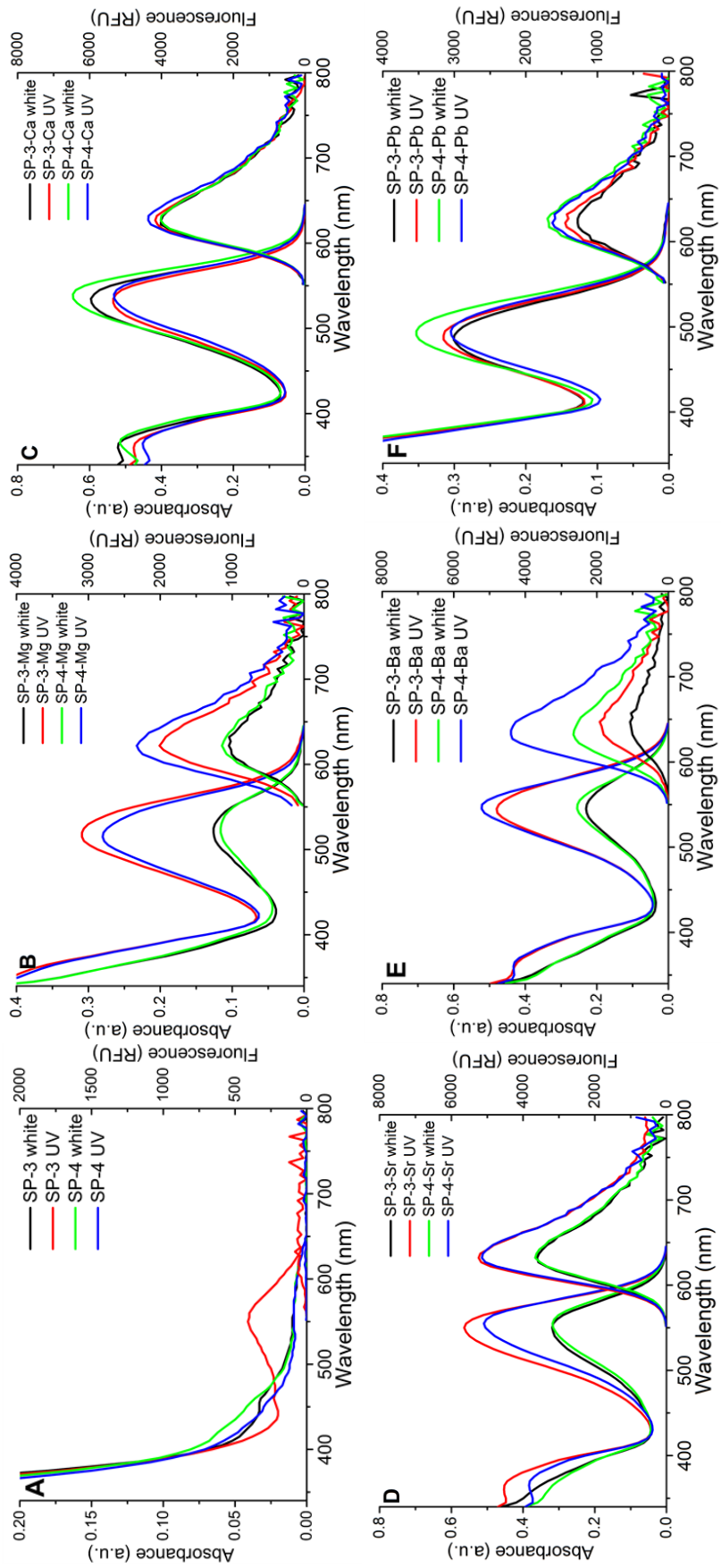

FIGURE 4-16: Absorbance and fluorescence (λ_{EX} = 532nm) spectral changes upon photoswitching for **SP-3** and **SP-4**, spectra shown is after the second white and UV352nm cycle. (A) with no metal ions; and in the presence of metal ions (B) Mg^{2+}; (C) Ca^{2+}; (D) Sr^{2+}; (E) Ba^{2+}; and (F) Pb^{2+}. After irradiation with: **SP-3** white light (black); **SP-3** UV352nm light (red); **SP-4** white light (green); **SP-4** UV352nm light (blue).

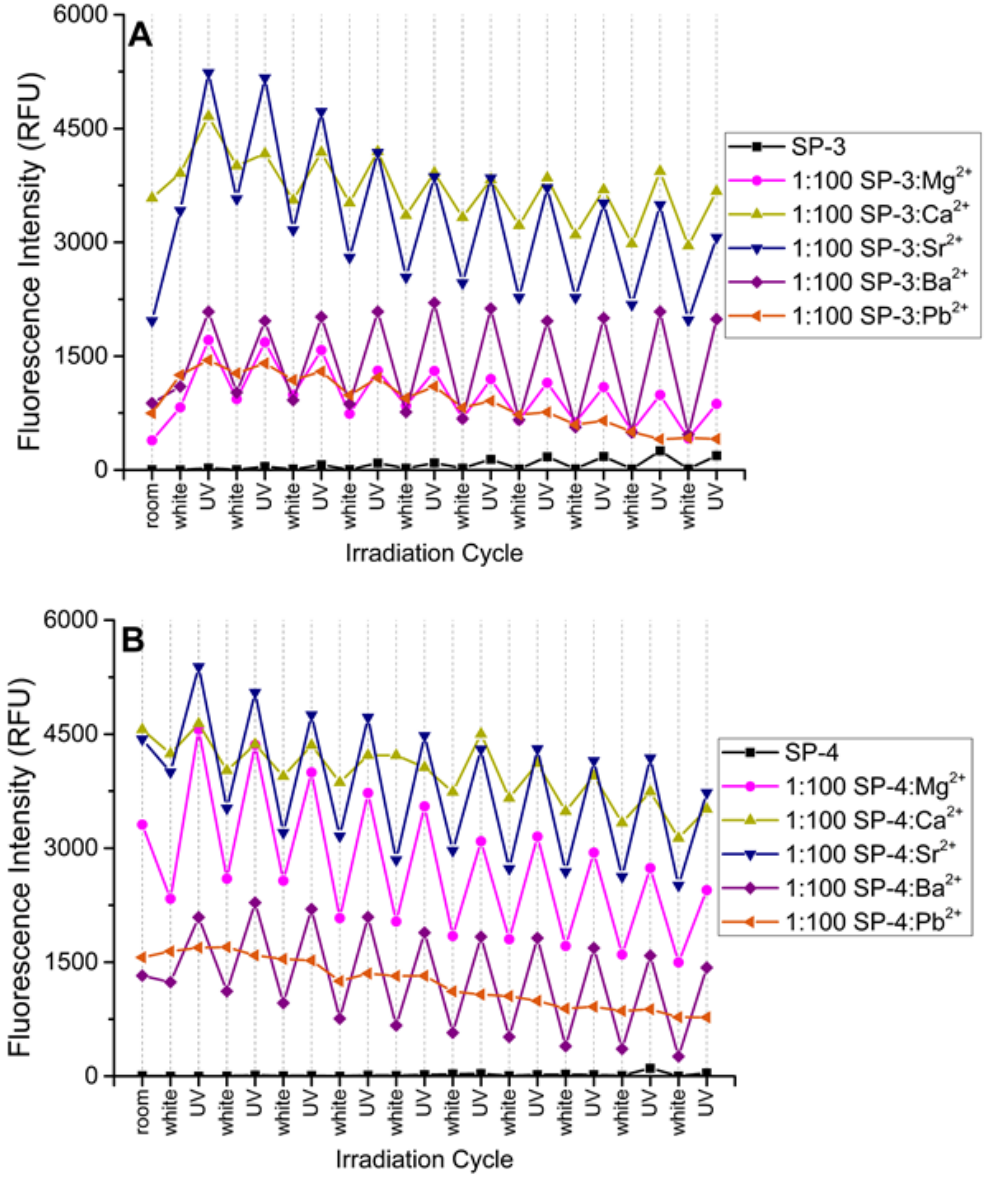

FIGURE 4-17: Changes in peak fluorescence intensity (λ_{em} = 640 nm) with photoswitching (with UV356nm (UV), or Halogen (white)) of A) **SP-3** and B) **SP-4** in the presence of excess metal salts in acetonitrile.

4.3.1.6 Sensing of Ca^{2+} Ions in Cells Using SP-4.

The ability of spiropyran **SP-4** to sense Ca^{2+} in live cells was then examined. **SP-4** was chosen for this in investigation due to its increased selectivity to Ca^{2+} over other biologically relevant metals compared to **SP-3**, as well as binding to Ca^{2+} in a 1:1 stoichiometry (as presented above). The experiments presented in this section were performed by Mr. Jinxin Victor Pei. This work contributed to a submission of a publication (PAPER 5) presented in Appendix D.3.

HEK 293 cells were first prepared by separate treatment with 0, 1, 2 and 5 μM of ionomycin; ionomycin increases the intracellular levels of Ca^{2+}.[28] Spiropyran **SP-4** was then incubated with the cells overnight and subsequent irradiation of the cells with a microplate reader (λ_{ex} = 532 nm) resulted in fluorescence (λ_{em} = 630 nm) from the treated cells (Figure 4-18). The results showed increasing fluorescence that is dependent on increasing ionomycin concentration; demonstrating that **SP-4** is able to detect differences in the intracellular Ca^{2+} concentrations produced by different ionomycin dose.

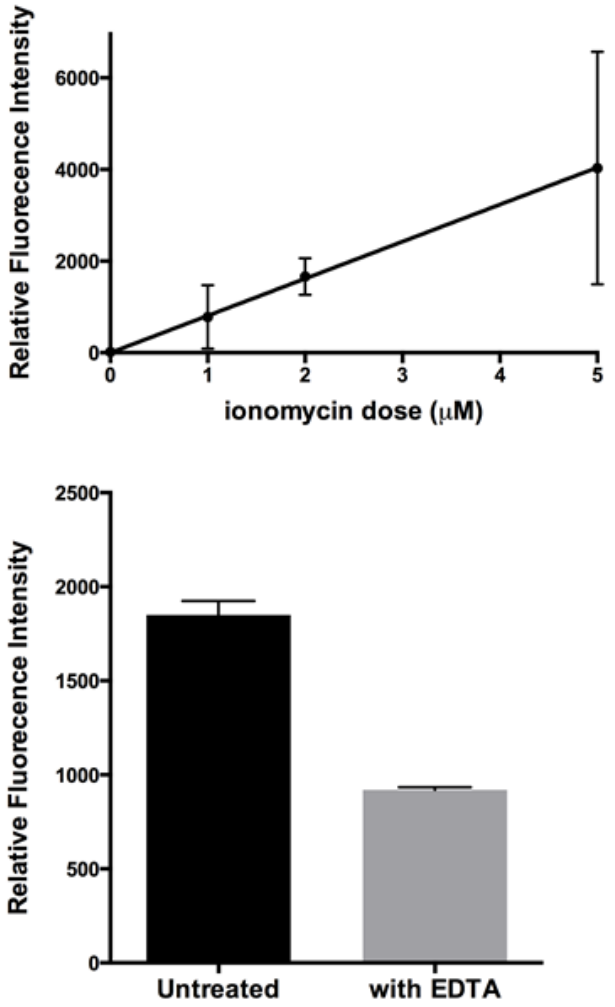

FIGURE 4-18: **SP-4** cellular fluorescence intensity in HEK 293 cells stimulated for increased intracellular Ca^{2+} by ionomycin.

Examination of the cells treated with **SP-4** and 5 μM ionomycin using confocal microscope (λ_{ex} = 559 nm and λ_{em}= 570 – 670 nm) showed fluorescence from the

Ca^{2+} bound **SP-4-Ca^{2+}** complex in the intracellular region (Figure 4-19A). Subsequent exposure of the same cells to visible light for 10 min gave rise to a decrease in fluorescence that is consistent with a photostationary state enriched in the non-fluorescent ring-closed SP isomer (Figure 4-19B). After which, the cells were again exposed to UV 365 nm light for 15 min in order to re-form the ring-opened **MC-4** isomer with rebinding of Ca^{2+}, resulting in the regeneration of fluorescence within the cells (Figure 4-19C). Thus, demonstrating the ability of **SP-4** to be "turned on" and "off" repeatedly in a cellular system, giving the sensor reversibility, allowing for multiple measurements at different time intervals to be made on a single sample.

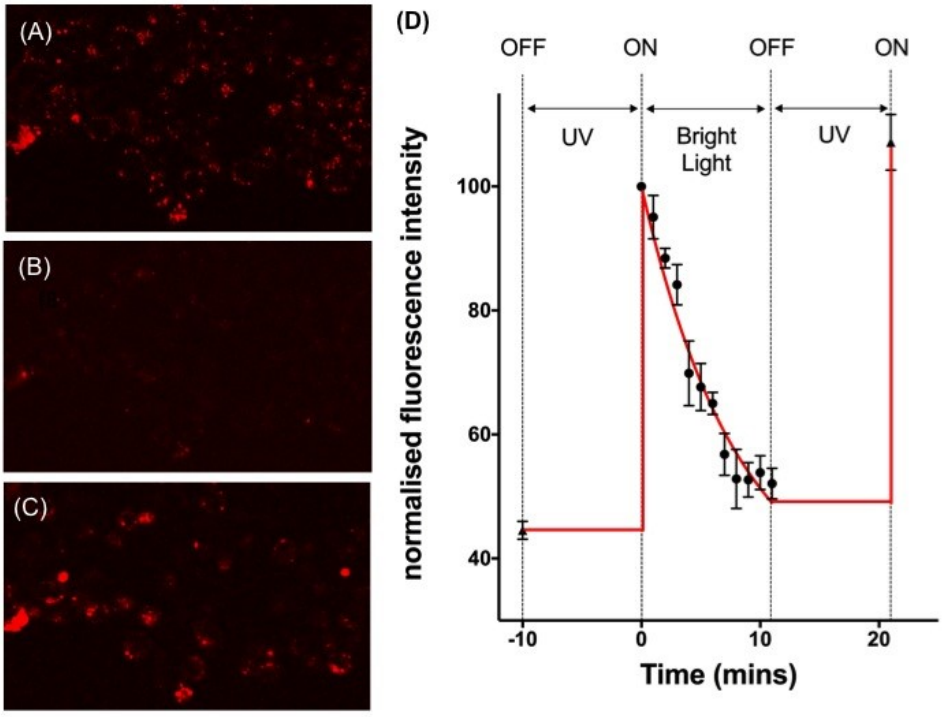

FIGURE 4-19: Confocal microscopy images of HEK 293 cells incubated with ionomycin and **SP-4** after 18 h of incubation at 37 °C. Cellular images obtained at A) t = 0 min; B) after exposing the cells to visible light for 11 min; and C) after exposing the cells to UV (λ = 365 nm) for 10 min. D) Normalized fluorescence intensity as a function of time during visible light irradiation.

4.4 CONCLUSIONS TO CHAPTER 4

Two spiropyrans containing the aza-18-crown-6-ether moiety, **SP-3** and **SP-4,** were synthesised with different N-indoline substitution, a methyl and ethoxy, respectively. These spiropyrans were systematically designed to contain a reactive carboxyl group which could later be used for attachment to a device/surface, such as a microstructured optical fibre. The absorbance and fluorescence spectra of these two photoswitches were obtained and compared in acetonitrile as well as the metal ion induced spectral responses from a series of 15 different biologically relevant metal ions. It was found that both systems have a strong increase in fluorescence signal in the presence of the larger divalent alkaline earth metal ions (Ca^{2+}, Sr^{2+} and Ba^{2+}), and the N-ethoxy indoline spiropyran expressed greater selectivity to these ions over the transition metal ions. Both fluorophores also had a large spectral response in the presence of Pb^{2+}. Both of these spiropyrans were found to bind to the metal ions in a 1:1 ratio, this was different to what was observed for the smaller crown ether spiropyran **SP-1** which binds to these larger ions in a 2:1 spiropyran to metal ion ratio. In the photoswitched state **SP-3** formed a 2:1 complex, but **SP-4** did not, suggesting that the ethoxy group blocks the formation of 2:1 complexes. Therefore, the spiropyran **SP-4** may be more suitable for applications in which the 2:1 complex cannot form, such as attached to a glass surface. These complexes were found to be photoswitchable with good repeatability over 8 cycles. However, in a large excess of metal ion (such as in all the samples investigated) a complete visible light induced decrease in signal, representing a photoswitchable elimination of metal ion, was not observed; possibly due to a rapid reformation of the spiropyran-ion complex. Therefore, due to the increased selectivity and a more favourable 1:1 binding ratio **SP-4** is a better photoswitchable metal ion sensor for alkaline earth metal ions, such as calcium ions, for biological applications. Finally, the cell uptake and Ca^{2+} sensing of **SP-4** in HEK 293 Cells was demonstrated. This then allows for the further use of these spiropyrans for further use as biological sensors, and for sensing when attached to surfaces such as MOFs.

4.5 MATERIALS AND METHODS

4.5.1 SYNTHESIS OF SPIROPYRAN FLUOROIONOPHORES

The synthesis for **SP-1, SP-3** and intermediate indoline (**5**) is shown previously in Section 3.2.5.2.[25]

4.5.1.1 Materials

All ^{13}C NMR and ^{1}H NMR spectra were recorded on an Agilent Technologies 500 MHz NMR with DD2 console in $CDCl_3$ or DMSO-d_6 (Cambridge Isotope Laboratories, Cambridge, MA). Chemical shifts (δ) are reported in ppm, with $CDCl_3$ (δ_C = 77.1 ppm), DMSO-d_6 (δ_C = 39.52 ppm) or TMS (δ_H= 0.0 ppm) used as internal standards. High resolution mass spectrometry was performed on the Agilent 6230 TOF LC-MS. All commercially available chemicals were reagent grade and used without further purification.

4.5.1.2 Synthesis of N-ethylalcohol aza-18-crown-6 spiropyran (SP-4)

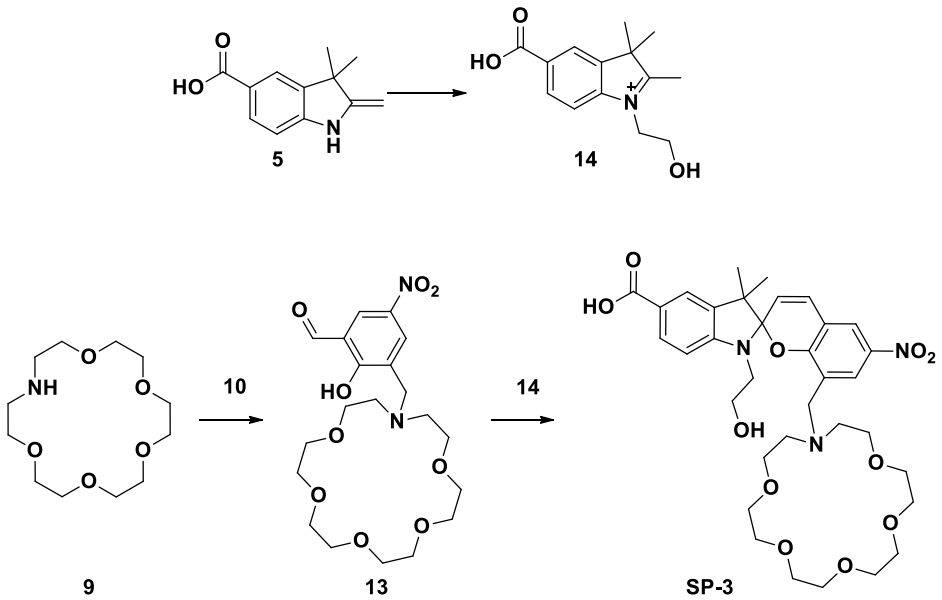

3,3-dimethyl-2-methyleneindoline-5-carboxylic acid (**5**, 1.6 g, 7.7 mmol) was dissolved in acetonitrile (30 mL). To this was added bromoethanol (0.82 mL, 12 mmol), and solution was stirred at 95 ^{o}C for 48 h. Solution was cooled to room temperature and the precipitate was removed by filtration and washed with acetonitrile to give **14** (0.56 g) as a crude mixture with **5** and was used without further purification. ^{1}H NMR (500 MHz, DMSO) δ 8.39 (s, 1H), 8.17 (d, J = 8.1 Hz,

1H), 8.10 (d, *J* = 8.1 Hz, 1H), 4.64 (s, 2H), 3.88 (s, 2H), 2.89 (s, 3H), 1.60 (s, 6H). ^{13}C NMR (126 MHz, DMSO) δ 206.5 (s), 199.0 (s), 166.4 (s, 2C), 145.2 (s), 141.9 (s), 131.6 (s), 130.3 (s), 124.2 (s), 115.3 (s), 54.2 (s), 34.9 (s), 30.7 (s), 21.5 (s, 2C), 14.5 (s). HRMS (m/z) for $C_{14}H_{18}NO_3$ ($[M]^+$) calcd 248.1287; found 248.1296. To 1-aza-15-crown-6 (**9**, 0.13 g, 0.47 mmol) in dry THF (3 mL) was added triethyl amine (0.08 mL, 1.1 mmol) and cooled in an ice bath. To this mixture was added dropwise a solution of 3-(chloromethyl)-2-hydroxy-5-nitrobenzaldehyde (**10**, 0.11 g, 0.5 mmol) in dry THF (5 mL). Solution was allowed to warm to room temperature for 0.5 h then refluxed for 18 h. The precipitate was removed by filtration and the solvent was removed to give thick orange oil (**13**, 0.23 g). ^{1}H NMR (500 MHz, DMSO) δ 10.23 (s, 1H), 8.27 (d, *J* = 3.1 Hz, 1H), 8.13 (d, *J* = 3.1 Hz, 1H), 4.38 (s, 2H), 3.84 – 3.79 (m, 4H), 3.54 (d, *J* = 15.9 Hz, 16H), 3.33 – 3.27 (m, 5H); ^{13}C NMR (126 MHz, DMSO) δ 190.4 (s), 179.1 (s), 131.1 (s), 131.0 (s), 126.5 (s), 124.3 (s), 122.7 (s), 70.3 (s), 70.3 (s), 70.2 (s), 69.9 (s), 65.1 (s), 56.5 (s), 52.5 (s). HRMS (m/z) for $C_{20}H_{30}N_2O_9$ + H ($[M+H]^+$) calcd 443.2030; found 443.2009. Without further purification compounds **13** (0.22 g, 0.49 mmol) and **14** (0.13 g, 0.51 mmol) were combined and dissolved in ethanol (10 mL) and refluxed for 3 h. Solvent was removed *in vacuo* to give purple crude solid (0.34 g) which was purified twice by C18 reverse phase silica chromatography eluting with a gradient of 0-30 % acetonitrile in water to give pure product (**SP-4**, 80 mg, 0.12 mmol, 25 % from **5**). mp. 123-127^{o}C; ^{1}H NMR (500 MHz, DMSO) δ 12.11 (s, 1H), 8.12 (s, 2H), 7.79 (d, *J* = 8.3 Hz, 1H), 7.66 (s, 1H), 7.21 (d, *J* = 10.4 Hz, 1H), 6.72 (d, *J* = 8.2 Hz, 1H), 6.02 (d, *J* = 10.4 Hz, 1H), 4.76 (s, 1H), 3.66 – 3.18 (m, 30H), 1.24 (s, 3H), 1.12 (s, 3H); ^{13}C NMR (126 MHz, DMSO) δ 167.4 (s), 156.5 (s), 150.7 (s), 140.1 (s), 135.6 (s), 130.8 (s), 128.3 (s), 126.9 (s), 126.0 (s), 123.0 (s), 121.5 (s), 121.1 (s), 120.9 (s), 118.3 (s), 106.0 (s), 105.8 (s), 69.9 (s), 69.9 (s), 69.8 (s), 69.6 (s), 68.8 (s), 58.9 (s), 53.3 (s), 51.8 (s), 51.6 (s), 45.4 (s), 25.7 (s), 19.3 (s). HRMS (m/z) for $C_{34}H_{45}N_3O_{11}$ + H^+ ($[M+H]^+$) calcd 672.3092; found 672.3105.

4.5.2 ION BINDING STUDIES

4.5.2.1 Ion Specificity

Stock solutions of spiropyrans (**SP-1**, **SP-3** or **SP-4)** (100 μM) and metal ion salts (10 mM) were prepared in HPLC grade acetonitrile. Salt solutions were prepared from vacuum dried $LiClO_4$, $NaClO_4$, $KClO_4$, Cs_2SO_4, $Mg(ClO_4)_2$, $Ca(ClO_4)_2$, $Sr(ClO_4)_2$, $Ba(ClO_4)_2$, $Mn(ClO_4)_2$, $Fe(II)(ClO_4)_2$, $Co(ClO_4)_2$, $Ni(ClO_4)_2$, $Cu(ClO_4)_2$, $Zn(ClO_4)_2$, $Cd(ClO_4)_2$, and $Pb(ClO_4)_2$. To separate 96 well assay trays each spiropyran (100 μL) was mixed separately with each of the metal solutions (100 μL) in triplicate to give 1:100 ratio of spiropyran/metal ion. The absorbance and fluorescence spectra were recorded between 300 and 800 nm, and 552 and 802 nm, respectively, at 25 ^{o}C using a BioTek Synergy H4 Hybrid Multi-Mode Microplate Reader scanning with a resolution of 5 nm. Fluorescence excitation was at 532 nm with bandgap of 9 nm. The assay tray was then removed and photoswitching was performed by exposing to 352 nm UV light from a filtered 8 W Hg lamp (UVP), or halogen white lamp for 10 min each, with the absorbance and fluorescence spectra obtained after each irradiation. The average spectrums were calculated and integrated between 425 nm and 650 nm for the absorbance spectra or 552 and 802 for the fluorescence spectra.

4.5.2.2 Job's Plot with SP-1

On a single 96 well assay tray three different Job's plots were recorded at a single run. From the stock solutions of $LiClO_4$, $Ca(ClO_4)_2$, or $Cd(ClO_4)_2$ different concentrations of metal ions [M] and spiropyran [**SP-1**] were combined in triplicate such that the total concentration of metal and spiropyran was constant ([M] + [**SP-1**] = 50 μM) with [**SP-1**] = 0, 5, 10, 15, 20, 25, 30, 35, 40, 45, and 50 μM and volume of 200 μL. After mixing the UV-Vis absorption and fluorescence (λ_{ex} = 532 nm) spectra of each concentration was recorded using a Synergy H4 Hybrid Multi-Mode Microplate Reader and the average spectrum obtained. The peak absorbance (λ = 540 nm) or fluorescence intensity (λ = 627 nm) was plotted against percent spiropyran ([**SP-1**]/([**SP-1**]+[M]) x 100).

4.5.2.3 Job's Plot with SP-3 and SP-4

On a single 96 well assay tray three different Job's plots were recorded in a single run. 100 μM stock solutions of the metal salts $Ca(ClO_4)_2$, $Sr(ClO_4)_2$ and $Ba(ClO_4)_2$ were prepared. On the assay tray the metal ion solutions were diluted in triplicate with either spiropyran in various concentration ratios such that total concentration of metal ion and spiropyran was constant ([M] + [SP] = 50 μM); *i.e.* [SP] = 0, 5, 10, 15, 20, 25, 30, 35, 40, 45, and 50 μM. After mixing the UV-Vis absorption and fluorescence (λ_{ex} = 532 nm) spectra was recorded using a Synergy H4 Hybrid Multi-Mode Microplate Reader and the average spectrum obtained. The peak fluorescence intensity (λ_{em} = 627 nm) was plotted against percent spiropyran ([SP]/([SP]+[M]) x 100) to find the optimal binding ratio of spiropyran to metal ion.

4.5.2.4 Ion Affinity Assay with SP-1

On a single 96 well assay tray **SP-1** (50 μM) was mixed in triplicate with different concentrations of metal ions of $LiClO_4$, $Ca(ClO_4)_2$, or $Cd(ClO_4)_2$ from the stock solutions such that [M] = 0, 5, 10, 20, 30, 40, 50, 100, 250, 500 μM to give the ratios of [M]/[SP] = 0, 0.1, 0.3, 0.5, 0.7, 0.9, 1.0, 1.5, 2, 5, 10 in a total volume of 200 μL. After mixing the UV-Vis absorption and fluorescence (λ_{ex} = 532 nm) spectra at each concentration was recorded using a Synergy H4 Hybrid Multi-Mode Microplate Reader and the average spectrum obtained. The peak fluorescence intensity (λ_{max} = 627 nm) was plotted against ratio [M]/([SP])

4.5.2.5 Ion Affinity Assay with SP-3 and SP-4

On a single 96 well assay tray three different analysis was recorded in a single run. Spiropyran ([SP] = 33.3 μM) was mixed in triplicate with different concentrations of metals ([M] = 0, 1.67, 3.3, 10.0, 16.7, 23.3, 30, 33.3, 50, 66.7, 333 μM) to give the ratios of [M]/[SP] = 0, 0.05, 0.1, 0.3, 0.5, 0.7, 0.9, 1.0, 1.5, 2, 10 in 300 μL acetonitrile. After mixing the UV-Vis absorption and fluorescence (λ_{ex} = 532 nm) spectra was recorded using a Synergy H4 Hybrid Multi-Mode Microplate Reader and the average spectrum obtained. The peak fluorescence intensity (λ_{em} = 627 nm) was plotted against ratio [M]/[SP].

4.5.2.6 Photoswitchability Assay with SP-1

On a single 96 well assay tray solution of **SP-1** (100 μM, 100 μL) in acetonitrile was mixed with solutions of metal perchlorates ($LiClO_4$, $NaClO_4$, $KClO_4$, $Mg(ClO_4)_2$, $Ca(ClO_4)_2$, $Sr(ClO_4)_2$, $Ba(ClO_4)_2$, $Cd(ClO_4)_2$, and $Pb(ClO_4)_2$) in acetonitrile (10 mM or 100 μM (100 μL)) and the tray was sealed with a plastic film to prevent evaporation. After mixing the UV-Vis absorption and fluorescence (λ_{ex} = 532 nm) spectra was obtained using a Synergy H4 Hybrid Multi-Mode Microplate Reader. Photoswitching cycling was achieved by irradiation with a white light source (halogen lamp) for ten minutes, or a UV light source (UVP mercury lamp, 8 W, 352 nm BRB tube) (UV352nm) for 5 min. Photocycling was repeated for 6 white - UV cycles.

4.5.2.7 Photoswitching Assay with SP-3 and SP-4

To two different 96 well assay plates (Plate 1 and Plate 2) 12 wells were prepared on each plate by adding to 6 wells each per plate 100 μL of spiropyran **SP-3** and **SP-4** (100 μM) in acetonitrile. Then to each spiropyran solution was added metal perchlorate solution of either Mg^{2+}, Ca^{2+}, Sr^{2+}, Ba^{2+}, and Pb^{2+} (10 mM, 100 μL) in acetonitrile, or acetonitrile only (control) (as shown in Figure 4-20). The wells were covered with a plastic slip to prevent evaporation. The UV-Vis absorption (between 340 and 650 nm) and fluorescence (λ_{ex} = 532 nm) spectra was obtained at 5 nm increments using a Synergy H4 Hybrid Multi-Mode Microplate Reader at 25 ^{o}C. Photoswitching cycling was achieved by irradiation with a white light source (halogen lamp) for ten minutes, or a UV light source (Plate 1: UVP mercury lamp, 8 W, 352 nm BRB tube (UV352nm), Plate 2: UVP mercury lamp, 8 W, 254 nm tube (UV254nm)) for 5 min with plastic slip removed. Photocycling was repeated for at least 7 white - UV cycles. For Plate 1 after 8 cycles 100 μL of acetonitrile was added to each well. The peak absorbance intensity (λ_{max} = 540 nm) and the fluorescence intensity (λ_{em} = 627 nm) after each switching cycle was plotted.

SP-3 ACN	**SP-4 ACN**	**SP-3 Ca^{2+}**	**SP-4 Ca^{2+}**
SP-3 Sr^{2+}	**SP-4 Sr^{2+}**	**SP-3 Mg^{2+}**	**SP-4 Mg^{2+}**
SP-3 Ba^{2+}	**SP-4 Ba^{2+}**	**SP-3 Pb^{2+}**	**SP-4 Pb^{2+}**

FIGURE 4-20: Left) The layout of the photoswitching assay tray; Right, the colour difference between the spiropyrans with 100-fold excess metal ion salts, taken after the final spectra acquisition.

4.5.3 COMPUTATIONAL MODELLING

The lowest energy structure, frequencies and orbitals of spiropyrans **SP-3** and **SP-4** without and with the metal ions Mg^{2+}, Ca^{2+}, Sr^{2+}, and Ba^{2+} in a 1:1 ratio in a vacuum was determined using computational methods. Structure and frequency calculations were performed using Gaussian 09[29], the level of theory used was UB3PLY and the 6-31g(d) basis set for the atoms H, C, N, and O and LanL2DZ for the metal ions. Computations were completed using the Tizard supercomputer at e-RSA. Images of energy minimalised structures are shown in Appendix C, Figure C-2.

4.6 REFERENCES FOR CHAPTER 4

1. Chibisov, A. K.; Gorner, H. Photochromism of spirobenzopyranindolines and spironaphthopyranindolines. *Physical Chemistry Chemical Physics* 2001, *3* (3), 424-431.
2. Winkler, J. D.; Bowen, C. M.; Michelet, V. Photodynamic Fluorescent Metal Ion Sensors with Parts per Billion Sensitivity. *Journal of the American Chemical Society* 1998, *120* (13), 3237-3242.
3. Paramonov, S. V.; Lokshin, V.; Fedorova, O. A. Spiropyran, chromene or spirooxazine ligands: Insights into mutual relations between complexing and photochromic properties. *Journal of Photochemistry and Photobiology C: Photochemistry Reviews* 2011, *12* (3), 209-236.
4. Kang, S. O.; Llinares, J. M.; Day, V. W.; Bowman-James, K. Cryptand-like anion receptors. *Chemical Society Reviews* 2010, *39* (10), 3980-4003.
5. Gokel, G. W.; Leevy, W. M.; Weber, M. E. Crown ethers: Sensors for ions and molecular scaffolds for materials and biological models. *Chemical Reviews* 2004, *104* (5), 2723-2750.
6. Fabbrizzi, L.; Licchelli, M.; Rabaioli, G.; Taglietti, A. The design of luminescent sensors for anions and ionisable analytes. *Coordination Chemistry Reviews* 2000, *205* (1), 85-108.
7. Amendola, V.; Fabbrizzi, L.; Mangano, C.; Pallavicini, P.; Poggi, A.; Taglietti, A. Anion recognition by dimetallic cryptates. *Coordination Chemistry Reviews* 2001, *219–221* (0), 821-837.
8. Kimura, K.; Teranishi, T.; Yokoyama, M.; Yajima, S.; Miyake, S.; Sakamoto, H.; Tanaka, M. Cation complexation, isomerization, and photoresponsive ionic conduction of a crown ether derivative carrying two spirobenzopyran units. *Journal of the Chemical Society, Perkin Transactions 2* 1999, (2), 199-204.
9. Tanaka, M.; Nakamura, M.; Salhin, M. A. A.; Ikeda, T.; Kamada, K.; Ando, H.; Shibutani, Y.; Kimura, K. Synthesis and photochromism of spirobenzopyran derivatives bearing an oxymethylcrown ether moiety: Metal ion-induced switching between positive and negative photochromisms. *Journal of Organic Chemistry* 2001, *66* (5), 1533-1537.
10. Kimura, K.; Sakamoto, H.; Kado, S.; Arakawa, R.; Yokoyama, M. Studies on metal-ion complex formation of crown ether derivatives incorporating a photoionizable spirobenzopyran moiety by electrospray ionization mass spectrometry. *Analyst* 2000, *125* (6), 1091-1095.
11. Heng, S.; Nguyen, M.-C.; Kostecki, R.; Monro, T. M.; Abell, A. D. Nanoliter-scale, regenerable ion sensor: sensing with a surface functionalized microstructured optical fibre. *RSC Advances* 2013, *3* (22), 8308-8317.
12. Natali, M.; Soldi, L.; Giordani, S. A photoswitchable Zn (II) selective spiropyran-based sensor. *Tetrahedron* 2010, *66* (38), 7612-7617.
13. Natali, M.; Aakeroy, C.; Desper, J.; Giordani, S. The role of metal ions and counterions in the switching behavior of a carboxylic acid functionalized spiropyran. *Dalton Transactions* 2010, *39* (35), 8269-8277.
14. Sakamoto, H.; Yamamura, T.; Takumi, K.; Kimura, K. Absorption- and fluorescence-spectral sensing of alkali metal ions in anionic micelle

solutions containing crowned spirobenzopyrans. *Journal of Physical Organic Chemistry* 2007, *20* (11), 900-907.

15. Kimura, K.; Yamashita, T.; Yokoyama, M. Cation-specific isomerization of crowned spirobenzopyrans. *Journal of the Chemical Society, Chemical Communications* 1991, (3), 147-148.
16. Kimura, K.; Yamashita, T.; Yokoyama, M. Synthesis, cation complexation, isomerization and photochemical cation-binding control of spirobenzopyrans carrying a monoaza-crown moiety at the 8-position. *Journal of the Chemical Society-Perkin Transactions 2* 1992, (4), 613-619.
17. Kimura, K.; Yano, H.; Kitazawa, S.; Shono, T. Synthesis and selectivity for lithium of lipophilic 14-crown-4 derivatives bearing bulky substituents or an additional binding site in the side arm. *Journal of the Chemical Society, Perkin Transactions 2* 1986, (12), 1945-1951.
18. Kimura, K.; Yamashita, T.; Kaneshige, M.; Yokoyama, M. Crowned spironaphthoxazine: lithium ion-selective colouration and ion-regulated thermal stability of its coloured form. *Journal of the Chemical Society, Chemical Communications* 1992, (13), 969-970.
19. Kimura, K.; Yamashita, T.; Yokoyama, M. Photochemical switching of ionic-conductivity in composite films containing a crowned spirobenopyran. *Journal of Physical Chemistry* 1992, *96* (13), 5614-5617.
20. Kimura, K.; Kaneshige, M.; Yamashita, T.; Yokoyama, M. Cation Complexation, Photochromism, and Reversible Ion-Conducting Control of Crowned Spironaphthoxazine. *The Journal of Organic Chemistry* 1994, *59* (6), 1251-1256.
21. Roxburgh, C. J.; Sammes, P. G. Substituent tuning of photoreversible lithium chelating agents. *Dyes and Pigments* 1995, *28* (4), 317-325.
22. Kimura, K.; Kanokogi, S.; Yokoyama, M. Extraction Spectrophotometry of Lithium Ions Based on Cation- and Photo-Induced Isomerization of Crowned Spirobenzopyran. *Analytical Sciences* 1996, *12* (3), 399-403.
23. Masiker, M. C.; Mayne, C. L.; Boone, B. J.; Orendt, A. M.; Eyring, E. M. 7Li NMR chemical shift titration and theoretical DFT calculation studies: solvent and anion effects on second-order complexation of 12-crown-4 and 1-aza-12-crown-4 with lithium cation in several aprotic solvents. *Magnetic Resonance in Chemistry* 2010, *48* (2), 94-100.
24. Kostecki, R.; Heng, S.; Ebendorff-Heidepriem, H.; Abell, A. D.; Monro, T. M. Functionalization of exposed core fibers with multiligand binding molecules for fluorescence based ion sensing. In *23rd International Conference on Optical Fibre Sensors*, López-Higuera, J. M.; Jones, J.; López-Amo, M.; Santos, J. L., Eds. 2014; Vol. 9157, 915788.
25. Stubing, D. B.; Heng, S.; Abell, A. D. Crowned spiropyran fluoroionophores with a carboxyl moiety for the selective detection of lithium ions. *Organic & Biomolecular Chemistry* 2016, 14 (15), 3752-7.
26. Hughes, D. L. Progress in the fischer indole reaction. a review. *Organic Preparations and Procedures International* 1993, *25* (6), 607-632.
27. Renny, J. S.; Tomasevich, L. L.; Tallmadge, E. H.; Collum, D. B. Method of continuous variations: applications of job plots to the study of molecular associations in organometallic chemistry. *Angewandte Chemie* 2013, *52* (46), 11998-2013.

28. Stubing, D. B.; Heng, S.; Monro, T. M.; Abell, A. D. A comparative study of the fluorescence and photostability of common photoswitches in microstructured optical fibre. *Sensors and Actuators B: Chemical* 2017, *239*, 474-480.
29. Frisch, M. J.; Trucks, G. W.; Schlegel, H. B.; Scuseria, G. E.; Robb, M. A.; Cheeseman, J. R.; Scalmani, G.; Barone, V.; Mennucci, B.; Petersson, G. A.; Nakatsuji, H.; Caricato, M.; Li, X.; Hratchian, H. P.; Izmaylov, A. F.; Bloino, J.; Zheng, G.; Sonnenberg, J. L.; Hada, M.; Ehara, M.; Toyota, K.; Fukuda, R.; Hasegawa, J.; Ishida, M.; Nakajima, T.; Honda, Y.; Kitao, O.; Nakai, H.; Vreven, T.; Montgomery Jr., J. A.; Peralta, J. E.; Ogliaro, F.; Bearpark, M. J.; Heyd, J.; Brothers, E. N.; Kudin, K. N.; Staroverov, V. N.; Kobayashi, R.; Normand, J.; Raghavachari, K.; Rendell, A. P.; Burant, J. C.; Iyengar, S. S.; Tomasi, J.; Cossi, M.; Rega, N.; Millam, N. J.; Klene, M.; Knox, J. E.; Cross, J. B.; Bakken, V.; Adamo, C.; Jaramillo, J.; Gomperts, R.; Stratmann, R. E.; Yazyev, O.; Austin, A. J.; Cammi, R.; Pomelli, C.; Ochterski, J. W.; Martin, R. L.; Morokuma, K.; Zakrzewski, V. G.; Voth, G. A.; Salvador, P.; Dannenberg, J. J.; Dapprich, S.; Daniels, A. D.; Farkas, Ö.; Foresman, J. B.; Ortiz, J. V.; Cioslowski, J.; Fox, D. J. *Gaussian 09*, Gaussian, Inc.: Wallingford, CT, USA, 2009.

CHAPTER 5

SURFACE FUNCTIONALISATION AND MOF SENSORS

5.1 INTRODUCTION

5.1.1 THE CURRENT LITERATURE ON PHOTOSWITCHABLE SENSING SURFACES

The combination of the fields of fluorescence sensors, surface functionalisation and photochromism in one sensing device allows for the exploitation of the combined advantages from each field. As discussed in Chapter 1 the advantages of attaching a photoswitch to an optical fibre core include: removal of the need to contaminate analyte with fluorophore; a known fluorophore concentration on the surface, allowing for easier local calibration; and repeatable/reusable sensing with the same device.

Despite the increased attention to photoswitchable materials in recent times,[1-6] the majority of studies have focused on photoswitchable polymers[2, 7-9] and nanoparticles,[10, 11] there is currently, to our knowledge, few publications on photoswitchable glass surfaces.[12, 13] This is likely due to the poor electronic and reflective properties of glass compared to other materials, such as gold or silicon, making it difficult to characterise the analyte binding and photoswitching of such systems (*e.g.* using SPR,[14] or grazing angle IR). Likewise, despite the interest in photoswitchable ion chelators, there are few reports for the chemical attachment of these sensors to a material for use as an integrated sensing device. Several of these reports are highlighted below.

Scarmagnani *et al.*[15] in 2008 attached a NO_2-Spiropyran to polystyrene microbeads. This spiropyran in the merocyanine form, like most spiropyrans, has a broad affinity to metal ions. The microbeads were able to photoreversibly detect Cu^{2+} by colour changes, however no fluorescence sensing was reported. Liu *et al.*[16] in 2011 attached the same spiropyran as Scarmagnani to the surface of gold nanoparticles via an alkanethiol linker. It was shown that in the presence of copper ions the copper was able to bind to and bridge two spiropyrans on different nanoparticles; this caused aggregation, which was detected with UV-Vis spectroscopy, zeta potential, and dynamic light scattering (DLS). Connel *et al.*[17] in 2010 created a microstructured polymer network with surface attached NO_2-spiropyran which showed a strong colour change in the presence of Pd^{2+}. And Fries *et al.*[18, 19] reported this spiropyran

attached to a polymer on a glass surface which showed a colour response to a range of transition metal ions.

Sensors made with photoswitchable molecules directly attached to a silica surface have been reported by Kim *et al*.[20] and Sanchez *et al*.[11] In both of these systems azobenzene derivatives were attached to silica nanoparticles and was able to detect Hg^{2+} via a strong colour change. However, in this study no fluorescence sensing was performed, and the photoswitchability of the ion binding was not reported. This is possibly due to the photoswitching centre having no influence on the ion affinity; therefore, these are not photoreversible sensing systems.

Although the above examples have a photoswitchable molecule as a sensor in a material, these systems either lack any metal specificity, or are not photochromic, or show no reported fluorescence sensing. To the best of our knowledge, there are no reports of a targeted sensing system that is photochromic and attached directly to a silica surface. This chapter aims to fill this void by producing a photoresponsive silica surface, capable of performing fluorescence sensing for metal ions. This is achieved by modifying the MOF core surface with a photoswitchable ionophore. This investigation is separated into three sections: firstly, in Section 5.2 the methods of surface attachment of photoswitchable fluorophores is trialled on bulk glass slide in order to determine the optimum conditions for functionalising the glass surface. The surface attachment, photoswitching, and ion sensing is monitored and characterised by contact angle measurements and scanning fluorescence imaging. Secondly, in Section 5.3 an investigation of photoswitch surface attachment and photoswitchable metal ion sensing is performed in microstructured optical fibres. This fibre based work is discussed with respect to an investigation of the Ca^{2+} sensitive spiropyran photoswitch **SP-3**, and thirdly, in Section 5.4 the use of MOFs in two publications in which two different spiropyran based photoswitchable sensors selective for $Ca^{2+}$and Cd^{2+} (**SP-6/SP-7**), and Zn^{2+} (**SP1**) is presented.

5.1.2 FUNCTIONALISATION OF SILICA SURFACES

5.1.2.1 Surface Silanisation with APTES

The silane reagent used primarily in this study was aminopropyltriethoxy silane (APTES) (Figure 5-1), which contains a primary amine four atoms away from the silicon. This amino group imparts the silica surface with alternate reactivity, allowing for further modification with standard amide coupling reactions; and therefore, it is the most commonly used silane reagent.[21-24] However, due the structure of APTES, the surface attachment process is not as straightforward as other silanes (Chapter 1.3.2); which has led to the surface attachment process being well studied.[25-29] Issues with silanisation are due to the primary amine of APTES, which is able to coordinate to the silicon atom either intra- or inter- molecularly, forming a highly reactive pentacoordinate intermediate (Figure 5-1).[29] This intermediate is highly subjective to nucleophilic attack either by the surface hydroxyls or by water in the solution. Therefore, in the presence of water APTES is able to self-catalyse its hydrolysis in solution, increasing the rate of hydrolysis and leading to the formation of polymers either in the solution or on the surface (Figure 5-2 e, c). Also, due to the polar nature of the amine it is able to form hydrogen bonding to the surface, blocking the surface and contributing to polymerisation (Figure 5-2 b, d, f). These factors disrupt the formation of a uniform SAM which provides a smooth, regular, and reproducible surface coverage of amine groups, and therefore an even distribution of fluorophore.

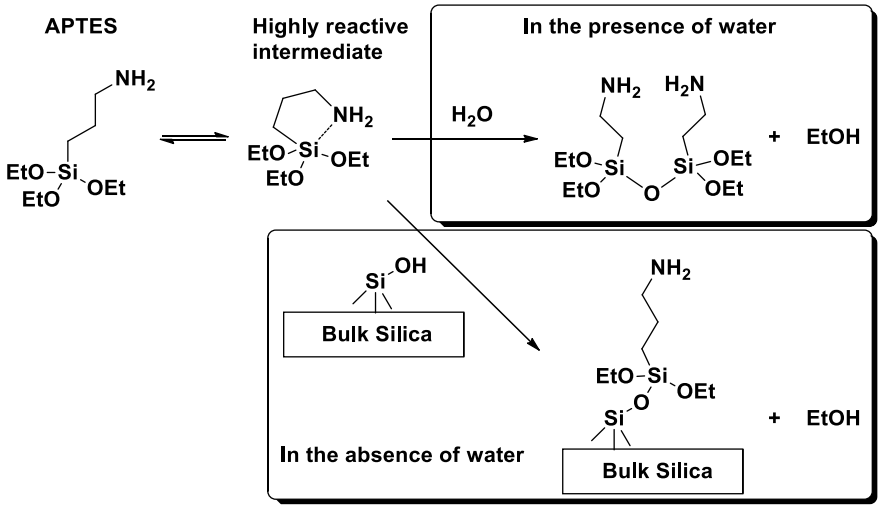

FIGURE 5-1: Self-catalysed hydrolysis of APTES in the presence of water.

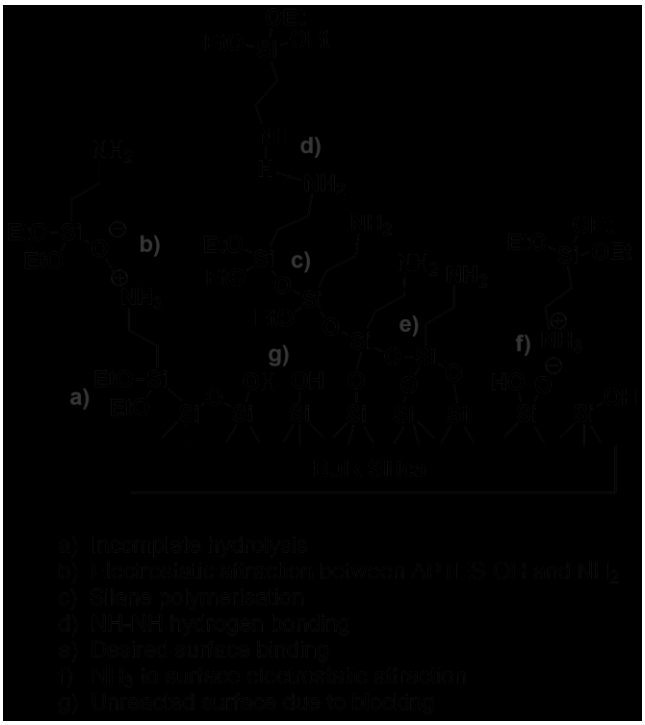

FIGURE 5-2: Possible binding modes for APTES to a silica surface.

To overcome these issues standard reaction conditions have been well investigated and optimised as reported in the literature.[25, 27, 30] In general, the APTES silanization must be done in purely anhydrous conditions, with dry glass surfaces and in anhydrous toluene, unlike with other silanes which can be used in water or other protic solvents. Also, the reaction time is critical, as the reaction needs sufficient time to form a complete monolayer, yet longer times lead to increased

polymerisation and a thicker surface layer. Pre-treatment of the surface has also been found to have a profound effect on the silanization efficiency; the surface needs to be clean of all contaminants and have the largest possible composition of free hydroxyl groups. The optimum silica surface for APTES silanization has been found to be produced from a series of treatments in acids (HCl/MeOH, or HNO_2) and oxidising Piranha solution (7:3 H_2SO_4/30 % $H_2O_{2(aq)}$), followed by washing and oven drying (Scheme 5-1).[30] Post-silanisation hydrolysis of the aminated surface is required to remove non-specific and incomplete binding.

5.1.2.2 Surface Amide Coupling Reaction

As shown previously in Figure 1-8, the silanization process can impart various functionality to the surface. This functionality can be used to attach organic molecules (e.g., fluorophores) to the surface using standard organic chemistry; such as through functional group transformations, esterification, metathesis cross-coupling, Azide-Alkyne Huisgen Cycloaddition ("click" chemistry), or acrylic polymerisation.[31, 32] Modification of an amine (APTES) coated surface can be achieved through an amide coupling reaction involving an activated carboxylic acid functional group.[33] Two such coupling reactions involve activation with NHS via the carbonimide, EDC, or with HATU with Hunigs base (DIPEA). Both of these activated coupling processes have been well published for the attachment of functionalisation to aminated or carboxylated surfaces.[22, 34-41] The NHS ester pathway has the benefit of a more stable activated acid, thereby allowing purification of the activated form, prior to surface attachment, which limits the amount of side products and gives a cleaner reaction.[38]

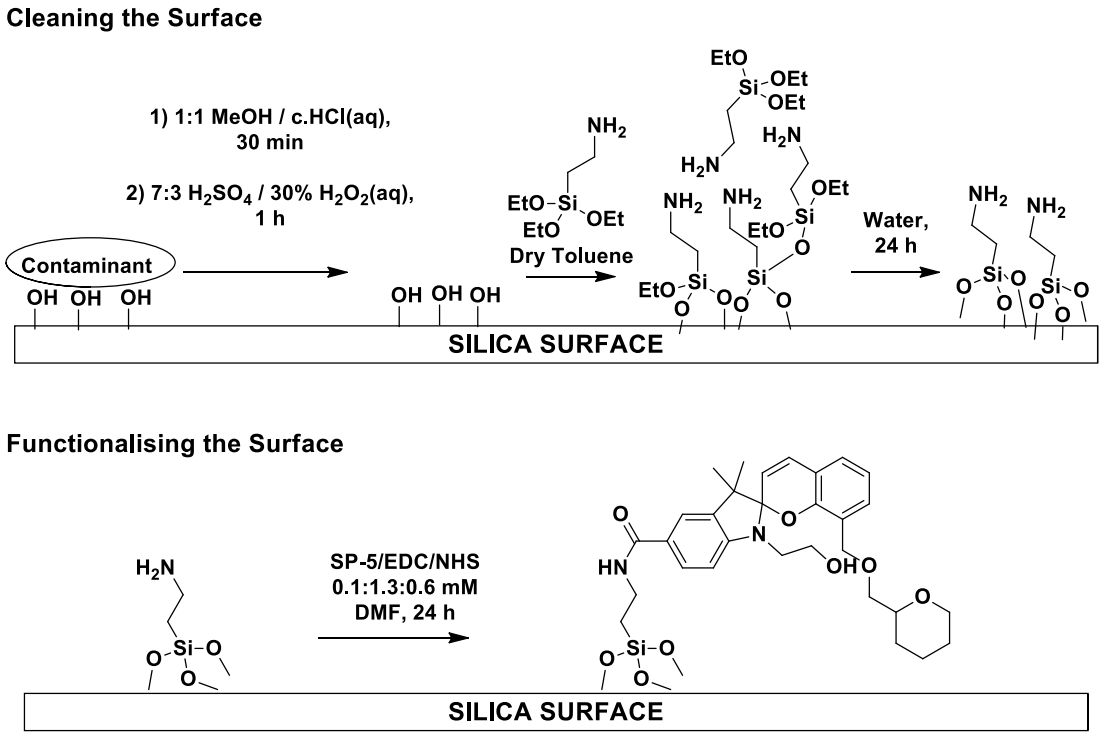

SCHEME 5-1: Protocol for the functionalisation of the silica surface. The surface is first cleaned of contaminant and hydroxylated with 1:1 MeOH/c.HCl and Piranha solution. Silanisation of the surface with APTES in dry toluene for 1 hour. Hydrolysis of unreacted silane with water for 24 hours. Coupling to the aminated surface with **SP-5**.

5.1.3 GLASS SLIDE SURFACE CHARACTERISATION TECHNIQUES

5.1.3.1 Surface Contact Angle

Surface contact angle is the angle of incident at a liquid-solid-air interface, it can be used to quantify the surface energy of the material, *i.e.* the hydrophobicity. There are generally three methods to measure contact angle for a drop of liquid on a surface, the sessile drop method, the dynamic drop method and the pendant drop method. The sessile drop method is the simplest form of measurement and the contact angle determined is taken as the internal angle of a stationary drop on top of a flat surface (Figure 5-3A).

The measurement of contact angles is generally achieved through the use of a goniometer (Figure 5-3B). This consists of a pipette/syringe aligned perpendicular to an illuminated surface with a measurement tool (such as a protractor or digital camera with processing software) in the plane of the surface. For a pure water liquid drop, a contact angle of <90° indicates a hydrophilic surface and >90° indicates a hydrophobic surface.

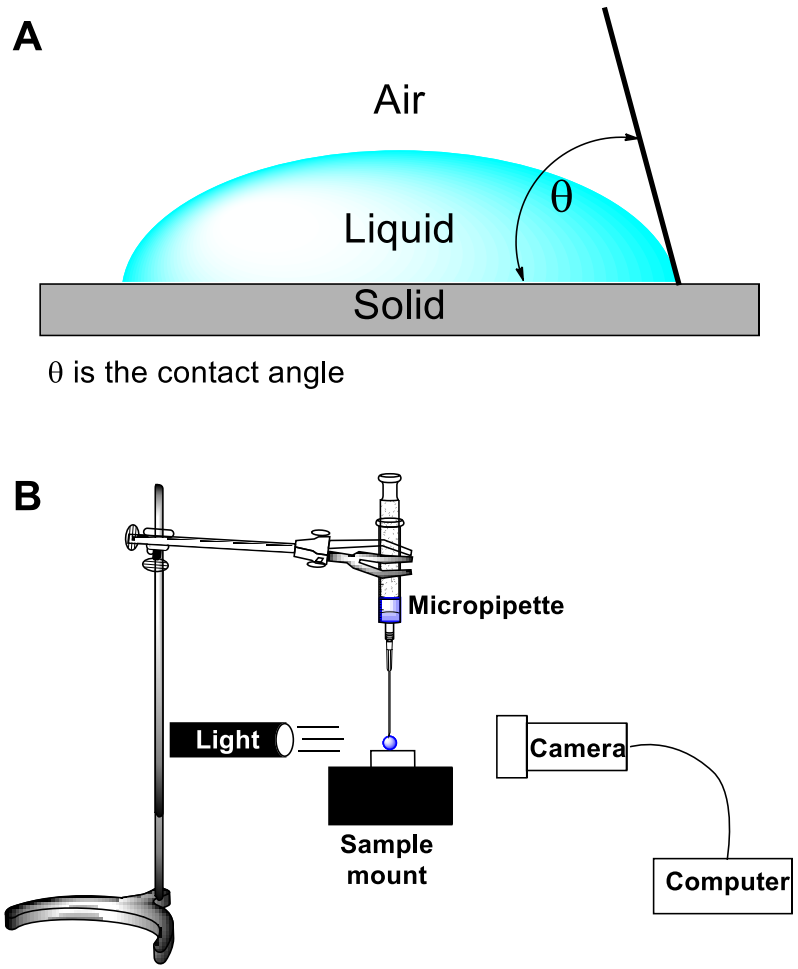

FIGURE 5-3: A) The contact angle of a liquid drop on a solid material; B) Goniometer apparatus for determining drop contact angle.

5.1.3.2 Scanning Fluorescence Imaging

Two-dimensional images of the fluorescence of a material can be achieved using a Typhoon variable mode imager. More commonly used for biological gels, this instrument works similarly to conventional imaging scanners; however, illumination of the sample is achieved with a laser of a specific wavelength (488 nm, 532 nm or

633 nm) then the emitted fluorescence of the sample is captured and amplified with a PMT and converted to an image of the fluorescence. The amount of fluorescence can be quantified by comparing the relative intensity in each pixel to an internal standard. Advantages of scanning fluorescence imaging over spectroscopic techniques is that rapid 2D data can be achieved over a large area (43 cm x 35 cm), therefore, allowing a fast comparison between many samples, as well as an analysis of the distribution and uniformity of fluorescence within the same sample. However, unlike spectroscopic techniques no characterisation of the fluorescence spectra is achieved; therefore, there is some uncertainty in the origin of the observed fluorescence signal.

5.2 ATTACHMENT OF PHOTOSWITCHES TO GLASS SURFACES

To perform surface sensing using microstructured optical fibres, the surface of the suspended core need to be functionalised. However, due to the enclosed structure of MOFs, characterisation of the functionalised surface is difficult. Most commonly used methods to characterise surfaces, such as AFM, [24,26,31] and XPS,[42, 43] are unable to be used to examine the MOF core.

Therefore, to investigate the surface attachment processes and to test different chemical conditions of the functionalisation of photoswitchable ionophores to glass surfaces, the functionalisation protocols were first tested on glass slides before latter transferring the protocols to a microstructured optical fibre. The surfaces were characterised through non-destructive chemical methods of sessile drop contact angle measurements,[25, 30, 44-46] and scanning fluorescence imaging[47]. Other techniques such as grazing angle IR spectroscopy[43, 46-47] (using a Perkin Elmer spectrum 400 FT-IR/FT-FIR spectrometer with a liquid N_2 cooled MCT detector) and surface zeta potential[48-50] measurements were attempted; however, these were found to not be suitable due to either a high silica IR background absorption and low material surface reflection, or lengthy data acquisition, respectively.[§]

In a preliminary investigation into the surface treatment conditions the APTES silanization conditions are thus investigated and verified using these methods by coupling of a fluorophore to the surface. Then two different coupling conditions are compared; the HATU mediated coupling and EDC/NHS coupling.

[§] A discussion on the investigation of monitoring surface chemistry and photoswitching by zeta potential is presented in Appendix B.

5.2.1 RESULTS AND DISCUSSION

5.2.1.1 Experiment 1: APTES Silanization and Photoswitch Coupling to Borosilicate Glass Slides

APTES SAM on borosilicate glass slides

Firstly, in order to verify the glass cleaning procedure and the compare subsequent APTES silanization reaction times, sessile drop contact angles were obtained after four different treatment conditions and the surface wettability was compared. The four different treatments compared were: 1) untreated borosilicate glass (as supplied); 2) washed glass slide (Slide **XVII**); 3) APTES treatment for 1 hour (Slide **VI**); and 4) APTES treatment for 5 hours (Slide **XIV**) (Figure 5-4). The contact angle of the water drops indicates a clear change in the surface hydrophobicity/wettability between the different treatments. Cleaning the slide produced a very hydrophilic surface, as expected, due to an increased amount of free hydroxyls on the surface. The observed average angle of around 10^{o} was higher than expected compared to that reported by Cras *et al.* ($\leq 2.5^{o}$).[30] However, the actual angle was most likely lower than calculated due to the increased error in defining the droplet shape in the images at lower angles due to droplet spreading. There was no significant difference between 1 hour APTES and 5 hour APTES treatments, which both showed angles of around 22^{o}, which was significantly lower than expected for APTES SAMs ($40\text{-}60^{o}$).[51, 52] (However, later APTES coating experiments under the same conditions produced contact angles closer to 40^{o}, therefore this discrepancy could be due to variation and experimental error in the goniometer technique.)

Therefore, due the increased risk of multiple layers forming with 5 hours of APTES (Figure 5-2), subsequent surface silanization on glass slides was performed over a 1 hour period, and only slides coated with APTES for 1 hour are compared further.

Coupling of SP-5 to APTES coated glass sides

The aminated surface was then functionalised with a fluorescent spiropyran photoswitch, **SP-5**, in order to verify the formation of the APTES layer, and to test different reaction times for complete surface coupling. This photoswitchable carboxylic acid functionalised spiropyran was synthesised by Dr. Sabrina Heng in a

similar manner to spiropyran **SP-4** (Chapter 4), and was shown to be selective towards Pb^{2+} (Scheme 5-2).[**] Therefore, it was chosen as a model system to investigate surface functionalisation, and photoswitching towards a Pb^{2+} sensitive surface sensor. This coupling reaction was performed using the EDC/NHS methodology. To Slides **I** to **IV**, with an APTES SAM, four different coupling conditions were examined. They were: 1) reaction in the dark for 2 hours; 2) reaction in the dark for 5 hours; 3) reaction in the dark for 24 hours; and 4) reaction under the influence of 352 nm light for 5 hours (a summary of all the treated slides is shown in Table 5-1). These conditions were used to determine the minimal optimal time required to achieve a fluorophore coated surface.

The fourth reaction condition under UV irradiation was to compare and investigate the effect of the reaction occurring when **SP-5** is in the photoswitched state (**MC-5**). During the surface coupling this reaction solution was observed to change colour from the yellow of the spiro-form to blue of the merocyanine, then fading to a clear solution by the end of the 5 hours. This bleaching of the solution colour could have been from either: photobleaching of the spiropyran from the UV light; a loss of colour in the merocyanine state when activated to the NHS ester; or degradation due to reacting with the NHS or EDC while in the merocyanine form. This phenomenon was not investigated further due to successful reaction to the surface under the other conditions.

[**] Unpublished data.

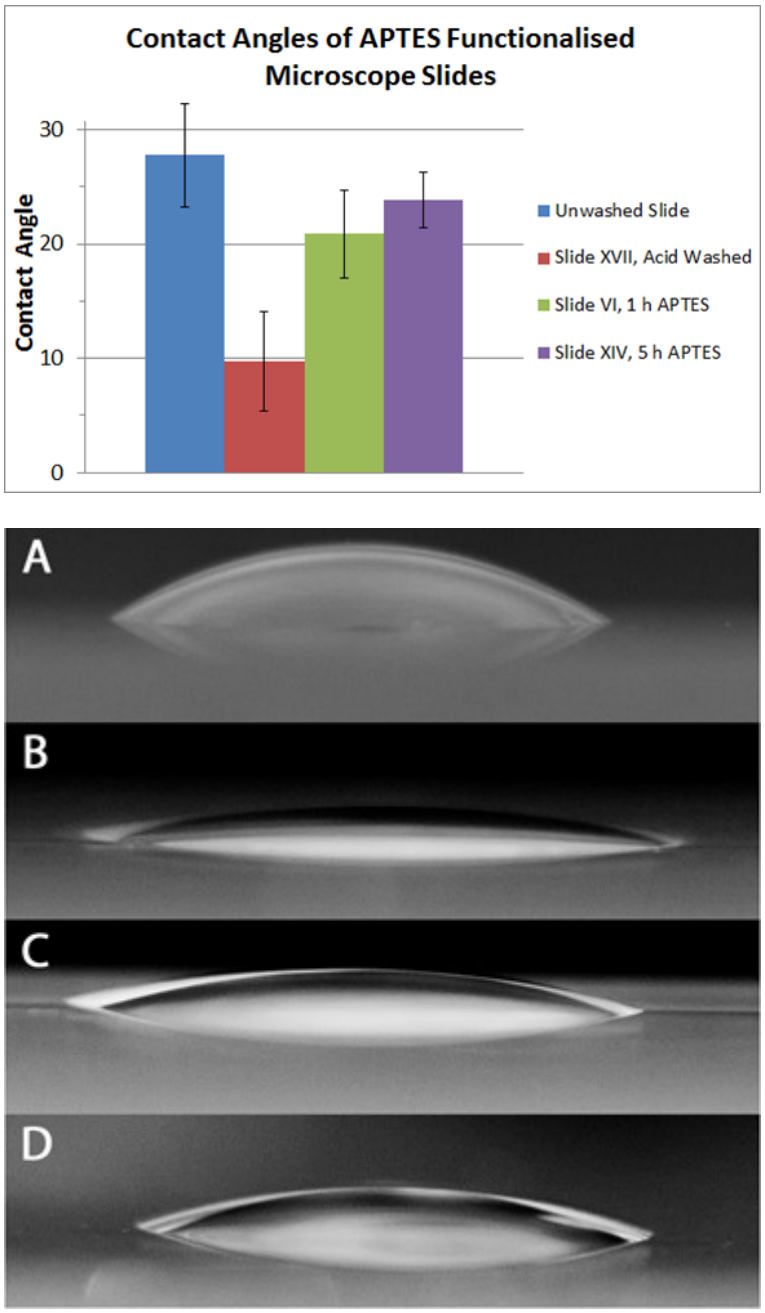

FIGURE 5-4: Graph showing the measured contact angle after various treatments and example images of 2 µL water drops on glass slides, A) Untreated; B) Cleaned with Piranha; C) 1 h APTES; D) 5 h APTES.

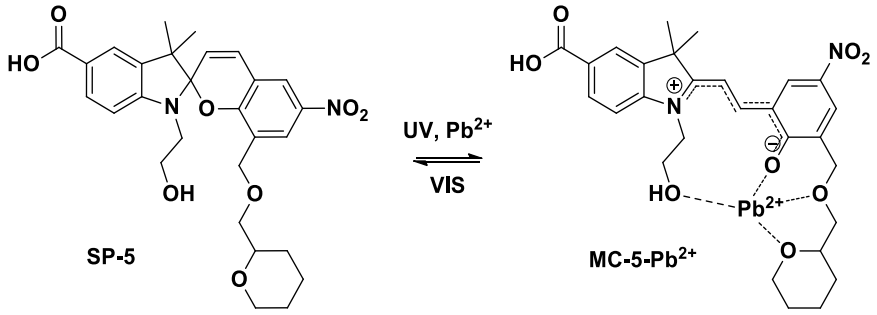

SCHEME 5-2: The structure of **SP-5** and proposed mechanism for binding Pb^{2+}.

Quantification of the relative amount of reaction to the surface was attempted via three methods: 1) UV-vis absorption spectral measurements of the reaction solution and glass slides before and after reaction; 2) scanning fluorescence imaging using the typhoon imager; and 3) contact angle measurements.

The UV-vis absorbance spectra of the reaction solutions sampled after each reaction time showed no apparent trend in the relative absorbance intensities (**SP-5** concentration) (**Figure 5-5**). However, there was a noticeable blue shift from 440 nm to 430 nm and reduced overall absorbance in all samples with activated **SP-5** (including an activated control not exposed to a APTES surface); therefore, this change can be attributed to the formation of the NHS ester of **SP-5**. This shows that reactions to the carboxylic acid group produces a spectral change which could later influence the observed fluorescence signal, causing a difference between the solution and the surface bound emissions. The lack of the expected trend of decreasing **SP-5** concentrations for longer reaction times was likely due to the influence of other variables; such as, evaporation of the solution or non-specific binding to the surface of the slides and glassware having a greater influence on concentration than the reaction to the amine monolayer. Similarly, no change in the UV-vis absorption/transmittance was observed in the glass slides (not shown), possibly due to the weak absorption of a fluorophore monolayer being below the detection limit of the instrument, as well as the presence of a large silica background signal.

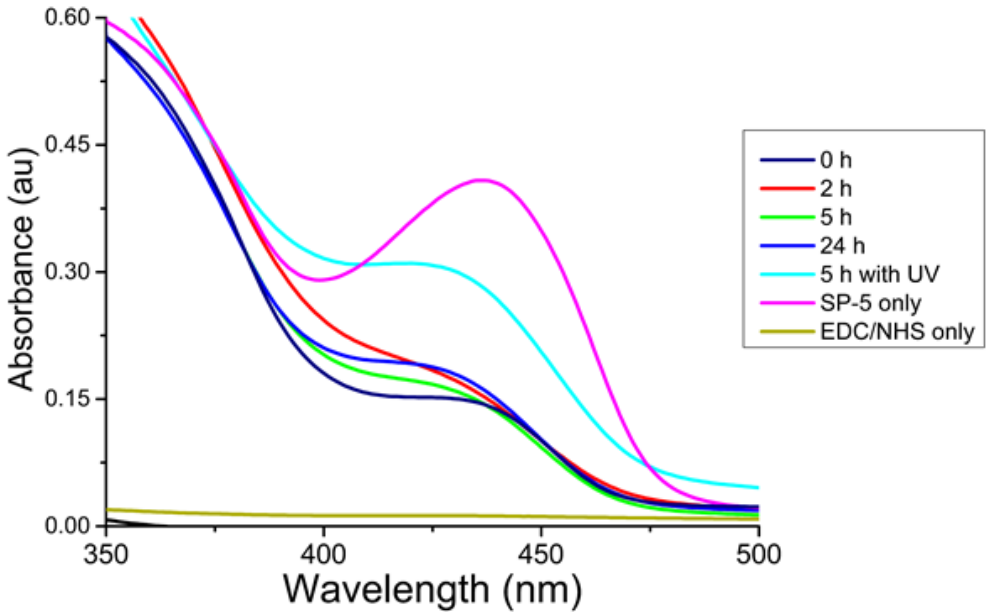

FIGURE 5-5: Absorbance spectra of the slide coupling reaction solutions before (navy) and after reaction with the aminated glass slides. Slide I (red); Slide II (green); Slide III (dark blue); Slide IV (light blue); **SP-5** only control (pink); NHS/EDC reagent solution only control (brass).

The fluorescence of the slides was compared using a Typhoon imager as described in Section 5.6.1.6. The Typhoon images of the treated slides **I**, **II**, **III**, **IV**, and control slides **VI** and **XX** are shown in Figure 5-6. To investigate if these slides on the Typhoon imager could detect the presence of Pb^{2+} in solution, to each slide was placed two 75 µL drops; the upper drop consisting of pure water and the lower drop an aqueous solution of 10 mM $Pb(ClO_4)_2$. Acetonitrile was first attempted to be used as solvent (due to preliminary binding affinity studies of **SP-5** towards Pb^{2+} being performed in acetonitrile (similarly to spiropyrans **SP-1** to **SP-4** in Chapter 4)); however, acetonitrile was found to evaporate within the image acquisition timescale. After exposure to ambient light conditions (Figure 5-6A) there was no observable difference between the six slides, or between the solution droplets. The slides were then irradiated on the imager stage with UV352nm blacklight for 4 min (Figure 5-6B). The control slides as well as the Slide **IV** (which was treated with spiropyran under UV irradiation) did not express any increased fluorescence. However, after irradiation Slide **I** to Slide **III**, which were treated with **SP-5** for 2 to 24 hours, showed a distinct increase in fluorescence dependent on reaction time. This

observable fluorescence was a result of increased fluorescence signal from the more fluorescent **MC-5** isomer, demonstrating the photoswitchability on the surface in the solid state. Interestingly the areas covered with the water drops showed a decreased signal, this could possibly have been due to: fluorescence quenching by the water; increased scattering of the signal interfering with the Typhoon image; absorption/reflection of the UV light resulting in no/reduced photoswitching; or thermoswitching of **MC-5** to **SP-5** in solution within the experiment acquisition timescale (<30 min). The drop with Pb^{2+} appeared the same as the drop with just water; therefore, from these images there is no evidence of binding and sensing of Pb^{2+} in water from the surface attached spiropyran **SP-5**.

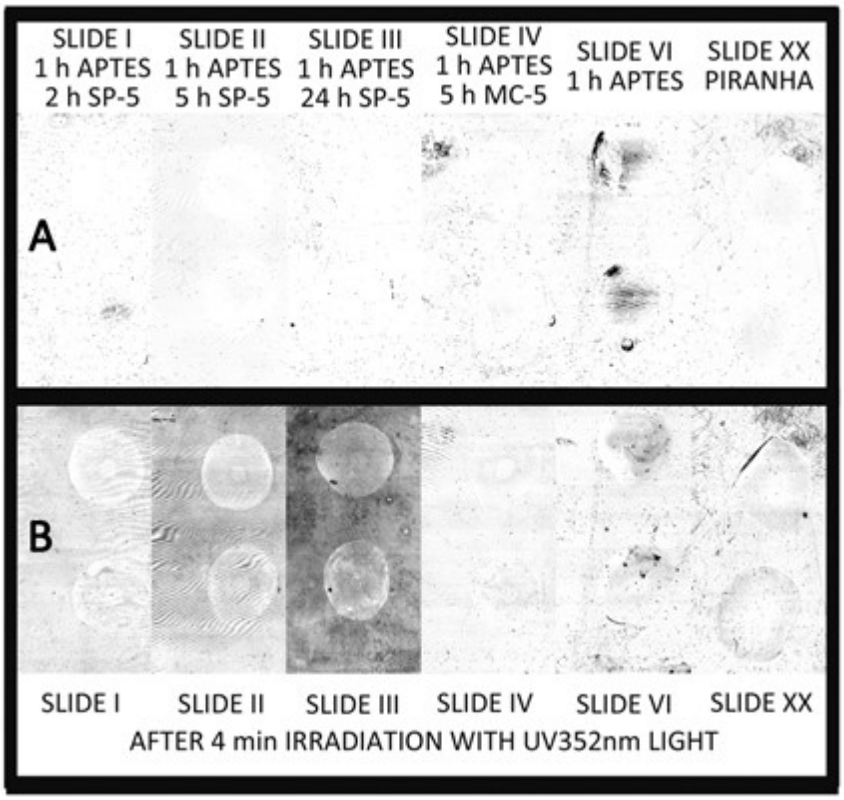

FIGURE 5-6: Scanning fluorescence images of treated microscope slides: A) before; and B) after exposure to UV352nm light for 4 min. Each slide contains two drops, the upper drop of Milli-Q water, and the lower drop 10 mM $Pd(ClO_4)_{2(aq)}$

The contact angle of 2 μL water droplets on the spiropyran functionalised slides was also investigated using the goniometer setup described below. Due to a large error in drop angles no significant difference was able to be determined between the different

treatments, including the APTES only control (Figure 5-7), with each treatment producing a hydrophilic surface with contact angles between 30 and 45 degrees. This lack of difference could have been due to **SP-5** coated surfaces exhibiting a similar hydrophobicity to APTES coated surfaces. Therefore, functionalisation of the APTES surface could not be monitored by contact angle measurements; however, with a fluorophore with a greater difference in hydrophobicity, this method should be able to monitor this reaction.

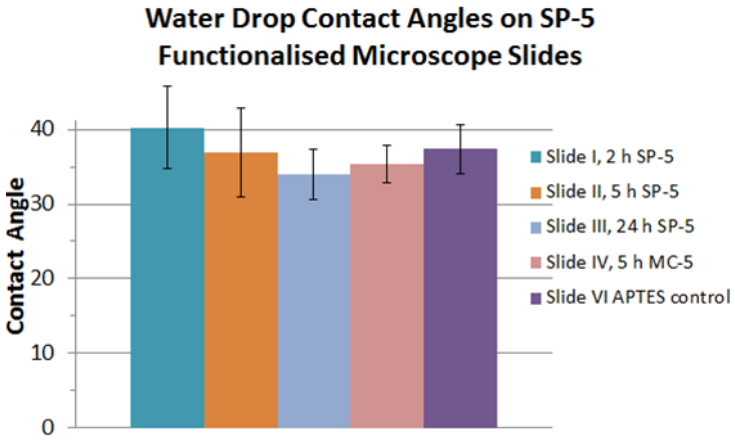

FIGURE 5-7: Average sessile drop contact angles of 2 µL water drops on spiropyran functionalised slides treated for different reaction times.

5.2.1.2 Experiment 2: Comparing Two Amide Coupling Conditions.

After establishing the APTES coating procedure and characterisation techniques in Experiment 1 (Section 5.2.1), here we aimed to perform a similar investigation in which two coupling conditions are compared. For this comparison a lumogallion derivative, **Azo1** (Chapter 2), was used as the photoswitchable unit for attaching to the silanized surface. **Azo1** has previously been shown to bind to Al^{3+} ions and produce a detectable fluorescence signal when attached to polymer coated glass slides and MOFs (Scheme 5-3).[53, 54] The two coupling conditions compared are the EDC/NHS method (Slide **XXIII**, **XXV**) (as used in Experiment 1 with **SP-5**), and the HATU method (Slide **XXIV**, **XXIV**).

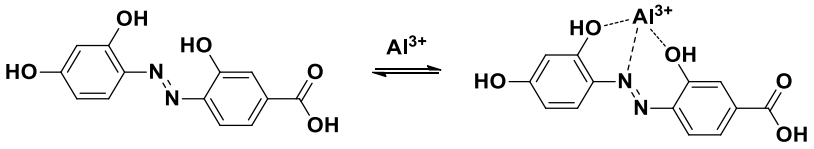

SCHEME 5-3: Structure of **Azo1** and binding to Al^{3+}.

Sessile drop contact angle measurements of Slides **XXIII** to **XXVI** and **XXXII** were performed to confirm amide coupling of **Azo1** to the APTES surfaces and to compare between the two coupling methods. The average contact angle of drops of 2 µL and 10 µL was also compared to determine if the size of the water droplet affected the observed contact angle. The results are plotted in Figure 5-8. The 2 µL drop contact angle for each slide (apart from Slide **XXIII**) showed an angle of 40-50 degrees. Therefore, these different treatments were indistinguishable from each other. These values, although higher than the contact angles measured in Experiment 1, are within the reported range for APTES coated silica. The 10 µL contact angle results gave a decreased value for the APTES and EDC/NHS coated slides compared to the 2 µL drop angles; the HATU method angles were unchanged. Therefore, with the 10 µL drops a difference in the surface chemistry was observable between the EDC/NHS coupling method and the HATU coupling method, with the HATU method producing a more hydrophobic surface.

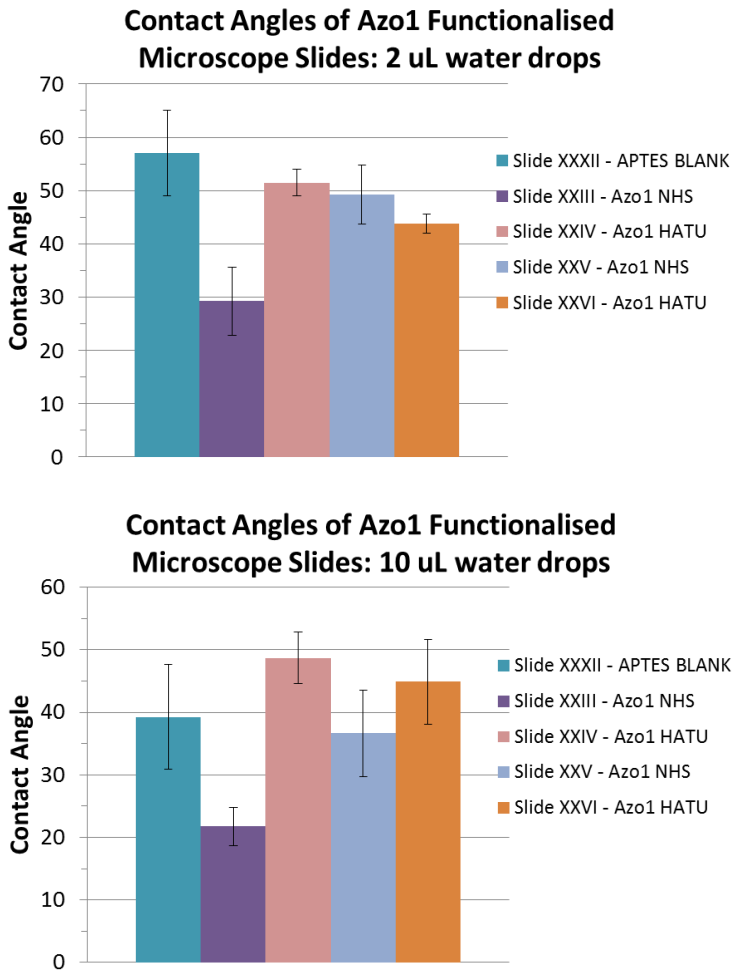

FIGURE 5-8: Graphs of the contact angles comparing slides treated with **Azo1** with either the EDC/NHS or HATU methods.

The fluorescence and sensing capability of the slides were then imaged using a Typhoon Imager (Figure 5-9). The fluorescence image shows that the APTES only control shows no fluorescence, as expected due to the absence of fluorophore. The slides coated with the EDC/NHS method showed no fluorescence signal, and were indistinguishable from the APTES slide; thereby indicating that no surface coupling occurred in these conditions. This was not expected due the successful coupling of the spiropyran **SP-5** shown in Experiment 1. Both slides treated with the HATU method showed an increase in the fluorescence emission, indicating the presence of **Azo1**. This difference between the EDC/NHS and HATU coupling methods verifies the difference observed in the 10 μL drop contact angles. This lack of surface

coating with the EDC/NHS method may possibly be due to errors from a bad reagent solution, however, repetition of these conditions was not performed to verify this.

The ability of the **Azo1** coated slides to detect the presence of aluminium ions was then examined through a preliminary investigation. A 1 mM stock solution of $KAl(SO_4)_2$ was prepared in acetonitrile. This stock Al^{3+} ion solution was then diluted 10 and 100 fold with either acetonitrile or Milli-Q water to give 0.1 mM and 0.01 mM stock solutions, respectively. To the **Azo1** treated slides four 75 µL drops of solution were added containing either: Milli-Q water; 0.1 mM Al^{3+} in acetonitrile; 0.1 mM Al^{3+} in 10 % acetonitrile in water; or 0.01 mM Al^{3+} in 1 % acetonitrile in water. The fluorescence of the plates was then imaged (Figure 5-9). The ion solution with only acetonitrile (top right drop) evaporated during image acquisition, this left a salt residual that was visible in the image on all slides. The other drops showed a reduced fluorescence compared to the regions of slide without water (similarly to observed in Experiment 1), and there was no difference in fluorescence signal between each of the drops (Figure 5-9C). A large increase in fluorescence intensity of the Al^{3+} drops was expected, as was observed in previous reports of Typhoon images of **Azo1** in polymer coated slides.[26] The lack of this strong signal is likely due to the reduced surface density of **Azo1** in a SAM compared to a three-dimensional polymer.

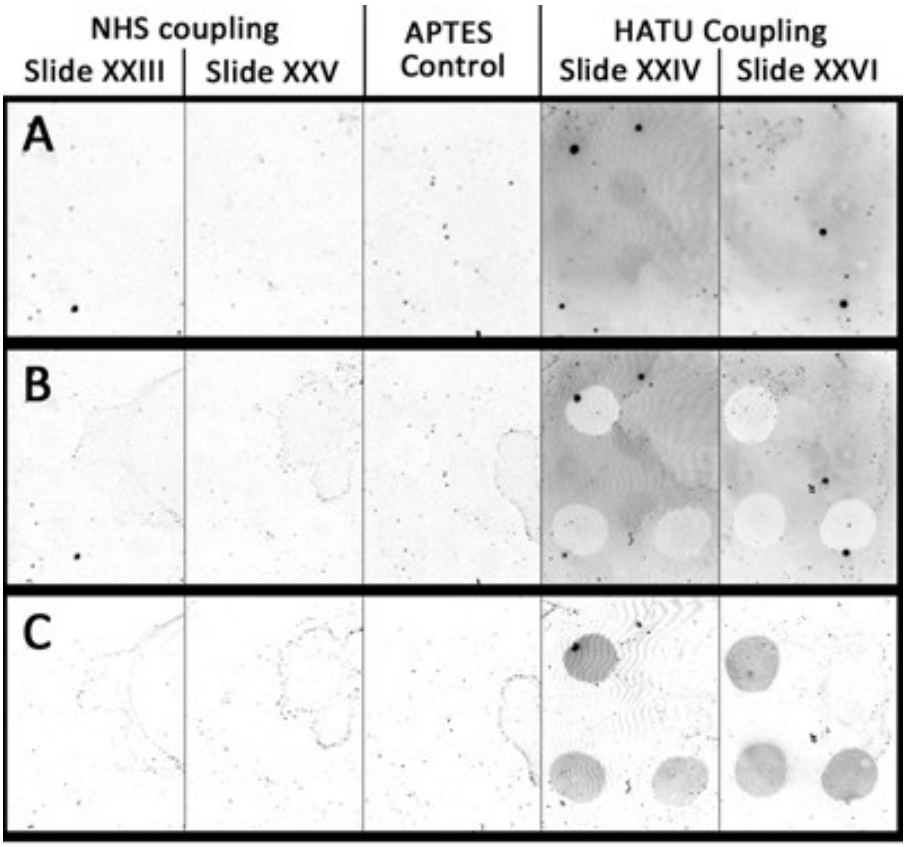

FIGURE 5-9: A) Typhoon fluorescence image of slides coated with **Azo1** in different coupling conditions. B) Typhoon fluorescence image of functionalised slides with four drops of solution arranged on each. Top left) Water only; Top right) 0.1 mM Al^{3+} in acetonitrile; Bottom left) 0.1 mM Al^{3+} 90 % H_2O; Bottom Right) 0.01 mM Al^{3+} 99 % H_2O. C) Difference between the image with solution and without solution.

5.2.2 CONCLUSIONS TO SECTION 5.2

The above surface coating experiments on glass slides demonstrate successful silanization of the borosilicate surface with APTES after one hour reaction time. This was demonstrated by observing the changes in surface hydrophobicity by comparing the sessile drop contact angle on each surface. Successful coupling of a spiropyran and azobenzene photoswitchable fluorophores to the surface was achieved using two coupling protocols, EDC/NHS and HATU/DIPEA, respectively, and demonstrated with the Typhoon Imager. It was found that the amide coupling to the surface with spiropyrans (**SP-5**) is improved if left for 24 hours, compared to 2 hours and 5 hours reaction times. Photoswitching of **SP-5** on the surface was

observed as an increase in fluorescence in the merocyanine form. However, the ability for either the **SP-5** or **Azo1** surface to bind to and detect the metal ions Pb^{2+} or Al^{3+}, respectively, in an aqueous solution could not be determined using the Typhoon imager.

5.3 INVESTIGATION OF PHOTOSWITCHABLE SENSORS IN MOFS

This section describes an investigation into the use of MOFs as a sensing platform for metal ions using a photoswitchable fluorophore. Firstly, sensing in the fibre is investigated with the spiropyran fluorophore, **SP-3,** premixed with Ca^{2+} ions in solution. **SP-3** was the fluorophore of choice due to its strong selective ion binding and fluorescence in the presence of alkaline metals, such as Ca^{2+}, and was shown to bind to Ca^{2+} in a 1:1 stoichiometry (Chapter 4.3), which is preferable when chelating to ions when fixed to a surface.[39] This is followed by attaching this photoswitch to the surface via silanization and coupling reactions to create a reusable sensing system. Therefore, this investigation aimed to create a fibre based sensor for detecting Ca^{2+} for future applications in sensing in IVF samples.

5.3.1 RESULTS AND DISCUSSION

5.3.1.1 MOF Fluorescence Sensing with SP-3 in Solution

The fluorescence and sensing behaviour of **SP-3** using MOFs was first investigated when in solution prior to attachment to the MOF core. This examines the use of **SP-3** in a premixed analyte solution and would lead to applications of fibre based measurements in solutions which allow for premixing of a biological sample and fluorophore, such as IVF media (*i.e.* without the presence of embryos).

To emulate premixed conditions, in which the fluorophore in acetonitrile is mixed with media, four analyte solutions were prepared by mixing **SP-3** (10 μM) in acetonitrile with aqueous $Ca(ClO_4)_2$ stock solutions (100 μM, 10 μM, or 1 μM) and Milli-Q water in a 1:1 volumetric ratio. A series of untreated MOFs (approx. 25 cm long) were coupled to the optics setup (see section 5.6.2.3) and while aligned to the laser each fibre was completely filled with an analyte solution by dipping the 'fill' end in solution for 5 min. The fibre was then exposed to ten 8 ms pulses of 532 nm laser light (approx. 50-60 μW) with the fluorescence spectra recorded after each pulse.

Fluorescence of SP-3 in fibre without Ca^{2+}

The background spectrum from an empty fibre showed only a small feature peaking below 570 nm before being cut off by the 550 LP filter (Figure 5-10A). This peak is from the Raman spectra of the exposed glass fibre and is typical of empty MOFs. The intensity of this feature can be used to optimise the coupling of the fibre to the optics setup in lieu of fibre transmission power. Also, as its intensity is dependent on the coupling of the fibre to the laser optics, the intensity of Raman spectra should be able to be used to account for variations (e.g., in optics coupling) between different fibres. After filling the fibre with **SP-3** solution the fluorescence spectra from **SP-3** is observed with a peak at around 628 nm (Figure 5-10B); this is similar to the 625 nm maximum observed with the microplate reader (Section 4.3.1.2). In these irradiation conditions the spiropyran peak experienced an approximate 30 % decrease in signal intensity over 10 laser pulses due to photobleaching or/and reverse photochromism (a similar decrease was observed for **SP1** over 50 pulses in Chapter 2). The fibre was then externally irradiated with UV light for 10 min and a fourfold increase in signal was observed, due to an increase in **MC-3** concentration from photoswitching, with no change in the peak wavelength (Figure 5-10C). This new peak rapidly decreased with pulsing green light by approximately 80 % over 10 pulses, to give a spectrum with intensity similar to the original unswitched compound; indicating reverse, **MC-3** to **SP-3**, photoswitching with the laser excitation light over 10 pulses.

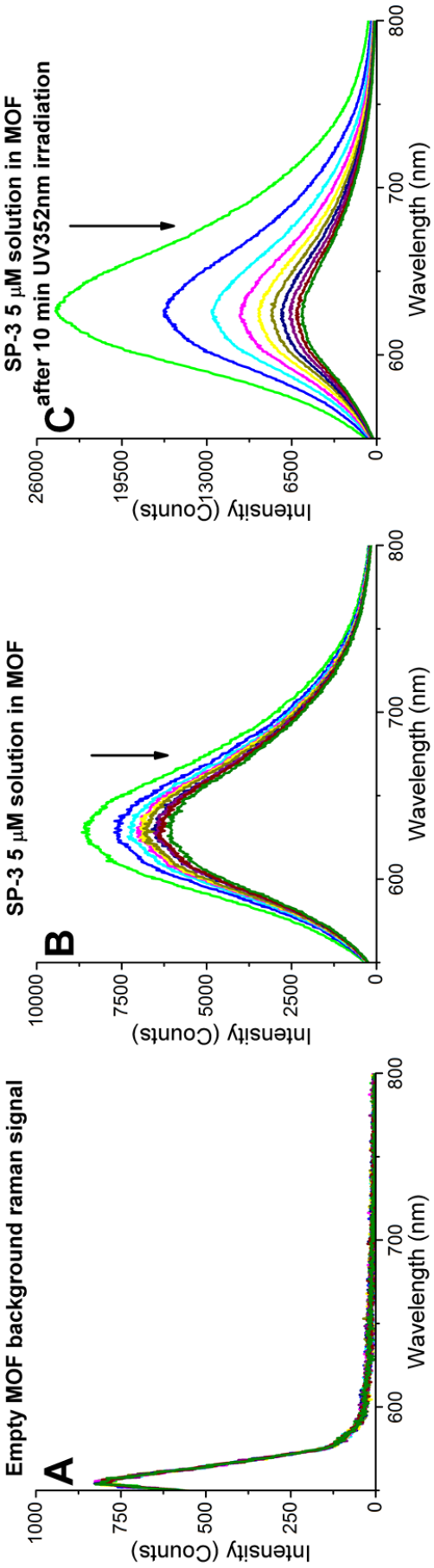

FIGURE 5-10: Typical MOF fluorescence spectra of: A) an empty MOF; B) MOF filled with **SP-3** (5 μM) in 1:1 acetonitrile/water; C) **SP-3** after 10 min of irradiation with UV352nm light while in the MOF.

Photoswitchability of SP-3 in solution in MOF

To test the repeatability of the photoswitching process a MOF filled with **SP-3** solution was exposed to UV352nm light on five consecutive occasions. The fluorescence peak intensities (λ_{max} = 628 nm) over time are shown in Figure 5-11. After the first set of green pulses the fibre was left in the dark for 5 min before exposure to the next set, this showed that there was no recovery in fluorophore intensity over time due to thermal switching. The fibre was then exposed to UV352nm for 10 min, followed by a set of green excitation pulses, this was repeated five times. The repeated UV exposures showed a good recovery in **MC-3** signal, with a 30 % weaker signal observed after the fifth UV exposure compared to the first.

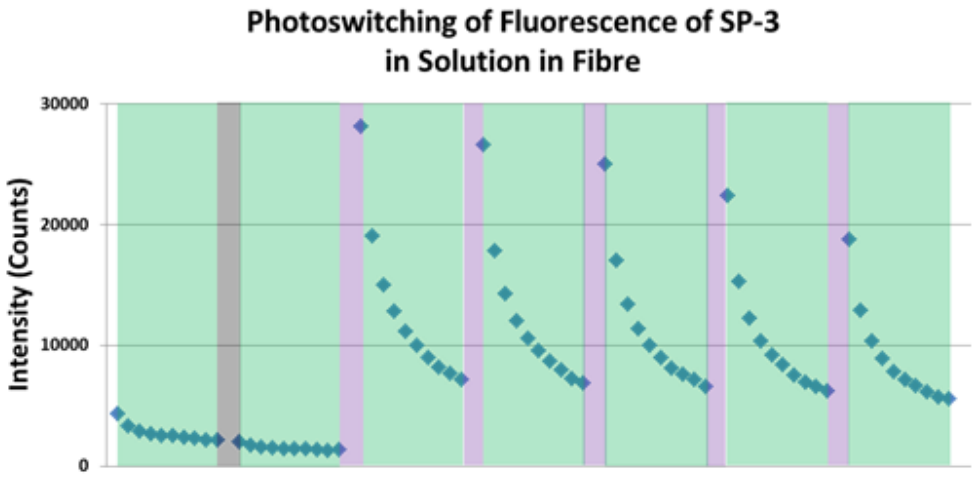

FIGURE 5-11: Multiple photoswitching of an **SP-3** solution in MOF. Each point represents peak fluorescence intensity after 8 ms excitation with green 532 nm light. Green background represents 532 nm exposure, grey represents leaving in the dark for 5 min and pink represents UV352nm exposure for 10 min.

SP-3 in the presence of Ca^{2+}

Each of the four premix analyte solutions (containing **SP-3**:Ca^{2+} concentrations of 5:0, 5:0.5, 5:5, 5:50 μM:μM) were filled into two empty MOFs each and the fluorescence obtained before and after filling, and after external exposure to UV352nm light for 10 min. Due to an error a fibre filled with the 50 μM Ca^{2+}

solution it has been omitted from this discussion. The fluorescence spectra from the first pulse after fibre filling and UV irradiation is shown in Figure 5-12 A and B, respectively.

The **SP-3** fluorescence intensity in the absence of any Ca^{2+} ions was weaker compared to with Ca^{2+}, as expected due to the fluorescence turn on effect of binding to Ca^{2+}, with a peak maximum at 628 nm. With the samples with Ca^{2+} the fluorescence signal appeared to increase as Ca^{2+} concentration increased; however, due to variations in the intensity of the sample with 0.5 μM Ca^{2+} (5:0.5 **SP-3**:Ca^{2+}) the large error makes it difficult to distinguish from the 5 μM Ca^{2+} (5:5 **SP-3**:Ca^{2+}) sample. A large difference in signal intensity was also observed between the two fibres without Ca^{2+} ions.

After exposure of the fibre to UV352nm light all samples expressed a varied increase in fluorescence signal which appeared to be non-dependent on relative ion concentration (Figure 5-12B). Fibres with **SP-3** alone had the greatest increase in fluorescence, to give a signal greater than the 0.5 and 5 μM.

The observed variation in signal intensity between fibres that had undergone identical treatment could possibly be due to experimental variations that can occur between fibres, such as; misalignment of the core causing variations in laser intensity, or moving of the core during the experiment acquisition, from solution drying at the ends of the fibre. In an attempt to develop an analysis method to account for differences in the coupling of the fibre to the optics, the intensity of each spectrum was normalised by dividing by the maximum intensity observed in the initial Raman spectra of the empty fibre; the resulting spectra are shown in Figure 5-13. This Raman signal, as an inherent property of the silica fibre, should be directly related to the optics coupling strength and laser intensity. After this manipulation a greater difference is observed between solutions containing Ca^{2+} than without, however, there was no trend between the intensities of the solutions containing Ca^{2+} ions that could account towards a concentration dependent change in fluorescence intensity.

Therefore, it was determined that these fibre sensors are able to distinguish between samples containing and not containing Ca^{2+} at concentration levels below normal extracellular Ca^{2+} concentrations (2 mM);[55] however, it was not possible to accurately determine the Ca^{2+} concentration. Also, forcing the photoswitching of **SP-3** to **MC-3** in these fibres from an external source produced a larger change with the unbound **SP-3**. Therefore, photoswitching in fibre to the 'ON' state of spiropyrans does not provide an accurate representation of ion concentration, and the fibre is best used to photoswitch the spiropyrans to the 'OFF' state. This was discussed previously in Chapter 4.

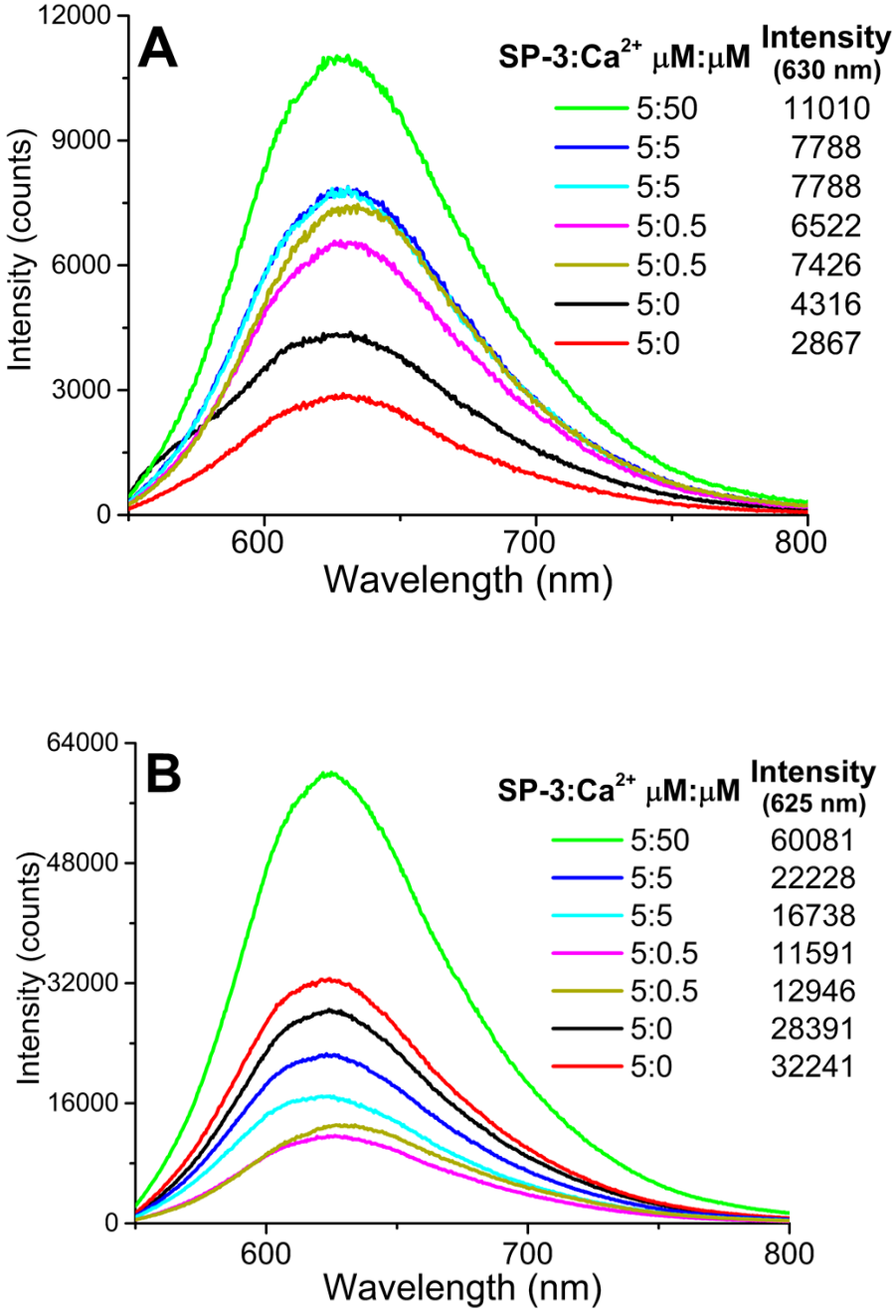

FIGURE 5-12: Calibration of fluorescence sensing of premixed solutions containing **SP-3** (5 μM) and $CaClO_4$ (0, 0.5, 5, and 50 μM) in 1:1 acetonitrile/water. A) Immediately after filling the fibre; B) After 10 min UV 352nm irradiation while within the fibre.

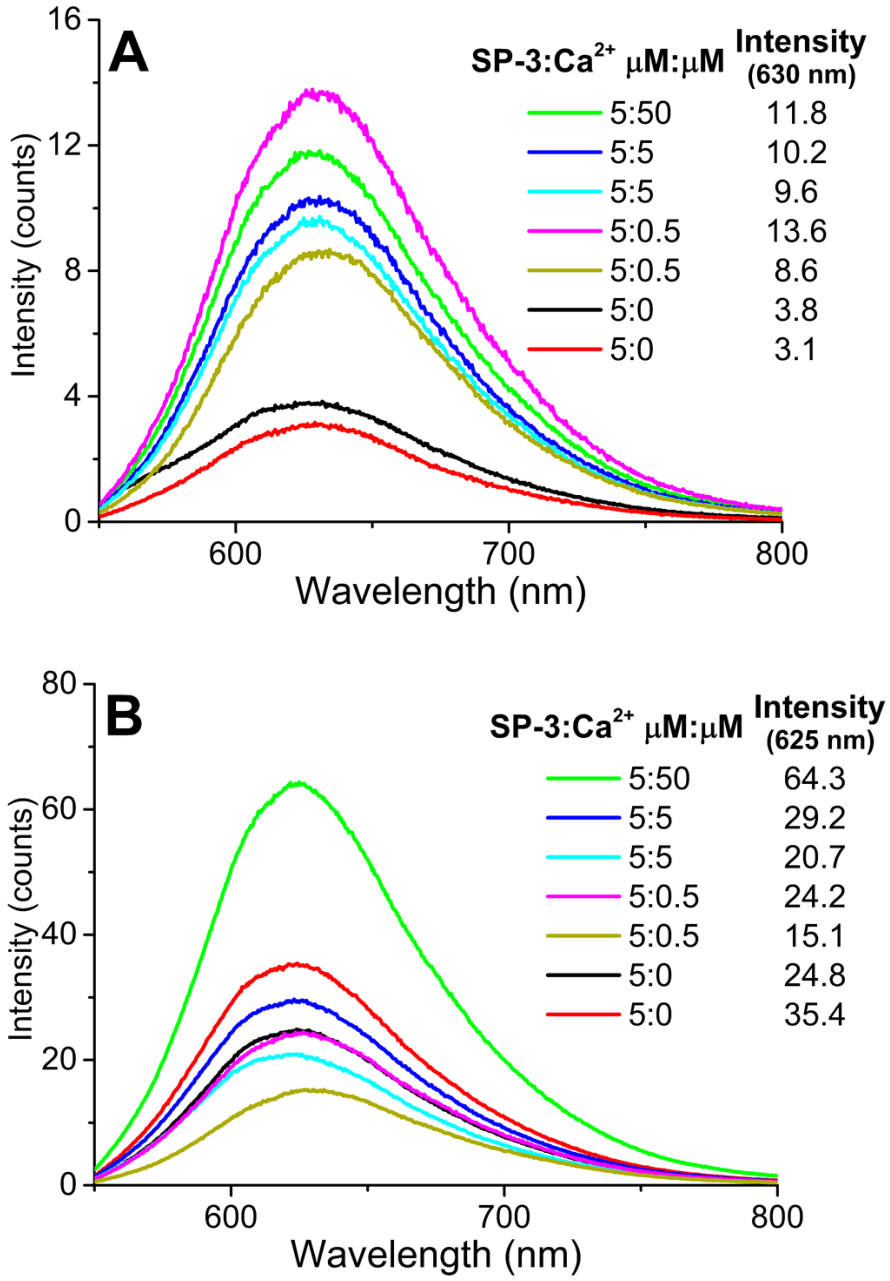

FIGURE 5-13: Calibration of fluorescence sensing of premixed solutions containing **SP-3** (5 µM) and $CaClO_4$ (0, 0.5, 5, and 50 µM) in 1:1 acetonitrile/water. Fluorescence spectra are normalised to the Raman signal intensity. A) Immediately after filling the fibre; B) After 10 min UV352nm irradiation while within the fibre.

Fill and cut fibre sensing technique

To try to improve the system to get a calibration curve a new experiment was devised with two major differences: 1) fibres were only partially filled with analyte solution;

and 2) only one long fibre was used for all measurements. This way a single fibre could first be calibrated and then used on multiple samples. The motivation behind these two changes is discussed below.

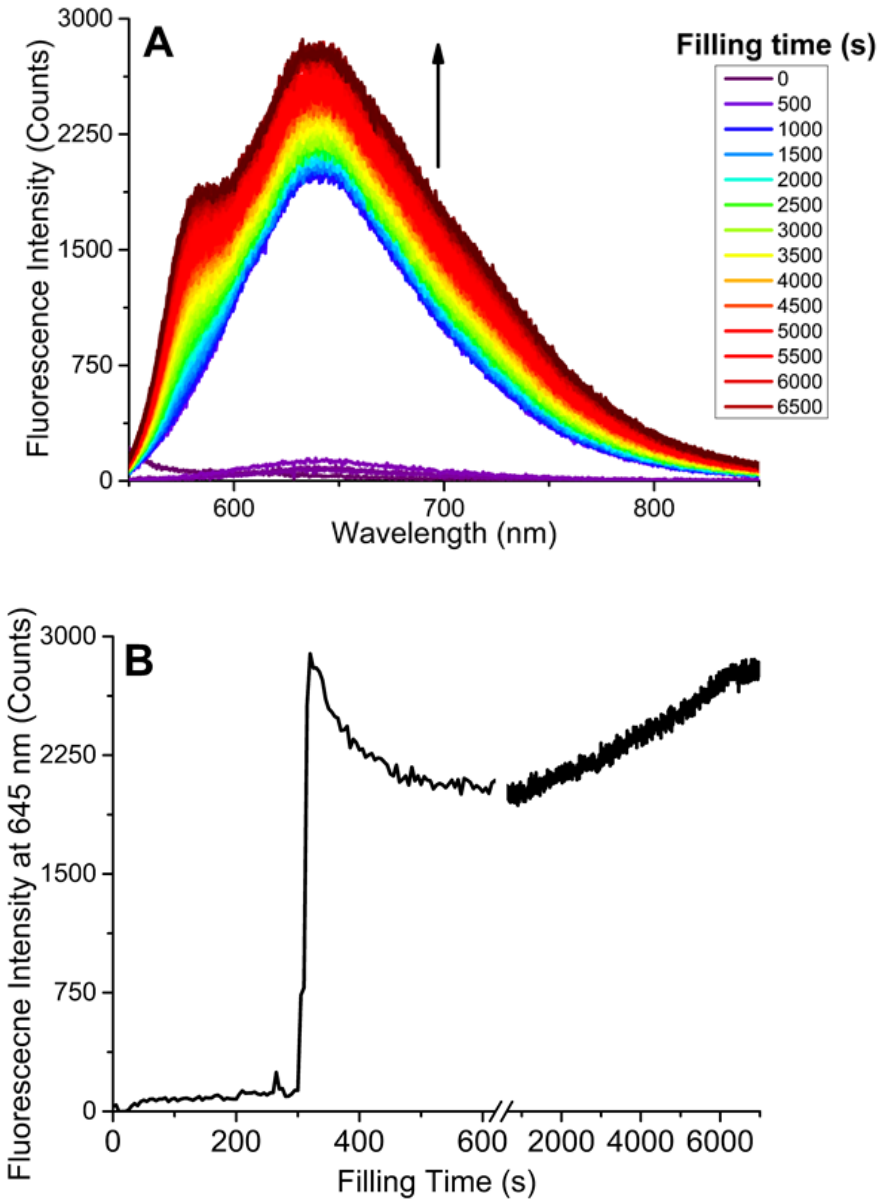

FIGURE 5-14: A) Changing fluorescence spectra of a fibre of 20 cm being filled with a solution of a spiropyran **SP1** in DMSO for 2 h. B) Fluorescence intensity at 625 nm over time.

Firstly, the change to using partially filled fibres was derived from an investigation into changes in the observed fluorescence signal during fibre filling. This investigation looked at the rate of filling and time required to completely fill a fibre

by capillary forces. Fibres (20 cm) were dipped into a solution of spiropyran (**SP1**) in DMSO (1 mM) (as described in Chapter 2) for 2 hours and the fluorescence spectra was observed every five seconds. A small increase in the fluorescence intensity was observed over the first 280 s as the fibre was being filled. After 280 s, corresponding to the solution reaching the 'optics' tip of the fibre, a sharp increase in the fluorescence intensity is observed (Figure 5-14). Therefore, the interference of the solution with the coupling was likely being observed and the solution in the tip of the fibre was being sensed, as well as the solution within the fibre. Therefore, to remove this possible influence on sensing signal the fibres will need to be only partially filled with solution. In a test similar to the above experiment a fibre was filled with solution for 1 min. After an extended period there was no sharp increase in signal; however, a minor gradual increase in signal was still observed. Visual observation of the fibre showed that although the solvent front in the fibre remained unchanged, there was an increase in fluorescence beyond the solvent front; this appeared to be from a sublimation-like process depositing fluorophore on the dry section of the fibre core.

Secondly, by using only one fibre coupled to the optics for all measurements, rather than having to align many fibres, any differences between fibres due to variations in the optics alignment should be negated.

The following experiment continues from the **SP-3** ion affinity assay performed using the microplate reader described in Section 4.5.2.5, as this series of concentrations had been shown to provide a large concentration dependent variation in the observed signal intensities (Figure 4-12A). A 150 cm MOF coupled to the optical setup was sequentially dipped into the **SP-3-Ca**$^{2+}$ solutions from microplate assay tray for 30 s. After the 30 s the fibre was removed from the solution and fluorescence spectra was obtained from excitation with a 32 ms, 0.8 mW pulse of 532 nm light. The section of fibre containing the fluorophore solution was then removed. The clean fibre tip was then dipped into another analyte solution for 30 s. This procedure was repeated on 11 occasions with random sampling of the different analyte concentrations before the fibre became too short to be used. The resulting spectra are shown in Figure 5-15. The fluorescence spectra appeared to be random in fluorescence intensity and gave no correlation between calcium ion concentration

and fluorescence intensity. This was exemplified by the repeating measurements of the 0.5:1, 0.7:1, and 1:1 Ca^{2+}:**SP-3** solutions, which gave very different fluorescent intensities. Therefore, a concentration dependent calibration plot could not be produced. It is unknown why there was a large difference in the spectrums, or why samples 0.05:1, 0.1:1, and 0.3:1 gave an extra peak around 580 nm; there was no correlation to the fill order, indicating that the fibre did not uncouple from the optics during these fills or that the difference in fibre length was responsible. Possible errors causing the observed variations could have arisen due to: variations in optical power; consistency of the filling; movement of the optics; blockages of the fill end; or difference in the fibre tip quality due to the fibre cleavage required to remove the previous sample.

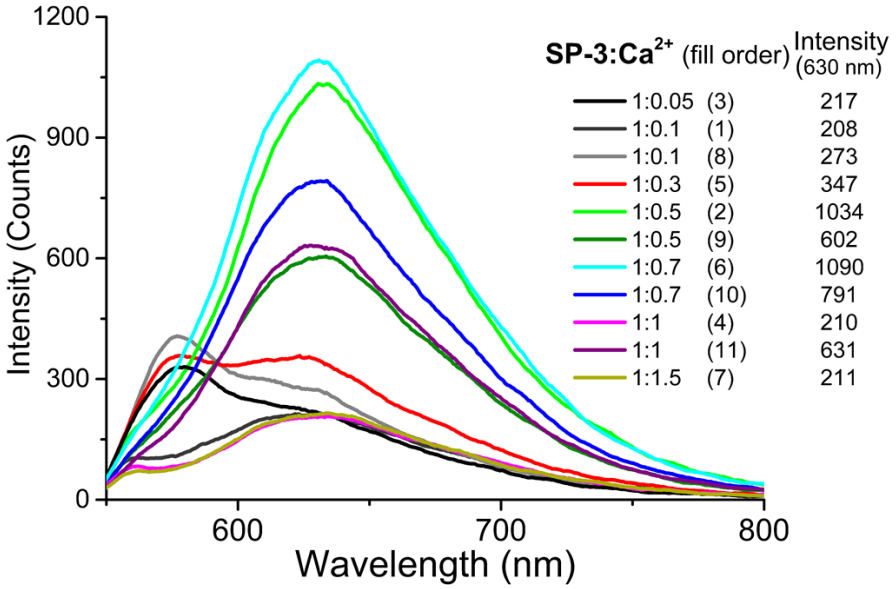

FIGURE 5-15: Fluorescence spectra of **SP-3**/Ca^{2+} solutions after sequentially dipped into a single fibre for 30 s, with cutting of the previously filled section after each measurement.

5.3.1.2 Investigations Towards a Surface Functionalised MOF Sensor for Ca^{2+}.

A series of fibres were prepared with a SAM of **SP-3** via the APTES silanization reaction (as described below in Section 5.6.2) in order to investigate creating a single reusable MOF for the fluorescence based sensing of Ca^{2+}. For this series, 16 fibres

of an initial 40 mm were prepared. Coupling of the **SP-3** fluorophore was achieved using the EDC/NHS amide coupling reaction.

Firstly, two control fibres were prepared by treating with **SP-3** in the absence of coupling reagent. This was performed in order to determine if there was excess spiropyran adsorbed to the fibre surface after coupling and to optimise the MOF washing procedure. The presence of adsorbed **SP-3** on the fibre core was then determined by observing the fibre fluorescence spectra after different washing procedures. After a single wash a fluorescence spectrum indicative of the presence of non-covalently attached spiropyran was observed; therefore, further washing was necessary. After washing the fibres at least three more times with DMF (1.5 mL) the adsorbed **SP-3** was undetectable. Therefore, after the amide coupling reaction all of the fibres were thoroughly washed with DMF four times to remove adsorbed **SP-3**. As the non-specific binding of **SP-3** once activated and onto a functionalised surface would be different to in the absence of coupling reagent, the washing procedure after coupling was also monitored by observing fluorescence of **SP-3** in the waste solvent eluting from the fibre during washing using another blank MOF as a sensitive sensing device.

Photoswitching of SP-3 on the fibre surface

The reproducibility of photoswitching of **SP-3** attached to the fibre surface was then investigated in a functionalised fibre filled with acetonitrile, and compared to the photoswitching in solution (above). A 23 cm **SP-3** functionalised MOF was prepared and coupled to the optics setup. Due to the risk of photobleaching of the fluorophore on the surface during alignment, coupling to the optics was done as quickly as possible with the laser light filtered to a minimal usable intensity by ND filters. Ideally for future applications this coupling would be done in an automated system[56] with a light source which is not absorbed by the fluorophore (*i.e.* >800 nm for the **SP-3** system);for these experiments such a setup was not available. Also, due to an increased absorption/scattering with the functionalised surface, the fibre transmission intensity (optical power of irradiation) could not be obtained with functionalised fibres; therefore, the fibre transmission intensity could not be used to compare different functionalised fibres. The power of the excitation light required

for sensing was thus determined by decreasing the filter density until sufficient fluorescence signal was obtained.

The resulting fluorescence spectra of the **SP-3** coated MOF before and after repeated UV photoswitching to **MC-3** is shown in Figure 5-16. The fluorescence spectra of the empty fibre revealed an emission peak around 600 nm. Filling the fibre with acetonitrile, by dipping the 'fill' end in acetonitrile for 5 min, caused a decrease in the signal intensity, as well as a shift in the emission peak to around 630 nm. This was observable in all fibres and could be attributed to the change in the refractive index of the MOF's holes and interference by the solution at the fibre ends, causing a change in the transmission properties of the fibre, and a change in the fluorescence properties of the solvated fluorophore compared to the solid state, respectively. External irradiation of the fibre to UV352nm light for 10 min produced an increase in the fluorescence intensity due to the photoswitching of the **SP-3** isomer to the **MC-3** isomer. A rapid decrease in intensity upon repeated 532 nm exposure was observed; this decrease was due to reverse photoswitching as well as photobleaching (Figure 5-17). Repeated UV exposure was able to cycle between the **SP-3** and **MC-3** state, as was observed when photoswitching in solution; however, a greater bleaching of the fluorescence after several cycles was observed when attached to the surface. This is likely due to the restricted mobility of surface bound fluorophore compared to the diffusion of fluorophore in solution, as well as an increased relative concentration of fluorophore in the brightest region of the evanescence field producing relatively more bleaching events, as discussed in Chapter 2.

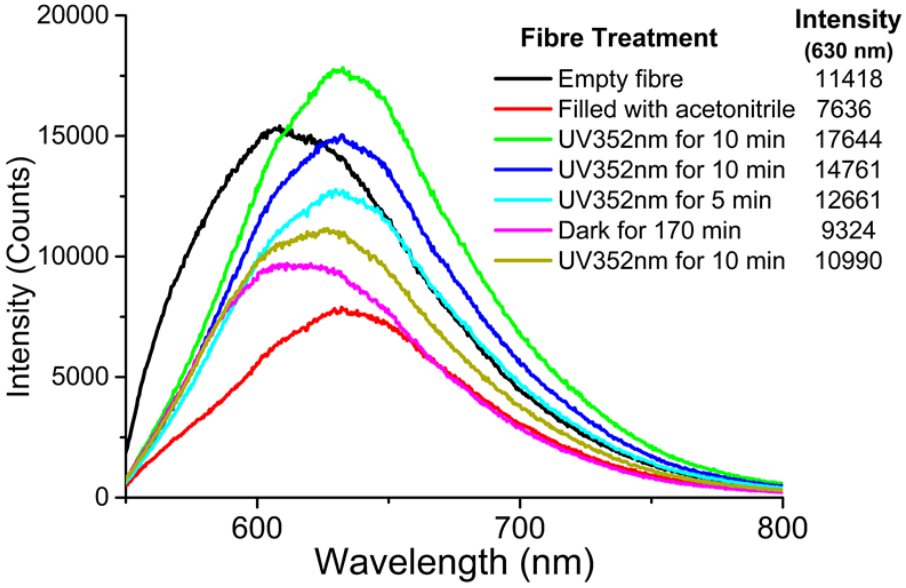

FIGURE 5-16: The initial fluorescence spectrums of a **SP-3** functionalised fibre after various UV treatments.

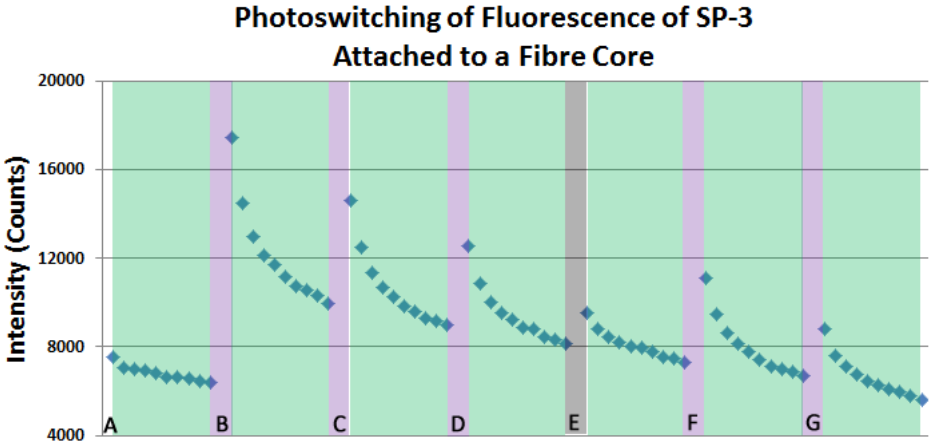

FIGURE 5-17: Changes in fluorescence intensity due to pulsing with 532 nm excitation light. After a) filling with acetonitrile, b) 10 min UV352nm exposure, c) 10 min UV352nm exposure, d) 5 min UV352nm exposure, e) in the dark 170 min, f) 10 min UV352nm exposure, g) 10 min UV352nm exposure

Repeated filling with Ca^{2+} solution

The ability to detect a difference between a fibre filled with just acetonitrile solution or an Ca^{2+} acetonitrile solution was then investigated with a different functionalised fibre. The fibre was first filled with acetonitrile, as in the above experiment this

produced a decrease and bathochromic shift in the fluorescence spectra (Figure 5-18, red). This fibre was then removed from the optics setup and dried by flushing with N_2 in the MOF reaction chamber. After recoupling to the optics setup the fibre was filled with a 10 mM $Ca(ClO_4)_2$ acetonitrile solution and the fluorescence spectra was taken. The fluorescence spectra were normalised with respect to the maximum fluorescence intensity of the unfilled fibre; thereby, accounting for differences in coupling efficiency, excitation power, and photobleaching between measurements. The fluorescence signal of the **SP-3** fibre with Ca^{2+} caused an increase in the fluorescence at around 625 nm (Figure 5-18, lt. blue), approximately 1.5 fold greater than the unfilled fibre. The fibre was then removed from the optics set up and washed by flushing with acetonitrile. After recoupling to the optics, the fibre was filled with 100 mM Ca^{2+}. This produced the same increase in fluorescence as observed with the 10 mM Ca^{2+} solution, suggesting a possible saturation of surface fluorophore at these high ion concentrations.

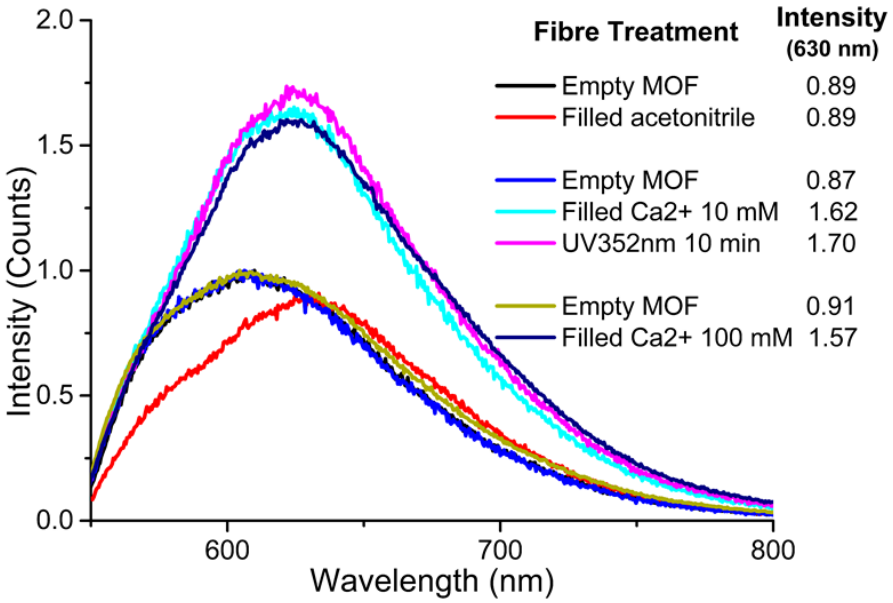

FIGURE 5-18: Sensing of Ca^{2+} in acetonitrile with a MOF functionalised with **SP-3** consecutively sensing three different solutions. Fluorescence intensity normalised to the maximum intensity of the fibre before filling with analyte solution.

Ca^{2+} detection limits and reusability of the same fibre on the set up

The above experiment showed that these fibres could be used on multiple occasions if the contamination could be removed and there was a way to calibrate each fibre. The above process, of decoupling from the optical setup to flush out the fibre and wash away contaminating solution, is not desirable to achieve multiple measurements of a single sample. Therefore, it was investigated whether a simple apparatus to remove analyte solutions could be used while the fibre is attached to the optics. The detection limits of sensing using this method were also investigated.

With the optics setup as described it is impossible to manipulate the 'optics' end of the fibre to wash the solution through the fibre.[57] Therefore, to remove the solution from the MOF while attached to the optics, a system which creates a negative pressure at the 'fill' end was devised (Figure 5-19).

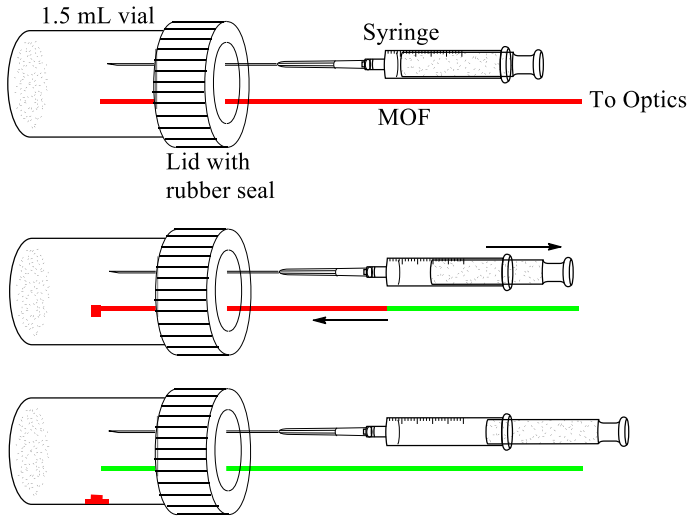

FIGURE 5-19: Process of removing analyte from the laser coupled MOF. The tip of a MOF is inserted through syringe needle in a rubber seal of a HPLC glass vial, removing of the needle and enclosing the tip in the vial creates a sealed environment at the fill end. A negative pressure is imparted to the fill end via a syringe in the rubber seal. The fibre is then refilled with solution by removing the vial from its lid and dipping the fibre tip into solution.

Multiple fibres were investigated incorporating this filling and emptying technique, the combined fluorescence spectra of two fibres filled with increasing Ca^{2+} concentrations between 1 pM and 1 μM is shown in Figure 5-20. In both fibres the

background fluorescence spectra were obtained before and after filling with acetonitrile. The fibres were then emptied, background fluorescence observed and then filled with either 1 pM or 10 nM Ca^{2+} solution. At both of these concentrations an increase in fluorescence was observed at around 650 nm, indicating the ability for these **SP-3** coated fibres to bind to and detect Ca^{2+} at picomolar concentrations. However, after emptying the fibre and refilling with subsequent, more concentrated (10 and 100 pM, and 10 nM and 1 μM, respectively), calcium ion solutions this increase in signal was not observed.

This is possibly from a combination of factors, including: an increase in background signal from Ca^{2+} contamination from previous fills reducing the normalised signal intensity; photobleaching of the photoswitch, from the green and UV light; also from small movements in the alignment of the core to the optics, although this was minimised by fixing the fibre to a stage. Other attempts to wash the fibre while the photoswitch was forced into the spiropyran form, by 532 nm light or external white light, did not show improvement in sensing capacity. To fully remove Ca^{2+} contamination and fully regenerate the fibre surface, the fibres may need to be washed several times under visible light (however, this increases the risk of photodegradation), or the fibres could be washed with a competing chelating agent, such as EDTA; however, this was not investigated due to its risk of contamination and its implementation deviating from the goal of a sensing system that is completely intrinsically reversible by the photoswitching process.

Solutions of Ca^{2+} concentrations lower than 1 pM were not investigated; in order to determine the absolute limits of detection. This was primarily due to the large errors in the sensing, as already discussed, as well as the high abundance of Ca^{2+} in biological systems well above this level. Further improvements in sensitivity could possibly be produced by: only partially functionalising the fibre with fluorophore, such that all fluorophore is exposed to analyte, and thereby, reducing the background signal. Attempts to achieve this were trialled. Also improvements in fibre and spectrometer technology could reduce loss and increase signal.

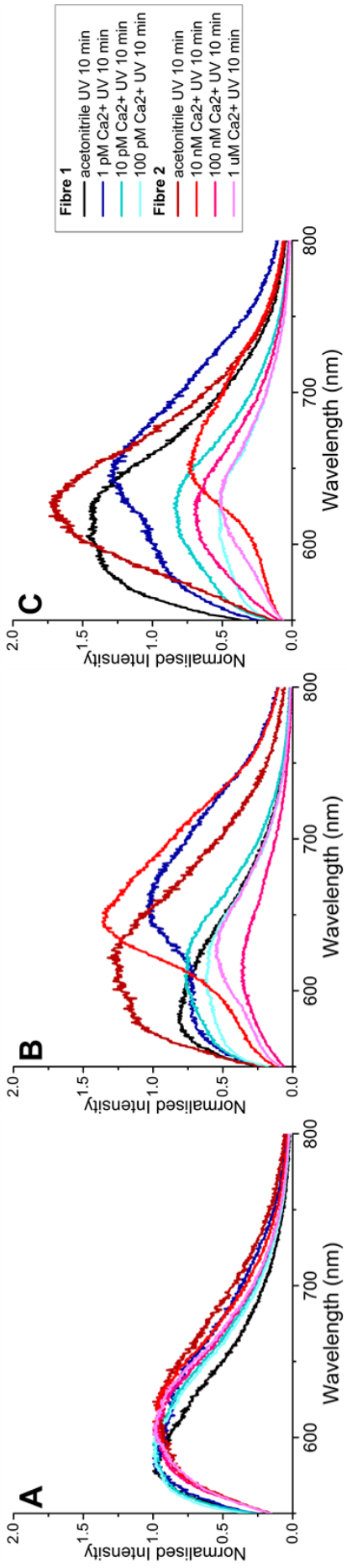

FIGURE 5-20: Combined fluorescence spectra of two fibres filled and emptied on the optics setup normalised to the maximum intensity of the emptied fibre. Fibre 1 sequentially filled with acetonitrile, 1 pM, 10 pM, and 100 pM Ca^{2+}; Fibre 2 filled with acetonitrile, 10 nM, 100 nM and 1 µM Ca^{2+}. A) The normalised empty fibres showing variations in the spectra before addition of analyte; B) The spectra after filling with analyte; C) The spectra after exposure to UV352nm light for 10 min.

5.3.2 CONCLUSIONS TO SECTION 5.3

The sensing capabilities of MOFs with the Ca^{2+} selective spiropyran fluoroionophore **SP-3** was investigated. Firstly, the fibres were used as a dip sensor with the fluorophore premixed in solution, different filling methods were investigated and analyte concentrations, in order to determine whether a reproducible calibrated sensing system could be created. It was found that the fibres could clearly distinguish between samples with and without Ca^{2+} ions; however, due to inconsistencies in fibre coupling to the optics, fibre filling, fibre preparation, cleaving, and possibly other unidentified causes, obtaining a calibratable fibre sensor is likely very difficult due to the sensitivity of the system. The fibres were then internally coated with an aminosilane monolayer, to which was then covalently attached a layer of **SP-3**. The fluorescence of this fluorophore monolayer was detected using the optics setup and photoswitching was observed. A significant spectral change was observed with solutions containing picomolar concentrations of Ca^{2+} in acetonitrile; which is well below the detection limit required to detect intracellular free Ca^{2+} (100 nM).[55] However, like in solution, calibration of the sensor for comparison between different fibres was not possible. The reusability of the functionalised fibre was investigated, however, due to likely contamination from previous analyte solution, and with further issues with calibration, reproducible sensing using a single fibre was not achieved. These issue may be overcome with other fluorophores that rely on ratiometric sensing rather than intensiometric sensing (as discussed in Section 1.1.2); by using a ratiometric sensor the fluorophore itself provides an internal method for calibration.

5.4 PHOTOSWITCHABLE MOF METAL ION SENSORS IN PUBLISHED ARTICLES

This final section presents highlights into the use of MOFs as photoswitchable sensors from two published papers in which photoswitches and MOFs were utilised to create fibre based switchable metal ion sensors. This section presents my contribution to these papers; the full articles are presented as PAPER 3 and PAPER 4 in Appendix D.

5.4.1 PAPER 3: A DUAL SENSOR FOR CD(II) AND CA(II): SELECTIVE NANOLITRE-SCALE SENSING OF METAL IONS[58]

5.4.1.1 Summary of the Publication

The publication titled "A Dual Sensor for Cd(II) and Ca(II): Selective nanolitre-scale sensing of metal ions" investigates two different spiropyran fluoroionophore for the detection of Ca^{2+} and Cd^{2+} (Appendix D.1).

The importance for a sensor for metal ions, such as Ca^{2+}, was discussed in Chapter 1. It has been reported that, while low concentrations of Cd^{2+} (below 100 ρM) significantly stimulate cell proliferation and DNA synthesis, Cd^{2+} exposure at concentrations above 1 mM inhibits DNA synthesis and cell division. Therefore, it is important to have a sensing system that is capable of detecting such low concentrations of Cd^{2+} in biological samples.

This publication presents the design, synthesis and characterisation of the ion binding properties of two new spiropyran fluorophores (**SP-6** and **SP-7**, Scheme 5-4)[††] for the specific detection of Ca^{2+} and Cd^{2+}. The design of these spiropyrans was based on the scaffold introduced in Chapter 4 without the surface attachable R_5, carboxylic acid group. In place of the crown ether ionophore at R_8 the spiropyrans were substituted with a diether alkyl chain ($-CH_2OCH_2CH_2OCH_3$). The two spiropyrans have a structural variations at the indole nitrogen, with either an ethoxy group for

[††] For continuity the labels **SP-6** and **SP-7** have been altered from their originally published names (Compound **1** and Compound **2**, respectively)

SP-6 (similar to **SP-4**, Chapter 3), or a butanoic acid group for **SP-7**. In similar assays to those undertaken with the series of **SP-1** to **SP-4** in Chapter 4, these spiropyrans were shown to exhibit a strong preference to Ca^{2+} and Cd^{2+} over a range of other biologically relevant metal ions and binding to these ions was occurring in a 2:1 ratio, making them suitable for a MOF dip sensor.

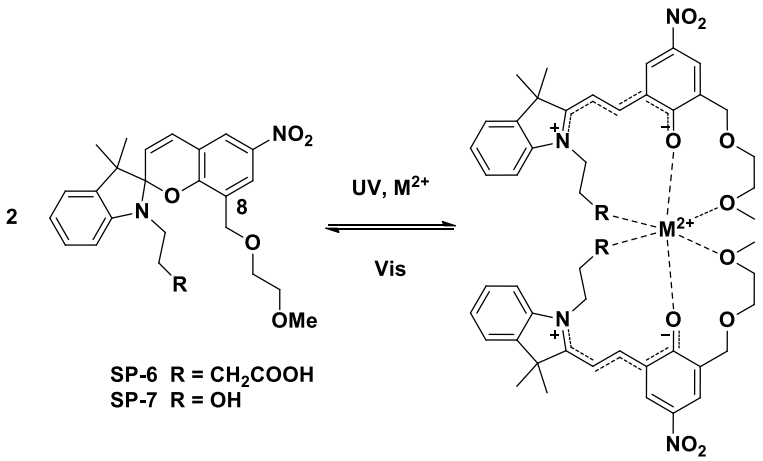

SCHEME 5-4: Structures of **SP-6** and **SP-7**, showing the proposed binding mechanism to a divalent metal ion. Computationally determined complex structures are shown in Appendix Figure D-3.

In this context a MOF was used as a dip sensor for sensing in solutions containing **SP-6** with Ca^{2+}, or Cd^{2+} or mixed ion solutions as a first step toward realizing a selective, nanoscale and regenerable dip-sensor for Ca^{2+} and Cd^{2+} that is able to yield significant signal-to-background changes with minimal sample volumes.

5.4.1.2 Results and Discussion

One end of a 20 cm length of MOF fibre was dipped into pre-mixed solutions containing 100 ρM of Cd^{2+} and 5 μM of **SP-6** or 100 pM of Ca^{2+} with 5 μM of **SP-6**. The solution is drawn into the air holes of the fibre by capillary action. The fibres were filled with 150 - 180 nL of the solution respectively. Detailed information on the fibre and optical setup employed can be found below in the Experimental Section (Section 5.6.2). The fibre core was then exposed to light from a 532 nm laser and the fluorescence generated within the sample chambers was collected by the fibre core. The resulting fluorescence spectra was obtained by capturing the fluorescence travelling in the backwards direction and from this a significant increase in

fluorescence intensity in the presence of 100 ρM Cd^{2+} and Ca^{2+} was observed (Figure 5-21A), given that only 2 % of the **SP-6** are bound to any ions ([M^{2+}]/[**SP-6**]).

On/off binding experiments were also carried out to examine the reversibility of this new sensor system. The results in Figure 5-21B show that the binding of Cd^{2+} can be turned off, on and off again by exposing the system to white light for 5 min, followed by exposure to UV for 5 min and white light again for 5 min.

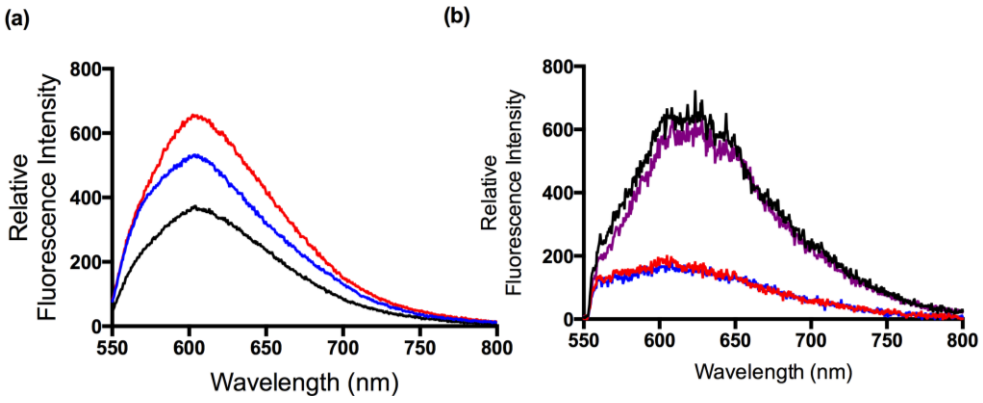

FIGURE 5-21: (a) Fluorescence results of the optical fibre-based nanoscale dip-sensor. black) 5 µM **SP-6**, no ions; red) 100 ρM of Ca^{2+} premixed with 5 µM of **SP-6**; blue) 100 ρM of Cd^{2+} premixed with 5 µM of **SP-6**. Experiments were carried out in acetonitrile with excitation wavelength of 532 nm. The signal-to-noise ratio between the free and complexed-form were calculated to be 1:1.7 for Cd^{2+} and 1:1.8 for Ca^{2+}. Information on fibre, optical set-up and results from a duplicate run can be found in the Supporting Information Section (Appendix D.1.6). (b) Photoswitching experiments within a single MOF (λ_{ex} = 532 nm). black) First "On Cycle"; red) First "Off Cycle"; purple) Second "On Cycle"; blue) Second "Off Cycle". Experiments were performed with the same sample of 10 mM of **SP-6** premixed with 1 µM of Cd^{2+} in 30 cm of MOF.

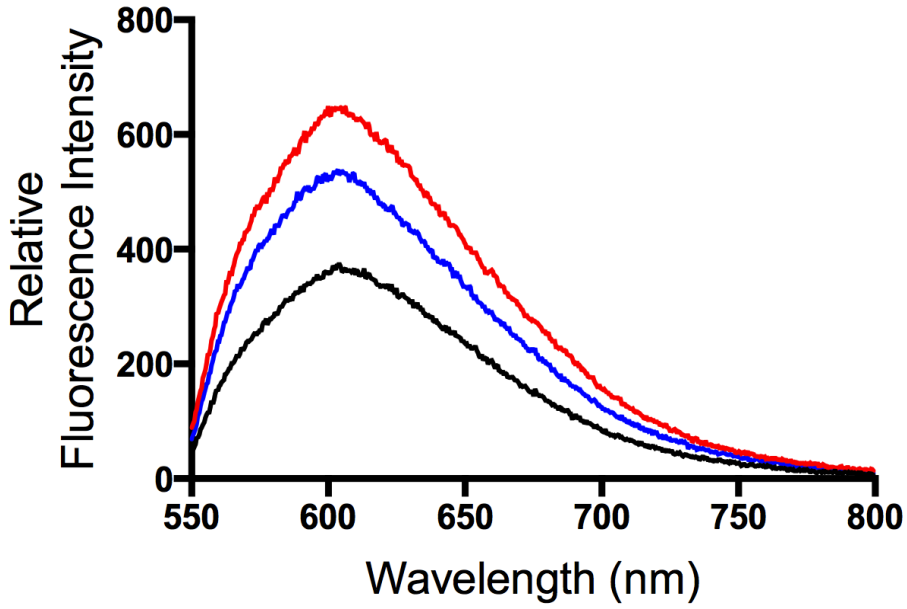

FIGURE 5-22: Fluorescence results of the optical fibre-based nanoscale dip-sensor. Duplicate Run. (black) 5 μM **SP-6**, no ions (red) 100 ρM of Ca^{2+} premixed with 5 μM of **SP-6**, (blue) 100 ρM of Cd^{2+} premixed with 5 μM of **SP-6**. Experiments were carried out in acetonitrile with excitation wavelength = 532 nm.

5.4.1.3 Conclusion to PAPER 3

In summary, we have designed a selective, dual sensor for Ca^{2+} and Cd^{2+} capable of detection at 100 ρM concentrations. Molecular modelling was used to provide insights on the binding modes between the respective ions and **SP-6** and **SP-7**. A first step toward a nanolitre-scale dip sensor for the dual sensing of Ca^{2+} and Cd^{2+} was demonstrated using a microstructured optical fibre as the sensing platform; which is important for sensing in confined spaces such as the medium surrounding cell clusters. In addition, this system displays picomolar sensitivity for these ions, with an added ability to reproducibly turn ion-binding on/off.

5.4.2 PAPER 4: MICROSTRUCTURED OPTICAL FIBRES AND LIVE CELLS: A WATER-SOLUBLE, PHOTOCHROMIC ZINC SENSOR[59]

5.4.2.1 Summary of the Publication

Many organic ionophores have limited use in biological applications due to their poor solubility in aqueous solutions and/or incompatibility with biological media. This general lack of solubility arises largely from the fact that in order to have a visible absorbance or fluorescence the molecules need to have large regions of conjugation, which is largely from non-polar aromatic units. It is a common difficulty in designing fluorophore systems to increase the aqueous solubility of the fluorophores while still maintaining fluorophore function. This paper presents a new non-synthetic method for increasing the solubility of poorly soluble fluorophores while still maintaining function and biocompatibility. A spiropyran fluorophore (**SP1**)[‡‡] was designed with a bis(2-pyridylmethyl) amine ionophore and was shown to be selective to Zn^{2+}. This spiropyran sensor was incorporated into a liposome structure (**LSP1**), which improved its aqueous solubility. As part of the liposome the sensor was able to be mixed in an aqueous solution and was able to quantitatively sense Zn^{2+} ions in standard solutions and near apoptotic HEC 293 cells. The ability for these liposomes to be used within MOFs as a dip sensor was then investigated.

5.4.2.2 Results and Discussion

LSP1 was combined with a microstructured optical fibre (MOF) as a first step toward realizing a nanoscale dip-Sensor for Zn(II) that is able to yield significant signal-to-background changes with minimal (sub-cellular-scale) sample volumes. The MOF also provides a platform for sensing Zn(II) in confined spaces such as the medium surrounding cell clusters, oocytes and embryos, and in the in-vivo environment.[54] One end of the fibre was dipped into pre-mixed **LSP1.Zn(II)** solutions and this mixture drawn into the air-holes by capillary action. Each fibre was filled with 150 - 180 nL of the solution (see Experimental Section 5.6.2). The fibre core was then exposed to light from a 532 nm laser and the fluorescence generated within the sample chambers was collected by the fibre core. By capturing

[‡‡] For continuity with Chapter 2 and PAPER 1 the labels **SP1** and **LSP1** have been altered from their originally published names (**SP2** and **LSP2**, respectively).

the fluorescence travelling in the backwards direction the sampling end of the fibre can be left *in-situ* within the environment being sampled. The results shown in Figure 5-23 show a dramatic increase in fluorescence intensity in the presence of 100 ρM Zn(II); emission was not detected in the absence of zinc ions. These results are highly reproducible and graphs from repeated experiments can be seen in Figure D-16 (Appendix D.1.6). Binding of Zn(II) can be turned off by exposing the system to white light for 2 min (Figure 5-24). The ability to turn binding of Zn(II) on or off is an important advance towards developing sensors that are reusable and/or capable of continuous or repeated measurements.

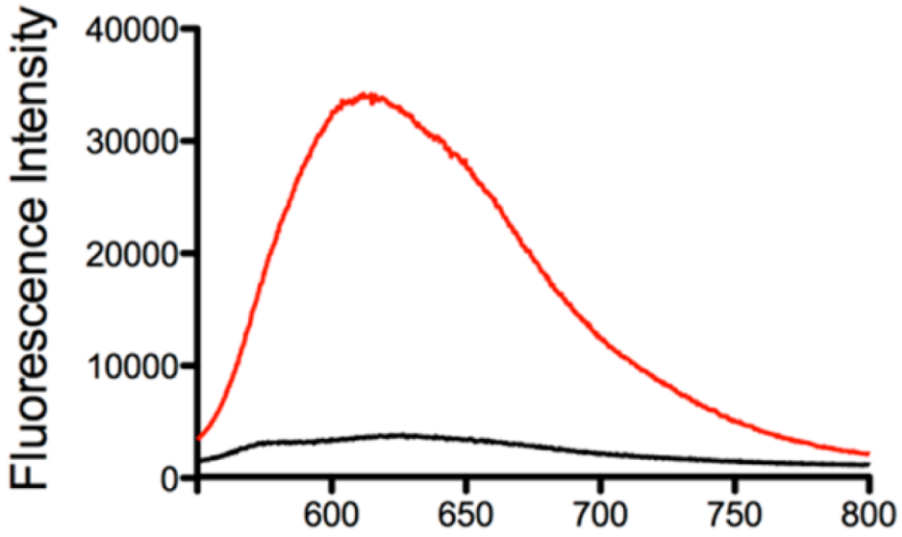

FIGURE 5-23: Fluorescence results of the optical fibre-based nanoscale dip-sensor. **LSP1** in the absence (−black) and in 100 ρM (red) of Zn(II).

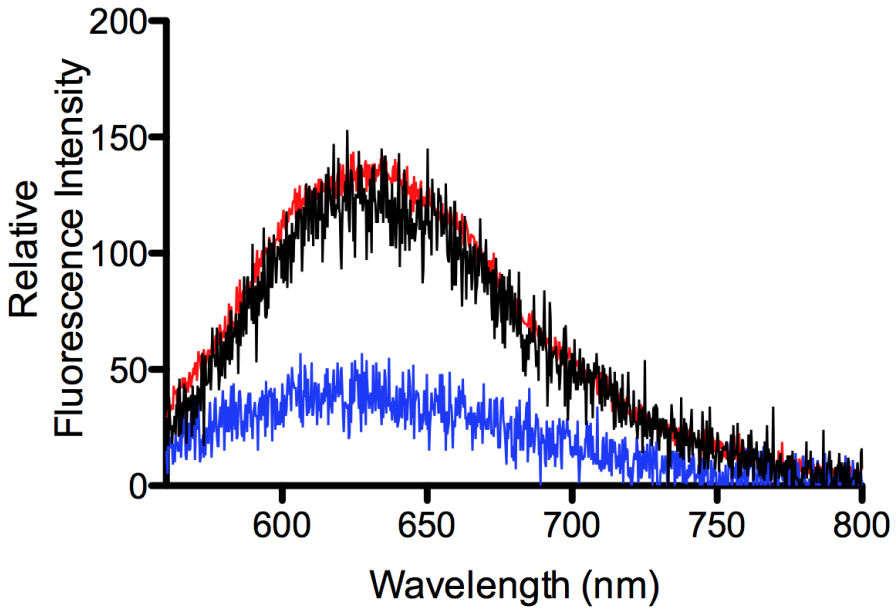

FIGURE 5-24: Photoswitching of **LSP1** in MOF. red) "On cycle" **LSP1** with 10 nM of Zn(II); blue) "Off-cycle" **LSP1** with 10 nM of Zn(II), exposed to white light for 2 min; and black) "On-cycle" **LSP1** with 10 nM Zn(II) exposed to UV (λ = 365 nm) for 7 min.

Photobleaching experiments were also carried out to determine the chemical and photostability of **LSP1** under the conditions of the experiment. A solution of **LSP1** pre-mixed with 10 nM of Zn(II) and exposed to the 532 nm laser for 10 x 16 ms. Minimal photobleaching of less than 10 % was observed (Figure 5-25). More importantly, it was shown that exposure to UV light for 7 min returned **LSP1** to the same fluorescence intensity as before demonstrating that the minimal photo discolouration was not due to any photodestruction of the molecules, but is most likely due to some spiropyran molecules switching back to the non-fluorescent spiro form under the influence of the 532 nm laser light. The stability of this system under these optical experimental conditions show that **LSP1** is suitable for development into a fibre-based dip-sensor suitable for the detection of Zn(II) in biological applications such as the monitoring of zinc spark events during the developmental cell cycle of mammalian eggs.[60]

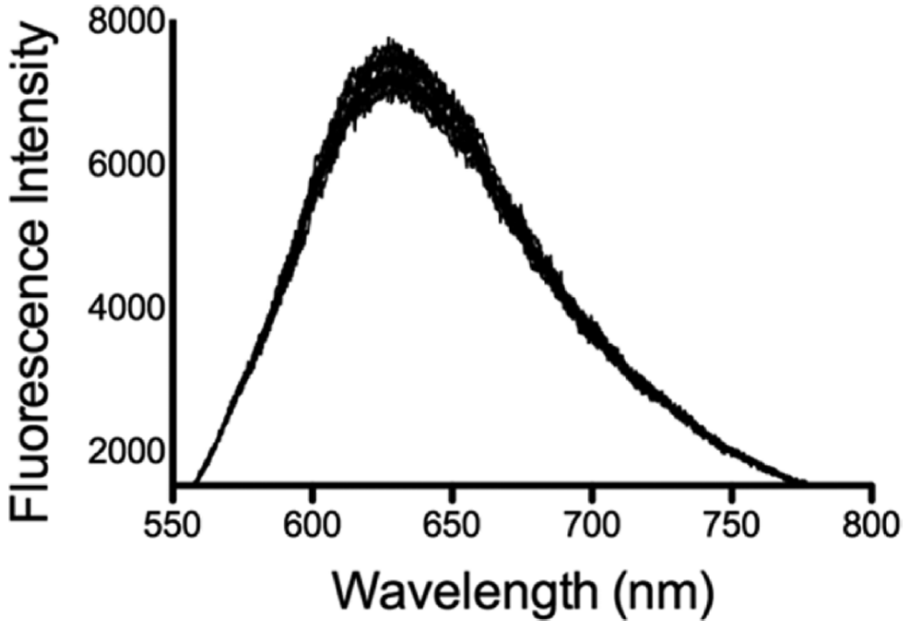

FIGURE 5-25: Photobleaching experiments within the optical fibre dip sensor. In the presence of 10 nM Zn(II) where the sample was exposed to 10 x 16 ms of light from the 532 nm laser. The optical power is 35 μW.

5.4.2.3 Conclusion to PAPER 4

In this work, a new biologically compatible Zn(II) sensor was fabricated by embedding Zn(II) sensing spiropyran molecules within the surface of the liposome (**LSP1**). Solution-based experiments with increasing Zn(II) concentrations demonstrate that this new sensor has improved aqueous solubility and sensitivity compared to the original spiropyran molecule (**SP1**). Cell based experiments showed that **LSP1** is capable of sensing Zn(II) efflux from apoptotic HEK 293 cells with preliminary data indicating that sensing is localized near the plasma membrane of the cells. This provides a significant advantage over other zinc fluorescent sensors, such as FluoZin-3[61] that operates in the bulk solution and hence lacks sensitivity and an ability to operate at a local level. **LSP1** is also suitable for development into a nanolitre scale, dip-sensor for Zn(II) using microstructured optical fibre as the sensing platform. Here Zn(II) can be detected within the range of 100 ρM with no signs of photobleaching. The results reported in this paper demonstrate an approach for developing existing spiropyran molecules into biologically compatible sensors for use in a wide range of applications.

5.5 CONCLUSION TO CHAPTER 5

This chapter presented work into the investigation into the coating, photoswitching, and sensing capability of glass surfaces, in particular microstructured optical fibres, coated with photoswitchable ionophores. The first part of this investigation looked at optimising the surface functionalisation procedures on glass slides as a model surface. Using non-destructive surface characterisation techniques of sessile drop contact angle analysis and 2D scanning fluorescence an APTES SAM was found to be produced after a 1 hour silanization reaction. Spiropyran (**SP-5**) and azobenzene (**Azo1**) photoswitches were then successfully attached the glass slides with optimal surface coupling occurring after 24 hour reaction time. The sensing capability for these photoswitchable surfaces was investigated in the presence of aqueous solutions of Pb^{2+} or Al^{3+}, respectively, using the Typhoon Imager; however, using the Typhoon Imager it was not possible to detect differences in the fluorescence emission intensities. The second part then continued on from Chapter 4 and investigated the sensing capabilities of MOFs using the spiropyran fluorophore **SP-3** in a fibre. Sensing using **SP-3** was investigated in solution as well as when covalently attached to the surface using the protocols determined in the first part. Photoswitching of **SP-3** was observed in fibre in solution as well as when attached to the surface. In both conditions the fibre was able to detect the presence of Ca^{2+} ions (as low as picomolar concentrations when attached to the surface); however, due to intrinsic issues with the calibration of the fibres, accurate determinations of Ca^{2+} concentrations in an unknown solution was not achieved. Finally, in the third part two more studies are presented (PAPER 3 and PAPER 4) which use photoswitchable spiropyran fluoroionophores in MOFs for the sensing of the metal ions Ca^{2+} and Cd^{2+}, and Zn^{2+}. Both of these systems again showed the ability to detect the presence of the metal ions at picomolar concentrations in solution, with the advantage of the liposome system improving aqueous solubility of the sensor.

This work is now leading towards sensing of calcium ions in IVF Media, with the aim of creating a sensor capable of sensing the media surrounding an oocyte during and after fertilisation. By detecting changes in ion concentration overtime it will allow further understanding of how changes in Ca^{2+} concentration correlate to

embryo development, health and viability for uterus implantation. Preliminary work in this is currently in the process of being written for publication.

5.6 MATERIALS AND METHODS

5.6.1 GLASS SLIDE EXPERIMENTS

5.6.1.1 Materials

Borosilicate glass microscope slides, 'Universal Premium Microscope Glass Slides' Pathology grade, plain unfrosted glass slides, were prepared for functionalisation by first cutting the 76.2 mm by 25.4 mm sized slides in half to give 20 slides of dimensions 38 mm by 25 mm. The slides were labelled by scratching a roman numeral I to XX on the front top left corner. All glassware used for glass functionalisation was new and was cleaned of potential surface contaminants before each use by soaking in a solution of 1:1 MeOH/conc. HCl for a minimum of 30 min. APTES 95 % solution was acquired from Aldrich and stored under N_2. Toluene was dried by passing through a Pure Solv Micro solvent purification system (Innovative Technology).

5.6.1.2 Cleaning and Silanization of Glass Slides

The slides were prepared following a procedure from Cras *et al.*,[30] who investigated eight different cleaning procedures on soda lime glass. The procedure for the slide coating is shown in Scheme 5-1. Four slides at a time were soaked in 1:1 MeOH/conc. HCl in a petri dish for 30 min, followed by washing with Milli-Q water before drying by blowing N_2 gas. The slides were then soaked in piranha solution (7:3 H_2SO_4/30 % $H_2O_{2(aq)}$) for 30 min followed by washing with water and dried with N_2 then in an oven (150 ^oC) overnight. While still hot the slides were transferred to a N_2 atmosphere glovebox.

To a clean petri dish, four slides were arranged with the labelled side facing down. A 10 mL 5 % 3-aminopropyl triethoxysilane (APTES) solution was prepared fresh by mixing 0.5 ml of APTES with 9.5 mL dry toluene. The unlabelled side of each slide was covered in the 5 % APTES solution. Slides numbered **I** to **X** and **XV** to **XVI** were soaked in the APTES solution for 1 hour. Slides numbered **XI** to **XIV** were soaked in the APTES solution for 5 hours, Slide **XVII** was not treated with any solution, and Slide **XVIII** was only treated with toluene with no APTES (Table 5-1). After treatment, each slide was removed from the APTES solution followed by

washing with dry toluene. The slides were removed from the dry glovebox and washed further with methanol, and Milli-Q water (it was noticed that it was much easier to remove the adsorbed water after APTES treatment than with the untreated slides, indicating an increased hydrophobicity as per contact angle measurements). The slides were then soaked in H_2O overnight to promote hydrolysis of incompletely coupled APTES,[25] and followed by drying with blowing $N_{2(g)}$.

5.6.1.3 Coupling of SP-5 to Aminated Slides with EDC/NHS Method

Stock solutions of activated spiropyran ionophore **SP-5** were prepared by combining a stock solution of **SP-5** (547 μM) in DMF to a solution of NHS (2.26 mM) and EDC (5.32 mM) in DMF to make a solution of **SP-5** (100 μM), EDC (1330 μM), and NHS (565 μM) (*i.e.* an approximate ratio of 1:13:6 **SP-5**/EDC/NHS).[62] Slides **I** to **IV** were incubated in 5 mL of reaction solution under the following conditions: Slide **I** in the dark for 2 hours; Slide **II** in the dark for 5 hours; Slide **III** in the dark for 24 hours; and Slide **IV** was incubated under UV light irradiation (UV352nm) for 5 hours. After incubation, the slides were washed with methanol, followed by water and dried by N_2.

TABLE 5-1: Summary of numbered microscope slides and their respective surface coating treatments.

Slide Number	Wash	Piranha	APTES	Fluorophore	Coupling conditions
I	MeOH/HCl	yes	1 h	**SP-5**	2 h EDC/NHS dark
II	MeOH/HCl	yes	1 h	**SP-5**	5 h EDC/NHS dark
III	MeOH/HCl	yes	1 h	**SP-5**	24 h EDC/NHS dark
IV	MeOH/HCl	yes	1 h	**SP-5**	5 h EDC/NHS UV light
V	MeOH/HCl	yes	1 h		
VI	MeOH/HCl	yes	1 h		APTES Control
XI	MeOH/HCl	yes	5 h		
XII	MeOH/HCl	yes	5 h		
XIII	MeOH/HCl	yes	5 h		
XIV	MeOH/HCl	yes	5 h		APTES Control
XVII	MeOH/HCl	yes	none		Washing Control
XVIII	MeOH/HCl	yes	toluene only		
XX	MeOH/HCl	yes	none		Washing control

5.6.1.4 Coupling of Azo1 to Aminated Slides

A new series of APTES coated microscope slides were prepared as previously described using a 1 hour coupling time. These slides were labelled from **XX** to **XXXII,** as shown in Table 5-2. A 1 mM stock solution of the **Azo1** was made in DMF. HATU reaction solution was prepared by mixing the **Azo1** stock solution (0.5 mL, 1 mM) with HATU (0.14 mL, 20 mM) and DIPEA (0.25 mL, 20 mM) and diluted in DMF (4.11 mL) to give a 5 mL solution of 100 µM **Azo1**, 560 µM HATU, and 1 mM DIPEA. EDC/NHS reaction solution was prepared as described previously with **Azo1** in place of **SP-5**. Slide **XXIII** was soaked in the **Azo1**/EDC/NHS reaction solution for 24 hours, as per determined in Experiment 1 (Section 5.2.1). Slide **XXIII** was then removed from the reaction solution before adding Slide **XXV** to the same reaction solution for 24 hours. Slide **XXIV** was incubated in the HATU/DIPEA reaction solution for 24 hours, followed by Slide **XXVI** for 24 hours. After reaction the slides were washed with methanol and water, dried by blowing with N_2 and stored in atmosphere for 2 days before contact angles were acquired.

TABLE 5-2: The numbered microscope slides and their respective surface coating treatments.

Slide Number	Wash	Piranha	APTES	Fluorophore	Coupling conditions
XXIII	MeOH/HCl	yes	1 h	Azo1	24 h EDC/NHS
XXIV	MeOH/HCl	yes	1 h	Azo1	24 h HATU
XXV	MeOH/HCl	yes	1 h	Azo1	24 h EDC/NHS
XXVI	MeOH/HCl	yes	1 h	Azo1	24 h HATU
XXXII	MeOH/HCl	yes	1 h		

5.6.1.5 Sessile Drop Contact Angle Experimental

Goniometer setup (Figure 5-3) was built in-house containing a 2-20 µL Gilson micropipette, adjustable scissor-lift platform, and Canon EOS 500D camera with a Canon EF-S 15-85mm f/3.5-5.6 IS USM lens. Either 2 or 10 µL drops of Milli-Q water were slowly placed on the glass slide on the platform and the surface was retracted from the pipette. The resulting images were processed using 'Image J

1.47v' freeware (http://imagej.nih.gov/ij) and the contact angle plugin 'DropSnake' (http://bigwww.epfl.ch/demo/dropanalysis).[63] The left and right contact angle was measured for 5-6 drops per slide and the average contact angle was obtained.

5.6.1.6 Typhoon Fluorescence Imager Experimental

Surface fluorescence from slides was measured using a Molecular Dynamics Typhoon TM 8600 variable mode imager. Samples were excited with a 532 nm green laser and the emission filtered through a 560 nm long pass filter. The sensitivity setting used was high, with a resolution of 50 μm and the PMT voltage of 500 V. A background image of the imager screen was first obtained. Then the microscope slides were arranged on the screen with the functionalised side facing upwards and image obtained. On the screen the slides were irradiated with light from a 352 nm UV blacklight from a filtered 8 W Hg lamp (UVP) to promote photoswitching. Images were processed using Image J 1.47v freeware (http://imagej.nih.gov/ij) by subtracting the background fluorescence image from the sample image.

5.6.2 MICROSTRUCTURED OPTICAL FIBRE EXPERIMENTS

5.6.2.1 Materials

The wagon wheel suspended core microstructured optical fibres (MOFs) used in these experiments were made from high purity silica F300 glass by the fibre drawing technique, and fabricated in-house.[64] The fibres have a core size of 1.5 μm and hole diameters of 27.7 μm, providing a total fill volume of 18 nL/cm.

All solvents used were HPLC grade obtained from Sigma-Aldrich and were used as supplied. APTES was sourced from Aldrich and used as supplied. The spiropyran fluorophore, **SP-3**, was synthesised using previously demonstrated methods (PAPER 2). $Ca(ClO_4)_2$ was sourced from Sigma-Aldrich and dried under reduced pressure before use.

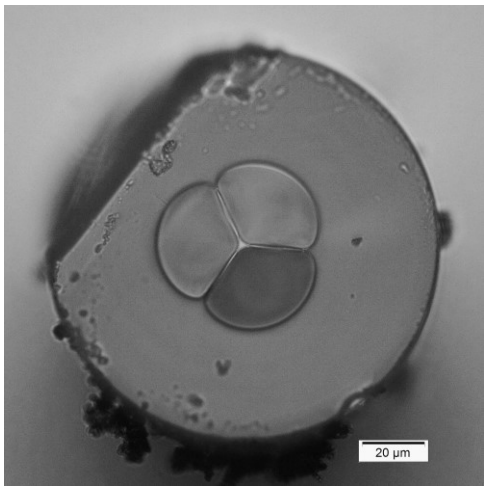

FIGURE 5-26: Cross section microstructured optical fibre taken with OLYMPUS BX51 light microscope, MPlanFLN-BD 50x/0.80 objective lens and fitted with OLYMPUS SC100 camera. Each hole has a diameter of 27.7 µm and an effective area of 600 μm^2. The length of each fibre used was between 9.5 to 11 cm. This equates to a maximum fill volume of approximately 180 nL/10 cm of fibre.

5.6.2.2 General Fibre Coating Procedure

The core of the fibre was prepared for silanization via similar chemical methods as investigated on the glass slides (Section 5.6.1), with the exception that with the MOFs the surface was not first washed with 1:1 MeOH/conc. $HCl_{(aq)}$ solution. This alteration was made due to advice from Mr. Roman Kostecki that, based on previous observations, this treatment was likely to cause damage the microstructured struts, and therefore, lead to poor quality light guiding; this however was not personally investigated. To lengths of fibre (45-60 cm), approximately 3-5 cm of the polymer coating was removed from each end, as to avoid contact between reagents and polymer; which would cause the polymer to dissolve and contaminate the sample. The ends of 2-4 fibres were then inserted into each pressurised reaction chamber (Figure 5-27) via a syringe needle in the rubber seal.

To clean and activate the fibre core for silanisation, Piranha solution (7:3 H_2SO_4/30 % $H_2O_{2(aq)}$) was prepared fresh and transferred to a 1.5 mL vial while still hot and installed into the pressure chamber. The chamber was then sealed and using a positive pressure the viscous Piranha solution was flowed through the fibre for 1

hour with regular monitoring of flow rate at the 'waste' end to ensure consistent flow and no blockages. The fibres were then rinsed by flowing with Milli-Q water for 1 hour, then with ethanol for at least 30 min, and then dried with N_2 for at least 1 hour.

In a N_2 atmosphere glovebox a 5 % APTES solution in dry toluene was prepared (as in Section 5.6.1.2) and transferred to a 1.5 mL vial. This vial was then quickly placed in the pressure chamber. The pressure chamber was first flushed with N_2 with tap open to remove atmospheric air and humidity, then the MOF was flushed with the 5 % APTES solution for 2 hours. The aminated fibres were then cleaned by flushing with toluene for 30 min, then ethanol for 30 min, then with water 1.5 mL/chamber and dried with N_2.

SP-3 coupling solution was prepared as described in Section 5.6.1.3. The aminated MOF in the reaction chamber was first solvated by flushing with DMF solution 30 min, then with the **SP-3** reaction solution for 24 hours. The fibres where then thoroughly washed with DMF (4 x 1.5 mL), then dried with N_2.

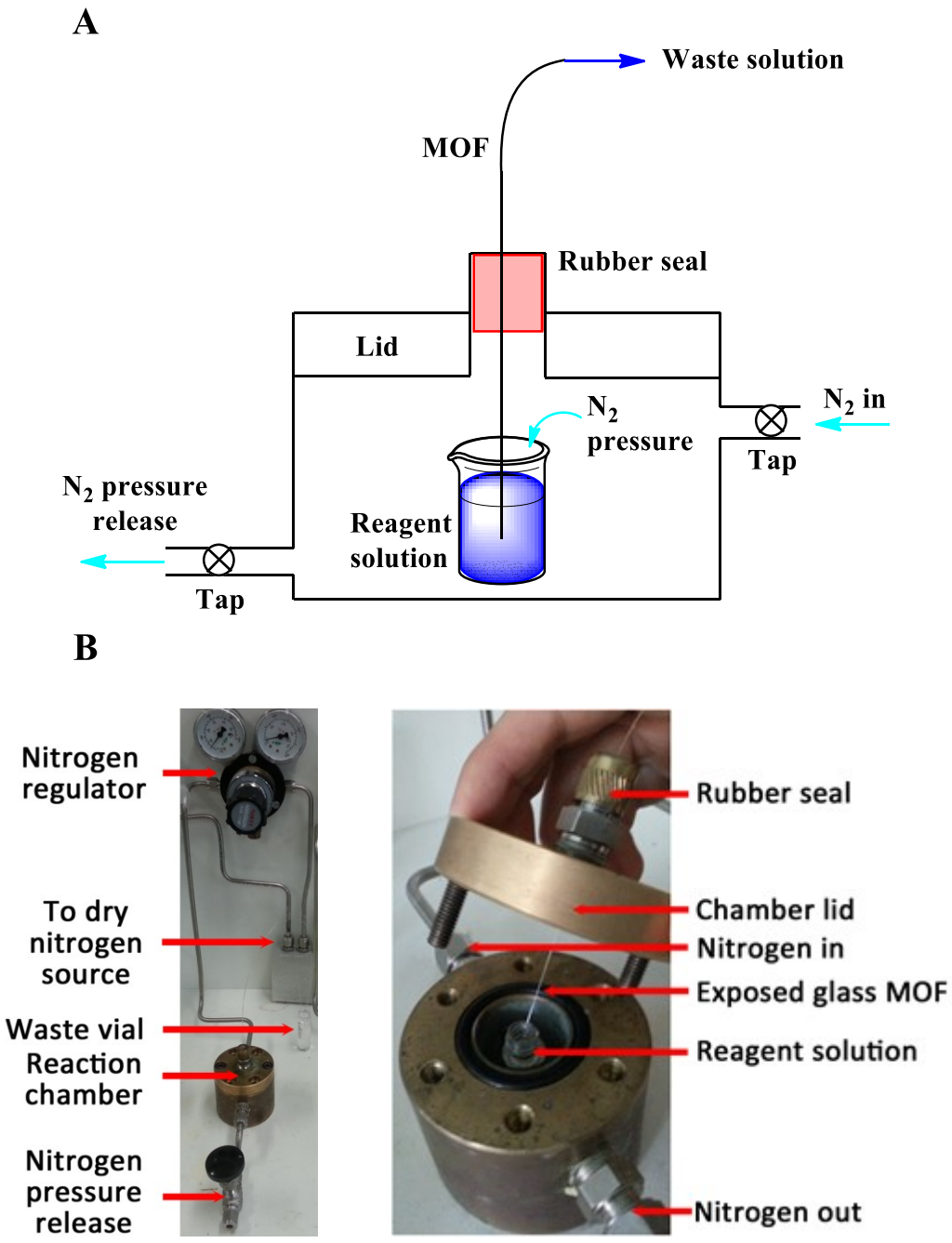

FIGURE 5-27: A) Cross section of the MOF pressurised reaction chamber. B) The filling scaffold and the reaction pressure chamber. MOF is inserted into the chamber via a syringe needle in the rubber seal and after removal of the needle a seal is produced surrounding the fibre. Within the chamber the end of the MOF is inserted into a solution in a 1.5 mL vial. A positive pressure in the chamber from a N_2 source forces the solution up through the three holes surrounding the core of the MOF and out the other end, where it is collected as waste.

5.6.2.3 General Fibre Fluorescence Measurement Procedure

The fluorescence of the fibres was measured using the custom optics setup shown in Figure 5-28. An attenuated 25 mW fibre coupled laser light source (CrystaLaser) with a wavelength of 532 nm was coupled into the MOF core at one end (the 'optics' end) of the MOF. Optimal alignment of the MOF core to the focused laser beam was achieved by monitoring the optical power transmitted by the fibre at the distal 'fill' end using a power meter (Thorlabs) while adjusting the location of the fibre tip at the 'optics' end with a 3-axis NanoMax-T5 stage (Thorlabs) (Figure 5-29). The MOF was filled with analyte solution by dipping the 'fill' end into the solution and allowing the solution to move along the fibre by capillary forces for a set time or distance before removing the tip from solution. The MOF was exposed to pulses of 532 nm light and the resulting fluorescence emission propagation in the backward direction[65] was filtered through a 550 nm LP filter, to remove scattering from the excitation light source, before being detected by a Horiba iHR550 spectrometer with Synapse CCD detector (100 g/mm grating, 0.5 mm entrance slit width). Ultra-violet light induced photoswitching of the photoswitch within the fibre was performed by externally irradiating (Figure 5-28, blue box) the filled MOF with a mercury lamp (UVP, 8 W, 352 nm (filtered BLB)) (UV352nm).

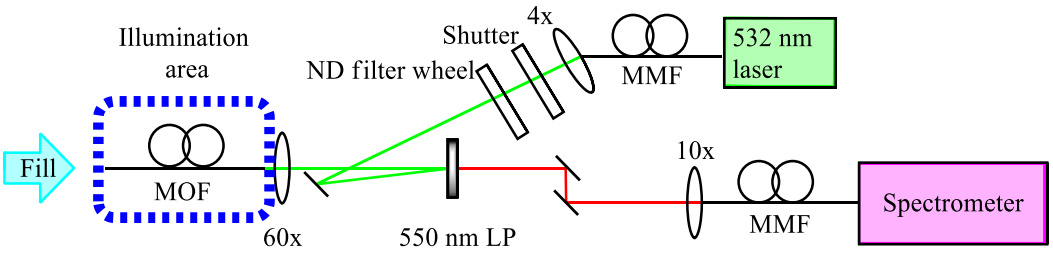

FIGURE 5-28: The MOF sensor optics setup.

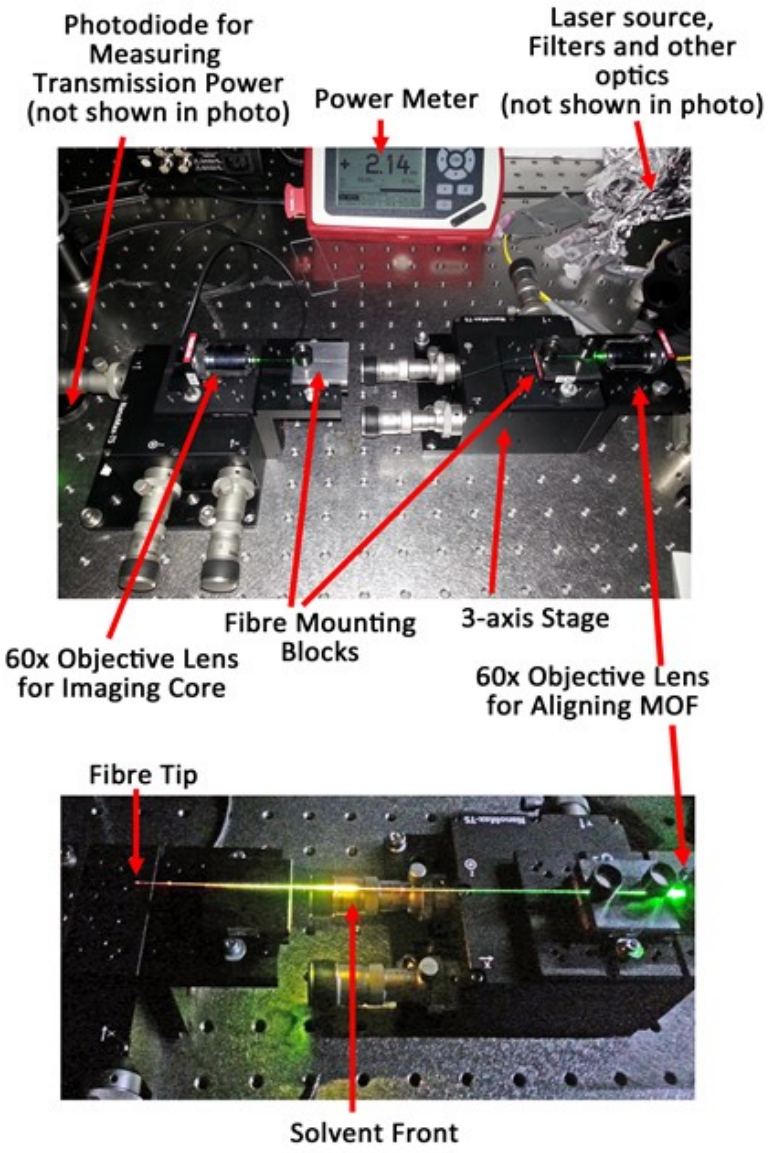

FIGURE 5-29: Image of the MOF optical setup. Top) alignment of the fibre to the laser optics; Bottom) after half filling with a strongly fluorescent rhodamine B solution, showing scattered yellow fluorescence from the rhodamine B along the fibre length.

5.7 REFERENCES FOR CHAPTER 5

1. Klajn, R. Spiropyran-based dynamic materials. *Chemical Society Reviews* 2014, *43* (1), 148-84.
2. Florea, L.; Diamond, D.; Benito-Lopez, F. Photo-Responsive Polymeric Structures Based on Spiropyran. *Macromolecular Materials and Engineering* 2012, *297* (12), 1148-1159.
3. Browne, W. R.; Feringa, B. L. Light Switching of Molecules on Surfaces. *Annual Review of Physical Chemistry* 2009, *60* (1), 407-428.
4. Klajn, R. Immobilized azobenzenes for the construction of photoresponsive materials. *Pure and Applied Chemistry* 2010, *82* (12), 2247.
5. Bossi, M. L.; Aramendía, P. F. Photomodulation of macroscopic properties. *Journal of Photochemistry and Photobiology C: Photochemistry Reviews* 2011, *12* (3), 154-166.
6. Katsonis, N.; Lubomska, M.; Pollard, M. M.; Feringa, B. L.; Rudolf, P. Synthetic light-activated molecular switches and motors on surfaces. *Progress in Surface Science* 2007, *82* (7-8), 407-434.
7. Suzuki, T.; Kitsukawa, T.; Hirata, Y.; Tanaka, S.; Iwasaki, N. Swelling-shrinking behavior of hydrated noncross-linked copolymer films in response to photoreversible isomerizaton and metal complexation of spiropyran units of the copolymers. *Polymers for Advanced Technologies* 2014, 25 (1), 123-129.
8. Luo, Q.; Cheng, H.; Tian, H. Recent progress on photochromic diarylethene polymers. *Polymer Chemistry* 2011, *2* (11), 2435-2443.
9. Byrne, R. J.; Stitzel, S. E.; Diamond, D. Photoregenerable surface with potential for optical sensing. *Journal of Materials Chemistry* 2006, *16* (14), 1332-1337.
10. Erno, Z.; Yildiz, I.; Gorodetsky, B.; Raymo, F. M.; Branda, N. R. Optical control of quantum dot luminescence via photoisomerization of a surface-coordinated, cationic dithienylethene. *Photochemical & Photobiological Sciences* 2010, *9* (2), 249-253.
11. Sanchez, G.; Curiel, D.; Ratera, I.; Tarraga, A.; Veciana, J.; Molina, P. Modified mesoporous silica nanoparticles as a reusable, selective chromogenic sensor for mercury(II) recognition. *Dalton Transactions* 2013, *42* (18), 6318-6326.
12. Rosario, R.; Gust, D.; Hayes, M.; Jahnke, F.; Springer, J.; Garcia, A. A. Photon-Modulated Wettability Changes on Spiropyran-Coated Surfaces. *Langmuir* 2002, *18* (21), 8062-8069.
13. Florea, L.; Hennart, A.; Diamond, D.; Benito-Lopez, F. Synthesis and characterisation of spiropyran-polymer brushes in micro-capillaries: Towards an integrated optical sensor for continuous flow analysis. *Sensors and Actuators B: Chemical* 2012, *175* (0), 92-99.
14. Pearson, D.; Downard, A. J.; Muscroft-Taylor, A.; Abell, A. D. Reversible Photoregulation of Binding of α-Chymotrypsin to a Gold Surface. *Journal of the American Chemical Society* 2007, *129* (48), 14862-14863.
15. Scarmagnani, S.; Walsh, Z.; Slater, C.; Alhashimy, N.; Paull, B.; Macka, M.; Diamond, D. Polystyrene bead-based system for optical sensing using

spiropyran photoswitches. *Journal of Materials Chemistry* 2008, *18* (42), 5063-5071.
16. Liu, D.; Chen, W.; Sun, K.; Deng, K.; Zhang, W.; Wang, Z.; Jiang, X. Resettable, Multi-Readout Logic Gates Based on Controllably Reversible Aggregation of Gold Nanoparticles. *Angewandte Chemie International Edition* 2011, *50* (18), 4103-4107.
17. Connal, L. A.; Franks, G. V.; Qiao, G. G. Photochromic, Metal-Absorbing Honeycomb Structures. *Langmuir* 2010, *26* (13), 10397-10400.
18. Fries, K. H.; Driskell, J. D.; Sheppard, G. R.; Locklin, J. Fabrication of Spiropyran-Containing Thin Film Sensors Used for the Simultaneous Identification of Multiple Metal Ions. *Langmuir* 2011, *27* (19), 12253-12260.
19. Fries, K. H.; Driskell, J. D.; Samanta, S.; Locklin, J. Spectroscopic Analysis of Metal Ion Binding in Spiropyran Containing Copolymer Thin Films. *Analytical Chemistry* 2010, *82* (8), 3306-3314.
20. Kim, E.; Seo, S.; Seo, M. L.; Jung, J. H. Functionalized monolayers on mesoporous silica and on titania nanoparticles for mercuric sensing. *Analyst* 2010, *135* (1), 149-156.
21. Mela, P.; Onclin, S.; Goedbloed, M. H.; Levi, S.; Garcia-Parajo, M. F.; van Hulst, N. F.; Ravoo, B. J.; Reinhoudt, D. N.; van den Berg, A. Monolayer-functionalized microfluidics devices for optical sensing of acidity. *Lab on a Chip* 2005, *5* (2), 163-170.
22. Flink, S.; van Veggel, F. C. J. M.; Reinhoudt, D. N. Functionalization of self-assembled monolayers on glass and oxidized silicon wafers by surface reactions. *Journal of Physical Organic Chemistry* 2001, *14* (7), 407-415.
23. Lokajova, J.; Tiala, H.; Viitala, T.; Riekkola, M.-L.; Wiedmer, S. K. Covalent binding of phospholipid vesicles on fused silica capillaries for electrochromatography. *Soft Matter* 2011, *7* (13), 6041-6050.
24. Szegedi, A.; Popova, M.; Goshev, I.; Klébert, S.; Mihály, J. Controlled drug release on amine functionalized spherical MCM-41. *Journal of Solid State Chemistry* 2012, *194* (0), 257-263.
25. Zhu, M.; Lerum, M. Z.; Chen, W. How To Prepare Reproducible, Homogeneous, and Hydrolytically Stable Aminosilane-Derived Layers on Silica. *Langmuir* 2011, *28* (1), 416-423.
26. Asenath Smith, E.; Chen, W. How To Prevent the Loss of Surface Functionality Derived from Aminosilanes. *Langmuir* 2008, *24* (21), 12405-12409.
27. Howarter, J. A.; Youngblood, J. P. Optimization of Silica Silanization by 3-Aminopropyltriethoxysilane. *Langmuir* 2006, *22* (26), 11142-11147.
28. Wang, W.; Vaughn, M. W. Morphology and Amine Accessibility of (3-Aminopropyl) Triethoxysilane Films on Glass Surfaces. *Scanning* 2008, *30* (2), 65-77.
29. Kanan, S. M.; Tze, W. T. Y.; Tripp, C. P. Method to Double the Surface Concentration and Control the Orientation of Adsorbed (3-Aminopropyl)dimethylethoxysilane on Silica Powders and Glass Slides. *Langmuir* 2002, *18* (17), 6623-6627.
30. Cras, J. J.; Rowe-Taitt, C. A.; Nivens, D. A.; Ligler, F. S. Comparison of chemical cleaning methods of glass in preparation for silanization. *Biosensors and Bioelectronics* 1999, *14* (8–9), 683-688.

31. Gooding, J. J.; Ciampi, S. The molecular level modification of surfaces: from self-assembled monolayers to complex molecular assemblies. *Chemical Society Reviews* 2011, *40* (5), 2704-2718.
32. Nicosia, C.; Huskens, J. Reactive self-assembled monolayers: from surface functionalization to gradient formation. *Materials Horizons* 2014, *1* (1), 32-45.
33. Valeur, E.; Bradley, M. Amide bond formation: beyond the myth of coupling reagents. *Chemical Society Reviews* 2009, *38* (2), 606-631.
34. Foo, H. T. C.; Ebendorff-Heidepriem, H.; Sumby, C. J.; Monro, T. M. Towards microstructured optical fibre sensors: surface analysis of silanised lead silicate glass. *Journal of Materials Chemistry C* 2013, *1* (41), 6782-6789.
35. Sam, S.; Touahir, L.; Salvador Andresa, J.; Allongue, P.; Chazalviel, J. N.; Gouget-Laemmel, A. C.; Henry de Villeneuve, C.; Moraillon, A.; Ozanam, F.; Gabouze, N.; Djebbar, S. Semiquantitative Study of the EDC/NHS Activation of Acid Terminal Groups at Modified Porous Silicon Surfaces. *Langmuir* 2010, *26* (2), 809-814.
36. Voicu, R.; Boukherroub, R.; Bartzoka, V.; Ward, T.; Wojtyk, J. T. C.; Wayner, D. D. M. Formation, Characterization, and Chemistry of Undecanoic Acid-Terminated Silicon Surfaces: Patterning and Immobilization of DNA. *Langmuir* 2004, *20* (26), 11713-11720.
37. Moraillon, A.; Gouget-Laemmel, A. C.; Ozanam, F.; Chazalviel, J. N. Amidation of Monolayers on Silicon in Physiological Buffers: A Quantitative IR Study. *The Journal of Physical Chemistry C* 2008, *112* (18), 7158-7167.
38. Heng, S.; Nguyen, M.-C.; Kostecki, R.; Monro, T. M.; Abell, A. D. Nanoliter-scale, regenerable ion sensor: sensing with a surface functionalized microstructured optical fibre. *RSC Advances* 2013, *3* (22), 8308-8317.
39. Kostecki, R.; Heng, S.; Ebendorff-Heidepriem, H.; Abell, A. D.; Monro, T. M. Functionalization of exposed core fibers with multiligand binding molecules for fluorescence based ion sensing. In *23rd International Conference on Optical Fibre Sensors*, López-Higuera, J. M.; Jones, J.; López-Amo, M.; Santos, J. L., Eds. 2014; Vol. 9157, p 915788.
40. Shin, Y. S. Micro- and nanotechnology - based platforms to study biology at small scale: from DNAs to single cells. California Institute of Technology, 2011.
41. Jose, B.; Antoci Jr, V.; Zeiger, A. R.; Wickstrom, E.; Hickok, N. J. Vancomycin Covalently Bonded to Titanium Beads Kills Staphylococcus aureus. *Chemistry & Biology* 2005, *12* (9), 1041-1048.
42. Silberzan, P.; Leger, L.; Ausserre, D.; Benattar, J. J. Silanation of silica surfaces. A new method of constructing pure or mixed monolayers. *Langmuir* 1991, *7* (8), 1647-1651.
43. Chen, E. H.; Walter, S. R.; Nguyen, S. T.; Geiger, F. M. Arylsilanated SiOx Surfaces for Mild and Simple Two-Step Click Functionalization with Small Molecules and Oligonucleotides. *The Journal of Physical Chemistry C* 2012, *116* (37), 19886-19892.

44. Vistas, C. R.; Águas, A. C. P.; Ferreira, G. N. M. Silanization of glass chips—A factorial approach for optimization. *Applied Surface Science* 2013, *286* (0), 314-318.
45. Herder, P.; Vågberg, L.; Stenius, P. ESCA and contact angle studies of the adsorption of aminosilanes on mica. *Colloids and Surfaces* 1988, *34* (2), 117-132.
46. Kurth, D. G.; Bein, T. Surface reactions on thin layers of silane coupling agents. *Langmuir* 1993, *9* (11), 2965-2973.
47. Ruan, Y.; Foo, T. C.; Warren-Smith, S.; Hoffmann, P.; Moore, R. C.; Ebendorff-Heidepriem, H.; Monro, T. M. Antibody immobilization within glass microstructured fibers: a route to sensitive and selective biosensors. *Optics Express* 2008, *16* (22), 18514-18523.
48. Parida, S. K.; Dash, S.; Patel, S.; Mishra, B. K. Adsorption of organic molecules on silica surface. *Advances in Colloid and Interface Science* 2006, *121* (1–3), 77-110.
49. Haensch, C.; Hoeppener, S.; Schubert, U. S. Chemical modification of self-assembled silane based monolayers by surface reactions. *Chemical Society Reviews* 2010, *39* (6), 2323-2334.
50. Kralj, S.; Drofenik, M.; Makovec, D. Controlled surface functionalization of silica-coated magnetic nanoparticles with terminal amino and carboxyl groups. *Journal of Nanoparticle Research* 2011, *13* (7), 2829-2841.
51. Lee, M. H.; Brass, D. A.; Morris, R.; Composto, R. J.; Ducheyne, P. The effect of non-specific interactions on cellular adhesion using model surfaces. *Biomaterials* 2005, *26* (14), 1721-1730.
52. Toworfe, G. K.; Composto, R. J.; Shapiro, I. M.; Ducheyne, P. Nucleation and growth of calcium phosphate on amine-, carboxyl- and hydroxyl-silane self-assembled monolayers. *Biomaterials* 2006, *27* (4), 631-642.
53. Warren-Smith, S. C.; Heng, S.; Ebendorff-Heidepriem, H.; Abell, A. D.; Monro, T. M. Fluorescence-based aluminum ion sensing using a surface-functionalized microstructured optical fiber. *Langmuir* 2011, *27* (9), 5680-5.
54. Monro, T. M.; Warren-Smith, S.; Schartner, E. P.; Francois, A.; Heng, S.; Ebendorff-Heidepriem, H.; Afshar, S. Sensing with suspended-core optical fibers. *Optical Fiber Technology* 2010, *16* (6), 343-356.
55. Clapham, D. E. Calcium Signalling. *Cell* 1995, *80* (2), 259-268.
56. Warren-Smith, S. C.; Nie, G. Y.; Schartner, E. P.; Salamonsen, L. A.; Monro, T. M. Enzyme activity assays within microstructured optical fibers enabled by automated alignment. *Biomedical Optics Express* 2012, *3* (12).
57. Cubillas, A. M.; Unterkofler, S.; Euser, T. G.; Etzold, B. J.; Jones, A. C.; Sadler, P. J.; Wasserscheid, P.; Russell, P. S. Photonic crystal fibres for chemical sensing and photochemistry. *Chemistry Society Reviews* 2013, *42* (22), 8629-48.
58. Heng, S.; Mak, A. M.; Stubing, D. B.; Monro, T. M.; Abell, A. D. Dual Sensor for Cd(II) and Ca(II): Selective Nanoliter-Scale Sensing of Metal Ions. *Analytical Chemistry* 2014, *86* (7), 3268-3272.
59. Heng, S.; McDevitt, C. A.; Stubing, D. B.; Whittall, J. J.; Thompson, J. G.; Engler, T. K.; Abell, A. D.; Monro, T. M. Microstructured optical fibers and live cells: a water-soluble, photochromic zinc sensor. *Biomacromolecules* 2013, *14* (10), 3376-9.

60. Kim, A. M.; Bernhardt, M. L.; Kong, B. Y.; Ahn, R. W.; Vogt, S.; Woodruff, T. K.; O'Halloran, T. V. Zinc Sparks Are Triggered by Fertilization and Facilitate Cell Cycle Resumption in Mammalian Eggs. *ACS Chemical Biology* 2011, *6* (7), 716-723.
61. Krenn, B. M.; Gaudernak, E.; Holzer, B.; Lanke, K.; Van Kuppeveld, F. J.; Seipelt, J. Antiviral activity of the zinc ionophores pyrithione and hinokitiol against picornavirus infections. *Journal of Virology* 2009, *83* (1), 58-64.
62. Pence, J. C. Control of covalent and non-covalent presentation of biomolecules within collagen GAG scaffolds. University of Illinois at Urbana-Champaign, 2012.
63. Stalder, A. F.; Kulik, G.; Sage, D.; Barbieri, L.; Hoffmann, P. A snake-based approach to accurate determination of both contact points and contact angles. *Colloids and Surfaces A: Physicochemical and Engineering Aspects* 2006, *286* (1–3), 92-103.
64. Webb, A. S.; Poletti, F.; Richardson, D. J.; Sahu, J. K. Suspended-core holey fiber for evanescent-field sensing. *Optical Engineering* 2007, *46* (1), 010503.
65. Afshar V, S.; Ruan, Y.; Warren-Smith, S. C.; Monro, T. M. Enhanced fluorescence sensing using microstructured optical fibers: a comparison of forward and backward collection modes. *Optics Letters.* 2008, *33* (13), 1473-1475.

CHAPTER 6

OVERALL CONCLUSIONS

This thesis presents a systematic investigation in which the principals of photoswitchable molecules, fluorescent sensors, silica surface functionalisation, and optical sensing with microstructured optical fibres were combined to create a new reusable metal ion sensor for biosensing applications.

Chapter 1 introduced the design and principals of the target biosensor. Chapter 2 provided an investigation into different classes of photoswitches to determine which type of photoswitches provide the most desirable properties for the optical fibre sensor. In particular, the viability of four different photoswitches (an azobenzene, spiropyran, indolylfulgide and diarylalkenes) were investigated within a MOF environment. The fluorescence and photostability of these photoswitches was compared in controlled comparable conditions in solutions of acetonitrile and DMSO, as well as adsorbed to the fibre core. It was found that both the azobenzene and spiropyran photoswitches showed favourable photostability in fibre, as well as the added benefits of improved synthesis, fluorescence yields, and absorbance wavelengths compared to the other switches.

Due to the ability for spiropyrans to inherently bind to and sense metal ion further investigation into the design and synthesis of a series of spiropyrans is then presented in Chapter 3 and 4. The synthesis of four spiropyrans (**SP-1**, **SP-2**, **SP-3**, and **SP-4**) with differing crown ether moieties, or N-indoline modifications was completed and the ability for these sensors to bind to and detect the presence of a series of biologically relevant metal ions was investigated. A comparison of the absorbance and fluorescence of **SP-1**, **SP-2** and **SP-3** in the presence of group 1 metals Li^+, Na^+, K^+, and Cs^+ was published as PAPER 2, where it was shown that spiropyran **SP-2** showed the most selective sensing towards Li^+. It was also shown that these spiropyrans (**SP-1** to **SP-3**) produce a strong response in the presence of group 2 metal ions, however binding was found to occur in a 2:1 metal ion to spiropyran ratio. **SP-4** with an ethoxy substituted N-indoline, was found to have a more favourable selectivity to group 2 metal ions, as well as prefer binding in a 1:1 ratio; due to the added size of the ethoxy moiety. These photoswitches were found to have good photoreversibly, with the ability to cyclise between the open (ion bound) merocyanine state and the closed spiropyran state on multiple occasion with white (halogen) and UV light (352 nm), respectively.

The designed and characterised photoswitchable sensor **SP-3** was then continued as a Ca^{2+} selective fluorophore for fibre sensing and functionalisation in Chapter 5. Where using pre-investigated surface coating methods **SP-3** was covalently attached to a MOF surface and was found to be photoswitchable on the surface as well as able to sense picomolar concentrations of metal ions.

The next aim for this research is to use these spiropyran fibre sensors in practical biologically relevant application, such as detecting Ca^{2+} fluctuations during IVF processes. However, further system design and optimisation is required to overcome some of the issues identified with the current suspended core MOFs and surface functionalisation. For example, different surface attachment methods, such as polymer coatings, could provide a more consistent and characterisable sensing layer with a greater surface density and improved ion binding thermodynamics. Also, a different fibre architecture, such as exposed core fibres, may improve reusability of the system due to the more accessible core; allowing for easier cleaning and removing contaminants from the side of the fibre rather than the tips. However, these exposed core fibres do not allow for point based sensing of nanolitre volumes; and therefore, are not suitable for cell sensing.

Further improvements in the UV-vis absorption and fluorescence properties and ion binding selectivity of the photoswitchable unit will lead to more diverse and selective sensors. Changes to the ion binding domain at R_8 and $R_{1'}$ (Figure 4-1) could provide a wide variety of ion/biological sensors. For example, more ion binding sites could be introduced by adding additional crown ether rings, or the length of the alkyl chain at $R_{1'}$ on **SP-4** could be extended to probe the influence of chain length on binding, and the ability to hydrogen bond to the phenolate could be removed by modification to an methyl ether. Changes to the NO_2 moiety at R_6 (such as to -F) will change the photochemistry of the spiropyran, possibly making the ion binding event more controllable, thereby, giving greater reversibility of the sensor, enabling the sensor to be completely turned ‘off’ or ‘on’. Also, as discussed in PAPER 4, for use in aqueous environments the solubility of the fluorophores need to be improved.

In conclusion, the goal to design and create a new reversible metal ion sensor was achieved. The entire process of developing this new class of biosensors was investigated, this required the incorporation of principals from a varied range of fields, such as photochemistry, synthetic chemistry, supramolecular chemistry, surface chemistry, and optics and photonics. Ultimately, these new biologically compatible microstructured optical fibre photoswitchable fluorescence based sensors, will lead to a greater understanding of the roles of metal ions (such as Ca^{2+}, Li^{+}, and Zn^{2+}) in vital cellular process to lead to a greater understanding of these process and diseases and ultimately lead to better diagnosis's and treatments.

APPENDIX

Appendix A: SYNTHESIS AND CHARACTERISATION OF CF_3-FULGIDE

The following section shows the synthesis and characterisation of the indolylfulgide, **CF_3-fulgide**, used in Chapter 2 (PAPER 1). The synthesis of a fluorinated indolylfulgide was first reported by Yokoyama in 1996.[1] The trifluoromethylated version was reported to have better fatigue resistance compared to the methylated indolylfulgide, and therefore was an interest to our investigation. An improved synthesis was later reported in 2001;[2] this synthesis is since the more commonly used method.[3-7] **CF_3-fulgide** was prepared based closely on this method and the overall synthetic procedure is shown below in Scheme A-1 and discussed in Section A.2. This fulgide was prepared to investigate its photoswitching properties in fibre and in order to perform future structural modification in order to design and create a fulgide based surface attachable photochromic metal ion sensor.

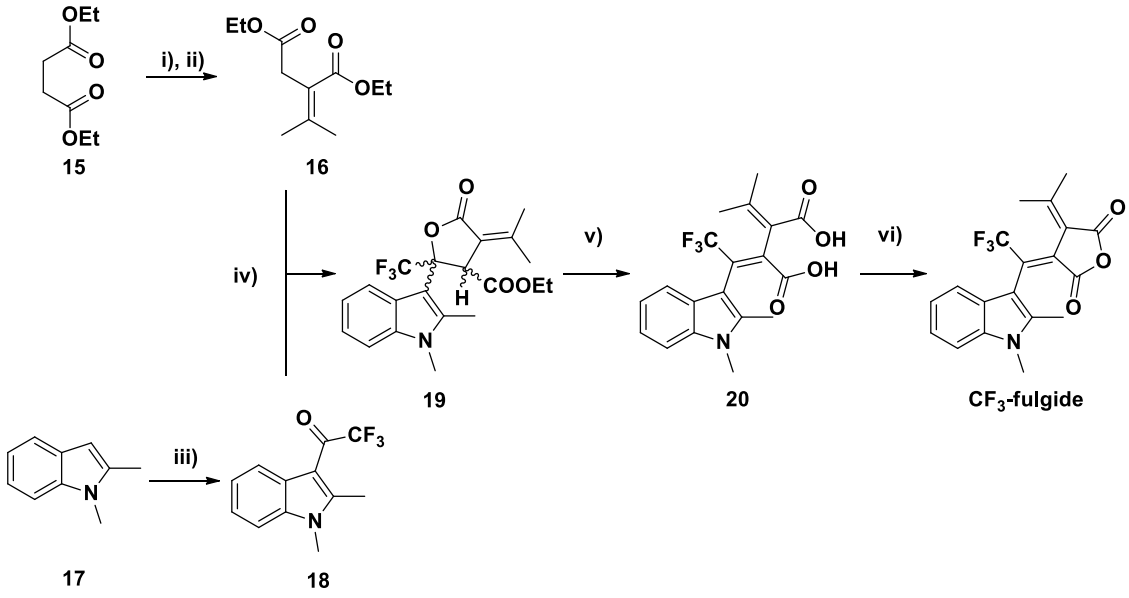

SCHEME A-1: Synthesis of trifluoromethylated indolylfulgide **CF_3-fulgide**. i) Acetone, t-BuOH, K^+ t-BuO^-, reflux 95 ^oC; ii) EtOH, HCl, r.t., 2d; iii) trifluoroacetic anhydride, 1,2-dichloroethane, 0 ^oC, 92 %; iv) LDA, Toluene, -78 ^oC; v) NaH, DMF, then H_2O, 25 %; vi) acetic anhydride, 72 %.

A.1 MATERIALS AND METHODS

A.1.1 Materials

All ^{1}H NMR, ^{13}C NMR, and ^{19}F NMR spectra were recorded on a Varian Gemini 2000 300 MHz or a Varian Inova 600 MHz NMR spectrometer in $CDCl_3$ (Cambridge Isotope Laboratories, Cambridge, MA). Chemical shifts (δ) are reported in ppm, with $CDCl_3$ (δ_C = 77.1 ppm) or TMS (δ_H = 0.0 ppm) used as internal standards, and trifluoroacetic acid (δ_F -78.5 ppm) used as external standard. Mass spectroscopy spectra were obtained using a Finnigan MAT LCQ MS. All reagents and solvents were from standard commercial sources and of reagent grade. Reactions were monitored by ascending TLC using pre-coated plates (silica gel 60 F_{254}, 250 μm, Merck, Darmstadt, Germany), spots were visualised under ultraviolet light at 254 nm or stained with basic potassium permanganate or Vanillin solutions. Column chromatography was performed with silica gel (40-63 μm, 60 Å, Davisil, Grace, Germany). Preparative thin layer chromatography was performed with Analtech inc, UNIPLATE^{TM}, Silica gel GF preparative layer with 254, 20 cm x 20 cm x 2000 μm.

A.1.2 Synthesis

diethyl 2-(propan-2-ylidene)succinate

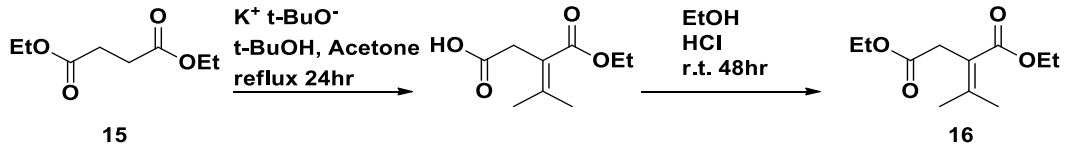

15 16

K^+t-BuO^- (9.2 g, 8.2 x 10^{-2} mol) was dissolved in t-BuOH (100 mL) and heated to 80 ^oC. Diethyl Succinate (**15**, 9.0 mL, 5.4 x 10^{-2} mol) was added and stirred for 5 min. Dry Acetone (8 mL) was added and the solution was heated at reflux at 95 ^oC for 17 h. The solution was acidified with conc. HCl (10 mL) and extracted with diethyl ether (3 x 40 mL). Organics were basified with 2M $NaOH_{(aq)}$ (pH 11) and washed with diethyl ether (3 x 40 mL). The aqueous solution was taken to pH 2 with concentrated HCl solution. Solution was extracted with diethyl ether and solvent was removed *in vacuo* to give a yellow oil. The oil was dissolved in ethanol (200 mL) and acidified with concentrated HCl (10 mL) and stirred at r.t. for 43 h. The ethanol was partially removed *in vacuo* and the remaining solution was quenched

with sodium carbonate and extracted with diethyl ether (20 mL) then ethyl acetate (2 x 50 mL), the organics were dried $MgSO_4$, and concentrated to red oil. **16** was isolated by vacuum distillation b.p. = 122 °C at 1.8 torr, yield 3.4 g, 30 %. ^{1}H NMR (300 MHz, $CDCl_3$) δ 4.19 (q, J = 7.1 Hz, 2H), 4.14 (q, J = 7.1 Hz, 2H), 3.38 (s, 2H), 2.15 (s, 3H), 1.87 (s, 3H), 1.29 (t, J = 7.1 Hz, 3H), 1.26 (t, J = 7.2 Hz, 3H).

1-(1,2-dimethyl-1H-indol-3-yl)-2,2,2-trifluoroethanone

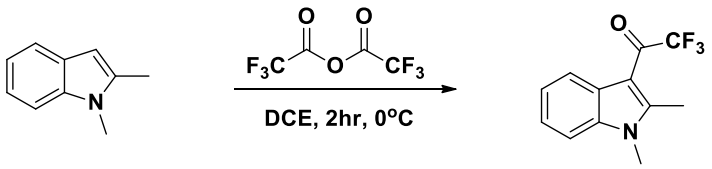

17 18

1,2-dimethylindolyl (**17**, 1.1 g, 7.6 x 10^{-3} mol) dissolved in 1,2-dichloroethane (3 mL) was added via cannula over 15 min to trifluoroacetic anhydride (1.1 mL, 8.6 x 10^{-3} mol) at 0 °C (ice bath). The solution was left to stir in an ice bath for 1.5 h, then at r.t. for 2 h. Solution was washed with sodium bicarbonate (200 mL) followed by extraction with dichloromethane (4 x 40 mL). Extracts were dried with $MgSO_4$ and solvent was removed *in vacuo* to give **18** as light brown crystals (1.7 g, 1 x 10^{-3} mol, 92 %). mp. 108-111°C; ^{1}H NMR (300 MHz, $CDCl_3$) δ 8.08 – 8.03 (m, 1H), 7.39 – 7.29 (m, 3H), 3.77 (s, 3H), 2.81 (s, 3H).

ethyl 2-(1,2-dimethyl-1H-indol-3-yl)-5-oxo-4-(propan-2-ylidene)-2-(trifluoromethyl)tetrahydrofuran-3-carboxylate

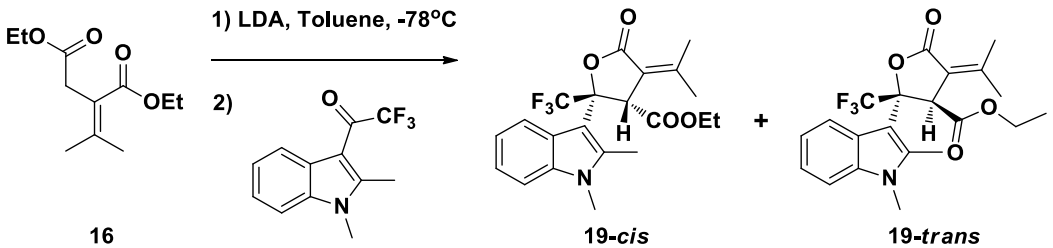

16 18 19-*cis* 19-*trans*

In four different reaction vessels diethyl 2-(propan-2-ylidene)succinate (**16**, 99 mg, 4.6 x 10^{-4} mol) was dissolved in dry toluene (5 mL) and cooled to -78 °C under nitrogen atmosphere. Freshly prepared 1.1 M LDA (0.6 mL, 6.6 x 10^{-4} mol) at -78 °C was added and stirred at -78 °C for 15 min, followed by heating to 0 °C (ice bath) for 10 min and cooling to -78 °C. **18** (107 mg, 4.4 x 10^{-4} mol) in dry toluene (3 mL)

was added drop wise via cannula over 15 min. Solution was then left to stir at r.t for 22 h. To the dark red solution water (10 mL) was added followed by acidification to pH 1 with 2M sulphuric acid (1 mL) then extracted with ethyl acetate (4 x 50 mL). Organic extracts of all four reactions were combined and dried with $MgSO_4$ and solvent removed *in vacuo*. The resulting red oil was purified by silica flash chromatography eluting with 2:1 dichloromethane/petroleum ether to give yellow solid **19** as a mixture of distereoisomers (yield 33 %). Recrystallization from ethanol gave pure *cis*-isomer as white crystals in a total yield of 25 %. **19-*Cis*** (as a mixture of atropisomers); mp. 163-165 ^{o}C; ^{1}H NMR (600 MHz, $CDCl_3$) δ 8.25 (d, J = 8.2 Hz, 0.3H), 7.55 (d, J = 8.1 Hz, 0.7H), 7.24 – 7.03 (m, 3H), 4.76 (s, 0.7H), 4.56 (s, 0.3H), 3.67 (s, 2H), 3.63 (s, 1H), 3.56 (dq, J = 10.8, 7.1 Hz, 0.7H), 3.46 (dq, J = 10.8, 7.1 Hz, 1.3H), 2.67 (s, 2H), 2.42 (s, 1H), 2.35 (s, 1H), 2.34 (s, 2H), 2.07 (s, 2H), 2.02 (s, 1H), 0.59 (t, J = 7.1 Hz, 2H), 0.33 (t, J = 7.1 Hz, 1H); ^{19}F NMR (300 MHz, $CDCl_3$) δ -80.04 (s); ^{13}C NMR (600 MHz, $CDCl_3$) δ 168.1, 167.9, 166.8, 166.6, 154.4, 153.6, 137.6, 136.7, 136.4, 133.5, 127.1, 125.8, 124.2, 123.9, 122.1, 121.6, 121.1, 120.4 (q, J = 3 Hz), 120.3, 119.2, 118.6, 118.5, 108.9, 108.4, 103.4, 102.1, 61.2, 61.1, 53.1, 51.8, 29.5, 29.5, 24.2, 20.6, 20.4, 13.7 (q, J = 3.7 Hz), 13.1, 12.8, 12.1; MS. $C_{21}H_{22}F_3NO_4$+H^+, expected 410.16, observed 410.1. **19-*Trans*** (calculated from a mixture of isomers); ^{1}H NMR (300 MHz, $CDCl_3$) δ 8.00 (d, J = 7.4 Hz, 1H), 7.25 – 6.99 (m, 3H), 4.89 (s, 1H), 4.43 – 4.22 (m, 2H), 3.68 (s, 3H), 2.63 (s, 3H), 2.25 (s, J = 21.1 Hz, 3H), 1.74 (s, 3H), 1.37 (t, J = 7.1 Hz, 3H).

3-(1-(1,2-dimethyl-1H-indol-3-yl)-2,2,2-trifluoroethylidene)-4-(propan-2-ylidene)dihydrofuran-2,5-dione - (CF_3-fulgide)

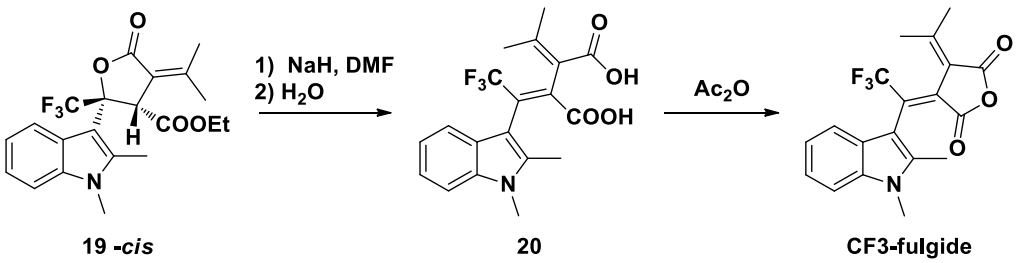

19 -*cis* 20 CF3-fulgide

Cis-lactone (**19-*cis***, 120 mg, 2.9 x 10^{-4} mol) in dry DMF (8 mL) was stirred at 0 ^{o}C (ice bath). NaH, 60 % in mineral oil (85 mg, 2.2 x 10^{-3} mol) added and stirred in ice bath for 10 min, then at r.t. for 2 h. Water (0.8 mL) was added and stirring continued for 17 h. The solvent was removed *in vacuo* to give an orange and white powder.

Acetic anhydride (2 mL) was added neat and stirred for 12 min. Water was added and solution was extracted with dichloromethane and solvent was removed *in vacuo* to give red solid. **CF_3-fulgide** was isolated by multiple recrystallizations from 2-propanol, yield 75 mg, 72 %. **E-isomer**; mp. 142-144 ^oC, ^1H NMR (300 MHz, $CDCl_3$) δ 7.47 – 7.09 (m, 4H), 3.76 (s, 3H), 2.50 (s, 3H), 2.36 (s, 3H), 2.30 – 2.25 (m, 3H); ^{19}F NMR (300 MHz, $CDCl_3$) δ -64.67. **Z-isomer** (from a mixture of isomers) ^1H NMR (300 MHz, $CDCl_3$) δ 7.46 – 7.08 (m, 10H), 3.72 (s, 3H), 2.28 (s, 3H), 2.17 (s, 3H), 0.98 (s, 3H); ^{19}F NMR (300 MHz, $CDCl_3$) δ -58.72. **C-isomer** (from a mixture of isomers) ^1H NMR (300 MHz, $CDCl_3$) δ 7.47 – 7.09 (m, 4H), 2.96 (s, 3H), 1.78 (s, 3H), 1.36 (s, 3H), 1.24 (s, 3H). HRMS (m/z) for $C_{19}H_{16}F_3NO_3$ +H ($[M+H^+]^+$); calcd 364.1160, found 364.1160.

A.2 DISCUSSION OF THE FULGIDE SYNTHESIS

Fulgides are typically synthesised by two Stobbe condensation reactions, named after its discoverer and the discoverer of fulgides, Hans Stobbe.[8, 9] The Stobbe condensation reaction is a Claisen condensation type reaction between a diethyl ester derivative and a carbonyl compound in the presence of a base, such as potassium tert-butanol (K^+ t-BuO^-) or lithium diisopropylamide. This reaction produces a C-C double bond via a lactone intermediate, and results in the loss of an ethoxy group. The mechanism for the Stobbe condensation reaction is shown in Scheme A-2. The basic synthetic process for creating the CF_3-Indolylfulgide **CF_3-fulgide** is very similar to other fulgides. The synthesis is performed by first performing a Stobbe condensation reaction between diethyl succinate **15** and acetone in K^+ t-BuO^- to insert an isopropyl unit, followed by esterification back to the diester **16**. Separately the CF_3-acylindolyl **18** is formed in excellent yields by addition of 1,2-dimethylindolyl **17** to trifluoroacetic anhydride at 0 ^oC. A second Stobbe condensation reaction between the acylindolyl and the isopropyl succinate gives an isolatable lactone intermediate **19**, which after an elimination and condensation gives the desired fulgide.

A.2.1 1st Stobbe Reaction

Compound **16** was prepared on three occasions. Each occasion gave a large proportion of unreacted diethyl succinate before distillation (best yield was 20:1 product to diethyl succinate), which was difficult to remove. Thorough acid-base liquid-liquid extraction procedures were attempted after the initial condensation and subsequent esterification; however, this was unsuccessful in removing diethyl succinate in the final crude product. This was possibly due to an undesired base catalysed hydrolysis at the ester in the first step to give the monoethyl succinate, which then was re-esterified in the next step. Initially a few flash chromatography columns were attempted however separation was difficult due to many side products and streaking (as shown by TLC with 9:1 petroleum ether/ethyl acetate, viewing with Vanillin stain). It was thus determined that vacuum distillation was the best way to purify. Expected boiling point of product was 100-102 ^{o}C at 2 Torr,[10] and for the starting material expected 70-75 ^{o}C at 4 Torr.[11, 12] The measured boiling points were higher and with less separation in temperatures. However, distillation never was able to completely remove all diethyl succinate.

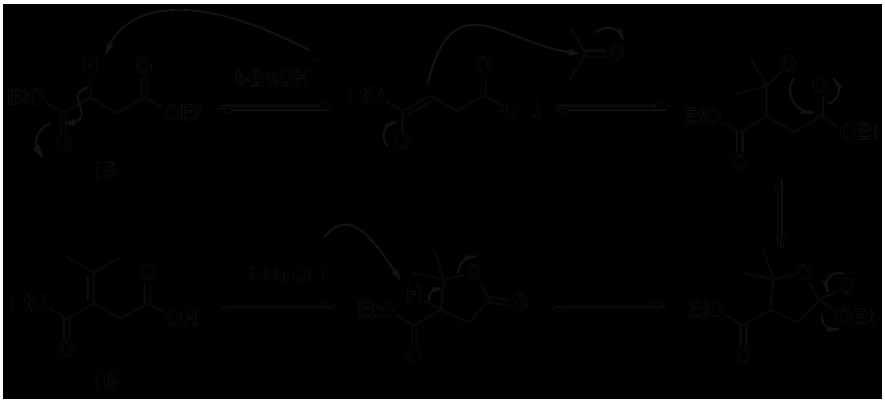

SCHEME A-2: Stobbe condensation reaction between diethyl succinic anhydride (15) and acetone.

A.2.2 Acylation of the Indolyl

This reaction was performed multiple times with multiple scale synthesis with yields varying from 52 % to 92 %. Initial attempts gave an impure compound after extraction which was purified by flash chromatography (2:3 ethyl acetate/petroleum ether), monitoring by TLC (2:3 ethyl acetate/petroleum ether, R_f = 0.60), which was

partially responsible for the lower yields obtained. However, it was found on larger scales with thorough quenching and extraction, pure product could be obtained without the need for chromatography. The acylindole was found to be unstable after extended storage on the bench, as observed by a discolouring of the crystals exposed to air.

A.2.3 2nd Stobbe Reaction

This reaction has provided the most issues and has been repeated on over 15 separate occasions (see Table A-1). Each time the reaction conditions and/or scale was altered. The reported yield for this reaction is low, Thomas *et al*. reports a total yield of 36 %.[2] Yields obtained varied between 20 % and 3 %, there was one exception (reported in experimental above) to this which provided a yield greater than 30 %. Variation to the yields appeared to be random. Even if the same conditions in two flasks on the same day, same batch of lithium diisopropylamide (LDA), same source of reagents, and same solvents two completely different outcomes may occur. LDA was sourced from Sigma-Aldrich, or prepared fresh from n-BuLi and isoproplyamine (see below). The main product isolated by column chromatography was the trifluoroacylindolyl starting material which indicates that activation of the succinate is difficult/not occurring in these conditions or once formed readily degrades back to give the indolyl. It was also observed that on occasions with an extended reaction time of more than one day, the reaction led to another unknown compound with a NMR spectra characteristic of an indolyl.

A.2.4 Synthesis and Verification of LDA

Lithium diisopropylamide was prepared fresh before each reaction from n-BuLi and isopropylamine. Firstly, the n-BuLi (Sigma-Aldrich, 2.5 M in hexanes) in a syringe was titrated dropwise into diphenylacetic acid (100 mg) in dry THF (8 mL) in a round bottom flask stirring at room temperature to determine the concentration of the base. Endpoint of titration was determined by the formation of a constant yellow tint.

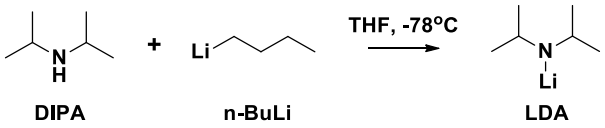

SCHEME A-3: Synthesis of lithium diisopropylamine.

Then to a dry round bottom flask was added diisopropylamide (1.25 mL, 8.8 mmol) and cooled to -78 ^{o}C with dry ice/acetone bath. To this was added n-BuLi (1 eq) dropwise, and solution was left to stir for 12 min before allowing to warm to 0 ^{o}C for 10 min then temporary sored at -78 ^{o}C. Final concentration of LDA was either calculated from amount of n-BuLi used or titrated with diphenylacetic acid, as above, then added directly to Stobbe condensation reaction via cannula using a N_2 positive pressure.

Table A-1: Summary of reaction conditions and yields investigated for the 2nd Stobbe condensation reaction. Yellow – pure yield; tan – point of variation; similar reactions are grouped between bold columns. (* followed alternate protocol by Balenko *et al.*[13])

Entry number	1	2	3	4	5	6	7	8	9	10	11	11	11	12 *	13	14	15	15	15
Mass diisopropyl succinate (mg)	113	93	91	690	300	322	448	500	507	108	108	99	116	127	1000	268	151	204	255
Mol diisopropy succinate (mol)	5.27E-04	4.34E-04	4.25E-04	3.22E-03	1.40E-03	1.50E-03	2.09E-03	2.33E-03	2.37E-03	5.04E-04	5.04E-04	4.62E-04	5.41E-04	5.93E-04	4.67E-03	1.25E-03	7.05E-04	9.52E-04	1.19E-03
Mass trifluoroacyl indolyl (mg)	125	101	100	760	340	360	498	522	532	115	116	107	110	104	1000	298	101	102	206
Mol trifluoroacyl indolyl (mol)	5.18E-04	4.19E-04	4.15E-04	3.15E-03	1.41E-03	1.49E-03	2.06E-03	2.16E-03	2.21E-03	4.77E-04	4.81E-04	4.44E-04	4.56E-04	4.31E-04	4.15E-03	1.24E-03	4.19E-04	4.23E-04	8.54E-04
LDA source	made from old n-BuLi	made from new n-BuLi	sigma new 2M	LDA (sigma)	LDA (sigma)	LDA (sigma)	LDA (sigma)	LDA (sigma)	LDA (sigma)	made from n-BuLi	made from n-BuLi	made from n-BuLi	made from n-BuLi	NaH, DIPA, THF	fresh THF	fresh THF	fresh THF	fresh THF	fresh THF
LDA concentration by titration (mol/L)	0.586	0.55	1.13	1	1.7	1.3	1.3	1.3	1.4	0.75	1.1	0.75	0.75	-	0.47	0.47	0.76	0.76	0.76
Toluene volume (mL) suc + ind+extra	5 + 5	5 + 5	1 + 1.5 +1	1 + 10	3 + 3 + 1.5	3 + 4	4 + 5	5 + 6	5 + 13	5 +3	5 +3	5 +3	5 +3		? + 15 +5	? + 15 +5	1+1.5+1	2+3+1	2+3+1
Total volume (mL)	10	10	3.5	11	7.5	7	9	11	18	8	8	8	8	9 (THF)			4.5	6	6
Reactant ratio succinidbase (mol)	1:0.98:1.05	1:0.96:1.01	1:0.98:1.06	1:0.98:1.30	1:1.01:1.46	1:0.99:1.36	1:0.99:1.31	1:0.93:1.28	1:0.93:1.18	1:0.95:1.04	1:0.95:1.31	1:0.96:1.14	1:0.84:0.97	1:0.73:5.9	1:0.89:0.60	1:0.99:0.30	1:0.59:0.97	1:0.44:0.64	1:0.72:1.15
Time at -78 (min)	10	15	10	15	N/A	5-10	60	5	10	10	10	10	10		12	15	15	15	15
Time on ice (min)	10	15	15	15	N/A	10	0	15	10	10	10	10	10		12	19	19	20	17
Time recooling (min)	N/A	N/A	10	N/A	N/A	N/A	N/A	10	15	N/A	N/A	N/A	N/A		N/A	10	10	13	9
Time adding indolyl (min)	N/A	20	N/A	N/A	N/A	N/A	30	15	30	10	10	10	10		20	3	3	5	15
Time left stirring at -78 (min)	N/A	10	0	10	10	10	0	N/A	0	N/A	N/A	N/A	N/A		N/A	N/A	N/A	N/A	N/A
Reaction time (hr)	23	44	25	70	20	N/A	16.5	20	23	19	21	21	22	22	22	22	44	44	44
Infreaction pH	10	N/A	N/A	N/A	N/A	N/A	N/A	N/A	12	N/A	12	12	12	12	11	11	11	11	11
Quenching acid	HCl (2M)	H2SO4 (2M)	H2SO4 (2M)	H2SO4	H2SO4 (2M)	H2SO4 (2M)	N/A	H2SO4 (2M)	H2SO4 (2M)	H2SO4 (2M)	H2SO4 (2M)	H2SO4 (2M)	H2SO4 (2M)	H2SO4 (2M)	H2SO4 (2M)	H2SO4 (2M)	H2SO4 (2M)	H2SO4 (2M)	H2SO4 (2M)
Acidified pH	2						N/A		2		1	1	1		2	2	2	2	2
Crude yeild	73 mg	N/A	44 mg	1341 mg	N/A	775 mg	N/A	993mg	1104Img	251mg	246mg	257mg	218mg	231mg	1.9174	no reaction	1.9174	1.9174	1.9174
Total pure yeild %	0	26	4	0	26	17	4	11	N/A	9	24 combined	-	-	0	2		37 (column only)	26 (column only)	12 (column only)

A.2.5 Elimination and Condensation

This step requires different conditions than normally used in fulgide synthesis, and has been investigated by Thomas *et al.*[2] Thomas reports that although the *trans*-lactone is able to successfully undergo elimination and hydrolysis by the standard conditions of aqueous ethanoic potassium hydroxide at 70 ^{o}C, the *cis*-lactone degrades in these conditions, and as the *cis*-lactone is the major product for the lactone with the pendant CF_3 group (4:1 *cis*:*trans*) this resulted in a large loss of product. However, it was found that sodium hydride in DMF gave favourable conditions for the elimination. Due to the low yield of the previous step, and it propensity to recrystallise in ethanol only the cis-lactone is reported here. Initially the condensation reaction was done in toluene and acetic anhydride (as per Thomas *et al.*[2]), this was found to give many side products. Difficulty was initially found in attempts to purify the crude fulgide, as the product photoswitches and degrades on dried silica making purification impossible from preparative TLC and difficult from silica flash chromatography. Figure A-1 shows a preparative TLC plate of the crude product from three different reactions, as can be seen in the left image the reaction was not very clean. The yellow central bands was composed of the *cis*- and *trans*-fulgide (determined by comparing to a pure sample, and investigating the photoswitching on TLC plates by running the TLC in different light conditions (dark (red jar), 354 nm filtered UV, and sunlight).). The TLC on the right was taken after the silica containing yellow bands were removed from the plate, it can be seen that there was bleaching of the colour which indicated degradation of the product on aerated silica. No **CF_3-fulgide** was recovered from preparative TLC.

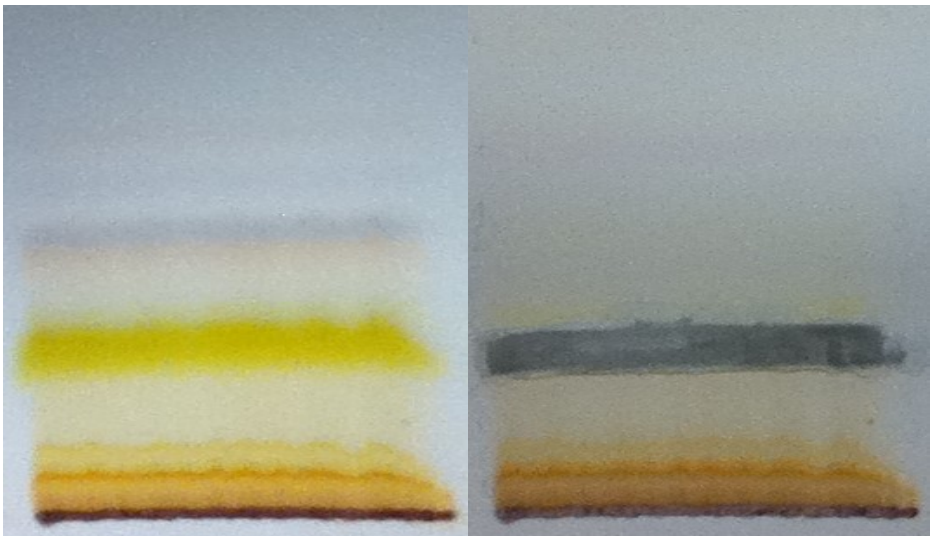

FIGURE A-1: Preparative TLC of crude products containing the pure fulgide (*cis*/*trans* yellow, cyclised blue). Left, freshly run plate; Right, after 40 min with thick yellow bands removed.

It was found that performing the condensation reaction in neat acetic anhydride (as described in the synthesis experimental, above) gave a much cleaner crude product which was able to be effectively purified by recrystallization from isopropanol. The added toluene was possibly leading to the unwanted side products as described by Wolak *et al.*[14]

A.3 CF_3-FULGIDE PHOTOSWITCHING SPECTROSCOPIC EXPERIMENTS

A.3.1 UV-Vis Absorbance Spectroscopy

UV-VIS absorbance spectroscopy of the synthesised **CF_3-fulgide** was observed on a Cary UV-Vis-5000 spectrometer. A solution of **CF_3-fulgide** (1×10^{-4} M) in HPLC grade ethanol was prepared from serial dilution of a 1×10^{-2} M stock solution (2.6 mg, 716 µL). Absorbance spectra were obtained in a 10 mm PMMA cuvette between 250 nm and 800 nm. Influence of light irradiation on the UV-vis absorption spectra of **CF_3-fulgide** in cuvette was observed after irradiation at multiple time intervals in four different light conditions; 254 nm germicidal UV lamp ($UV_{254\ nm}$), 352 nm filtered UV lamp (UV_{352nm}), as well as broad spectrum blue light from a halogen light source filtered with 525 nm shortpass filter ($SP_{<525nm}$) and red light from a halogen light source filtered with a 600 nm long pass filter (LP>600nm). The halogen light filter setup is shown in Figure A-2.

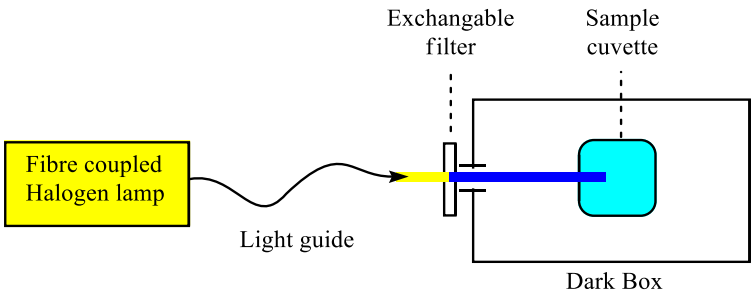

FIGURE A-2: Setup for benchtop broad spectrum photoswitching with a fibre coupled halogen light source.

The absorbance spectra of **CF_3-fulgide** during irradiation with UV light or visible light is shown in Figure A-3 and Figure A-4, respectively. The graphs show an initial spectrum consisting of the most stable non-cyclisable *trans*-isomer (Figure A-5) with a single visible peak at 439 nm. The calculated extinction coefficient is 2000-3000 $Lmol^{-1}cm^{-1}$, which is lower than previously reported in toluene (4000 - 6000 $Lmol^{-1}cm^{-1}$).[1, 4, 15, 16] Spectral responses due to photoswitching was initially observed using broad spectrum non-coherent UV light from a filtered Hg tube (black light)(UV352nm) and an unfiltered Hg tube (UV254nm) to initiate photoswitching. Exposure to UV352nm produced a decrease and a small shift in the 439 nm peak to 435 nm as well as a small increase around 570 nm. The shift in the 439 nm peak is associated with *trans*- to *cis*-photoisomerisation (Figure A-5).[15] The small increase at 570 nm indicates only a small amount of cyclisation; this could be expected due to the poor absorption of **CF_3-fulgide** and an overlapping absorbance of the cyclised form at 350 nm. Subsequent irradiation with UV254nm produced a decrease at 435 nm as well as large increases at around 358 nm and 572 nm. Thereby showing that 254 nm UV light induces a PSS with increased cyclised isomer than the 352 nm light.

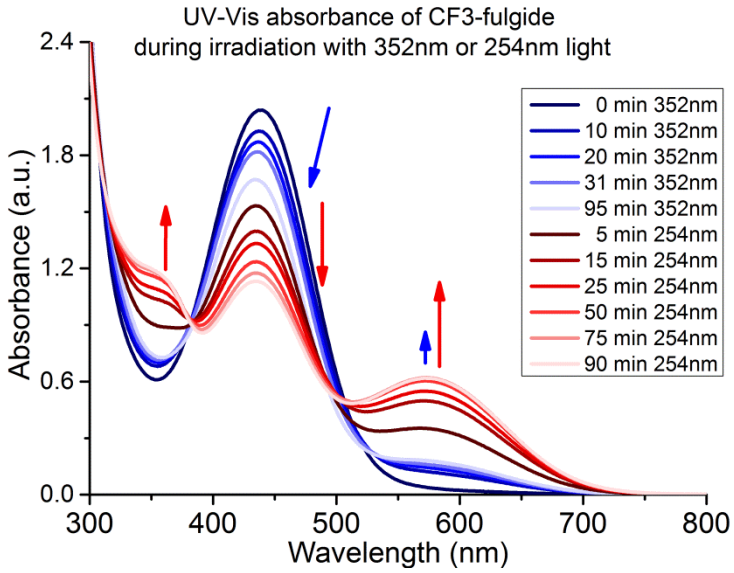

FIGURE A-3: UV-Vis absorbance of **CF_3-fulgide** during irradiation with UV light at the stated time intervals, 1 x 10^{-3} M in ethanol. Blue, irradiation using a UV352nm tube; red, irradiation using a UV254nm tube.

The photochemical switching was then investigated with broad spectrum visible light (Figure A-4). Using a fibre coupled halogen white light source blue light or red light was produced by using a 525 nm shortpass filter (SP<525nm) or a 600 nm longpass filter (LP>600), respectively. These filters were chosen to selectively irradiate the *trans*/*cis* isomers' 439/435 nm absorbance's (with SP<525nm), or only the cyclised absorbance (with LP>600nm), as can be deduced from the absorbance spectra given in Figure A-3. Irradiation of the *trans*-isomer with SP<525nm produced a large decrease at 439 nm, from a decrease in the *trans*/*cis* concentration, and an increase at 572 nm and 358 nm, from an increase in cyclised isomers (Figure A-4). Exposure to LP>600nm caused the removal of the 358 nm peak, restoration of the *cis*-isomer peak at 433 nm and a decrease at 572 nm to give a spectrum similar to that observed after UV352nm irradiation. This suggests that small peak around 572 nm could possibly be from a weak absorption in in *cis*-isomer and that UV352nm irradiation did not cause any cyclisation. These absorbance peaks show a small bathochromic shift compared to those reported by Wolak *et al.*, which reported peaks at 427 nm (*cis*-), 441 nm (*trans*-) and 571 nm (*cyclised*-) in toluene.[15]

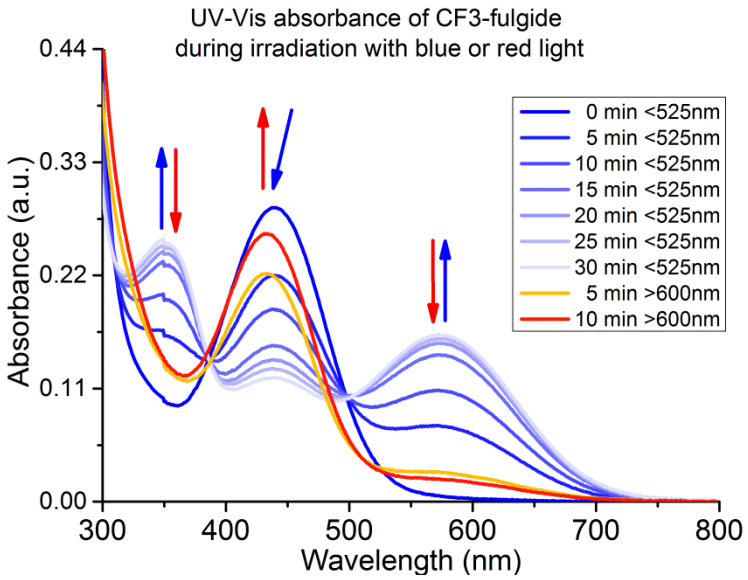

FIGURE A-4: UV-Vis absorbance of **CF_3-fulgide** during irradiation with filtered halogen light at 5 min time intervals, 1 x 10^{-4} M in ethanol. Blue, irradiation using the SP525nm filter; red, irradiation using the LP600nm filter.

A.3.2 ^{1}H NMR Spectroscopy

To confirm the structure of compounds produced from the photoswitching described above a visible-light photoswitching experiment was perform on an NMR sample and the resulting spectra were compared to that reported by Wolak *et al.*[14] A sample of **CF_3-fulgide** (3 mg) was dissolved in $CDCl_3$ (700 µL) in a standard NMR tube. ^{1}H NMR spectra was obtained at 0 min and timed intervals during irradiation with SP<525nm for a total of 170 min, then at timed intervals during irradiation with LP>600nm (as described above for the cuvette experiment). The resulting ^{1}H NMR spectra at 0 min, 170 min SP<525nm and 20 min LP>600nm is shown in Figure A-5 along with photos showing the colour change of the solutions. The spectral analysis of each isomer is given above in the experimental synthesis Section A.1. The initial ^{1}H NMR spectrum confirmed the presence of only pure *trans*- **CF_3-fulgide**. After the initial 30 min of SP<525nm irradiation *cis*- to *trans*- isomerisation could be observed then over the next 140 min the formation of resonance peaks from the cyclised isomer were observed. No other compounds were observed, suggesting there was no/little photodegradation occurring. When the irradiation was switched to the LP>600nm red light the signal of the closed isomer disappeared from the spectrum within 20 min, and only the *cis*- and *trans*- isomers remained. This

confirms the above UV-Vis observations and conclusions of the composition of the photo-stationary state upon photoswitching with these light sources.

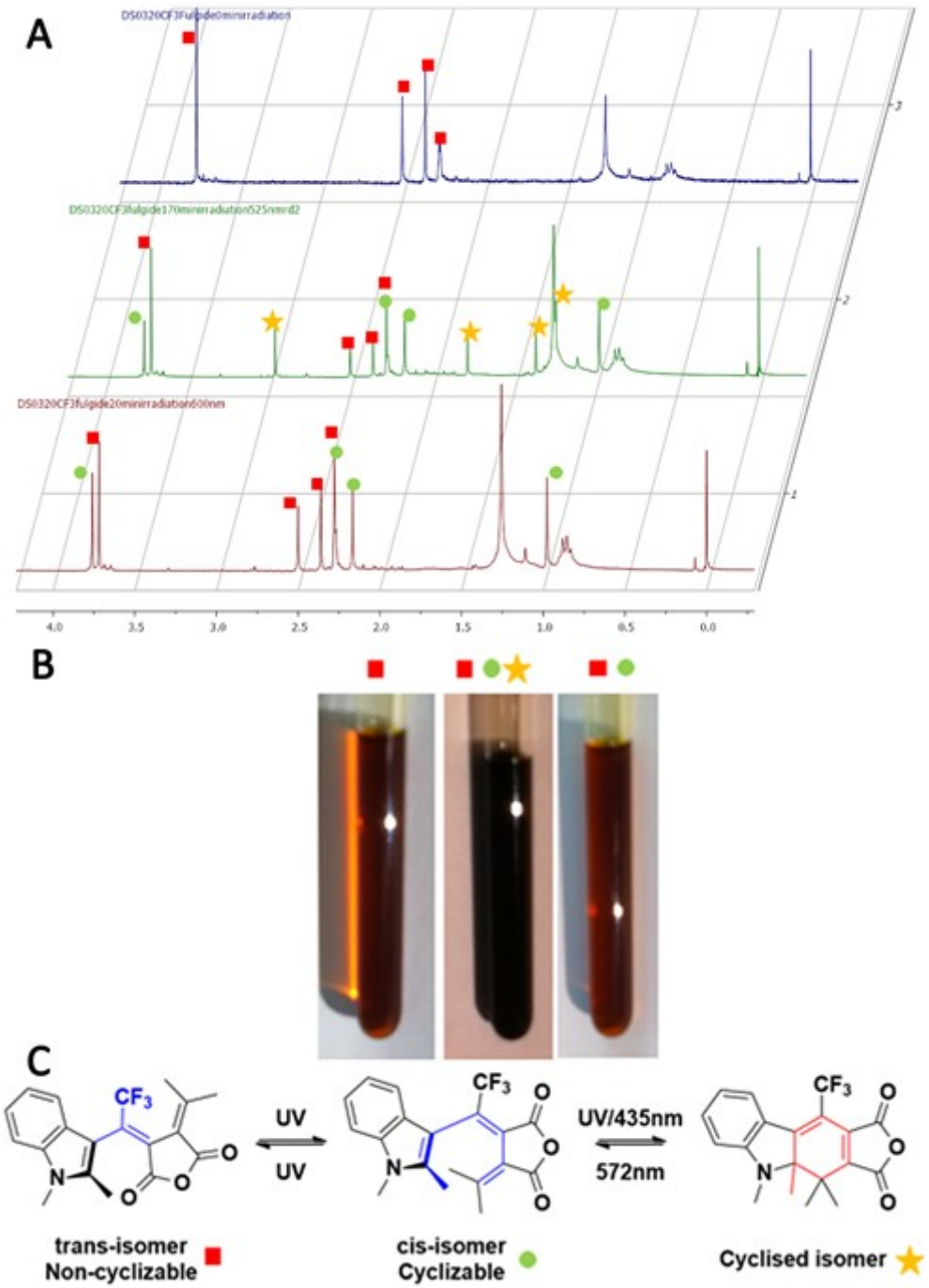

Figure A-5: A) ^{1}H NMR spectrum of **CF_3-fulgide**; Purple: non-irradiated sample, green: 190 min blue irradiation, brown: 20 min red irradiation. The peaks corresponding to each compound indicated as: red square for *trans*-fulgide; green circle for *cis*-fulgide; and yellow star for cyclised-fulgide B) Image of **CF_3-fulgide** in the NMR tube showing the colour of each solution. C) Photoswitching structural changes of CF_3-fulgide.

A.4 CONCLUSIONS TO APPENDIX A

The synthesis of the trifluoromethyl indolylfulgide, **CF_3-fulgide,** was achieved following a combination of literature methods. The synthesis was found to be difficult and low yielding, particularly due to a difficult, sterically hindered Stobbe condensation step to form the lactone intermediate. Therefore, due to the overall lengthy and low yielding synthesis it was not viable to further investigate fulgides as Photoswitchable sensors. That is, to perform further modifications to the completed fulgide (that is to modify the anhydride to give fulgimide derivatives) to create a series of fulgides capable of binding to metal ions for sensing. The same synthesis issues were encountered in attempts to synthesise a carboxylic acid functionalised indolylfulgide, as described by Strübe *et. al.,*[17] for surface attachment (data not shown). Characterisation of **CF_3-fulgide** was achieved by ^{1}H, ^{13}C and ^{19}F NMR, mass spectroscopy and by melting point and gave good correlation to previously reported data. Photoswitching of **CF_3-fulgide** was investigated using various wavelengths of light when dissolved in DMSO and ethanol; that is, filtered (352 nm) and unfiltered (254 nm) UV light from a Hg lamp as well as high energy (<525 nm) and low energy (>600 nm) broad spectrum light from a filtered halogen light source. The changes in UV-vis absorption spectra and ^{1}H NMR was observed during photoswitching and gave spectra similar to literature with absorbance peaks of 439 nm for *trans*- **CF_3-fulgide**, 433 nm for *cis*- **CF_3-fulgide** and 572 nm for the *cyclised*-**CF_3-fulgide**. The fluorescence and photoswitching properties of this fulgide were then investigated; as presented in Chapter 2 (PAPER 1).

A.5 REFERENCES FOR APPENDIX A

1. Yokoyama, Y.; Takahashi, K. Trifluoromethyl-substituted photochromic indolylfulgide. A remarkably durable fulgide towards photochemical and thermal treatments. *Chemistry Letters* 1996, (12), 1037-1038.
2. Thomas, C. J.; Wolak, M. A.; Birge, R. R.; Lees, W. J. Improved Synthesis of Indolyl Fulgides. *The Journal of Organic Chemistry* 2001, *66* (5), 1914-1918.
3. Brust, T.; Draxler, S.; Popp, A.; Chen, X.; Lees, W. J.; Zinth, W.; Braun, M. Stability and reaction dynamics of trifluorinated indolylfulgides. *Chemical Physics Letters* 2009, *477* (4-6), 298-303.

4. Islamova, N. I.; Chen, X.; Garcia, S. P.; Guez, G.; Silva, Y.; Lees, W. J. Improving the stability of photochromic fluorinated indolylfulgides. *Journal of Photochemistry and Photobiology A: Chemistry* 2008, *195* (2-3), 228-234.
5. Islamova, N. I.; Chen, X.; DiGirolamo, J. A.; Silva, Y.; Lees, W. J. Thermal stability and photochromic properties of a fluorinated indolylfulgimide in a protic and aprotic solvent. *Journal of Photochemistry and Photobiology A: Chemistry* 2008, *199* (1), 85-91.
6. Chen, X.; Islamova, N. I.; Garcia, S. P.; DiGirolamo, J. A.; Lees, W. J. Synthesis and Optical Properties of Aqueous Soluble Indolylfulgimides. *The Journal of Organic Chemistry* 2009, *74* (17), 6777-6783.
7. Chen, X.; Islamova, N. I.; Robles, R. V.; Lees, W. J. Photochromic properties of a water-soluble methyl carboxylic acid indolylfulgimide. *Photochemical & Photobiological Sciences* 2011, *10* (6), 1023-1029.
8. Stobbe, H. The colour of the 'fulgenic acid' and 'fulgide'. *Berichte Der Deutschen Chemischen Gesellschaft* 1905, *38*, 3673-3682.
9. Stobbe, H. Eine neue Synthese der Teraconsäure. *Berichte der deutschen chemischen Gesellschaft* 1893, *26* (3), 2312-2319.
10. Marvel, C. S.; Myers, R. L.; Saunders, J. H. The Preparation of 2-Alkylbutadienes1. *Journal of the American Chemical Society* 1948, *70* (5), 1694-1699.
11. Anderson, J. L.; Putnam, R. E.; Sharkey, W. H. Fluorodienes. I. Synthesis from Cyclobutenes. *Journal of the American Chemical Society* 1961, *83* (2), 382-385.
12. Watanabe, H.; Kuwata, S.; Koyama, S. Synthesis of cyclic peptide .1. preparation of cyclo-di-beta-alanyl from 1,4-cyclohexanedione. *Bulletin of the Chemical Society of Japan* 1963, *36* (2), 143-145.
13. Balenko, S. K.; Rybalkin, V. P.; Makarova, N. I.; Bezuglyi, S. O.; Shepelenko, E. N.; Popova, L. L.; Tkachev, V. V.; Aldoshin, S. M.; Metelitsa, A. V.; Bren', V. A.; Minkin, V. I. Synthesis, structures, and photochromic properties of N-aryl-3-indolylfulgides. Russian Chemical Bulletin 2009, 57 (7), 1435-1443.
14. Wolak, M. A.; Sullivan, J. M.; Thomas, C. J.; Finn, R. C.; Birge, R. R.; Lees, W. J. Thermolysis of a Fluorinated Indolylfulgide Features a Novel 1,5-Indolyl Shift. *The Journal of Organic Chemistry* 2001, *66* (13), 4739-4741.
15. Wolak, M. A.; Gillespie, N. B.; Thomas, C. J.; Birge, R. R.; Lees, W. J. Optical properties of photochromic fluorinated indolylfulgides. *Journal of Photochemistry and Photobiology A: Chemistry* 2001, *144* (2-3), 83-91.
16. Wolak, M. A.; Thomas, C. J.; Gillespie, N. B.; Birge, R. R.; Lees, W. J. Tuning the Optical Properties of Fluorinated Indolylfulgimides. *The Journal of Organic Chemistry* 2002, *68* (2), 319-326.
17. Strübe, F.; Rath, S.; Mattay, J. Functionalized Fulgides and Fluorophore-Photoswitch Conjugates. *European Journal of Organic Chemistry* 2011, *2011* (24), 4645-4653.

Appendix B: SURFACE POTENTIAL EXPERIMENTS ON QUARTZ GLASS

B.1 INTRODUCTION

The aim of this project was to test the Malvern Zetasizer Nano S surface potential device to determine if the apparatus is able to provide a viable method to monitor surface modification, photoswitching, and ion binding on glass slides. Using the change in zeta potential is advantageous compared to contact angle measurements as it is a direct measurement of a quantifiable surface property, rather than an indirect comparison of the surface hydrophobicity. Therefore, analysis of the zeta potential may provide a better comparison of surface composition after each surface treatment process. Also, as the zeta potential is a measurement of the surface charge it may be possible to observe changes that may arise from the photoswitching of a spiropyran SAM; as spiropyrans undergo a charge separation upon photoswitching to their merocyanine isomeric form. This surface charge may also be manipulated in the binding of a charged metal ion to the ionophore; therefore, the binding of metals to the surface may also be observed using this technique.

B.1.2 Zeta Potential and the Malvern Zetasizer Nano S

The Malvern Zetasizer Nano uses the electrophilic mobility of particles close to the surface to determine surface zeta potential, which is not a common method for the calculation of the zeta potential and there are almost no citations of its use in characterising silica surfaces (to our knowledge the only published reports have been from the Manufacturer[1-3]). Compared to the zeta potential of nanoparticles the zeta potential of bulk surfaces is not commonly reported in literature.[4, 5] We aimed to use surface zeta potential as a new method to differentiate between different stages of surface modification.

A charged material in a solution influences the charged particles/ions in that solution in a complex arrangement that forms several different layers on the surface. The first layer is the Stern layer, which is composed of oppositely charged particles adsorbing to the surface. Above this layer another layer is formed of particles attracted with weaker coulomb forces. This diffuse layer is able to interact and exchange with the

bulk solution. The point at which this layer interacts with the bulk solution is known as the slipping plane, the electronic potential at this plane is known as the zeta potential (Figure B-1).

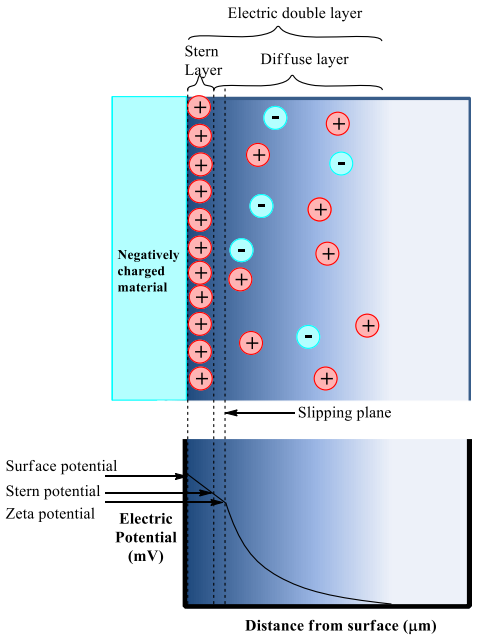

FIGURE B-1: The electric potential of a surface.

An electrical charge on the surface exhibits an electric field to the surrounding medium. This causes various electrokinetic effects in the medium, including electrophoresis and electroosmosis.

Electrophoresis is "the movement of a charged particle relative to the liquid it is suspended in under the influence of an applied electric field" and electroosmosis is "the movement of a liquid relative to a stationary charged surface under the influence of an electric field".[6]

The zeta potential of a particle is related to the electrophoretic mobility by the Henry equation. The Malvern Zetasizer Nano S uses the movement of particles during fast and slow pulsing of an electric field across the surface to calculate the electrophoretic mobility of particles in the solution at regular distance intervals from the surface (Figure B-2). Therefore, it is able to determine the zeta potential at each point away from the surface; then by extrapolating to the surface the surface zeta potential is

determined. Further information about this technique has been published by Corbett *et. al*.[3]

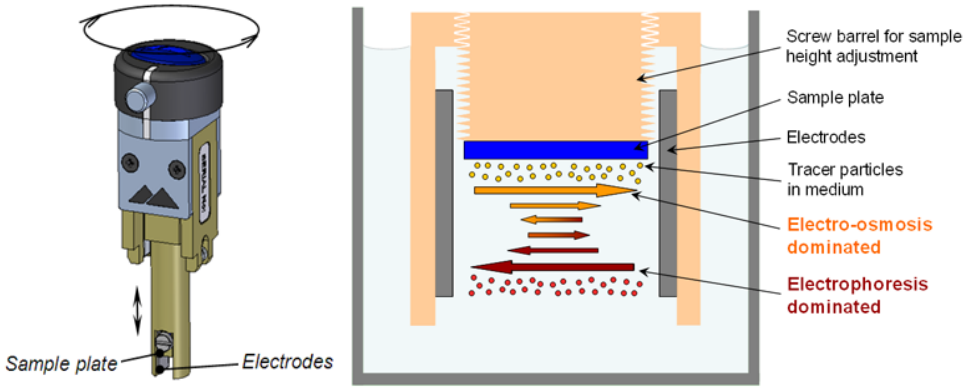

FIGURE B-2: The Zetasizer Nano S surface potential device, and the competing electroosmosis and electrophoresis processes utilised to determine the zeta potential.[1, 2]

B.2 RESULTS AND DISCUSSION

We aimed to observe and compare the zeta potential of quartz glass slides after the following six different treatments: 1) clean quartz, 2) APTES coated quartz, 3) CTES coated quartz, 4) spiropyran coated quartz, and 5) spiropyran coated quartz after photoswitching with i) spiropyran (Halogen white light) and ii) merocyanine (UV352nm light) (Figure B-3).

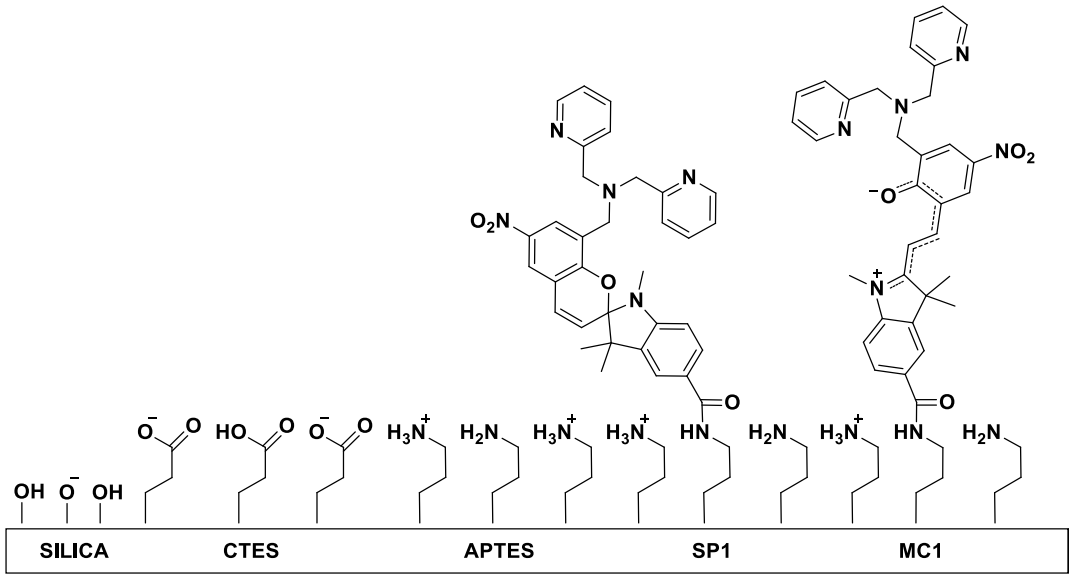

FIGURE B-3: Chemical composition of a silica surface after the differing surface treatments of 1) washing with piranha solution; 2) silanisation with CTES; 3) silanisation with APTES; 4) subsequent coupling with **SP1**; 5) subsequent irradiation with UV light to give the **MC1** isomer.

B.2.1 Preparing Microparticle Solution

The Zetasizer does not directly measure the surface potential, but the movement of microparticles in solution near the surface. Therefore, a standard microparticle buffer solution needed to be determined. The buffer solution needed to have a suitable ionic potential and contain microparticles of appropriate size with a surface potential compatible with the surface; *i.e.* a similar charge and magnitude to the surface (silica). A buffer system composed of phosphate-buffered saline (PBS) buffer with 0.3 μm polystyrene microbeads was chosen. The microbeads were first examined in solution with the Zetasizer to determine particle size and zeta potential. The microbeads were diluted to give 1 mM PBS solution 0.001 % particles. This solution concentration was used due to a reduced cloudiness compared to the more concentrated solutions, which would limit saturation of the laser beam path. Size measurements found that the average size distribution of the particles has a median around 372 nm with standard deviation of 105 nm in water, which is consistent with the supplier documentation stating 0.3-0.33 ± 0.03-0.05 μm. The zeta potential of the particles (0.001 % in 0.01 mM PBS) was determined to be -50 mV with std. error of 4.7 mV which is similar to the reported silica zeta potentials of between -35 and -

50 mV;[7-9] therefore, these particles are suitable for determining the zeta potential of silica surfaces.

B.2.2 Optimisation of Microparticle Buffer Solution

A clean quartz slide was attached to the sample plate (Figure B-2) with Loctite 406 adhesive and inserted into the surface potential device. Firstly, the surface zeta potential was obtained with a co-solution of 1 mM PBS and 0.001 % microparticles. However, it was observed that the solution turned cloudy brown after recording the first series of data, with a dark deposit on the electrode surface. This was thought to be a result of electrolysis of the electrode in the PBS buffer solution. This phenomenon may have not been observed earlier due to the extended data acquisition time required to determine particle zeta potential at multiple distances from the surface, compared to at a single distance. To confirm if the contamination was caused by the buffer and not the microparticles the surface zeta potential measurement was competed with negative controls containing just water, microparticles, or PBS buffer at 0.01 mM, 0.1 mM, and 1 mM. The water and microparticle solutions produced no change in solution quality. After one measurement with the 1 mM solution a change in the solution quality was visually observed, a lesser change was observed in the 0.1 mM solution. This electrolysis at the electrode by the buffer solution was not expected as Malvern has reported with similar concentrations of buffer solution using 0.1 - 50 mM KCl solution.[2, 3] Whereas a 1 mM PBS solution contains 0.27 mM KCl and 13.7 mM NaCl. Therefore, it is possible that the NaCl 13.7 mM is causing this deterioration of the buffer. Therefore, to determine this, co-solutions were tested with 10 and 1 mM KCl which gave a similar concentration dependent contamination of the solution during data acquisition as the PBS solutions. Therefore, to minimalize electrolysis/corrosion of the electrodes all future zeta potential acquisitions were done using fresh solutions of 0.01 mM PBS with 0.001 % polystyrene microparticles.

B.2.3 Zeta Potential of Different Surfaces for the Monitoring of the Reaction

The observed zeta potential of quartz surfaces coated with no silane, CTES and APTES was -45 ± 3.4 mV, -44.6 ± 4.7 mV, and -44.5 ± 9.3 mV, respectively. Indicating that there was no difference between the different surface coatings. This

was not expected due to the large expected difference in the charges at the experimental pH of 7.7 (Figure B-3). The uncoated and CTES surface showed an expected negative zeta potential of -44 mV, consistent with literature for silica.[7, 9] With the addition of the more positive amine layer a positive/less negative zeta potential was expected.[8] However, the APTES coated surface showed no change in zeta potential.

B.2.4 Zeta Potential of Photoswitching on Quartz

Slides functionalised with the spiropyran photoswitch **SP1** gave a zeta potential of around -30 mV. This reduced negative intensity compared to an uncoated surface was expected for a surface with a neutrally charged layer. However, like the APTES layer, it unexpectedly still showed a strong negative charge. Upon exposure of the coated surface with 352 nm UV light irradiation, in order to promote photoswitching to the open merocyanine form, a change in surface zeta potential was observed with a decrease in the intensity of the surface potential (Figure B-4). The glass slide was the allowed to sit in the dark overnight to thermally equilibrate to the closed form, this produced an increase in the intensity of the zeta potential. Irradiation with white light for 10 min also was observed to produce a small increase. Cycling of the surface zeta potential was observable over three UV – dark cycles with a decreasing difference in change in potentials observed in subsequent cycles. This observed change indicates that the photoswitching process alters the electronic state of the surface. This was expected as photoswitching with a spiropyran produces a charge delocalisation within the molecule. The increase in positive charge on the surface is possibly explained by an increased affinity of the spiropyran to positive ions in the solution, producing a more positive surface which would influence the observed zeta potential.

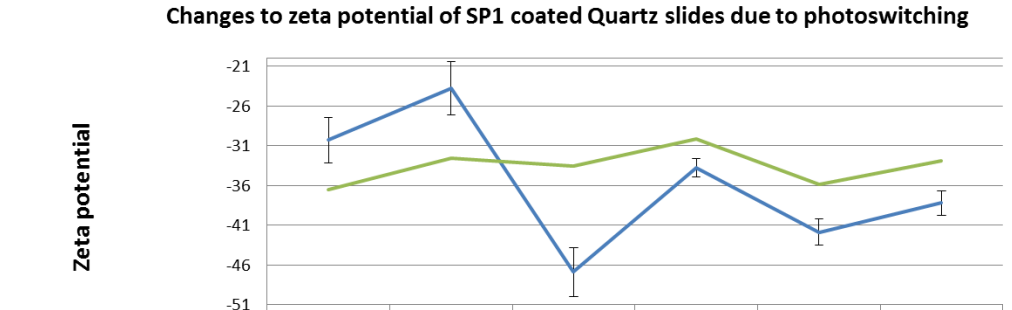

	SP1 quartz Slide	SP1 slide UV7min day 1	SP1 slide overnight	SP1 slide UV7min day 2	SP1 slide overnight 2	SP1 slide UV7min day 3
Surface zeta potential	-30.3	-23.8	-46.9	-33.8	-41.9	-38.2
Surface zeta potential error	2.85	3.38	3.09	1.18	1.64	1.55
microparticle zeta potential	-36.5	-32.6	-33.6	-30.2	-35.9	-32.9

FIGURE B-4: Changes in the zeta potential due to photoswitching of a **SP1** coated silica surface.

B.3 CONCLUSIONS FOR APPENDIX B

Using the Malvern Zetasizer Nano S the zeta potential of coated quartz slides was measured, however unexpectantly no discernible change in zeta potential was found between the three surface treatments of clean slides, CTES slides, and APTES slides. A difference in the photoswitched states of a quartz slide coated with a layer of spiropyran **SP1** via surface coupling to a APTES SAM was observed. Thus, its plausible that the photoswitching process for a range of photoswitches could be followed on surfaces in solution by observing the change in zeta potential, and in detecting binding of metal ions to the surface (provided that the ions don't interfere with the ionic potential of the co-solution and the particle zeta potential). However, using the Malvern Zetasizer Nano S for monitoring multiple steps and measurements was not a viable method for monitoring surface reactions, as 1) only a small sample can be used and the process was not transferrable to surfaces for alternative devices (such as fibres or curved surfaces). 2) Each reading needed to be performed manually and took over 40 min; therefore, to get statistically relevant measurements on many samples was not efficient, and it was likely surface switching was occurring over the experimental timescale. 3) There appeared to be a large degree of random error in the measurement process due to the crude mechanism to fix and align the glass surface to the sensor. Therefore, this method of surface evaluation was deemed unpractical and no more surface experiments were pursued to attempt to monitor zeta

potential changes associated with metal ion binding to the surface and hence quantify sensing of the surfaces.

B.4 MATERIALS AND METHODS

B.4.1 Materials

A pH 7.4 50 mM stock solution of PBS was produced following a standard procedure combining NaCl (8 g, 685 mM), KCl (0.2 g, 13.5 mM) Na_2HPO_4 (1.44 g, 50 mM), KH_2PO_4 (0.24 g, 10 mM) in 200 mL Milli-Q water and adjusted to the correct pH with $HCl_{(aq)}$ and $NaOH_{(aq)}$. Polystyrene LATEX beads LB-3 0.3 µm 10 % suspension (Corbett *et. al.*[3]) was sourced from Sigma-Aldrich. Quartz slides used were, SPI Supplies® QUARTZ SLIDE 25x76x0.5 mm THIN quartz slides.

B.4.2 Preparation of Quartz Slides for Zeta Potential Analysis

The quartz slides were cut to approximate 4 x 7 mm pieces in order to fit between the Zetasizer electrodes (Figure B-2). The quartz slides were cleaned as described earlier for the borosilicate slides (Section 5.6.1) by soaking in 1:1 MeOH/conc. HCl solution for 30 min, followed by washing with water then warm Piranha solution 1 hour then washing with water and methanol then dried in the oven at 150 ^{o}C.

Cleaned slides were then split into three groups to compare three different surfaces with different charges, *i.e.* clean (control), APTES coated and CTES coated. The APTES coated slides were further functionalised with a zinc selective spiropyran fluoroionophore **SP1** (Figure B-3) (Chapter 2). Slides were prepared in the general method described in Section 5.6.1.

APTES coated slides – In the glove box slides were incubated horizontally in 5 % APTES in dry toluene for 1 hour followed by washing with toluene, followed by ethanol, then water, then soaked in water for 24 hours and dried N_2.

CTES coated slides – On the bench slides were soaked in 5 % CTES in water for 1 hour followed by washing with water then ethanol and dried with N_2. The usual CTES surface coating procedure consists of a high temperature annealing step,[10] however, this was not performed as the current protocol was designed for

compatibility within MOF, and due to the polymer cladding MOF cannot be subjected to high temperatures.

SP1 coated slides – After several days APTES coated slides were soaked in a **SP1**/EDC/NHS (152 μM/2.24 mM/2.28 mM in 5 mL DMF) solution for 30 hours. Followed by washing with DMF water and ethanol and dried with N_2

Four different quartz slides were prepared from each treatment. Using fresh solutions of microparticle buffer solution containing 0.01 mM PBS at pH 7.7 and 0.001 % 0.3 μm polystyrene beads the electrophoretic mobility of the polystyrene particles, and thus their zeta potential, was recorded at distances of 125 μm, 250 μm, 375 μm, 500 μm, and 1 mm (bulk solution) from the surface of each coated slide using the Malvern Zetasizer Nano S and the surface zeta potential was extrapolated.

B.5 REFERENCES FOR APPENDIX B

1. Limited, M. I. Measuring Surface Zeta Potential using the Surface Zeta Potential Cell. http://www.malvern.com/en/pdf/secure/AN120917Surface-ZetaPotentialCell.pdf (accessed 15/05/2016).
2. Limited, M. I. Measuring the Surface Zeta Potential of Silica. http://www.malvern.com/en/pdf/secure/AN120914MeasSurfZPSilica.pdf (accessed 15/05/2016).
3. Corbett, J. C. W.; McNeil-Watson, F.; Jack, R. O.; Howarth, M. Measuring surface zeta potential using phase analysis light scattering in a simple dip cell arrangement. *Colloids and Surfaces A: Physicochemical and Engineering Aspects* 2012, *396* (0), 169-176.
4. Liu, D.; Chen, W.; Sun, K.; Deng, K.; Zhang, W.; Wang, Z.; Jiang, X. Resettable, Multi-Readout Logic Gates Based on Controllably Reversible Aggregation of Gold Nanoparticles. *Angewandte Chemie International Edition* 2011, *50* (18), 4103-4107.
5. Erdem, A.; Shahwan, T.; Çağır, A.; Eroğlu, A. E. Synthesis of aminopropyl triethoxysilane-functionalized silica and its application in speciation studies of vanadium(IV) and vanadium(V). *Chemical Engineering Journal* 2011, *174* (1), 76-85.
6. limited, M. I. Zetasizer Nano Series User Manual. Malvern Instruments limited: Grovewood Road, Malvern Worcestershire, WR14 1XZ, UK.
7. Kralj, S.; Drofenik, M.; Makovec, D. Controlled surface functionalization of silica-coated magnetic nanoparticles with terminal amino and carboxyl groups. *Journal of Nanoparticle Research* 2011, *13* (7), 2829-2841.
8. Soto-Cantu, E.; Cueto, R.; Koch, J.; Russo, P. S. Synthesis and Rapid Characterization of Amine-Functionalized Silica. *Langmuir* 2012, *28* (13), 5562-5569.

9. Anderson, T. H.; Min, Y.; Weirich, K. L.; Zeng, H.; Fygenson, D.; Israelachvili, J. N. Formation of Supported Bilayers on Silica Substrates. *Langmuir* 2009, *25* (12), 6997-7005.
10. González-Guerrero, A. B.; Alvarez, M.; Castaño, A. G.; Domínguez, C.; Lechuga, L. M. A comparative study of in-flow and micro-patterning biofunctionalization protocols for nanophotonic silicon-based biosensors. *Journal of Colloid and Interface Science* 2013, *393* (0), 402-410.

Appendix C: COMPUTATIONAL MODELS OF SPIROPYRAN-METAL ION 1:1 COMPLEXES

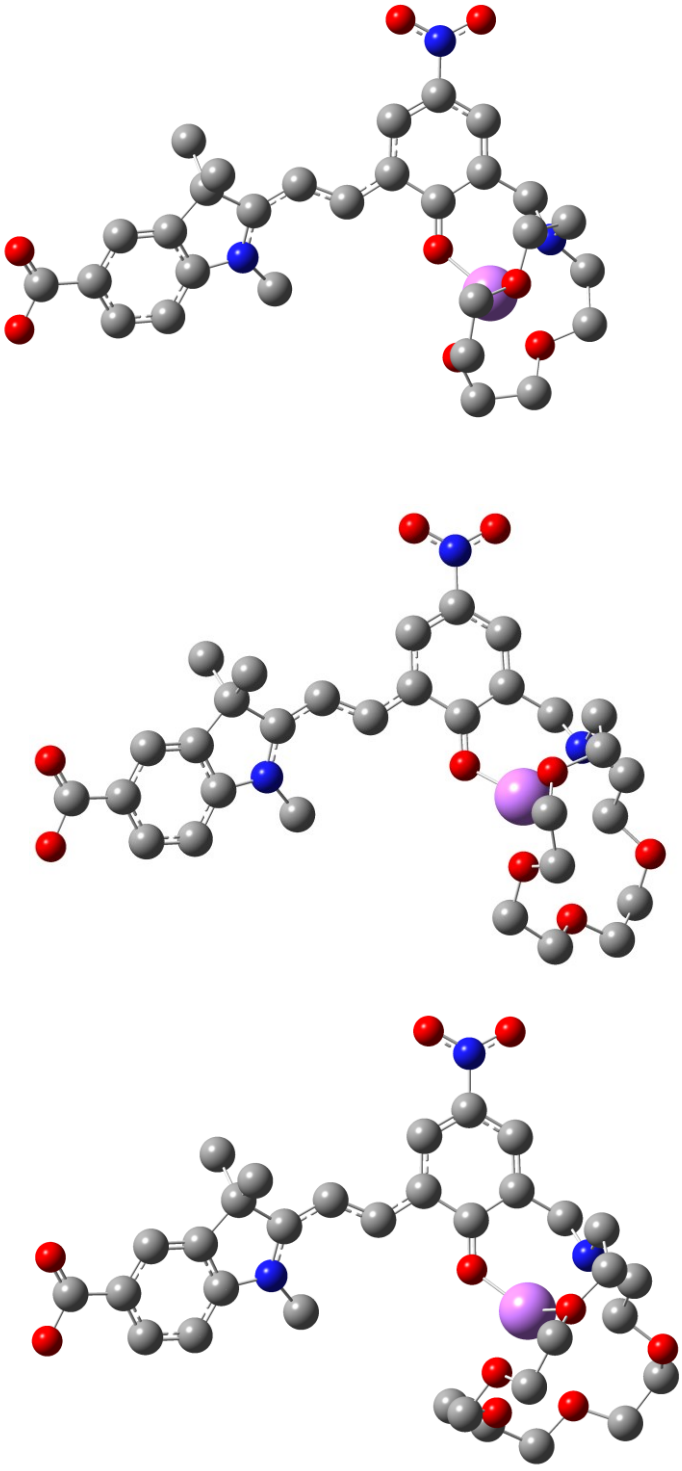

FIGURE C-1: 3D Computer generated model of the binding of Li^+ (pink) to **MC-1**, **MC-2**, **MC-3** in a 1:1 binding ratio. Hydrogens have been omitted for clarity. Calculations were performed as described in Section 4.5.3.

SP-3

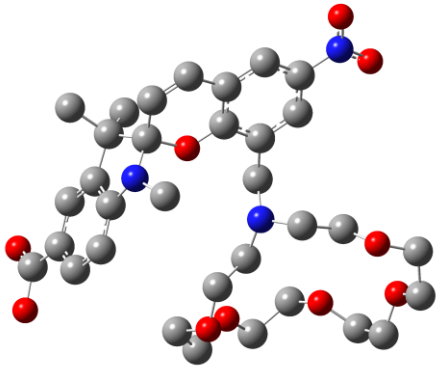

SP-4

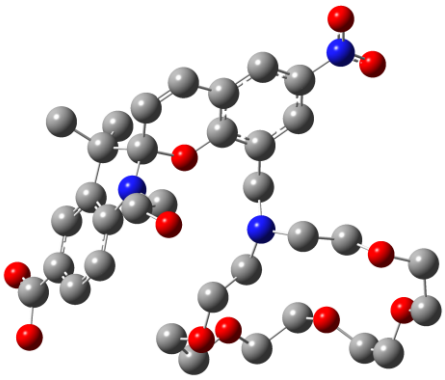

MC-3

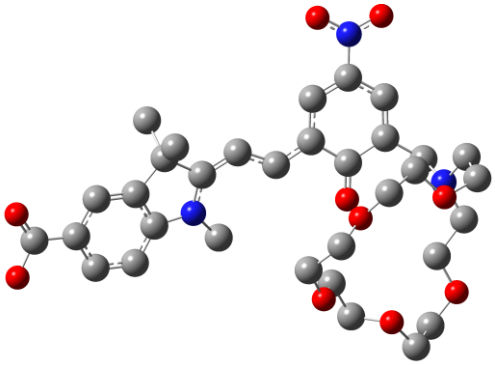

MC-4

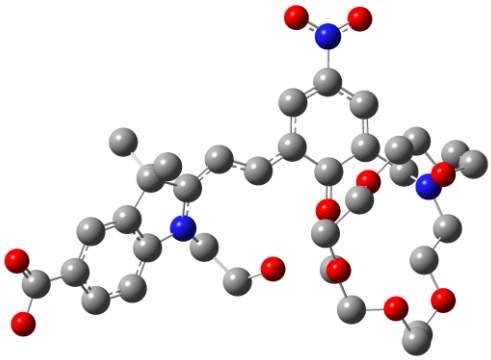

MC-3-Mg^{2+}

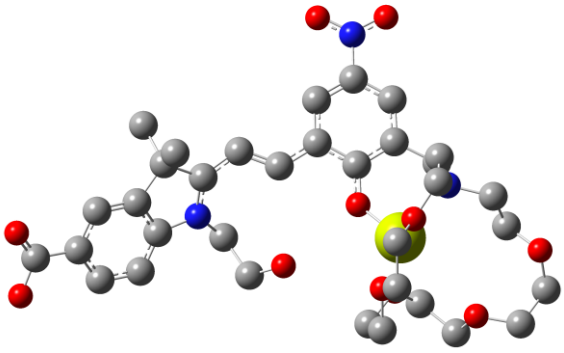

MC-4-Mg^{2+}

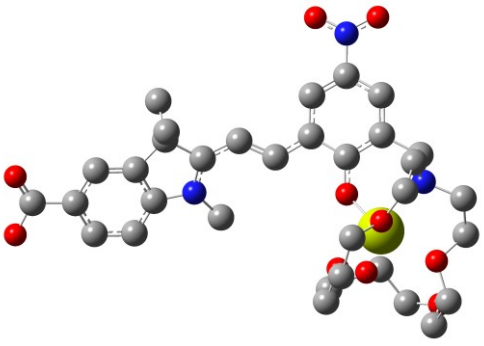

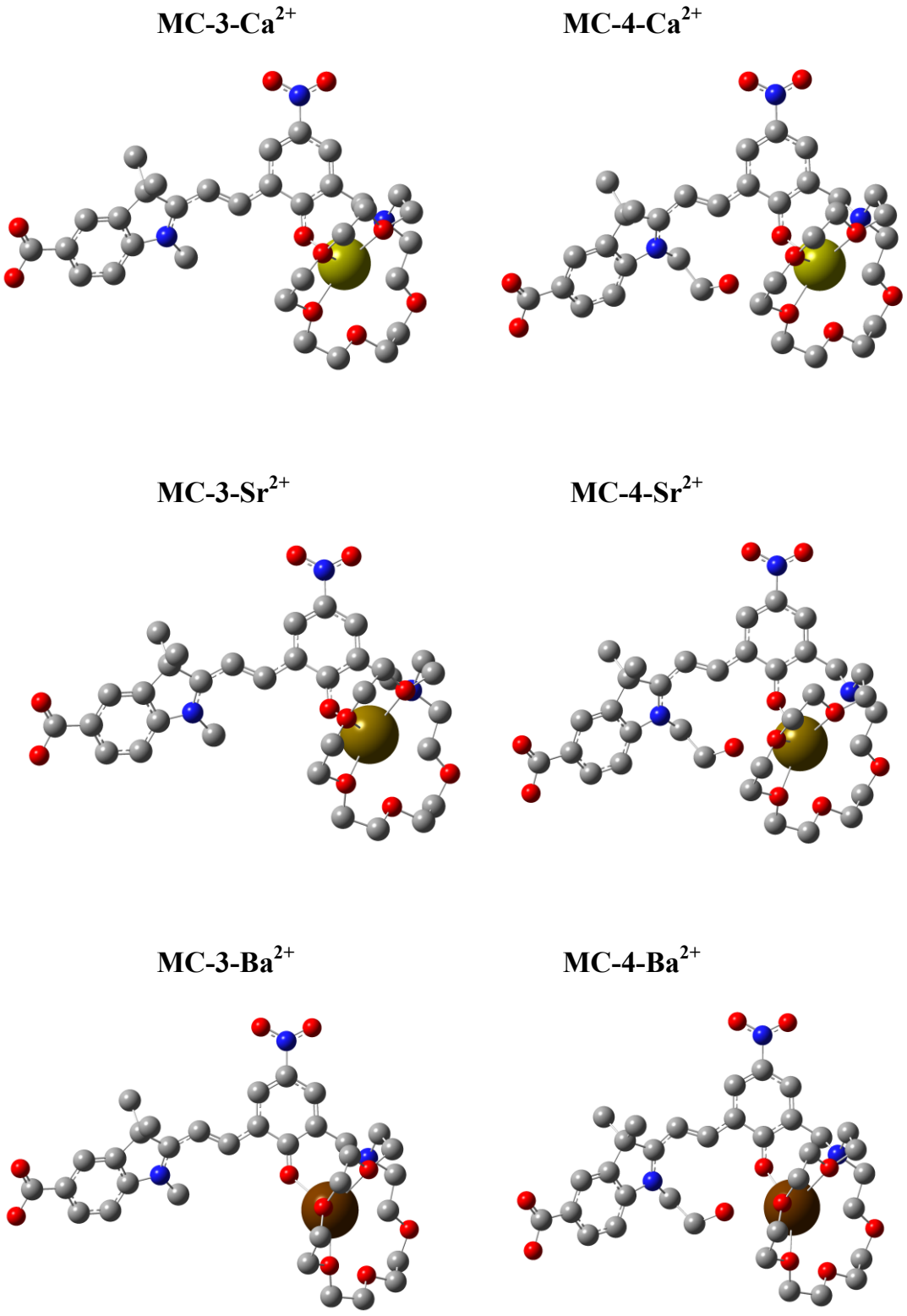

FIGURE C-2: Computational models of **SP-3** and **SP-4** with alkaline earth metals in a 1:1 binding ratio. Hydrogens have been omitted for clarity. Calculations were performed as described in Section 4.5.3.

Appendix D: OTHER PUBLICATIONS

The following section presents three papers mentioned within this thesis that have either been published or have been submitted for publication. The first two papers (PAPER 3 and PAPER 4) were partially discussed in Section 5.4, and involve the sensing of biologically relevant metal ions (Cd^{2+} and Ca^{2+}, and Zn^{2+}, respectively) in solution using MOFs. PAPER 5 was written based on the work presented in Section 4.3 and relates to the synthesis, biological testing and optical fibre based sensing of Ca^{2+} with **SP-4**.

D.1 PAPER 3: DUAL SENSOR FOR CD(II) AND CA(II): SELECTIVE NANOLITRE-SCALE SENSING OF METAL IONS

Statement of Authorship

Title of Paper	Dual Sensor for Cd(II) and Ca(II): Selective Nanolitre-Scale Sensing of Metal Ions
Publication Status	☑ Published ☐ Accepted for Publication ☐ Submitted for Publication ☐ Publication Style
Publication Details	Heng, S., A. M. Mak, D. B. Stubing, T. M. Monro and A. D. Abell (2014). "Dual Sensor for Cd(II) and Ca(II): Selective Nanolitre-Scale Sensing of Metal Ions." Analytical Chemistry 86(7): 3268-3272.

Principal Author

Name of Principal Author	Sabrina Heng		
Contribution to the Paper	Project conceptualisation. Synthesis of spiropyran fluorophores. Fluorescence assays of fluorophores. Project direction and writing of the manuscript		
Signature		Date	06.10.15

Co-Author Contributions

By signing the Statement of Authorship, each author certifies that:

i. the candidate's stated contribution to the publication is accurate;
ii. permission is granted for the candidate in include the publication in the thesis;
iii. the sum of all co-author contributions is equal to 100 % less the candidate's stated contribution.

Name of Co-Author (Candidate)	Daniel B. Stubing		
Contribution to the Paper	Microstructured optical fibre fluorescence measurements. Editing of manuscript		
Overall percentage (%)	20		
Signature		Date	08/09/2016

Name of Co-Author	Adrian M Mak		
Contribution to the Paper	Computational modelling and writing of manuscript.		
Signature		Date	08/09/2016

Name of Co-Author	Tanya M. Monro		
Contribution to the Paper	Project direction and editing of manuscript.		
Signature		Date	20/9/2016

Name of Co-Author	Andrew D. Abell		
Contribution to the Paper	Project direction and significant editing of manuscript.		
Signature		Date	13/09/2016

A DUAL SENSOR FOR CD(II) AND CA(II): SELECTIVE NANOLITRE-SCALE SENSING OF METAL IONS[1]

Sabrina Heng,[a*], Adrian M. Mak,[b] Daniel B. Stubing,[a] Tanya M. Monro,[a] Andrew D. Abell[a]

[a] ARC Centre of Excellence for Nanoscale BioPhotonics, Institute of Photonics & Advanced Sensing and School of Chemistry & Physics, The University of Adelaide, SA, Australia 5005.

[b] Institute of High Performance Computing, 1 Fusionopolis Way, #16-16 Connexis, Singapore 138632.

D.1.1 ABSTRACT

The first selective, dual sensor for Ca^{2+} and Cd^{2+} capable of detection at 100 ρM concentrations was designed and synthesized. The experimental observations made for the MC-cation complexes and the selectivity of Compounds **SP-6** and **SP-7** with Ca^{2+} and Cd^{2+} ions were further explored using density functional theory. A first step toward a nanolitre-scale dip sensor for the dual sensing of Ca^{2+} and Cd^{2+} was demonstrated using microstructured optical fibre as the sensing platform which is important for ion sensing in confined spaces such as the medium surrounding cell clusters. In addition, this system displays picomolar sensitivity for these ions, with an added ability to reproducibly turn ion-binding on/off.

D.1.2 INTRODUCTION

Cadmium (Cd^{2+}) is one of the most toxic heavy metal ions,[2, 3] with chronic exposure through inhalation and ingestion of contaminated smoke, soil and crops[4] giving rise to serious health disorders including osteoporosis,[5, 6] cancer[7-9] and neurodegenerative disorders such as Parkinson's disease,[10] Alzheimer's disease,[11, 12] and amyotrophic lateral sclerosis.[13, 14] In comparison, calcium (Ca^{2+}) is of major benefit as a ubiquitous intracellular signalling ion that is responsible for controlling numerous cellular processes including cell proliferation, differentiation, and survival/death.[15, 16] Despite these different profiles, the two metal ions are intricately related, where Cd^{2+} toxicity is known to arise from disruption of free intracellular Ca^{2+} homeostasis. This leads to apoptosis in a variety of cells, such as skin epidermal cells, hepatic

cells, lymphoblastoid cells, mesangial cells, thyroid cancer cells, and thymocytes.[17] Cd^{2+} is also able to act directly on bones, with animal studies showing that Cd^{2+} stimulates the formation and activity of osteoclasts to break down the collagen matrix in bones leading to osteoporosis.[18, 19] Despite the biological importance of these two ions, little is known about the molecular mechanisms of Cd^{2+} uptake by cells and its carcinogenesis due to Ca^{2+} hemostasis in humans and other mammals.[20] The development of non-invasive tools and techniques that is able to selectively sense Cd^{2+} and Ca^{2+} in the abovementioned examples and more would thus provide an important advance in the fields of cell biology, neurophysiology, and pathophysiology.[21]

Several sensors for the selective binding and detection of cadmium[22-27] and calcium[28] have been reported. However, a rationally designed sensor capable of binding both Cd^{2+} and Ca^{2+} with an ability to produce a unique fluorescence profile for each ion would provide an important advance to allow delineation of the relationship between the two ions.[22] Here we report the first specifically designed, photochromic sensor that has selectivity for both Cd^{2+} and Ca^{2+} (**SP-6**, Scheme D-1) when tested against other biologically relevant metal ions (Figure D-1a). A photochromic, spiropyran system was incorporated into the sensor to allow reversible switching and hence the capacity for continuous sensor operation. A spiropyran also provides low background fluorescence compared to non-photochromic sensors such as those based on rhodamine. A suitable ionophore capable of complexing with a metal ion or ions is then attached to the spiropyran to provide the functional metal ion sensor. This type of ion sensor will only fluoresce in the presence of the metal ion to which it is designed to bind. The resultant fluorescence occurs due to the isomerization of the sensor from the closed spirocyclic (SP) form to the ring opened merocyanine (MC) form in the presence of the metal ion (e.g. **SP-6** and **SP-7**, SP to MC, Scheme D-1).

The dual Ca^{2+} and Cd^{2+} sensor reported here was designed with the chemical similarities between Ca^{2+} (ionic radii 0.99 Å) and Cd^{2+} (0.97 Å) in mind. Selective binding of Ca^{2+} and Cd^{2+} compared to other metal ions was achieved by appending groups that are known to separately bind M^{2+} ions and Cd^{2+} respectively. We now combine these into the one structure for the first time, particularly (i) a butanoic acid group that is known to promote affinity for M^{2+} ions,[29] (ii) a 2-methoxyethoxy

moiety at position 8' of the benzopyran ring that is known to bind to Cd^{2+} specifically in such systems.[30] A control (**SP-7),** with a hydroxyethyl attached to the indolium nitrogen in place of the carboxylic acid of **SP-6**, was designed and prepared to have a reduced affinity towards M^{2+} ions. Both analogues contained the NO_2 moiety at the 6' of the benzopyran ring, as electron-withdrawing groups at that position are known to stabilize the ring-opened MC form thus favouring ion binding.

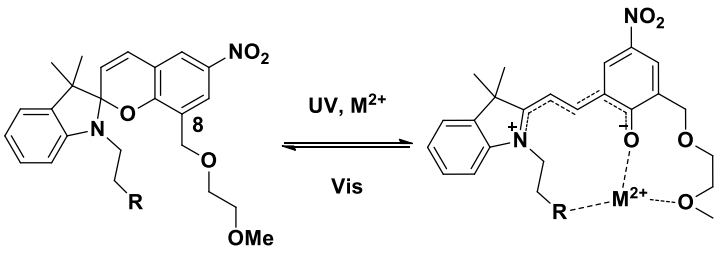

SP-6 R = CH_2COOH
SP-7 R = OH

SCHEME D-1: Structures of **SP-6** in the closed and metal ion induced opened form and SP-7. The dashed lines represent possible bindings of the metal ion to the MC ligand.

D.1.3 RESULTS AND DISCUSSION

Compounds **SP-6** and **SP-7** were prepared from 2,3,3-trimethylindolenine and 3-(chloromethyl)-2-hydroxy-5-nitrobenz aldehyde in 40 - 50 % overall yields using slight modifications to existing methodology.[31, 32] These compounds were characterized by ^{1}H, ^{13}C NMR and MS analysis respectively with details shown in supporting information.

To characterize the behaviour of **SP-6** and **SP-7**, fluorescence-based binding experiments with metal ions were performed. The selectivity of **SP-6** and **SP-7** toward biologically relevant metal ions Ca^{2+} and Cd^{2+} as well as Na^{+}, Be^{+}, Al^{3+}, K^{+}, Ni^{2+}, Mn^{2+}, Ce^{3+}, Mg^{2+}, Zn^{2+}, Fe^{2+}, Pb^{2+}, Cu^{2+}, and Co^{2+} were investigated by fluorescence spectroscopy, with the results shown in Figure D-1. These results reveal two important observations: Firstly, that **SP-6** is selective for Ca^{2+} and Cd^{2+} over Na^{+}, Be^{+}, Al^{3+}, K^{+}, Ni^{2+}, Mn^{2+}, Ce^{3+}, Zn^{2+}, Fe^{2+}, Pb^{2+}, and Cu^{2+}. Upon addition of Ca^{2+} and Cd^{2+} to **SP-6**, strong fluorescence at 590 - 595 nm were observed. The fluorescence observed here is due to the formation of the MC-M^{2+} complex and no other metal cations examined produced the same effect. The only exception was

with Mg^{2+} which gave half the fluorescence intensity relative to the MC-Ca^{2+} and MC-Cd^{2+} complexes as a result of the formation of a weakly complexing MC-Mg^{2+} system. While this is not surprising given the similarities between Ca^{2+} and Mg^{2+} and with **SP-6**, it is possible to differentiate between Mg^{2+} and Ca^{2+} in solution via absorbance spectroscopy since both **SP-6**-Mg^{2+} and **SP-6**-Ca^{2+} complexes gave different absorbance profile (Figure D-1b). The same fluorescence experiments were repeated using **SP-7** (Figure D-1a, red bars). Here, only Ca^{2+} and not Cd^{2+} showed a fluorescence response with the sensor that indicates the formation of the MC-M^{2+} complex (Figure D-1a). The absence of the carboxylate moiety in **SP-7** strongly suggests that Cd^{2+} coordinates to **SP-6** via a triad of functionalities that includes the carboxylic moiety at the indolium nitrogen, the 2-methoxyethoxy at position 8' of the benzopyran ring and phenoxy oxygen from the ring-opened MC moiety.

Secondly, **SP-6** showed little affinity for Zn^{2+} when compared to its affinity for Cd^{2+}, where the relative fluorescence intensity obtained for Zn^{2+} is less than 10 % of what was obtained in the presence of Ca^{2+} and Cd^{2+}. This is significant as many existing probes for Cd^{2+} also bind to Zn^{2+} due to both ions having closed shell d^{10} configurations.[33, 34] A useful sensor for Cd^{2+} must demonstrate selective fluorescence response to Cd^{2+} compared to Zn^{2+} under physiological conditions given that $Zn^{2+}$is ubiquitous in biology.

With respect to the simultaneous detection of multiple metal ions, the main challenge is finding a set of conditions under which all target metal ions can be detected as well as determining a method that produces distinguishable signals for each metal ion. With **SP-6** a subtle but potentially significant shift in the fluorescence spectrum was observed between the two MC-M^{2+} complexes of **SP-6** binding to Ca^{2+} and Cd^{2+} (Figure D-2a). In particular, the fluorescence maximum for **SP-6** with Ca^{2+} is 595 nm while **SP-6** with Cd^{2+} is 590 nm. On/Off binding of Cd^{2+} to **SP-6** and the detection of the second ion was demonstrated. **SP-6** was first saturated with 100 μM of Cd^{2+} (Figure D-2b, red dash lines) and λ_{max} = 590 nm was recorded. The solution was then exposed to white light, allowing the bound Cd^{2+} ions to be released back into solution. 100 μM of Ca^{2+} ions were then added to the solution and exposed to UV for 3 min. The resultant fluorescence curved showed a change where the

fluorescence maximum had shifted to approximately 595 nm (Figure D-2b, blue dash lines). This possibly demonstrates that **SP-6** has greater affinity for Ca^{2+} over Cd^{2+}. Understanding the binding affinity of **SP-6** towards the different ions is an important step towards designing compounds that can simultaneously identify both ions.[35]

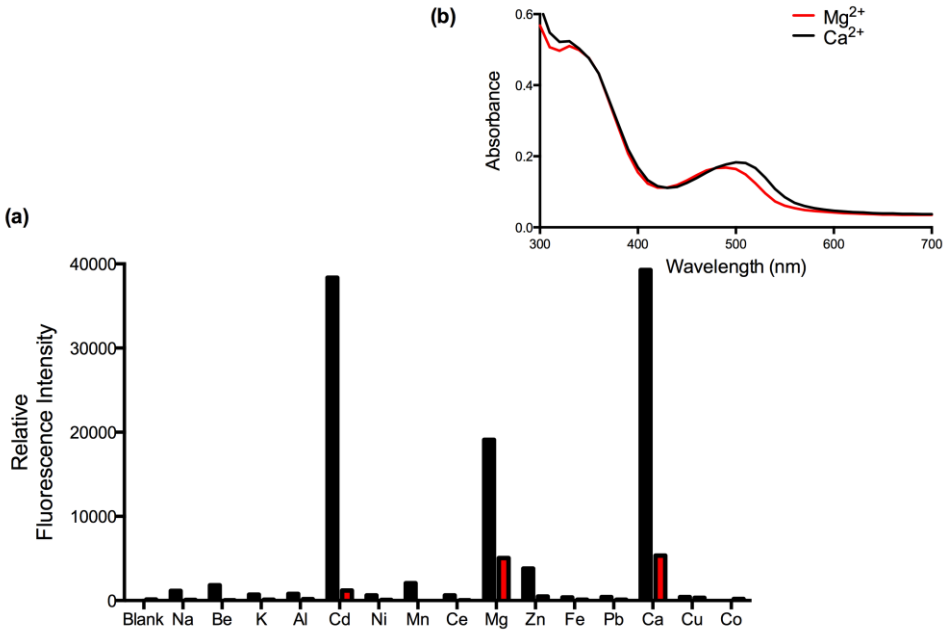

FIGURE D-1: (a) The bar graph shows the fluorescence (where λ_{ex} = 532 nm) of **SP-6** (50 µM, black) and SP-7 (50 µM, red) in the presence of various metal ions (100 µM). (b) Absorption spectra of **SP-6** (50 uM) in the presence of Mg^{2+} (100 µM, red) and Ca^{2+} (100 µM, black). All experiments were carried out using HPLC-grade acetonitrile and in 96-well plates at 25 °C and were performed in triplicates and results averaged.

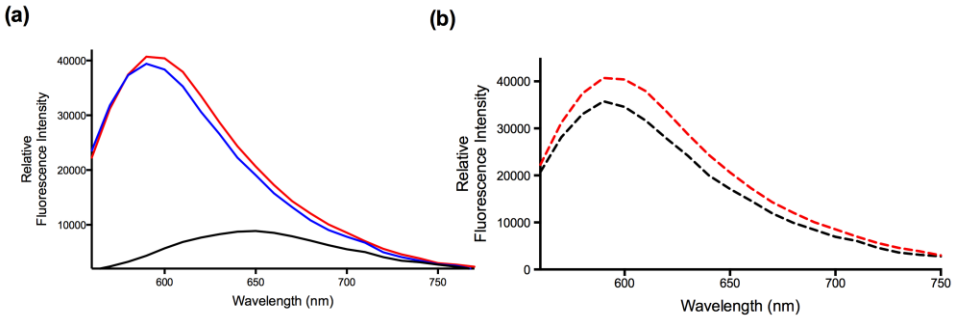

FIGURE D-2: (a) Fluorescence for **SP-6** (50 μM) in the absence (blank, black) and presence of Ca^{2+} (100 μM, red) and Cd^{2+} (100 μM, blue) respectively. Fluorescence maxima (where λ_{ex} = 532 nm) for **SP-6**-Ca^{2+} is 595 nm and **SP-6**-Cd is 590 nm. (b) Fluorescence for **SP-6** (50 μM) in the presence of Cd^{2+} (black dashed-lines) and in the presence of 1:1 Cd^{2+}: Ca^{2+} (100 μM each, red dashed-lines). All experiments were carried out using HPLC-grade acetonitrile and in 96-well plates at 25 °C. The excitation wavelength for these experiments was 532 nm.

Standard calibration experiments were performed for **SP-6** with Ca^{2+} and Cd^{2+} and for **SP-7** with Ca^{2+} respectively (Supporting Information, Figure D-7). The results showed increased fluorescence for **SP-6** and **SP-7** with increasing ion concentration. For **SP-6**, the limits of detection under these experimental conditions were 500 nM of Cd^{2+} and Ca^{2+} respectively while the limit of detection for **SP-7** with Ca^{2+} was determined to be 1 μM. As Ca^{2+} is reported to be the fifth most abundant ion in the cell and that the LC_{50} for Cd^{2+} related toxicity is in the low micromolar range[36] (reported to be between 20 to 60 μM), **SP-6** has the required sensitivity for sensing Ca^{2+} and Cd^{2+} in biological applications. From these experiments, it was also observed that maximum values for fluorescence intensity were reached after the addition of 0.5 equivalent of metal ions respectively. Thus, the binding stoichiometry of MC-M^{2+} complexes were determined by continuous analysis in order to define the species resulting from binding of **SP-6** to Ca^{2+} and Cd^{2+}. Similar methodology has been successfully applied to the characterization of other MC-cation complexes.[37] Here, Job's plot analysis shows a maximum fluorescence at X (=$[M^{2+}]/([M^{2+}] + [\textbf{SP-6}])$) = 0.3 for both Ca^{2+} and Cd^{2+} indicating that the observed fluorescence response for **SP-6** is due to the formation of a 2:1 MC-cation complex (Supporting Information, Figure D-6). This suggests that both Ca^{2+} and Cd^{2+} ions are sandwiched between two merocyanine molecules respectively.

The experimental observations made for the MC-cation complexes and the selectivity of **SP-6** and **SP-7** with Ca^{2+} and Cd^{2+} ions were further explored using density functional theory implemented in a development version of Q-Chem.[38] The BP86 functional[39, 40] was employed, along with the LANL2DZ basis set with effective core potentials for Ca^{2+} and Cd^{2+}, to carry out geometry optimizations for the compounds of interest. Calculation of the energy Hessian was carried out for each model by double differentiation of the energy with respect to spatial coordinates. A positive definite Hessian characterizes true energy local minima on the potential energy surface, with all harmonic frequencies being real.

For the M[**SP-6**(MC)]$_2$ species, the calcium ion is coordinated with eight oxygen atoms in the opened rings, while the Cd^{2+} ion is coordinated with six. These results are consistent with earlier observations that **SP-6** has greater affinity for Ca^{2+} over Cd^{2+}. In addition, Ca^{2+}…O distances are between 2.4 and 2.6 Å, and Cd^{2+}…O distances are between 2.3 and 2.6 Å. The overall reactions of the metal perchlorates with the closed spirocyclic form of **SP-6** are endergonic, at -94.3 and -230.6 kJ/mol for Cd^{2+} and Ca^{2+} respectively (Table D-1). For the M[**SP-7**(MC)]$_2$ species (**SP-7**), Ca^{2+} is still octa-coordinated and Cd^{2+} is hexa-coordinated. The more negative free energy of Reaction 1 compared to Reaction 2 in Table D-1 can be somewhat rationalized by examining the structures of the Cd-complexes. Oxygen atoms O41 and O105 of Cd[**SP-6**(MC)]$_2$ (indicated in Figure D-3) form ion-dipole interactions with the Cd centre which is ~3.0 Å away. This provides stabilization to the end product Cd[**SP-6**(MC)]$_2$ Correlating the reaction energies in Table D-1 with the fluorescence intensity bar graphs in Figure D-1(a), the difference in fluorescent yield of **SP-7** with Cd^{2+} and Ca^{2+} can be related with the difference in computationally obtained binding modes of Cd^{2+} and Ca^{2+} with **SP-7**.

TABLE D-1: Overall zero point vibrational energy corrected reaction energies at 0 K (ΔE_0), and overall Gibbs free energies of reaction at 298 K (ΔG_{298}) for the reactions of metal perchlorates with **SP-6** and **SP-7** to form the fluorescent end products and perchloric acid, at the BP86/LANL2DZ level of theory. Energies are given in kJ/mol.

Reaction	ΔE_0	ΔG_{298}
(1) $Cd(ClO_4)_2$ + 2[**SP-6**(SP)] → Cd[**SP-6**(MC)]$_2$ + $2HClO_4$	-107.5	-94.3
(2) $Cd(ClO_4)_2$ + 2[**SP-7**(SP)] → Cd[**SP-7**(MC)]$_2$ + $2HClO_4$	+52.2	+45.3
(3) $Ca(ClO_4)_2$ + 2[**SP-6**(SP)] → Ca[**SP-6**(MC)]$_2$ + $2HClO_4$	-244.8	-230.6
(4) $Ca(ClO_4)_2$ + 2[**SP-7**(SP)] → Ca[**SP-7**(MC)]$_2$ + $2HClO_4$	-49.5	-43.3

Finally, it has been reported that, while low concentrations of Cd^{2+} (below 100 ρM) significantly stimulate cell proliferation and DNA synthesis, Cd^{2+} exposure at concentrations above 1 mM inhibits DNA synthesis and cell division. Therefore, it is important to have a sensing system that is capable of detecting such low concentrations of Cd^{2+} in biological samples. In the final part of the study, **SP-6** was combined with a microstructured optical fibre (MOF) as a first step toward realizing a selective, nanoscale and regenerable dip-sensor for Ca^{2+} and Cd^{2+} that is able to yield significant signal-to-background changes with minimal sample volumes, a real advance in biological sensing that enables measurement on sub-cellular-scale samples. MOFs also provide a platform for sensing Ca^{2+} and Cd^{2+} in confined spaces such as the medium surrounding cell clusters.[41] MOFs provide the sensing platform of choice in this work since the constituent air holes within their cross-section can be used to control the interactions between light guided within the fibre core and matter located within the holes in the fibre cross-section. These voids simultaneously act as the micro sample chambers necessary for nanoscale sample collection.[41]

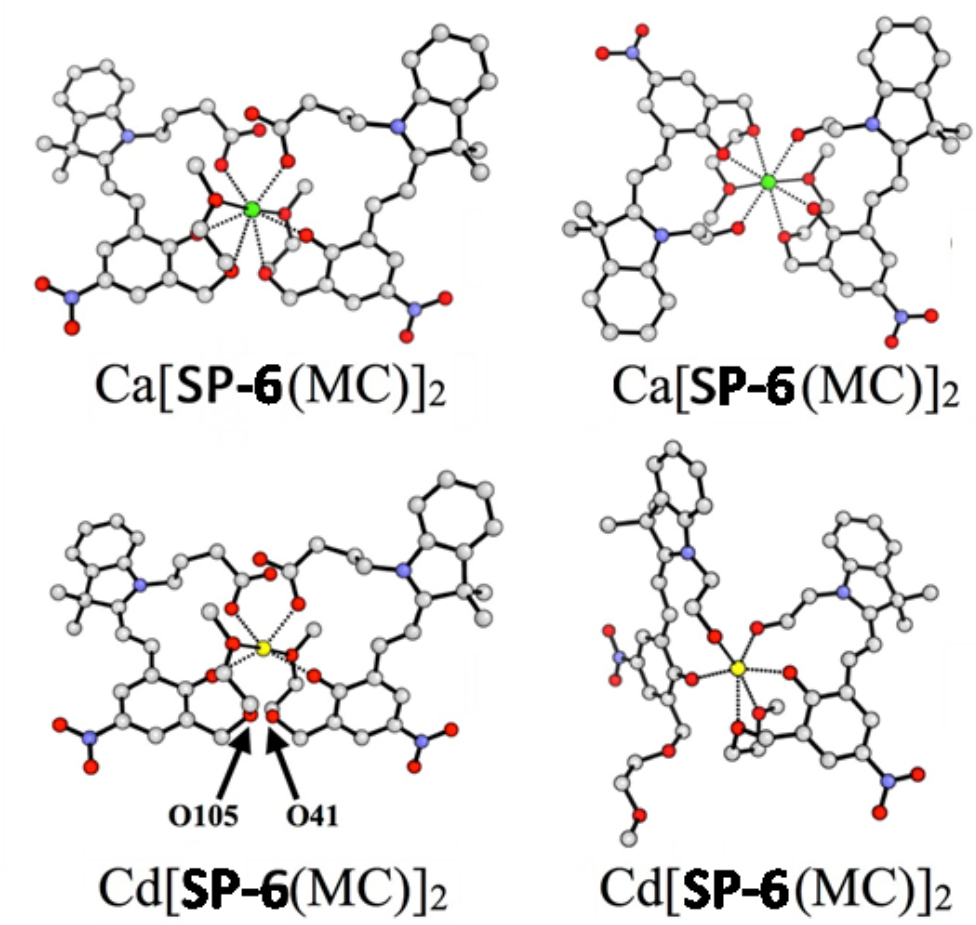

FIGURE D-3: BP86/LANL2DZ optimized structures of **SP-6** and **SP-7** bound to Ca^{2+} (green) and Cd^{2+} (yellow) in a 2:1 ratio. Hydrogens are omitted for clarity.

One end of a 20 cm length of fibre MOF fibre was dipped into pre-mixed solutions containing 100 ρM of Cd^{2+} and 5 μM of **SP-6**. The solution is drawn into the air holes of the fibre by capillary action. The fibres were filled with 150 - 180 nL of the solution respectively. Detailed information on the fibre and optical set up employed can be found in the supporting information section. The fibre core was then exposed to light from a 532 nm laser and the fluorescence generated within the sample chambers was collected by the fibre core. The same experiments was repeated with 100 ρM of Ca^{2+}. The resulting fluorescence spectra was obtained by capturing the fluorescence travelling in the backwards direction and from this a significant increase in fluorescence intensity in the presence of 100 ρM Cd^{2+} and Ca^{2+} were observed respectively (Figure D-4) given that only 2 % of the **SP-6** are bound to any ions.

On/off binding experiments were also carried out to examine the reversibility of this new sensor system. The results in Figure D-4 show that the binding of Cd^{2+} can be turned off/on and off again by exposing the system to white light for 5 min, followed by exposure to UV for 5 min and white light again for 5 min. On-going work is concerned with the surface attachment **SP-6** onto MOFs to yield a sensing platform for Ca^{2+} and Cd^{2+} that is reusable and/or capable of continuous or repeated measurements, one where the binding of ions can be turned off and expelled from the sensor through washing.[42] Such a sensor will have the advantages of making multiple measurements on a single sample or in a single sampling volume without the need to change the sensor, thereby potentially extending the sensor's useful lifetime. And as spiropyrans are known to have limited aqueous solubility, attachment onto surfaces such as MOFs or liposomes[31] will also eliminate the need to dissolve the compounds in an organic solvent, hence allowing sensing to be carried out in cellular environments.

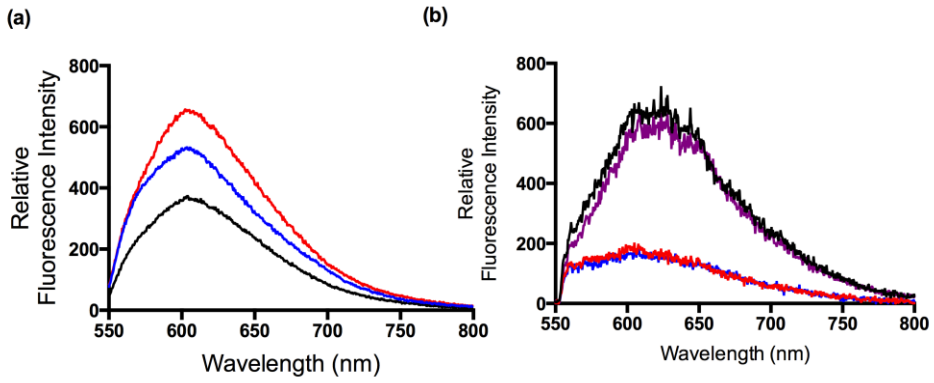

FIGURE D-4: (a) Fluorescence results of the optical fibre-based nanoscale dip-sensor. black) 5 μM **SP-6**, no ions; red) 100 ρM of Ca^{2+} premixed with 5 μM of **SP-6**; blue) 100 ρM of Cd^{2+} premixed with 5 μM of **SP-6**. Experiments were carried out in acetonitrile with excitation wavelength of 532 nm. The signal-to-noise ratio between the free and complexed-form were calculated to be 1:1.7 for Cd^{2+} and 1:1.8 for Ca^{2+}. Information on fibre, optical set-up and results from a duplicate run can be found in the Supporting Information Section. (b) Photoswitching experiments within a single MOF (λ_{ex} = 532 nm). black) First "On Cycle"; red) First "Off Cycle"; purple) Second "On Cycle"; blue) Second "Off Cycle". Experiments were performed with the same sample of 10 mM of **SP-6** premixed with 1 μM of Cd^{2+} in 30 cm of MOF.

D.1.4 CONCLUSION

In summary, we have designed a selective, dual sensor for Ca^{2+} and Cd^{2+} capable of detection at 100 ρM concentrations. Molecular modelling was used to provide insights on the binding modes between the respective ions and **SP-6** and **SP-7**. A first step toward a nanolitre-scale dip sensor for the dual sensing of Ca^{2+} and Cd^{2+}, was demonstrated using a microstructured optical fibre as the sensing platform which is important for sensing in confined spaces such as the medium surrounding cell clusters. In addition, this system displays picomolar sensitivity for these ions, with an added ability to reproducibly turn ion-binding on/off.

D.1.5 MATERIALS AND METHODS

D.1.5.1 Materials.

All ^{13}C NMR spectra (150 MHz) and ^{1}H NMR spectra (300 MHz) were recorded on a Varian Gemini 2000 spectrometer in $CDCl_3$ or DMSO-d_6. Chemical shifts (δ) are reported in ppm. Chemical shifts of $CDCl_3$ (δ_c = 77.1 ppm), DMSO-d_6 (δ_c = 39.52 ppm) or TMS (δ_H = 0.0 ppm) were used as internal standards in all ^{13}C NMR and ^{1}H NMR experiments respectively. High resolution mass spectrometry was performed on the microTOF-Q 10171. HPLC grade Acetonitrile was used in all related experiments. Anhydrous THF was distilled in the presence of benzophenone and sodium. All metal ions used in this work were in the form of perchlorate salt. All other reagents were purchased from Sigma-Aldrich and used without further purification.

D.1.5.2 Synthesis

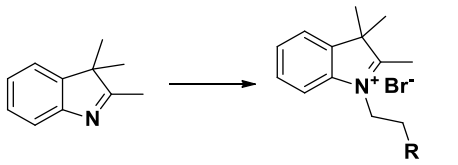

21

R = OH, **22a**
R = CH_2OEt, **22b**

1-(2-Hydroxyethyl)-2,3,3-trimethyl-3*H*-indolium (22a)

2,3,3-Trimethylindolenine (**21**, 500 mg, 3.14 mmol) and 2-Bromoethanol (334 µL, 4.7 mmol) were dissolved in anhydrous acetonitrile (15 mL) and set to reflux for 18 h. The reaction mixture was cooled to rt and excess solvent was removed under vacuo. Hexane (20 mL) was added to the oily residue and the mixture was placed in the sonicator for 10 min. The hexane layer was then discarded and the product was precipitated from the residue using CH_2Cl_2 to yield 1-(2-Hydroxyethyl)-2,3,3-trimethyl-3*H*-indolium (**5a**, 623 mg, 70 %) as a pink solid. ^{1}H NMR (DMSO-d_6, 300 MHz) δ 7.99 – 7.96 (m, 1H), 7.87 – 7.84 (m, 1H), 7.61 (dd, J = 5.7, 3.0 Hz, 2H), 4.61 (t, J = 5.0, 2H), 3.88 (t, J = 5.1, 2H), 2.83 (s, 3H), 1.55 (s, 6H); ^{13}C NMR (150 MHz) δ 198.5, 142.6, 142.0, 130.0, 129.6, 124.3, 116.5, 58.5, 55.1, 51.2, 22.8 (2C), 15.5. MS (m/z) for $C_{13}H_{18}NO^+$ ($[M]^+$) calcd 204.3; found 204.4.

1-(4-Ethoxy-4-oxobutyl)-2,3,3-trimethyl-3*H*-indolium (22b)

2,3,3-Trimethylindolenine (**21**, 500 mg, 3.14 mmol) and Ethyl 4-bromobutyrate (1.35 mL, 9.42 mmol) were dissolved in anhydrous acetonitrile (15 mL) and set to reflux for 48 h. The reaction mixture was cooled to rt and excess solvent was removed under vacuo. Product was precipitated from the viscous residue using 1:20 methanol:diethyl ether solution to yield 1-(4-Ethoxy-4-oxobutyl)-2,3,3-trimethyl-3*H*-indolium (**5b**, 615 mg, 60 %) as a pink solid. ^{1}H NMR ($CDCl_3$, 300 MHz) δ 7.99 (d, J = 7.2 Hz, 1H), 7.61 – 7.54 (m, 3H), 4.91 (t, J = 8.1, 2H), 4.11 (q, J = 7.2 Hz, 2H), 3.20 (s, 3H), 2.73 (t, J = 6.5 Hz, 2H), 2.28 – 2.23 (m, 2H), 1.65 (s, 6H), 1.24 (t, J =7.2 Hz, 3H); ^{13}C NMR (150 MHz) δ 196.9, 173.8, 141.9, 141,2, 129.4, 128.9 (2C), 123.6, 115.4, 54.2, 47.1, 40.4, 30.4, 22.5, 22.0 (2C), 14.2. MS (m/z) for $C_{17}H_{24}NO^+$ ($[M]^+$) calcd 274.2; found 274.2.

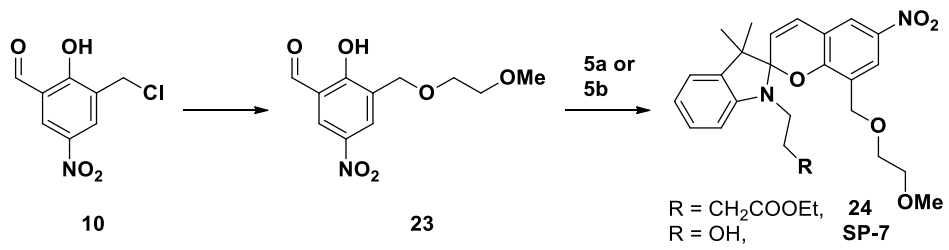

2-Hydroxy-3-((2-methoxyethoxy)methyl)-5-nitrobenzaldehyde (23)

Sodium hydride (60 % suspension in oil, 98 mg, approx. 2.4 mmol) was suspended in anhydrous THF (10 mL) and stirred at 0 °C. 2-Methoxyethanol (2.32 mmol, 183 µL) was added drop-wise to the above suspension. The reaction mixture was allowed to stir at 0 °C until the evolution of H_2 (g) stopped. A solution of **10**[42] in anhydrous THF (5 mL) was added drop wise to the reaction mixture. The reaction was set to heat at 50 °C for 2 h before quenching with water. The mixture was washed with CH_2Cl_2 and the CH_2Cl_2 layer was discarded. 1 M HCl was added to the aqueous layer until pH = 6. The aqueous layer was then extracted with ethyl acetate (3x) and the organic layer was combined, dried with sodium sulfate and excess solvent was removed under vacuum to yield 2-Hydroxy-3-((2-methoxyethoxy)methyl)-5-nitrobenzaldehyde (**23**, crude weight 560 mg) as a brown, viscous liquid, which was used in the next step without further purification. ^{1}H NMR ($CDCl_3$, 300 MHz) δ 10.01 (s, 1H), 8.61 (s, 1H), 8.49 (s, 1H), 4.70 (s, 2H), 3.80 – 3.76 (m, 2H), 3.67 – 3.64 (m, 2H), 3.43 (s, 3H).

2-(8-((2-Methoxyethoxy)methyl)-3',3'-dimethyl-6-nitrospiro[chromene-2,2'-indoline]-1'-yl)ethanol (SP-7)

Compounds **22a** (100 mg, 0.31 mmol) and **23** (79 mg, 0.31 mmol) were dissolved in anhydrous ethanol (10 mL) and set to reflux for 18 h. Excess solvent was removed under vacuum and the crude mixture was purified using normal phase silica gel (5 % CH_2Cl_2 in methanol) to yield 2-(8-((2-Methoxyethoxy)methyl)-3',3'-dimethyl-6-nitrospiro[chromene-2,2'-indoline]-1'-yl)ethanol (**SP-7**, 55 mg, 40 %) as a red solid. ^{1}H NMR ($CDCl_3$, 300 MHz) δ 8.14 (d, J = 3.0 Hz, 1H), 7.92 (d, J = 3.0 Hz, 1H), 7.16 (t, J = 6.8 Hz, 1H), 7.07 (d, J = 6.6 Hz, 1H), 6.88 (t, J = 5.9 Hz, 2H), 6.61 (d, J = 7.8 Hz, 1H), 5.86 (d, J = 10.5 Hz, 1H), 4.40 – 4.21 (m, 2H), 3.74 – 3.71 (m, 4H), 3.45 – 3.44 (m, 4H), 3.31 (s, 3H), 1.29 (s, 3H), 1.28 (s, 3H). ^{13}C NMR (150 MHz) δ 156.6, 146.8, 140.7, 135.7, 128.5, 128.4, 127.7, 125.6, 125.4, 122.2, 121.8, 121.6,

119.8, 118.3, 106.9, 71.8, 67.2, 66.6, 60.7, 59.0, 52.7, 46.0, 20.0 (2C). HRMS (m/z) for $C_{24}H_{28}N_2O_6$ + H ($[M+H]^+$) calcd 411.2020; found 411.2013

Ethyl 4-(8-((2-methoxyethoxy)methyl)-3',3'-dimethyl-6-nitrospiro[chromene-2,2'-indoline]-1'-yl)butanoate (24)

Compounds **22b** (100 mg, 0.35 mmol) and **23** (79 mg, 0.31 mmol) were dissolved in anhydrous ethanol and set to reflux for 18 h. Excess solvent was removed under vacuum and the crude mixture was purified using normal phase silica gel (5 % CH_2Cl_2 in methanol) to yield Ethyl 4-(8-((2-methoxyethoxy)methyl)-3',3'-dimethyl-6-nitrospiro[chromene-2,2'-indoline]-1'-yl)butanoate (**24**, 100 mg, 56 %) as a red solid. ^{1}H NMR ($CDCl_3$, 300 MHz) δ 8.17 (d, J = 1.5 Hz, 1H), 7.92 (d, J = 1.5 Hz, 1H), 7.16 (t, J = 3.0 Hz, 1H), 7.06 (d, J = 3.0 Hz, 1H), 6.89 (d, J = 6.0 Hz, 1H), 6.86 (t, J = 3.0 Hz, 1H), 6.62 (d, J = 3.0 Hz, 1H), 5.85 (d, J = 3.0 Hz, 1H), 4.28 (q, J = 6.0 Hz, 2H), 4.10 – 4.06 (m, 2H), 3.45- 3.42 (m, 4H), 3.33 (s, 3H), 3.19 – 3.09 (m, 2H), 2.35 – 2.28 (m, 2H), 2.0 – 1.94 (m, 1H), 1.90 – 1.85 (m, 1H), 1.25 (s, 3H), 1.21 (t, J = 3.0 Hz, 3H), 1.18 (s, 3H); ^{13}C NMR (150 MHz) δ 173.0, 156.6, 146.9, 140.7, 135.9, 128.4, 127.7, 126.0, 124.8, 121.8, 121.6, 121.4, 119.6, 118.0, 106.9, 106.8, 71.8, 70.2, 66.7, 60.4, 59.1, 52.4, 43.0, 31.7, 25.9, 24.0, 19.9, 14.2. HRMS (m/z) for $C_{28}H_{34}N_2O_7$ + H ($[M+H]^+$) calcd 511.2439; found 511.2428

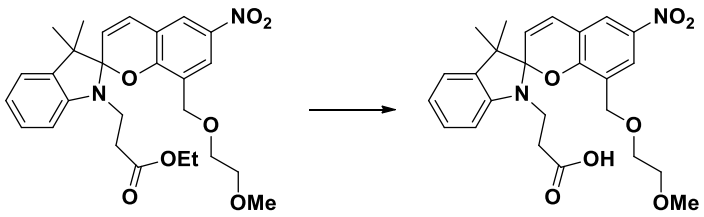

24 SP-6

4-(8-((2-Methoxyethoxy)methyl)-3',3'-dimethyl-6-nitrospiro[chromene-2,2'-indoline]-1'-yl)butanoic acid (SP-6)

Compound **24** (80 mg, 0.16 mmol) was dissolved in a solution of 2:1 methanol: 2M NaOH and the reaction mixture was set to heat at 50 °C for 18 h. Excess solvent was removed under vacuum and the crude reaction mixture was purified using C-18 reverse phase silica gel (5 % acetonitrile in water) to yield 4-(8-((2-Methoxyethoxy)methyl)-3',3'-dimethyl-6-nitrospiro[chromene-2,2'-indoline]-1'-yl)butanoic acid (**SP-6**, 40 mg, 54 %) as a red solid. ^{1}H NMR ($CDCl_3$, 300 MHz) δ

8.16 (dd, J = 9.3, 2.7 Hz, 1H), 7.92 (d, J = 2.7 Hz, 1H), 7.20 (t, J = 9.0 Hz, 1H), 7.08 (d, J = 6.0 Hz, 1H), 6.92 – 6.84 (m, 2H), 6.61 (d, J = 9.0 Hz, 1H), 5.87 (d, J = 9.0 Hz, 1H), 4.30 (s, 1H), 4.22 (s, 1H), 3.46 (s, 2H), 3.35 (dd, J = 15, 9 Hz, 2H), 3.34 (s, 3H), 3.24 – 3.15 (m, 2H), 2.40 (t, J = 7 Hz, 2H), 1.95 (m, 2H), 1.27 (s, 3H), 1.19 (s, 3H); ^{13}C NMR (150 MHz) δ 181.8, 156.3, 146.8, 136.0, 128.4, 127.7, 125.9, 124.9, 122.5, 121.8, 119.6, 118.0, 108.3, 106.8, 71.8, 70.3, 66.6, 59.0, 52.3, 44.2, 42.9, 38.8, 25.9, 24.4, 22.6, 20.0. MS (m/z) for $C_{26}H_{30}N_2O_7$ + H ($[M+H]^+$) calcd 483.2119; found 483.2119.

D.1.6 SUPPORTING INFORMATION

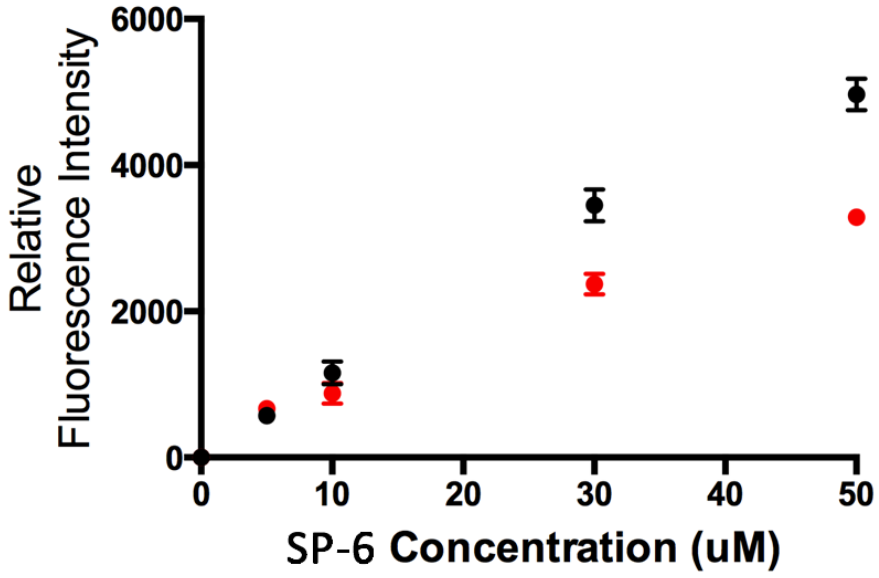

FIGURE D-5: Fluorescence measurements of increasing concentrations of **SP-6** with 100 μM of Ca^{2+} (black) and Cd^{2+} (red) respectively. The metal ions were in the perchlorate form. **SP-6** and the metal ions were dissolved HPLC grade acetonitrile respectively. The experiments were carried out in duplicates, at 25 °C, neutral pH and were preformed using 96-well plate reader. **SP-6** and the metal ions were dissolved in HPLC-grade acetonitrile. The excitation wavelength for these experiments were 532 nm.

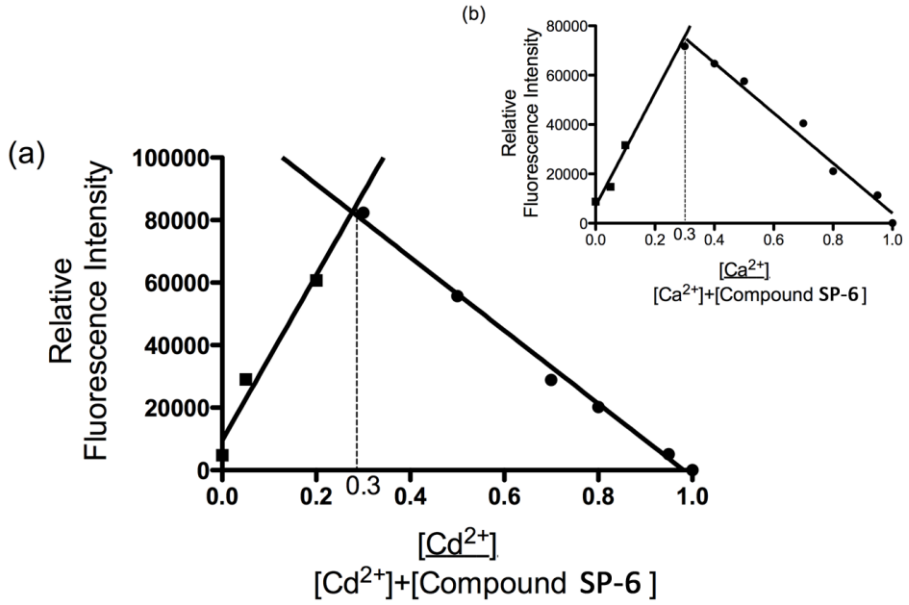

FIGURE D-6: Job's plot analysis for coloration of **SP-6** with (a) Cd^{2+} and (b) Ca^{2+} where ($[M^{2+}]$ + [**SP-6**] = 100 μM). The measurements were carried out in acetonitrile mixture after UV irradiation (λ = 320 nm) for 10 min.

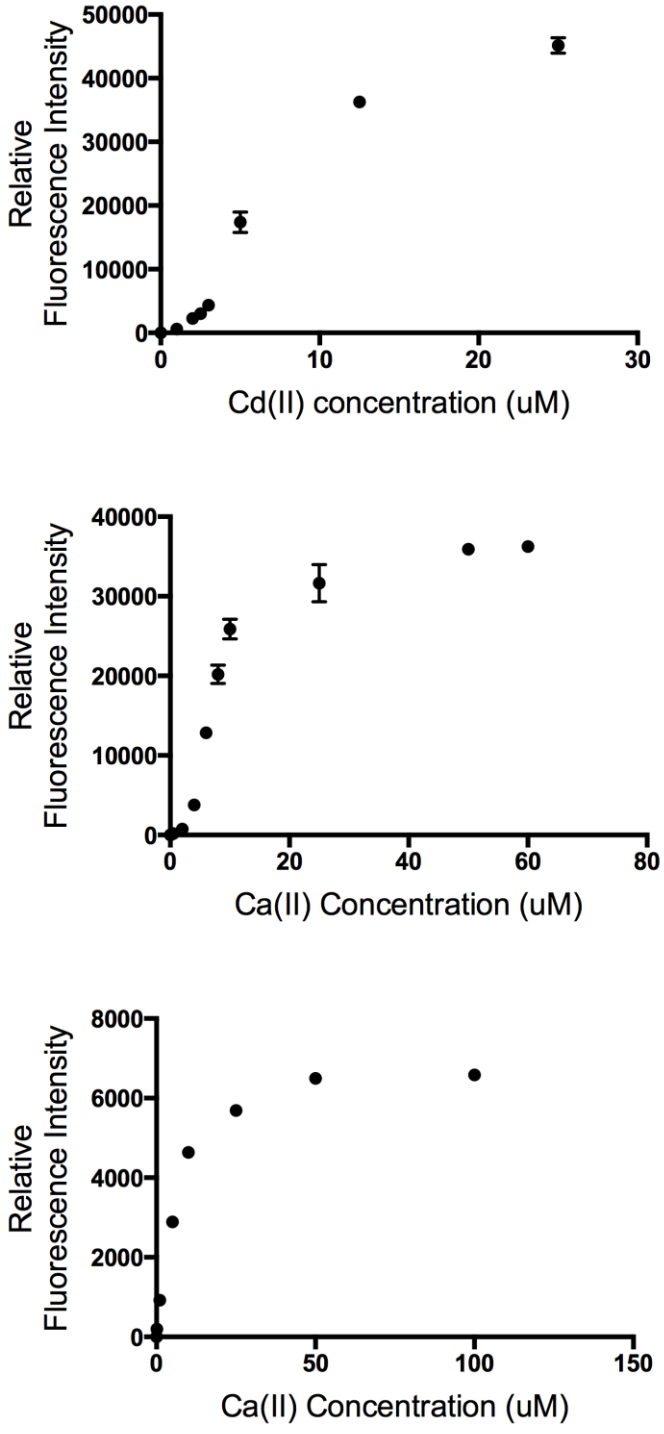

FIGURE D-7: Fluorescence measurements of **SP-6** (5 μM) with increasing concentrations of (a) Cd^{2+}, (b) Ca^{2+} and (c) **SP-7** (55 μM) with Ca^{2+} respectively. The metal ions were in the perchlorate form. **SP-6**, **SP-7** and the metal ions were dissolved HPLC grade acetonitrile respectively. The experiments were carried out at 25 °C, neutral pH and were preformed using 96-well plates with the excitation wavelength = 523 nm. Each experiment was performed in triplicates and the values in the graphs shown here were obtained by subtracting the value of zero and taking the average these runs.

Microstructured optical fibre (MOF) experiments.

The wagon wheel MOFs used in this work was fabricated in-house using high purity F300 silica glass.

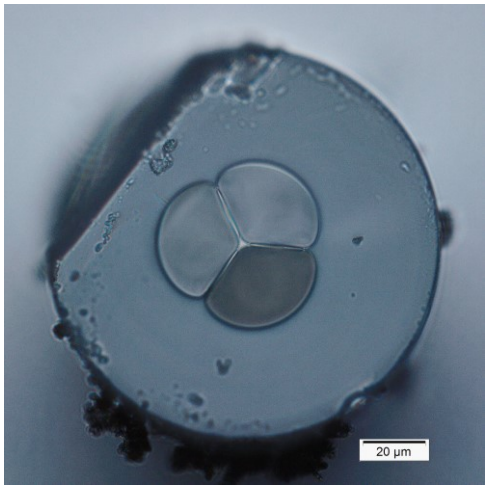

FIGURE D-8: Cross section microstructured optical fibre taken with OLYMPUS BX51 light microscope, MPlanFLN-BD 50x/0.80 objective lens and fitted with OLYMPUS SC100 camera. Each hole has a diameter of 27.7 µm and an effective area of 600 µm^2. This equates to a maximum fill volume of approximately 180 nl/10 cm of fibre.

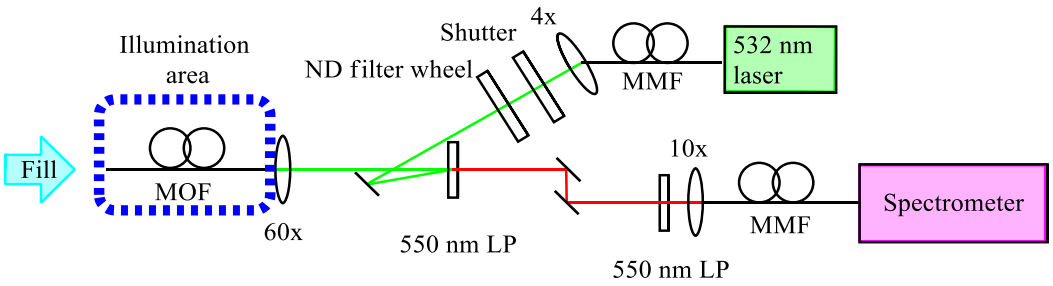

FIGURE D-9: The optics fluorescence setup. The MOF core was irradiated at 532 nm from a 25 mW fibre coupled laser (CrystaLaser). Optical power at filling end after fibre coupling recorded by a powermeter (Thorlabs) for calibration purposes. The 20 cm horizontal MOF was filled with sample solution by capillary action for 1 min (flow rate approx.14 cm/min). Solution volume is 180 nL/10cm. The sample was exposed to 8 ms 532 nm pulses of 0.017 mW and the back fluorescence was recorded with a Horiba iHR550 spectrometer with Synapse CCD detector (100 g/mm grating, 0.5 mm entrance slit width). Photoswitching was performed by externally irradiating the filled MOF with 365 nm light (filtered, 8W mercurylamp (UVP)) for 5 min.

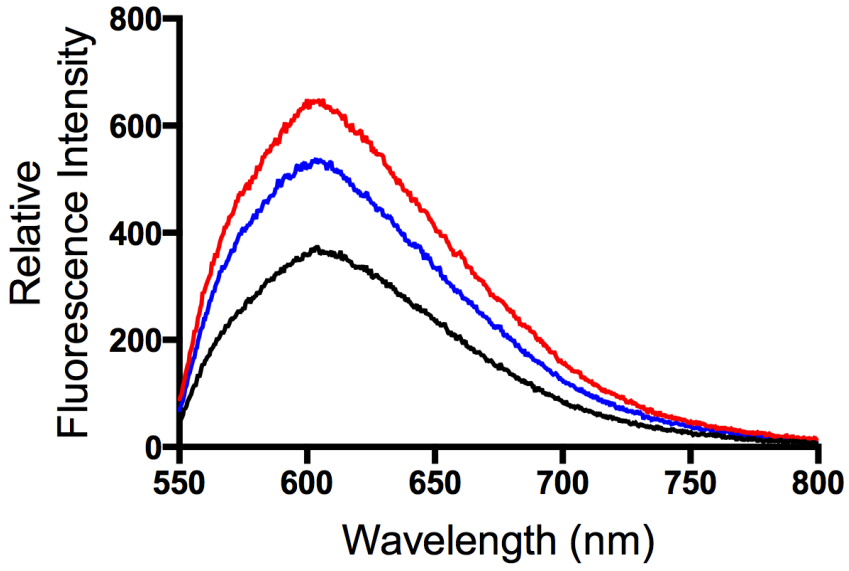

FIGURE D-10: Fluorescence results of the optical fibre-based nanoscale dip-sensor. Duplicate Run. (black) 5 μM **SP-6**, no ions (red) 100 ρM of Ca^{2+} premixed with 5 μM of **SP-6**, (blue) 100 ρM of Cd^{2+} premixed with 5 μM of **SP-6**. Experiments were carried out in acetonitrile with excitation wavelength = 532 nm.

D.1.7 REFERENCES

1. Heng, S.; Mak, A. M.; Stubing, D. B.; Monro, T. M.; Abell, A. D. Dual Sensor for Cd(II) and Ca(II): Selective Nanoliter-Scale Sensing of Metal Ions. *Analytical Chemistry* 2014, *86* (7), 3268-3272.
2. Wier, P. J.; Miller, R. K.; Maulik, D.; Disantagnese, P. A. Toxicity of cadmum in the perfused human placenta. *Toxicology and Applied Pharmacology* 1990, *105* (1), 156-171.
3. Godt, J.; Scheidig, F.; Grosse-Siestrup, C.; Esche, V.; Brandenburg, P.; Reich, A.; Groneberg, D. A. The toxicity of cadmium and resulting hazards for human health. *Journal of Occupational Medicine and Toxicology (London, England)* 2006, *1*, 22-22.
4. Yang, Y.; Li, F.; Bi, X.; Sun, L.; Liu, T.; Jin, Z.; Liu, C. Lead, Zinc, and Cadmium in Vegetable/Crops in a Zinc Smelting Region and its Potential Human Toxicity. *Bulletin of Environmental Contamination and Toxicology* 2011, *87* (5), 586-590.
5. Youness, E. R.; Mohammed, N. A.; Morsy, F. A. Cadmium impact and osteoporosis: mechanism of action. *Toxicology Mechanisms and Methods* 2012, *22* (7), 560-567.
6. Brzoska, M. M.; Moniuszko-Jakoniuk, J. Low-level exposure to cadmium during the lifetime increases the risk of osteoporosis and fractures of the

lumbar spine in the elderly: Studies on a rat model of human environmental exposure. *Toxicological Sciences* 2004, *82* (2), 468-477.

7. Asara, Y.; Marchal, J. A.; Carrasco, E.; Boulaiz, H.; Solinas, G.; Bandiera, P.; Garcia, M. A.; Farace, C.; Montella, A.; Madeddu, R. Cadmium Modifies the Cell Cycle and Apoptotic Profiles of Human Breast Cancer Cells Treated with 5-Fluorouracil. *International Journal of Molecular Sciences* 2013, *14* (8), 16600-16616.
8. Adams, S. V.; Passarelli, M. N.; Newcomb, P. A. Cadmium exposure and cancer mortality in the Third National Health and Nutrition Examination Survey cohort. *Occupational and Environmental Medicine* 2012, *69* (2), 153-156.
9. Beveridge, R.; Pintos, J.; Parent, M.-E.; Asselin, J.; Siemiatycki, J. Lung Cancer Risk Associated With Occupational Exposure to Nickel, Chromium VI, and Cadmium in Two Population-Based Case-Control Studies in Montreal. *American Journal of Industrial Medicine* 2010, *53* (5), 476-485.
10. Okuda, B.; Iwamoto, Y.; Tachibana, H.; Sugita, M. Parkinsonism after acute cadmium poisoning. *Clinical Neurology and Neurosurgery* 1997, *99* (4), 263-265.
11. Basun, H.; Lind, B.; Nordberg, M.; Nordstrom, M.; Bjorksten, K. S.; Winblad, B. Cadmium in blood in Alzheimer's disease and non-demented subjects: results from a population-based study. *Biometals : An international journal on the role of metal ions in biology, biochemistry, and medicine* 1994, *7* (2), 130-4.
12. Panayi, A. E.; Spyrou, N. M.; Iversen, B. S.; White, M. A.; Part, P. Determination of cadmium and zinc in Alzheimer's brain tissue using inductively coupled plasma mass spectrometry. *Journal of the Neurological Sciences* 2002, *195* (1), 1-10.
13. Bar-Sela, S.; Reingold, S.; Richter, E. D. Amyotrophic lateral sclerosis in a battery-factory worker exposed to cadmium. *International Journal of Occupational and Environmental Health* 2001, *7* (2), 109-12.
14. Vinceti, M.; Guidetti, D.; Bergomi, M.; Caselgrandi, E.; Vivoli, R.; Olmi, M.; Rinaldi, L.; Rovesti, S.; Solime, F. Lead, cadmium, and selenium in the blood of patients with sporadic amyotrophic lateral sclerosis. *Italian Journal of Neurological Sciences* 1997, *18* (2), 87-92.
15. Montell, C. The latest waves in calcium signaling. *Cell* 2005, *122* (2), 157-63.
16. Clapham, D. E. Calcium Signalling. *Cell* 1995, *80* (2), 259-268.
17. Bonner, F. W.; King, L. J.; Parke, D. V. The acute and sub-acute effects of cadmium on calcium homeostasis and bone trace-metals in the rat. *Journal of Inorganic Biochemistry* 1981, *14* (2), 107-114.
18. Nawrot, T.; Geusens, P.; Nulens, T. S.; Nemery, B. Occupational Cadmium Exposure and Calcium Excretion, Bone Density, and Osteoporosis in Men. *Journal of Bone and Mineral Research* 2010, *25* (6), 1441-1445.
19. Kazantzis, G. Cadmium, osteoporosis and calcium metabolism. *Biometals* 2004, *17* (5), 493-498.
20. Long, G. J. Cadmium perturbs calcium homeostasis in rat osteosarcoma (ROS 17/2.8) cells; A possible role for protein kinase C. *Toxicology Letters* 1997, *91* (2), 91-97.
21. Xu, B.; Chen, S.; Luo, Y.; Chen, Z.; Liu, L.; Zhou, H.; Chen, W.; Shen, T.; Han, X.; Chen, L.; Huang, S. Calcium Signaling Is Involved in Cadmium-

Induced Neuronal Apoptosis via Induction of Reactive Oxygen Species and Activation of MAPK/mTOR Network. *Plos One* 2011, *6* (4).
22. Zhou, X.; Li, P.; Shi, Z.; Tang, X.; Chen, C.; Liu, W. A Highly Selective Fluorescent Sensor for Distinguishing Cadmium from Zinc Ions Based on a Quinoline Platform. *Inorganic Chemistry* 2012, *51* (17), 9226-9231.
23. Goswami, P.; Das, D. K. A New Highly Sensitive and Selective Fluorescent Cadmium Sensor. *Journal of Fluorescence* 2012, *22* (1), 391-395.
24. Zhao, Q.; Li, R.-F.; Xing, S.-K.; Liu, X.-M.; Hu, T.-L.; Bu, X.-H. A Highly Selective On/Off Fluorescence Sensor for Cadmium(II). *Inorganic Chemistry* 2011, *50* (20), 10041-10046.
25. Xue, L.; Liu, C.; Jiang, H. Highly Sensitive and Selective Fluorescent Sensor for Distinguishing Cadmium from Zinc Ions in Aqueous Media. *Organic Letters* 2009, *11* (7), 1655-1658.
26. Cheng, T.; Xu, Y.; Zhang, S.; Zhu, W.; Qian, X.; Duan, L. A Highly Sensitive and Selective OFF-ON Fluorescent Sensor for Cadmium in Aqueous Solution and Living Cell. *Journal of the American Chemical Society* 2008, *130* (48), 16160-1.
27. Lu, C.; Xu, Z.; Cui, J.; Zhang, R.; Qian, X. Ratiometric and highly selective fluorescent sensor for cadmium under physiological pH range: A new strategy to discriminate cadmium from zinc. *Journal of Organic Chemistry* 2007, *72* (9), 3554-3557.
28. Verkhratsky, A.; Petersen, O. H. *Calcium Measurement Methods*. Humana Press: New York, 2010; Vol. 43.
29. Natali, M.; Aakeroy, C.; Desper, J.; Giordani, S. The role of metal ions and counterions in the switching behavior of a carboxylic acid functionalized spiropyran. *Dalton Transactions* 2010, *39* (35), 8269-8277.
30. Cardenas, G.; Ponce, A. Cadmium colloids from non-aqueous solvents. *Colloid and Polymer Science* 1996, *274* (8), 788-794.
31. Heng, S.; McDevitt, C. A.; Stubing, D. B.; Whittall, J. J.; Thompson, J. G.; Engler, T. K.; Abell, A. D.; Monro, T. M. Microstructured optical fibers and live cells: a water-soluble, photochromic zinc sensor. *Biomacromolecules* 2013, *14* (10), 3376-9.
32. Heng, S.; Nguyen, M.-C.; Kostecki, R.; Monro, T. M.; Abell, A. D. Nanoliter-scale, regenerable ion sensor: sensing with a surface functionalized microstructured optical fibre. *RSC Advances* 2013, *3* (22), 8308-8317.
33. Liu, X.; Zhang, N.; Zhou, J.; Chang, T.; Fang, C.; Shangguan, D. A turn-on fluorescent sensor for zinc and cadmium ions based on perylene tetracarboxylic diimide. *Analyst* 2013, *138* (3), 901-906.
34. Song, E. J.; Kang, J.; You, G. R.; Park, G. J.; Kim, Y.; Kim, S. J.; Kim, C.; Harrison, R. G. A single molecule that acts as a fluorescence sensor for zinc and cadmium and a colorimetric sensor for cobalt. *Dalton Transactions* 2013, *42* (43), 15514-20.
35. Fries, K. H.; Driskell, J. D.; Sheppard, G. R.; Locklin, J. Fabrication of Spiropyran-Containing Thin Film Sensors Used for the Simultaneous Identification of Multiple Metal Ions. *Langmuir* 2011, *27* (19), 12253-12260.
36. Shimoda, R.; Nagamine, T.; Takagi, H.; Mori, M.; Waalkes, M. P. Induction of apoptosis in cells by cadmium: Quantitative negative correlation between

basal or induced metallothionein concentration and apoptotic rate. *Toxicological Sciences* 2001, *64* (2), 208-215.

37. Shiraishi, Y.; Matsunaga, Y.; Hirai, T. Selective colorimetric sensing of Co(II) in aqueous media with a spiropyran-amide-dipicolylamine linkage under UV irradiation. *Chemical Communications* 2012, *48* (44), 5485-5487.
38. Shao, Y.; Molnar, L. F.; Jung, Y.; Kussmann, J.; Ochsenfeld, C.; Brown, S. T.; Gilbert, A. T.; Slipchenko, L. V.; Levchenko, S. V.; O'Neill, D. P.; DiStasio, R. A., Jr.; Lochan, R. C.; Wang, T.; Beran, G. J.; Besley, N. A.; Herbert, J. M.; Lin, C. Y.; Van Voorhis, T.; Chien, S. H.; Sodt, A.; Steele, R. P.; Rassolov, V. A.; Maslen, P. E.; Korambath, P. P.; Adamson, R. D.; Austin, B.; Baker, J.; Byrd, E. F.; Dachsel, H.; Doerksen, R. J.; Dreuw, A.; Dunietz, B. D.; Dutoi, A. D.; Furlani, T. R.; Gwaltney, S. R.; Heyden, A.; Hirata, S.; Hsu, C. P.; Kedziora, G.; Khalliulin, R. Z.; Klunzinger, P.; Lee, A. M.; Lee, M. S.; Liang, W.; Lotan, I.; Nair, N.; Peters, B.; Proynov, E. I.; Pieniazek, P. A.; Rhee, Y. M.; Ritchie, J.; Rosta, E.; Sherrill, C. D.; Simmonett, A. C.; Subotnik, J. E.; Woodcock, H. L., 3rd; Zhang, W.; Bell, A. T.; Chakraborty, A. K.; Chipman, D. M.; Keil, F. J.; Warshel, A.; Hehre, W. J.; Schaefer, H. F., 3rd; Kong, J.; Krylov, A. I.; Gill, P. M.; Head-Gordon, M. Advances in methods and algorithms in a modern quantum chemistry program package. *Physical Chemistry Chemical Physics : PCCP* 2006, *8* (27), 3172-91.
39. Becke, A. D. Density-functional exchange-energy approximation with correct asymptotic behavior. *Physical Review. A* 1988, *38* (6), 3098-3100.
40. Perdew, J. P. Density-functional approximation for the correlation energy of the inhomogeneous electron gas. *Physical Review. B, Condensed Matter* 1986, *33* (12), 8822-8824.
41. Monro, T. M.; Warren-Smith, S.; Schartner, E. P.; Francois, A.; Heng, S.; Ebendorff-Heidepriem, H.; Afshar, S. Sensing with suspended-core optical fibers. *Optical Fiber Technology* 2010, *16* (6), 343-356.
42. Heng, S.; Nguyen, M. C.; Kostecki, R.; Monro, T. M.; Abell, A. D. Nanoliter-scale, regenerable ion sensor: sensing with a surface functionalized microstructured optical fibre. *RSC Advances* 2013, *3* (22), 8308-8317.

D.2 PAPER 4: Microstructured Optical Fibres and Live Cells: A Water-Soluble, Photochromic Zinc Sensor

Statement of Authorship

Title of Paper	Microstructured Optical Fibres and Live Cells: A Water-Soluble, Photochromic Zinc Sensor
Publication Status	☑ Published ☐ Accepted for Publication ☐ Submitted for Publication ☐ Publication Style
Publication Details	Heng, S., C. A. McDevitt, D. B. Stubing, J. J. Whittall, J. G. Thompson, T. K. Engler, A. D. Abell and T. M. Monro (2013). "Microstructured Optical Fibres and Live Cells: A Water-Soluble, Photochromic Zinc Sensor." *Biomacromolecules*.

Principal Author

Name of Principal Author	Sabrina Heng		
Contribution to the Paper	Project conceptualisation. Design and Synthesis of spiropyran **SP1** fluoroionophore. Fluorescence assays of **SP1**. Project direction and writing of the manuscript		
Signature		Date	06.10.16

Co-Author Contributions

By signing the Statement of Authorship, each author certifies that:

i. the candidate's stated contribution to the publication is accurate;
ii. permission is granted for the candidate in include the publication in the thesis;
iii. the sum of all co-author contributions is equal to 100 % less the candidate's stated contribution.

Name of Co-Author (Candidate)	Daniel B. Stubing		
Contribution to the Paper	Microstructured optical fibre fluorescence measurements of **SP1** liposomes. Editing of manuscript		
Overall percentage (%)	15		
Signature		Date	08/09/2016

Name of Co-Author	Christopher A McDevitt		
Contribution to the Paper	Project design. Assembly and incorporation of SP1 into liposomes. Fluorescence measurements. Writing and editing of manuscript.		
Signature		Date	13/9/16

Name of Co-Author	J. J Whittall		
Contribution to the Paper	Assembly and incorporation of **SP1** into liposomes		
Signature		Date	12/9/16

Name of Co-Author	Jeremy G. Thompson		
Contribution to the Paper	Supplied HEK 293 cells and performed confocal microscopy experiments. Editing of manuscript.		
Signature		Date	9/9/16

Name of Co-Author	Timothy K. Engler		
Contribution to the Paper	Confocal microscopy experiments of HEK 293 cells		
Signature		Date	19/9/16

Name of Co-Author	Andrew D. Abell		
Contribution to the Paper	Project direction and significant editing of manuscript.		
Signature		Date	13/09/2016

Name of Co-Author	Tanya M. Monro		
Contribution to the Paper	Project direction and editing of manuscript.		
Signature		Date	20/9/2016

MICROSTRUCTURED OPTICAL FIBRES AND LIVE CELLS: A WATER-SOLUBLE, PHOTOCHROMIC ZINC SENSOR[1]

Sabrina Heng,[a] Christopher A. McDevitt,[a] Daniel B Stubing,[a] Jonathan J. Whittall,[b] Jeremy G. Thompson,[c] Timothy K Engler,[a] Andrew D. Abell,[a] Tanya M. Monro[a]

[a] Institute for Photonics and Advanced Sensing and School of Chemistry & Physics, The University of Adelaide, SA, Australia 5005.

[b] Research Centre for Infectious Diseases, School of Molecular and Biomedical Science, The University of Adelaide.

[c] The Robinson Institute, School of Pediatrics and Reproductive Health, The University of Adelaide.

D.2.1 ABSTRACT

A new biologically compatible Zn(II) sensor was fabricated by embedding Zn(II) sensing spiropyran within the surface of a liposome derived from *E.coli* lipids (**LSP1**). Solution-based experiments with increasing Zn(II) concentrations show improved aqueous solubility and sensitivity compared to the isolated spiropyran molecule (**SP1**). **LSP1** is capable of sensing Zn(II) efflux from apoptotic HEK 293 cells with preliminary data indicating that sensing is localized near the surface membrane of the cells. Finally, **LSP1** is suitable for development into a nanolitre scale, dip-sensor for Zn(II) using microstructured optical fibre as the sensing platform to detect Zn(II) in the range of 100 ρM with minimal photobleaching. Existing spiropyran based sensing molecules can thus be made biologically compatible, with an ability to operate with improved sensitivity using nanoscale liquid sample volumes. This work represents the first instance where photochromic spiropyran molecules and liposomes are combined to create a new and multifunctional sensing entity for Zn(II).

D.2.2 INTRODUCTION

Spiropyrans are amongst the most extensively studied class of photoswitchable molecules, with ability to reversibly switch from a non-fluorescent spiro form (e.g. as in **SP1)** to highly fluorescent ring opened form as depicted in Scheme D-2

(**MC1**).[2,3,4] These structures form the basis of a chemical sensor when coupled with a suitable ionophore (e.g., the bis(2-pyridylmethyl) amine of **SP1**) that is capable of complexing with a metal ion,[3] or another species such as an amino acid[5] and even a cyanide ion.[6] Switching is reversed on exposure to visible light or heat. Importantly, the two isomers have a high switching reliability and low fatigue, which maximizes the number of switching cycles.

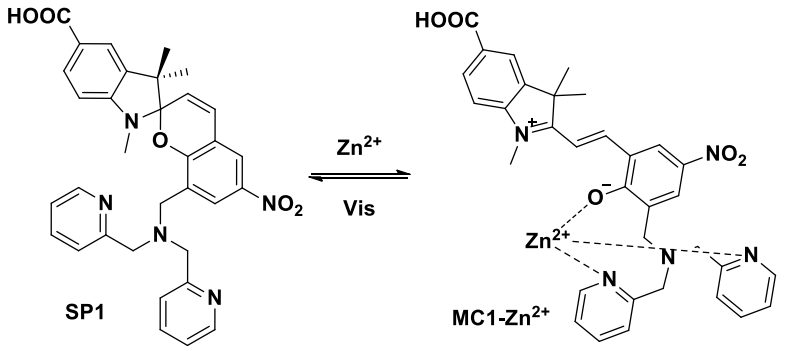

SCHEME D-2: Isomeric structures of spiropyran (**SP1**, closed, non-fluorescent), and the metal-induced ring opened **MC1-Zn^{2+}** complex (opened, fluorescent).

Spiropyrans offer advantages of reversibility of switching and low background fluorescence compared to non-photochromic molecules such as rhodamine.[7] However, they suffer from poor aqueous solubility,[8] a common problem among switchable molecules.[9] This prevents their widespread use in biological sensor-based applications.[10] Attempts to overcome this limitation using the sensor in co-solvents such as ethanol,[11, 1211] or to prepare water soluble derivatives[13] have failed to yield spiropyrans that are broadly applicable in biological environments.

Here we report a unique solution to this problem, where a spiropyran-based Zn(II) sensor (**SP1**) is integrated into the surface of liposome to provide an on/off Zn(II) sensor (spiropyran-liposome, **LSP1**) that is functional in an aqueous environment. This system is also able to detect Zn(II) effluxes from apoptotic cells. The new **LSP1** sensor platform can also be coupled with a microstructured optical fibre (MOF) to enable measurement within nanolitre sample volumes and allow the detection of low Zn(II) concentrations in biological samples. Zn(II) was chosen as the sensing target because it plays key roles in many important cellular activities

such as anti-oxidant enzyme activity (Cu, Zn superoxide dismutase), DNA structural integrity (Zn(II) fingers), oocytes maturation and fertilization.[14] At the same time, low nanomolar concentrations of free Zn(II) can be cytotoxic and the disruption of Zn(II) homeostasis has been implicated in various diseases including Alzheimer's,[15, 16] diabetes[17], cancer[18, 19] and heightening sensitivity to bacterial infections.[20] Despite the development of numerous highly selective probes for Zn(II), they generally lack the aqueous solubility required for biosensing applications.[21]

D.2.3 RESULTS AND DISCUSSION

The new spiropyran **SP1** was synthesized from 4-hydrazinobenzoic acid as detailed in supporting information.[22] The bis(2-pyridylmethyl)amine functionality was chosen as the ionophore in this work as it is known to form a complex with Zn(II) in aqueous solutions[11] (Scheme D-2). An aryl carboxylic acid was incorporated into the design to improve aqueous solubility. **LSP1** was then generated by dissolving **SP1** in DMSO (40 $mg.ml^{-1}$) and mixing it with a solution containing 0.04 mg of total *Escherichia coli* total lipids extracts in 20 mM 3-(N-morpholino)propanesulfonic acid (MOPS), pH 7.2. Unilamellar **SP1** liposomes were generated by re-suspending the lipid pellet in 20 mM MOPS, pH 7.2 and extruding the mixture through a 0.1 μm membrane to generate **LSP1**.

Solutions of **SP1** in 20 % acetonitrile in water and **LSP1** in MOPS buffer were then exposed to varying concentrations of Zn(II) in order to examine their affinities towards the ion (Figure D-11). We demonstrate that embedding **SP1** onto the surface of liposomes (as in **LSP1**) significantly improves solubility in MOPS buffer compared to the solubility of **SP1**, where 20 % acetonitrile is required as a co-solvent in order to achieve aqueous solubility.

Figure D-11 shows an increase in fluorescence for **LSP1** with increasing Zn(II) concentrations, due to **SP1** chelating to Zn(II). Spiropyrans are known to fluoresce only on ring-opening, as depicted in Scheme D-2. In addition, fluorescence was not observed for a control experiment using native liposomes without **SP1** embedded and Zn(II), demonstrating that the liposomes alone do not associate with Zn(II) ions in a way that can influence the fluorescence signal. The mean EC_{50} of **LSP1.Zn(II)** interactions from 4 independent reconstitutions was 23.8 ± 7 μM. This consistency

indicates that **SP1** can be reproducibly incorporated within the liposomes. With the liposome based sensor (**LSP1**), an increase in fluorescence was observed down to 1 μM of Zn(II) (signal to background ratio of 1.3:1).

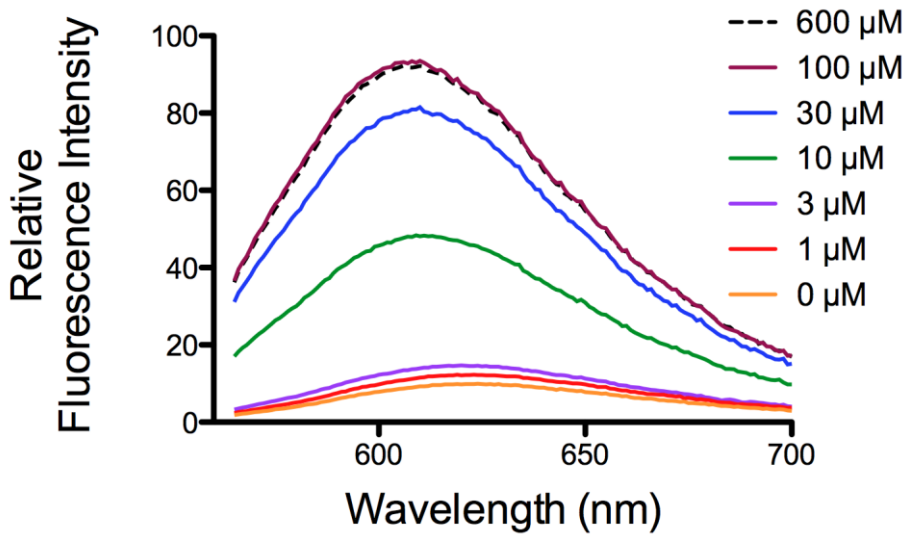

FIGURE D-11: Fluorescence for **LSP1**. Increase in fluorescence intensity with increasing Zn(II) concentrations with **LSP1**. Experiments were carried out using 96-well plates.

The interaction of **LSP1** with HEK 293 cells was next examined in apoptotic and non-apoptotic cells in order to determine the ability of this new sensing platform to detect cellular Zn(II). **LSP1** did not fluoresce in the presence of healthy cells, suggesting the absence of labile Zn(II) (Figure D-12a).[23] The absence of labile and hence detectable Zn(II) is most likely due to cellular Zn(II) readily transitioning to protein-complexes within intracellular compartments (Figure D-12a). This is also consistent with **LSP1** not being internalized into the eukaryotic cells due to their size (~100 nm) and bacterial lipid composition. By contrast, fluorescence was observed when **LSP1** was added to apoptotic HEK 293 cells, presumably due to the formation of the **LSP1.Zn(II)** complexes Figure D-12b and c). Cells undergoing early events of apoptosis are known to have increased levels of labile intracellular Zn(II) due to changes in the intracellular redox state liberating Zn(II) from protein thiolate bonds.[23] Intriguingly, in both experiments with the healthy and apoptotic cells, fluorescence was not observed between **LSP1** and the Zn(II) in the media

surrounding the cells. These unique observation suggest that **LSP1** is able to detect Zn(II) at the surface of cell membranes and further studies to understand this phenomenon are currently on-going.

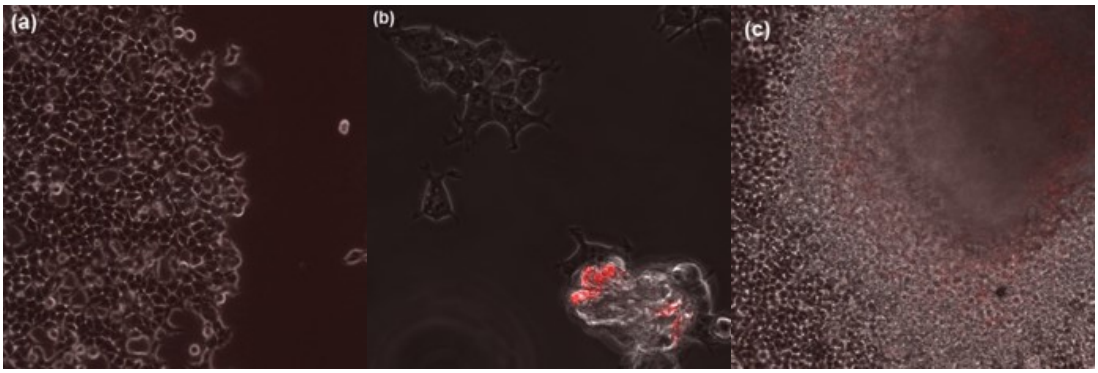

FIGURE D-12: Confocal microscope images of **LSP1** incubated with HEK 293 cells. HEK 293 cells were incubated overnight at 37 °C with 8 μL of **LSP1**. (a) Image of **LSP1** with non-apoptotic cells. (b) and (c) Images of **LSP1** with apoptotic cells where Zn(II) efflux were detected.

The spiropyran-liposome complex was observed to be non-toxic under these experimental conditions, with extended incubation of **LSP1** with HEK 293 cells for 18 hours having no observable effect on cell growth. In support, it is known that low concentrations of isolated spiropyrans (10^{-6}, 10^{-8}, and 10^{-9} M) do not induce any cytotoxic response after 24 and 72 h of exposure time.[24] This combination of a lack of toxicity and an ability to sense Zn(II) from apoptotic cells clearly demonstrates **LSP1** to be an effective sensor for detecting Zn(II) in cellular media.

In the final part of the study, **LSP1** was combined with a microstructured optical fibre (MOF) as a first step toward realizing a nanoscale dip-Sensor for Zn(II) that is able to yield significant signal-to-background changes with minimal sample volumes, a real advance in biological sensing that enables measurement on sub-cellular-scale samples. The MOF also provides a platform for sensing Zn(II) in confined spaces such as the medium surrounding cell clusters, oocytes and embryos, and in the in-vivo environment.[25] MOFs contain air holes within their cross-section that can be used to control the interactions between light guided within the fibre core and matter located within the holes in the fibre cross-section. These voids simultaneously act as the request micro sample chambers.[25] One end of the fibre was

dipped into pre-mixed **LSP1.Zn(II)** solutions and this mixture drawn into the air-holes by capillary action. Each fibre was filled with 150 - 180 nL of the solution (Supporting Information, Figure D-15). The fibre core was then exposed to light from a 532 nm laser and the fluorescence generated within the sample chambers was collected by the fibre core. By capturing the fluorescence travelling in the backwards direction the sampling end of the fibre can be left *in-situ* within the environment being sampled. The results shown in Figure D-13 shows a dramatic increase in fluorescence intensity in the presence of 100 ρM Zn(II); emission was not detected in the absence of zinc ions. These results are highly reproducible and graphs from repeated experiments can be seen in Figure D-16 in the Supporting Information section. Binding of Zn(II) can be turned off by exposing the system to white light for 2 min (Supporting Information, Figure D-13). The ability to turn binding of Zn(II) on/off is an important advance towards developing sensors that are reusable and/or capable of continuous or repeated measurements.

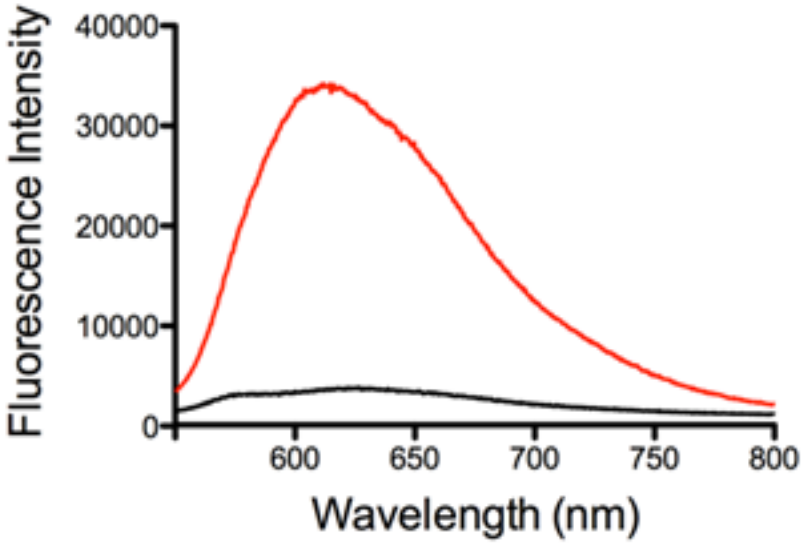

FIGURE D-13: Fluorescence results of the optical fibre-based nanoscale dip-sensor. **LSP1** in the absence (black) and in 100 ρM (red) of Zn(II).

Photobleaching experiments were also carried out to determine the chemical and photostability of **LSP1** under the conditions of the experiment. A solution of **LSP1** pre-mixed with 10 nM of Zn(II) and exposed to the 532 nm laser for 10 x 16 ms. Minimal photobleaching of less than 10 % was observed (Figure D-14). More

importantly, it was shown that upon exposure to UV light for 7 min returned **LSP1** to the same fluorescence intensity as before demonstrating that the minimal photodiscoloration was not due to any photodestruction of the molecules (Supporting Information, Figure D-17), but is most likely due to some spiropyran molecules switching back to the non-fluorescent spiro form under the influence of the 532 nm laser light. The stability of this system under these optical experimental conditions show that **LSP1** is suitable for development into a fibre-based dip-sensor suitable for the detection of Zn(II) in biological applications such as the monitoring of zinc spark events during the developmental cell cycle of mammalian eggs.[14]

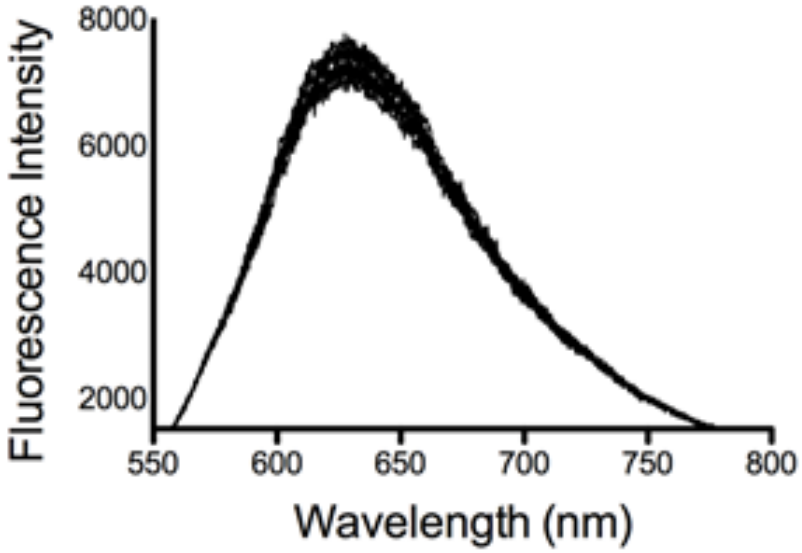

FIGURE D-14: Photobleaching experiments within the optical fibre dip sensor. In the presence of 10 nM Zn(II) where the sample was exposed to 10 x 16 ms of light from the 532 nm laser. The optical power is 35 μW.

D.2.4 CONCLUSION

In this work, a new biologically compatible Zn(II) sensor was fabricated by embedding Zn(II) sensing spiropyran molecules within the surface of the liposome (**LSP1**). Solution-based experiments with increasing Zn(II) concentrations demonstrate that this new sensor has improved aqueous solubility and sensitivity compared to the original spiropyran molecule (**SP1**). Cell based experiments showed that **LSP1** is capable of sensing Zn(II) efflux from apoptotic HEK 293 cells with preliminary data indicating that sensing is localized near the plasma membrane of the

cells. This provides a significant advantage over other zinc fluorescent sensors, such as FluoZin-3[26] that operates in the bulk solution and hence lacks sensitivity and an ability to operate at a local level. **LSP1** is also suitable for development into a nanolitre scale, dip-sensor for Zn(II) using microstructured optical fibre as the sensing platform. Here Zn(II) can be detected within the range of 100 ρM with no signs of photobleaching. The results reported in this paper demonstrate an approach for developing existing spiropyran molecules into biologically compatible sensors for use in a wide range of applications.

D.2.5 MATERIALS AND METHODS

D.2.5.1 Materials

All ^{13}C NMR spectra (150 MHz) and ^{1}H NMR spectra (300 MHz) were recorded on a Varian Gemini 2000 spectrometer in $CDCl_3$ or DMSO-d_6. Chemical shifts (δ) are reported in ppm. Chemical shifts of $CDCl_3$ (δ_c = 77.1 ppm), DMSO-d_6 (δ_c = 39.52 ppm) or TMS (δ_H = 0.0 ppm) were used as internal standards in all ^{13}C NMR and ^{1}H NMR experiments respectively. HPLC grade Acetonitrile was used in all related experiments. Anhydrous THF was distilled in the presence of benzophenone and sodium. All zinc ions used in this work were in the form of perchlorate salt. All other reagents were purchased from Sigma-Aldrich and used without further purification.

D.2.5.2 Synthesis of SP1

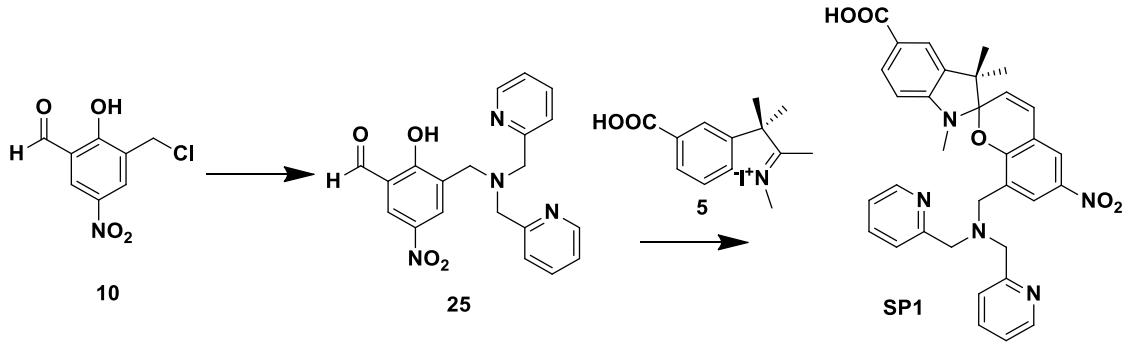

A solution of compound **10** (100 mg, 0.46 mmol) in anhydrous THF (15 mL) was added drop wise to a solution of di-(2-picolyl)amine (84 µL, 0.46 mmol) and Et_3N

(130 µL, 0.93 mmol) in anhydrous THF (5 mL) at 0 °C. The reaction mixture was allowed to warm to rt gradually and was set to reflux for 18 h. After removing the $Et_3N.Cl$ salt that formed using filtration, excess solvent was removed under reduced pressure and the crude product 3-((bis(pyridin-2-ylmethyl)amino)methyl)-2-hydroxy-5-nitrobenzaldehyde (**25**) was used in the next step without further purification. ^1H NMR ($CDCl_3$, 300 MHz) δ 10.59 (s, 1H), 8.62 – 8.58 (m, 3H), 8.23 (d, 1H, J = 3.0 Hz), 7.71 – 7.66 (m, 3H), 7.32 (d, 2H, J = 7.8 Hz), 7.23 (t, 2H, J = 6.0 Hz), 3.10 (s, 4H), 3.77 (s, 2H). MS (m/z) for $C_{20}H_{18}N_4O_4$ + H ($[M+H]^+$) calcd 379.4; found 379.4. After which, compounds **5** (100 mg, 0.46 mmol) and **25** (173 mg, 0.46 mmol) were dissolved in anhydrous ethanol (10 mL) and set to reflux for 18 h. Excess solvent was removed under vacuum and the crude mixture was purified using C-18 reverse phase silica gel (30 % acetonitrile:H_2O) to yield 8-((bis(pyridin-2-ylmethyl)amino)methyl)-1',3',3'-trimethyl-6-nitrospiro[chromene-2,2'-indoline]-5'-carboxylic acid (**SP1**, 200 mg, 75 %) as purple solid. ^1H NMR (DMSO-d_6, 300 MHz) δ 8.41 (d, 2H, J = 5.1 Hz), 8.20 (d, 1H, J = 2.7 Hz), 8.11 (d, 1H, J = 3.3 Hz), 7.81 (t, 1H, J = 8.1, 1.8 Hz), 7.71 – 7.65 (m, 3H), 7.30 (d, 2H, J = 7.8 Hz), 7.22 – 7.17 (m, 3H), 6.68 (d, 1H, J = 8.1 Hz), 6.08 (d, 1H, J = 10.2 Hz), 3.64 (s, 4H), 3.48 (s, 2H), 2.72 (s, 3H), 1.20 (s, 3H), 1.14 (s, 3H); ^{13}C NMR (150 MHz) δ 167.4, 158.4 (2C), 156.4, 151.1, 148.7 (2C), 140.3, 135.9 (2C), 130.8, 128.6, 126.3, 125.2, 122.9, 122.5 (2C), 122.1 (2C), 121.5, 121.3, 120.4, 118.5, 106.2, 105.9, 59.4 (2C), 51.2, 50.5, 45.7, 28.3, 25.5, 19.5. MS (m/z) for + H ($[M+H]^+$) calcd $C_{31}H_{39}N_3O_9$ 598.3; found 598.0; ($[M+Na]^+$) calcd 620.3; found 620.3. HRMS (ESI, m/z) for ($[M+H]^+$) calcd 598.2765 found 598.2757.

D.2.5.3 Construction of LSP1.

LSP1 was generated by dissolving **SP1** in DMSO (40 $mg.ml^{-1}$) and mixing it with a solution containing 0.04 mg of total *Escherichia coli* total lipids extracts in 20 mM MOPS, pH 7.2. Large multilamellar liposomes were formed by sonication and vortexing the lipid-**SP1** mixture for 15 minutes. The **LSP1** mixture was clarified to remove unincorporated insoluble **SP1** by high-speed centrifugation at 18,000 x *g* for 20 minutes at room temperature followed by ultracentrifugation at 120,000 x *g* for 60 minutes at 20 °C to isolate the **LSP1** fraction. The lipid pellet containing **LSP1** was washed twice with 20 mM MOPS, pH 7.2 to remove any soluble **SP1** and then

resuspended in 20 mM MOPS, pH 7.2. Unilamellar **SP1** liposomes were generated by resuspending the lipid pellet in 20 mM MOPS, pH 7.2 and extruding the mixture through a 0.1 μm membrane. After 11 passages **LSP1** liposomes with a median size distribution of ~100 nm in diameter were generated for analysis.

D.2.5.4 Solution Studies of SP1 and LSP1.

Solutions of **SP1** in 20 % acetonitrile in water and **LSP1** in MOPS buffer were then exposed to varying concentrations of Zn(II) in order to examine their affinities towards the ion (Figure D-11). We demonstrate that embedding **SP1** onto the surface of liposomes (as in **LSP1**) significantly improves solubility in MOPS buffer compared to the solubility of **SP1**, where 20 % acetonitrile is required as a co-solvent in order to achieve aqueous solubility.

D.2.5.5 Fluorescence Experiments.

Cuvette measurements of **SP1**. **SP1** and zinc chloride were dissolved in HPLC grade acetonitrile respectively. A solution of the appropriate solvent containing similar concentrations of **SP1** and metal ion was prepared and exposed to UV light (8 W, 365 nm filtered) for 7 min. Fluorescence spectra were recorded on a Varian 80 Cary Eclipse spectrofluorometer. The excitation and emission slit width were set at 5 mm. All measurements were recorded at 25 °C using 700 μL quartz cuvettes with an excitation path length of 10 mm. Photodecoloration experiments were performed by exposing the respective samples to white light (8 W, cool white).

Microplate measurements of **LSP1**. 20 μL of 40 $mg.ml^{-1}$ **LSP1** in 20 mM MOPS, pH 7.2 was incubated with $ZnSO_4$ at concentrations ranging from 0 to 600 μM for 10 minutes in the dark at 25 °C. The final assay volume for all samples was 100 μL in Greiner 96 well black plates. The fluorescence spectrum (565 nm - 700 nm, 2 nm slit width) recorded on a Biotek Synergy H1 using excitation at 535 nm with 10 flashes per reading. Data was analyzed using Prism version 5.0 (Graphpad Prism).

D.2.5.6 HEK 293 Cellular Experiments.

HEK 293 cells were grown in MEM with 10 % foetal bovine serum, at 37 °C in the presence of 6 % CO_2 in Air. The cells were plated and grown for 72 h with one media change. After which, 8 μL of **LSP1** were added to the cell media and the cells

were incubated with **LSP1** at 37 °C for an additional 12 h. Interactions between **LSP1** and HEK 293 cells were examined using confocal microscopy.

D.2.5.7 Microstructured Optical Fibre (MOF) Experiments.

The MOFs used in this work was fabricated in-house. Details of the fibre and optical set-up have been reported previously.[1] Respective solutions of **LSP1** with varying concentrations of Zn(II) were made up. The MOF was filled by immersing the left-hand tip into the solutions that were then left to fill via capillary forces. Fluorescence and photobleaching experiments were carried according to the method described in our previous work.[1]

D.2.6 SUPPORTING INFORMATION.

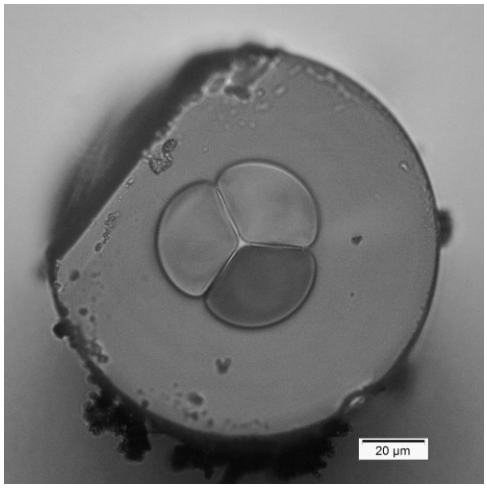

FIGURE D-15: Cross section microstructured optical fibre taken with OLYMPUS BX51 light microscope, MPlanFLN-BD 50x/0.80 objective lens and fitted with OLYMPUS SC100 camera. Each hole has a diameter of 27.7 µm and an effective area of 600 μm^2. The length of each fibre used was between 9.5 to 11 cm. This equates to a maximum fill volume of approximately 180 nl/10 cm of fibre.

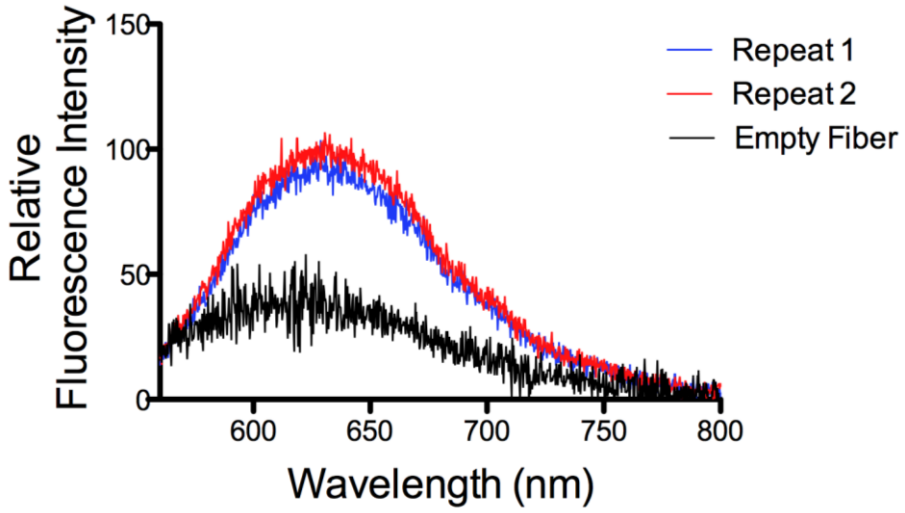

FIGURE D-16: Repeated fluorescence experiments of the optical fibre-based nanoscale dip-sensor. **LSP1** in the absence (black) and in 100 ρM of Zn(II) where (blue) and (red) represents repeated experiments 1 and 2 respectively.

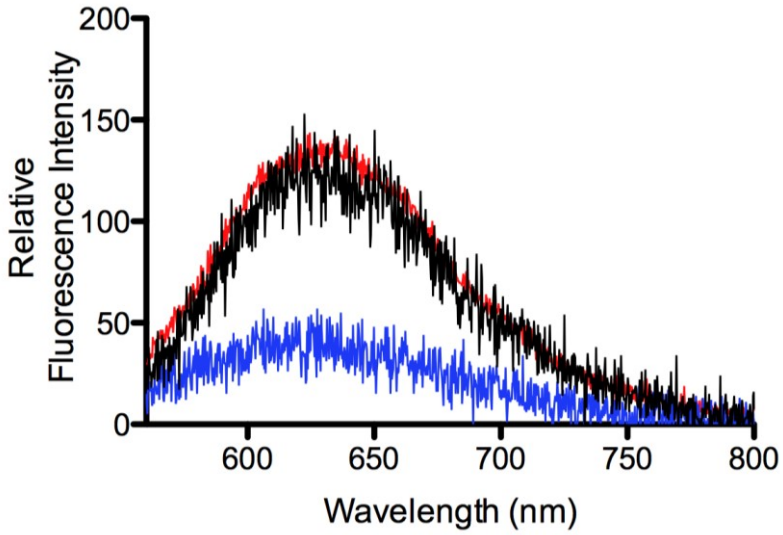

FIGURE D-17: Photoswitching of **LSP1** in MOF. (red) "On cycle". **LSP1** with 10 nM of Zn(II), (blue) "Off-cycle". **LSP1** with 10 nM of Zn(II), exposed to white light for 2 min and (black) "On-cycle". Same sample of **LSP1** with 10 nM Zn(II) exposed to UV (λ = 365 nm) for 7 min.

D.2.7 REFERENCES

1. Heng, S.; McDevitt, C. A.; Stubing, D. B.; Whittall, J. J.; Thompson, J. G.; Engler, T. K.; Abell, A. D.; Monro, T. M. Microstructured optical fibers and live cells: a water-soluble, photochromic zinc sensor. *Biomacromolecules* 2013, *14* (10), 3376-9.
2. Fischer, E.; Hirshberg, Y. Formation of coloured forms of spirans by low-temperature irradiation. *Journal of the Chemical Society* 1952, *868* (Nov), 4522-4524.
3. Natali, M.; Giordani, S. Molecular switches as photocontrollable "smart" receptors. *Chemical Society Reviews* 2012, *41* (10), 4010-4029.
4. Lukyanov, B. S.; Lukyanova, M. B. Spiropyrans: synthesis, properties, and applications. *Chemical Heterocyclic Compounds.* 2005, *41*, 281-311.
5. Shao, N.; Jin, J. Y.; Cheung, S. M.; Yang, R. H.; Chan, W. H.; Mo, T. A spiropyran-based ensemble for visual recognition and quantification of cysteine and homocysteine at physiological levels. *Angewandte Chemie-International Edition* 2006, *45* (30), 4944-4948.
6. Shiraishi, Y.; Adachi, K.; Itoh, M.; Hirai, T. Spiropyran as a Selective, Sensitive, and Reproducible Cyanide Anion Receptor. *Organic Letters* 2009, *11* (15), 3482-3485.
7. Kolmakov, K.; Belov, V. N.; Bierwagen, J.; Ringemann, C.; Mueller, V.; Eggeling, C.; Hell, S. W. Red-Emitting Rhodamine Dyes for Fluorescence Microscopy and Nanoscopy. *Chemistry - A European Journal* 2010, *16* (1), 158-166.
8. Garcia, A. A.; Cherian, S.; Park, J.; Gust, D.; Jahnke, F.; Rosario, R. Photon-controlled phase partitioning of spiropyrans. *Journal of Physical Chemistry A* 2000, *104* (26), 6103-6107.
9. Zhang, Z. H.; Burns, D. C.; Kumita, J. R.; Smart, O. S.; Woolley, G. A. A water-soluble azobenzene cross-linker for photocontrol of peptide conformation. *Bioconjugate Chemistry* 2003, *14* (4), 824-829.
10. Zhu, S.; Zhang, J.; Janjanam, J.; Bi, J.; Vegesna, G.; Tiwari, A.; Luo, F. T.; Wei, J.; Liu, H. Highly water-soluble, near-infrared emissive BODIPY polymeric dye bearing RGD peptide residues for cancer imaging. *Analytica chimica acta* 2013, *758*, 138-44.
11. Shao, N.; Wang, H.; Gao, X.; Yang, R.; Chan, W. Spiropyran-Based Fluorescent Anion Probe and Its Application for Urinary Pyrophosphate Detection. *Analytical Chemistry* 2010, *82* (11), 4628-4636.
12. Shao, N.; Jin, J.; Wang, H.; Zheng, J.; Yang, R.; Chan, W.; Abliz, Z. Design of Bis-spiropyran Ligands as Dipolar Molecule Receptors and Application to in Vivo Glutathione Fluorescent Probes. *Journal of the American Chemical Society* 2010, *132* (2), 725-736.
13. Tomizaki, K. Y.; Mihara, H. A novel fluorescence sensing system using a photochromism-based assay (P-CHROBA) technique for the detection of target proteins. *Journal of Materials Chemistry* 2005, *15* (27-28), 2732-2740.
14. Kim, A. M.; Bernhardt, M. L.; Kong, B. Y.; Ahn, R. W.; Vogt, S.; Woodruff, T. K.; O'Halloran, T. V. Zinc Sparks Are Triggered by Fertilization and Facilitate Cell Cycle Resumption in Mammalian Eggs. *ACS Chemical Biology* 2011, *6* (7), 716-723.

15. Wang, C. Y.; Wang, T.; Zheng, W.; Zhao, B. L.; Danscher, G.; Chen, Y. H.; Wang, Z. Y. Zinc overload enhances APP cleavage and Abeta deposition in the Alzheimer mouse brain. *Plos one* 2010, *5* (12), e15349.
16. Maynard, C. J.; Bush, A. I.; Masters, C. L.; Cappai, R.; Li, Q. X. Metals and amyloid-beta in Alzheimer's disease. *International Journal of Experimental Pathology* 2005, *86* (3), 147-159.
17. Long, A. E.; Gillespie, K. M.; Aitken, R. J.; Goode, J. C.; Bingley, P. J.; Williams, A. J. K. Humoral Responses to Islet Antigen-2 and Zinc Transporter 8 Are Attenuated in Patients Carrying HLA-A*24 Alleles at the Onset of Type 1 Diabetes. *Diabetes* 2013, *62* (6), 2067-2071.
18. VanLandingham, J. W.; Fitch, C. A.; Levenson, C. W. Zinc inhibits the nuclear translocation of the tumor suppressor protein p53 and protects cultured human neurons from copper-induced neurotoxicity. *Neuromolecular Medicine* 2002, *1* (3), 171-182.
19. Formigari, A.; Gregianin, E.; Irato, P. The effect of zinc and the role of p53 in copper-induced cellular stress responses. *Journal of Applied Toxicology* 2013, *33* (7), 527-536.
20. McDevitt, C. A.; Ogunniyi, A. D.; Valkov, E.; Lawrence, M. C.; Kobe, B.; McEwan, A. G.; Paton, J. C. A Molecular Mechanism for Bacterial Susceptibility to Zinc. *Plos Pathogens* 2011, *7* (11).
21. Jiang, P. J.; Guo, Z. J. Fluorescent detection of zinc in biological systems: recent development on the design of chemosensors and biosensors. *Coordination Chemistry Reviews* 2004, *248* (1-2), 205-229.
22. Heng, S.; Nguyen, M.-C.; Kostecki, R.; Monro, T. M.; Abell, A. D. Nanoliter-scale, regenerable ion sensor: sensing with a surface functionalized microstructured optical fibre. *RSC Advances* 2013, *3* (22), 8308-8317.
23. Truong-Tran, A. Q.; Ho, L. H.; Chai, F.; Zalewski, P. D. Cellular zinc fluxes and the regulation of apoptosis/gene-directed cell death. *Journal of Nutrition* 2000, *130* (5), 1459S-1466S.
24. Movia, D.; Prina-Mello, A.; Volkov, Y.; Giordani, S. Determination of Spiropyran Cytotoxicity by High Content Screening and Analysis for Safe Application in Bionanosensing. *Chemical Research in Toxicology* 2010, *23* (9), 1459-1466.
25. Monro, T. M.; Warren-Smith, S.; Schartner, E. P.; Francois, A.; Heng, S.; Ebendorff-Heidepriem, H.; Afshar, S. Sensing with suspended-core optical fibers. *Optical Fiber Technology* 2010, *16* (6), 343-356.
26. Krenn, B. M.; Gaudernak, E.; Holzer, B.; Lanke, K.; Van Kuppeveld, F. J. M.; Seipelt, J. Antiviral Activity of the Zinc Ionophores Pyrithione and Hinokitiol against Picornavirus Infections. *Journal of Virology* 2009, *83* (1), 58-64.

D.3 PAPER 5: A SELECTIVE AND REVERSIBLE CALCIUM SENSOR FOR BIOLOGICAL APPLICATIONS

Statement of Authorship

Title of Paper	A Selective and Reversible Calcium Sensor for Biological Applications
Publication Status	☐ Published ☐ Accepted for Publication ☑ Submitted for Publication ☐ Publication Style
Publication Details	Sabrina Heng, Xiaozhou Zhang, Roman Kostecki, Adrian M. Mak, Jinxin Pei, Daniel B. Stubing, Heike Ebendorff-Heidepriem, Andrew D. Abell. "A Selective and Reversible Calcium Sensor for Biological Applications".

Principal Author

Name of Principal Author	Sabrina Heng		
Contribution to the Paper	Project conceptualisation. Project direction and writing of the manuscript. Fluorescence assays of **SP-4** with ions.		
Signature		Date	06.10.16

Co-Author Contributions

By signing the Statement of Authorship, each author certifies that:

i. the candidate's stated contribution to the publication is accurate;
ii. permission is granted for the candidate in include the publication in the thesis;
iii. the sum of all co-author contributions is equal to 100 % less the candidate's stated contribution.

Name of Co-Author (Candidate)	Daniel B. Stubing		
Contribution to the Paper	Synthesis of spiropyran **SP-4** fluoroionophore, Fluorescence assays of **SP-4** with ions.		
Overall percentage (%)	20		
Signature		Date	08/09/2016

Name of Co-Author	Xiaozhou Zhang		
Contribution to the Paper	Cell studies and assistance with SCF experiments		
Signature		Date	13/9/16

Name of Co-Author	Roman Kostecki		
Contribution to the Paper	SCF experiments for sensing **SP-4** in solution and writing of manuscript.		
Signature		Date	15/9/2016

Name of Co-Author	Adrian M. Mak		
Contribution to the Paper	Computational modelling and writing of manuscript.		
Signature		Date	08/09/2016

Name of Co-Author	Jinxin Pei		
Contribution to the Paper	Cell studies and confocal microscopy		
Signature		Date	13/9/16

Name of Co-Author	Heike Ebendorff-Heidepriem		
Contribution to the Paper	Project direction and editing of manuscript.		
Signature		Date	13/9/2016

Name of Co-Author	Andrew D. Abell		
Contribution to the Paper	Project direction and significant editing of manuscript.		
Signature		Date	13/09/2016

A SELECTIVE AND REVERSIBLE CALCIUM SENSOR FOR BIOLOGICAL APPLICATIONS

Sabrina Heng,*[a] Xiaozhou Zhang,[a] Roman Kostecki,[a] Adrian M. Mak,[b] Jinxin Pei,[a,c] Daniel B. Stubing, [a] Heike Ebendorff-Heidepriem,[a] Andrew D. Abell. [a]

[a] ARC Center of Excellence for Nanoscale BioPhotonics, Institute for Photonics and Advanced Sensing, Department of Chemistry, School of Physical Sciences. The University of Adelaide, Adelaide, South Australia 5005, Australia.

[b] Institute of High Performance Computing, 1 Fusionopolis Way, No. 16-16 Connexis, Singapore 138632

[c] Department of Physiology, Faculty of Health Sciences, The University of Adelaide, South Australia.

D.3.1 ABSTRACT

A photoswitchable sensor for the selective detection of calcium ions (Ca^{2+}) was developed. Intra- and extra- cellular Ca^{2+} is known to fluctuate in the signalling of key biological processes; therefore, it is of interest to be able to detect the changing concentration of Ca^{2+} in a biological environment. This spiropyran based photoswitchable sensor is shown to be highly selective for Ca^{2+}over other biologically relevant metal ions. Job's analysis and HPC modelling was used to show the binding mechanism to Ca^{2+}. Incorporation of this sensor into Suspended Core microstructured optical Fibres (SCFs) allowed for the highly sensitive fluorescence sensing of nanomolar concentration in nanolitre volumes of mixed aqueous/acetonitrile solutions, and reversibility of the sensor is demonstrated.

D.3.2 INTRODUCTION

Calcium (Ca^{2+}) is a ubiquitous intracellular signalling ion that plays a critical role in the modulation of fundamental cellular processes; including cell proliferation, differentiation, and survival/death.[1] An ability to sense and determine its intracellular concentration is thus central to biology and medical applications. However, sensing Ca^{2+} is not straightforward as intracellular concentrations vary greatly during a typical cell cycle, with a variety of plasma membrane Ca^{2+} permeable channels and

intracellular sources contributing to fluctuations in levels.[2-4] While a number of highly selective and sensitive fluorescent chemosensors for one-off sensing of Ca^{2+} within a cell are known,[5-7] real-time continuous measurement is needed if we are to gain true insights into associated biological processes and exploit the outcomes of measurement. Such a sensor must be able to be 'switched' on and off on-demand with an external stimulus to allow multiple measurements on a single sample without the need to change the sensor.

The reversible Ca^{2+} sensor described here (Figure D-18) uses a spiropyran as a photoswitch to allow reversible switching and hence continuous sensing. A spiropyran has the advantage of low background fluorescence as compared to non-photochromic sensors such as those based on rhodamine.[8] A combination of a 1-aza-18-crown-6 substituent at C_8 of the benzopyran ring[9], and an ethoxy group on the indole nitrogen[9, 10] was used to promote affinity for Ca^{2+} in the ring opened merocyanine (MC) form as shown in Figure D-18. The sensor also contains an aryl carboxylate to increase hydrophilicity for biological applications.

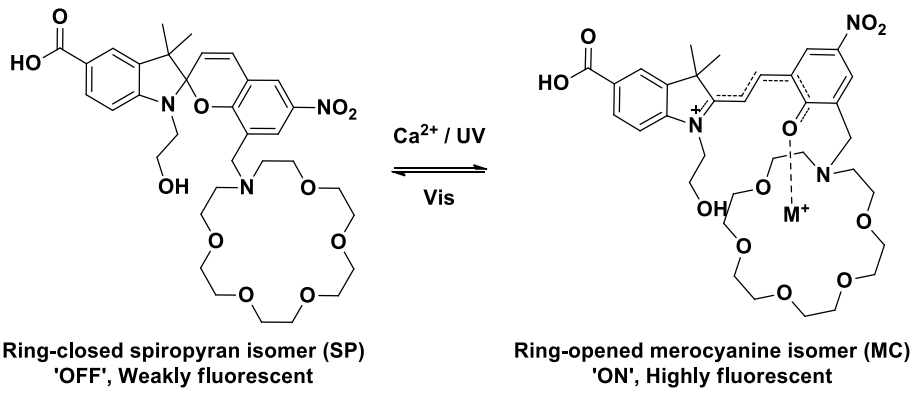

FIGURE D-18: Isomeric structures of the Ca^{2+} sensor (**SP-4**). The ring-closed spiropyran isomer is weakly fluorescent (**SP-4**, 'OFF'). The ring-opened Ca^{2+}-induced merocyanine isomer is highly fluorescent (**MC-4-Ca^{2+}**, 'ON').

D.3.3 RESULTS AND DISCUSSION

D.3.3.1 Synthesis and Ion Binding Characterization.

The Ca^{2+} Sensor **SP-4** was prepared from 4-hydrazinobenzoic acid and 1-aza-18-crown-6 in an overall yield of 47 % using a modification to existing methodology[11, 12] as detailed previously in Section 4.5.1.2. The addition of Ca^{2+} to **SP-4** gave rise to

strong fluorescence at 620 nm associated with the formation of the (**MC-4**)-Ca^{2+} complex depicted in Figure D-18. The sensor shows good selectivity over other metal ions (Co^{2+}, Mg^{2+}, Fe^{2+}, Cu^{2+}, K^{+}, Mn^{2+}, Na^{+} and Zn^{2+}) giving a significantly reduced signal (Figure D-20) compared to fluorescence signal obtained with Ca^{2+}. Increasing fluorescence was observed with increasing Ca^{2+} concentrations (see previous Section 4.3.1.3 for details), with maximum fluorescence observed after the addition of 1.0 equiv of Ca^{2+}. Job's plot analysis revealed a maximum fluorescence at 0.5 for Ca^{2+} indicating that the observed fluorescence response for **SP-4** is due to the formation of a 1:1 (**MC-4)**-Ca^{2+} complex (Figure D-20B).

Reaction energies of **SP-4** and the associated complex with Ca^{2+} were calculated using density functional theory in order to characterize the 'On' and 'Off' states, with the optimized geometries of ring closed SP isomer (**SP-4**) and the ring-opened MC form (**MC-4**) shown in Figure D-19. The model (**MC-4**)-Ca^{2+} shows five coordinate bonds formed between the sensor and the central metal ion. The average distances between the crown-based oxygen and Ca^{2+} were found to be 2.4 – 2.7 Å. More importantly, Ca^{2+} was found to coordinate to both the phenolic and ethoxy oxygens at 2.12 and 2.38 Å respectively. These molecular modelling results validate the sensor design and supports the 1:1 binding complex from Job's plot analysis.

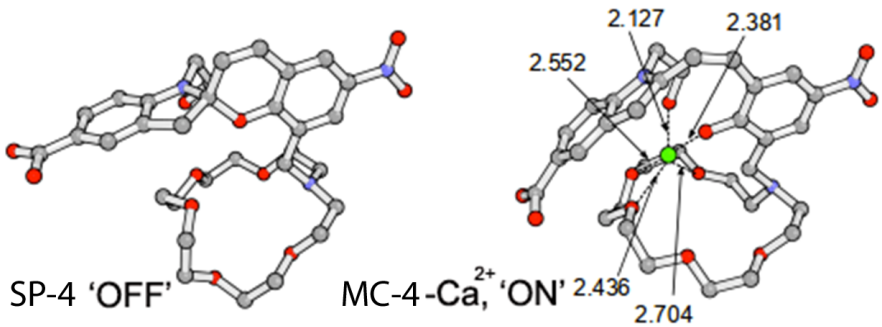

FIGURE D-19: Optimized structures of **SP-4** ('OFF') and **MC-4** ('ON'). Hydrogens are not depicted for clarity. Carbon atoms are in grey, oxygen atoms are in red, nitrogen atoms are in blue and calcium atoms are in green. Interatomic distances are given in Ångstroms.

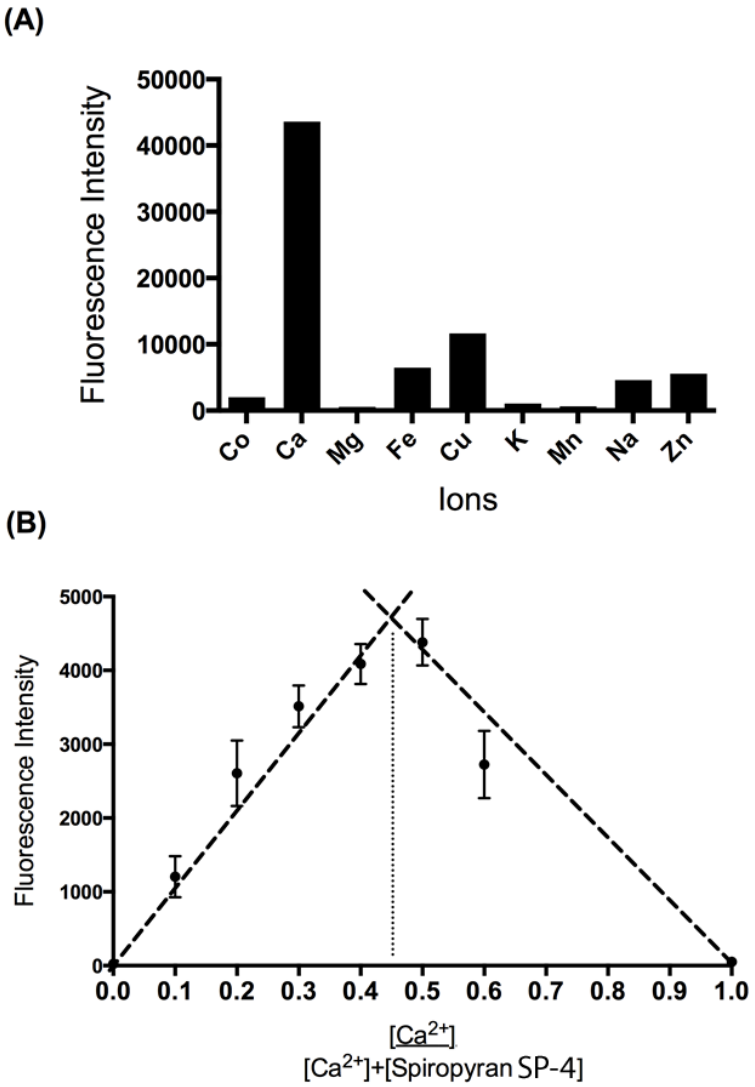

FIGURE D-20: (A) Bar graph showing fluorescence (where λ_{ex} = 532 nm) of **SP-4** (50 μM) in the presence of various biologically relevant metal ions (100 μM). (B) Job's plot analysis of (**MC-4**)-Ca^{2+} complex. All experiments were carried out in 96-well plates at 25 °C and were preformed in duplicates.

D.3.3.2 Sensing with Microstructured Optical Fibres.

Next, **SP-4** was combined with silica suspended-core microstructured optical fibre (SCF)[13] technology as a first step toward a reversible, non-disruptive and highly sensitive sensing platform for Ca^{2+} in the a cell, where the concentration of Ca^{2+} can be as low as 100 nM.[1] SCF is ideal for sensing in biological systems as the air holes within the cross-section of the SCF act as tiny sample chambers to allow measurements of nanoscale volumes enabling measurements on sub-cellular-scale samples.[14] With an overall size less then a couple of hundred μm, these light guiding

structures are suitable for sampling and hence sensing of ions in confined spaces such as the medium surrounding cell clusters, oocytes and embryos, and in the in-vivo environment.[15] With this in mind, one end of a 25 cm length SCF was dipped into solutions containing either **SP-4** only or **SP-4** premixed with 100 nM Ca^{2+}. Approximately 0.1 μL of the solution was drawn into the air holes of the fibre by capillary action. Fluorescence of both samples was measured following irradiation with 532 nm laser (10 × 10 ms pulses) down the fibre with the results shown in Figure D-21A. Details on the fibre and optical setup employed are provided in the Supporting Information section. Figure D-21A reveals an approximate 1.5x increase in fluorescence intensity in the presence of 100 nM Ca^{2+}.

Photoswitching between the (**MC-4**)-Ca^{2+} and SP isomers of the sensor was next characterized in detail using the fibre-based set up described above. In a typical switching experiment, an aqueous solution of **SP-4** (10 μM) was premixed with a solution of Ca^{2+} ions (10 μM) and drawn into the fibre via capillary action as previously described. The solution within the fibre was irradiated with the 532 nm laser (10 x 10 ms pulses), and the resulting increase in fluorescence was measured. The fibre was then illuminated with 532 nm green light for time 15 s in order to form the non-fluorescent SP isomer. Excitation with the 532 nm laser then revealed fluorescence comparable to that observed prior to the addition of Ca^{2+}. The sensor was 'turned-on' again by irradiating the fibre with UV (λ = 365 nm) to allow reformation of the MC isomer and hence sensing of Ca^{2+}, as measured by an associated increase in fluorescence. This procedure was repeated for 20 times and the results are summarized in Figure D-21B. This clearly demonstrates multiple photoswitching without any apparent photobleaching over the time course of the experiment. The photostability of the sensor within the optical fibre sensing system under high intensity light conditions demonstrates that the optical fibre based sensing platform be used to measure ion-induced changes in fluorescence with minimal sample volumes. This represents a real advance in biological sensing that enables measurements on subcellular-scale samples.

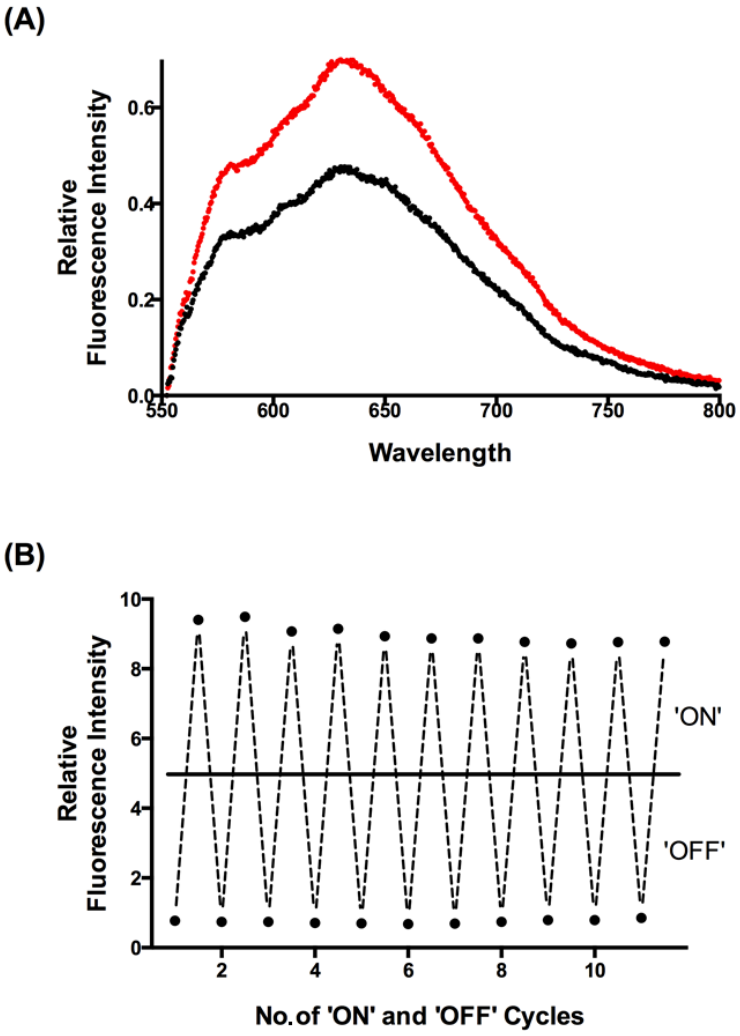

FIGURE D-21: Fluorescence results of the optical fibre-based (SCF) nanoscale sensor. (A) black = emission spectrum of **SP-4** (10 μM 9:1 H_2O:acetonitrile) in the absence of Ca^{2+} ions; red = emission spectrum resulting from 10 μM of SP-4 premixed with 100 nM of Ca^{2+}. (B) Photoswitching of **SP-4** within SCF. Each cycle represents an initial 'OFF' state where **SP-4** was exposed to the 532 nm laser for 15 sec and the subsequent 'On' state where **SP-4** was exposed to UV (λ = 365) for 5 min respectively.

D.3.3.3 In-vivo Experiments with HEK 293 cells.

The ability of **SP-4** to reversibly sense Ca^{2+} in live cells was determined next. HEK 293 cells were treated with ionomycin in a plate (4 wells, each well containing 0, 1, 2 and 5 μM, respectively) to promote rapid accumulation of intracellular Ca^{2+}.[16] A solution of **SP-4** (50 μM in water) was added to each well and the samples were incubated overnight. Irradiation of the cells within each well with the 532 nm light,

gave rise to fluorescence emission at λ_{em} maximum = 630 nm, indicating formation of the (**MC-4**)-Ca^{2+} isomer. Importantly, the observed fluorescence increased with increasing concentration of added ionomycin and hence the Ca^{2+} within the sample was subsequently detected (Figure D-22A). Formation of the associated (**MC-4**)-Ca^{2+} isomer is proportional to Ca^{2+} release as stimulated by ionomycin. The addition of EDTA (50 μM) to a group of cells similarly treated with 5 μM ionomycin revealed a decrease in intracellular fluorescence, see Figure D-22B. This is consistent with removal of Ca^{2+} and reformation of the SP isomer.

Finally, a group of cells treated with **SP-4** and 5 μM ionomycin was imaged by confocal microscopy in order to demonstrate in vivo photoswitching. Figure D-23A shows strong red intracellular fluorescence with an emission maximum at 630 nm was noted in the cells, consistent with results obtained in the plate reader. Subsequent exposure of the cells to visible light for 10 min, gave rise to a decrease in fluorescence, presumably due to formation of a photostationary state enriched in the non-fluorescent ring-closed SP isomer which then releases bound Ca^{2+} to set up the system for further round of Ca^{2+} sensing (Figure D-23B). The cells were again exposed to UV for 15 min. This re-forms the ring-opened MC isomer to allow the sensing of Ca^{2+} as measured by an increase in fluorescence (Figure D-23C). Collectively, these results clearly demonstrate the ability to permeate the cell membrane and also sense changes in intracellular Ca^{2+} concentrations reversibly and on-demand *in vivo* as per solution and fibre-based experiments. These are important findings and provide an opportunity for multiple measurements to be made on a single sample without the need to change the sensor. This is particularly attractive for biological experiments where sample availability and volumes often limit the number of experiments that can be performed.

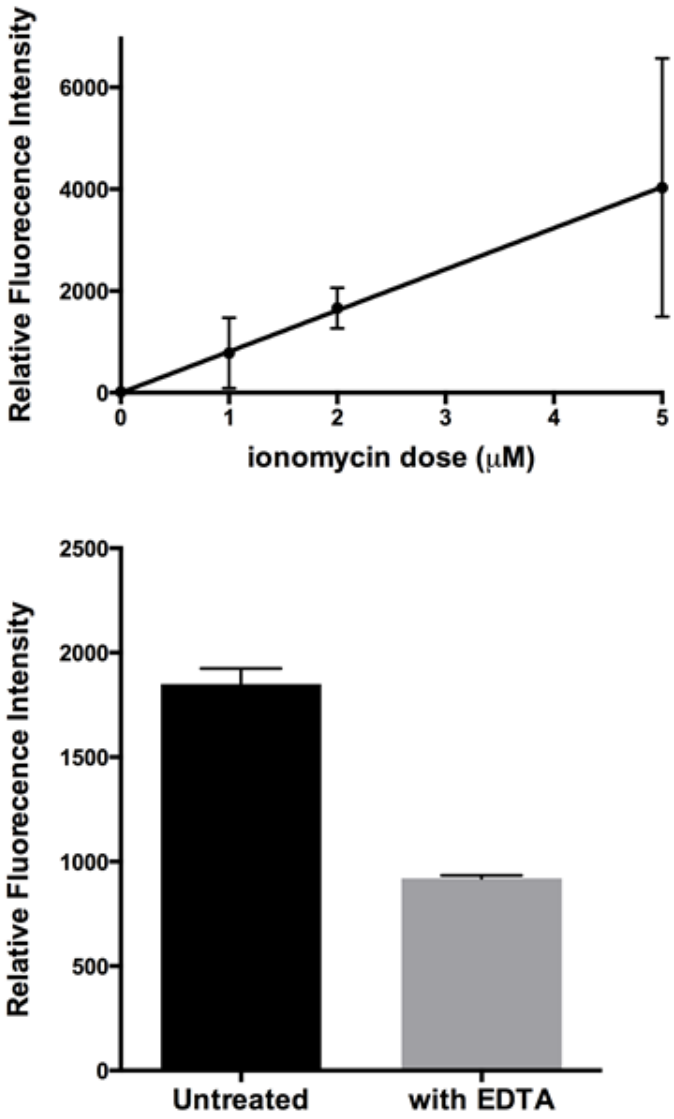

FIGURE D-22: (A) Fluorescence intensity is proportional to intracellular Ca^{2+} release stimulated by ionomycin doses. (B) Decrease in fluorescence after addition of EDTA where untreated represents cells that were not treated with EDTA.

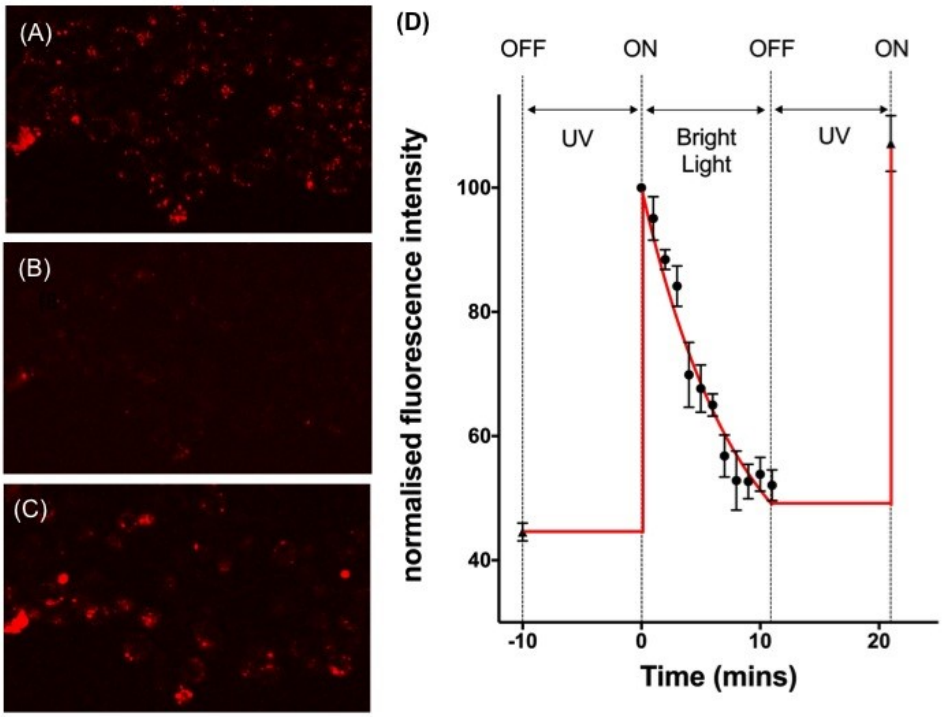

FIGURE D-23: Confocal microscopy images of HEK 293 cells incubated with ionomycin and **SP-4** after 18 h of incubation at 37 °C. Cellular images obtained at A) t = 0 min; B) after exposing the cells to visible light for 11 min; and C) after exposing the cells to UV (λ = 365 nm) for 10 min. D) Normalized fluorescence intensity as a function of time during visible light irradiation**.**

D.3.4 CONCLUSION

Calcium is a ubiquitous intracellular signalling ion that plays a critical role in the modulation of fundamental cellular processes. To properly characterize the role of Ca^{2+} in such processes, selective and reversible sensors for Ca^{2+} are required to quantify and monitor changes of ion concentrations in a biological application. With this in mind, we have designed a selective and reversible sensor for Ca^{2+}. The biocompatibility of the sensor was assessed using HEK 293 cells where the sensor was found to be readily soluble in aqueous media, cell permeable and able to detect changes in intracellular Ca^{2+}. In addition, the sensor is capable of ion detection at 100 nM concentrations using microstructured optical fibre with the sensor being unaffected by multiple rounds of photoswitching. The results in this work can potentially open up avenues for biologists to work with chemists to custom-design, regenerable and selective sensors for virtually any ions with known ionophores. In

addition, the modular synthesis of sensor **SP-4** allows modification of the ionophore, and allow for the rational design of selective and reversible sensors for a given metal ion. This will greatly expand our ability find answers to biological questions, such as the physical principles governing the changes in ion concentrations the cell, which cannot be obtained from non-selective and/or non-reversible ion sensors.

D.3.5 SUPPORTING INFORMATION

D.3.5.1 Fluorescence Measurements Using SCF: Setup

A UV lamp operating at 365 nm wavelength was used for switching SP to the fluorescent MC, ring-opened isomer. A 532 nm laser was used for both excitation of the MC fluorescence and switching of MC back to the non-fluorescent SP ring-closed isomer. The light from the 532 nm laser was coupled into the silica SCF core via a dichroic mirror and 60X objective. The fluorescence collected by the SCF core in backward direction was imaged using the same coupling objective, passed through the dichroic mirror and 550 nm long pass filter, and recorded using a Horiba iHR550 Imaging Spectrometer with Synapse CCD Detector. Each of these recorded measurements was a collection of ten spectra during 5 ms exposure to the 532 nm excitation laser with 5 ms pause in between. The results shown are the average of these ten measurements. The long pass filter was used to remove the excitation light from the light measured by the spectrometer, and all measurements were conducted in the dark.

D.3.5.2 Ca^{2+} Detection by SP-4 Using SCF:

Four 25 cm long silica SCF's were used for the experiments. Each of the four fibres was coupled to the setup to measure the fluorescence from one solution of **SP-4** (10 uM) and 0, 100 nM, 1 uM or 10 uM $CaCl_2$ in 90 % MeCN in water respectively. For each fibre, a measurement was taken straight after coupling and then straight after filling the fibre with the solution for 30 sec. During filling the excitation laser was on to ensure that the spiropyran in solution was the SP ring closed isomer. For subsequent MC ring opened isomer measurements, the SCF was exposed to UV light from the lamp for five minutes, and then a measurement was recorded. For

subsequent SP ring closed isomer measurements, the SCF was exposed to the 532 nm excitation light source for 15 sec before recording the spectra.

D.3.5.3 Photoswitching of SP-4 in a SCF:

The procedure discussed above was repeated 20 times using a mixture of **SP-4** (10 μM) and $CaCl_2$ (10 μM) in water to fill the fibre.

D3.6 REFERENCES

1. Clapham, D. E. Calcium signaling. *Cell* 2007, *131* (6), 1047-58.
2. Pinto, M. C.; Kihara, A. H.; Goulart, V. A.; Tonelli, F. M.; Gomes, K. N.; Ulrich, H.; Resende, R. R. Calcium signaling and cell proliferation. *Cellular Signalling* 2015, *27* (11), 2139-49.
3. Smyth, J. T.; Hwang, S. Y.; Tomita, T.; DeHaven, W. I.; Mercer, J. C.; Putney, J. W. Activation and regulation of store-operated calcium entry. *Journal of Cellular and Molecular Medicine* 2010, *14* (10), 2337-49.
4. Hoffmann, A.; Kann, O.; Ohlemeyer, C.; Hanisch, U. K.; Kettenmann, H. Elevation of basal intracellular calcium as a central element in the activation of brain macrophages (microglia): suppression of receptor-evoked calcium signaling and control of release function. *The Journal of neuroscience : the official journal of the Society for Neuroscience* 2003, *23* (11), 4410-9.
5. Verkhratsky, A.; Petersen, O. H. *Calcium Measurement Methods*. Humana Press: New York, 2010; Vol. 43.
6. Izumi, S.; Urano, Y.; Hanaoka, K.; Terai, T.; Nagano, T. A simple and effective strategy to increase the sensitivity of fluorescence probes in living cells. *Journal of the American Chemical Society.* 2009, *131* (29), 10189-200.
7. Barreto-Chang, O. L.; Dolmetsch, R. E. Calcium imaging of cortical neurons using Fura-2 AM. *Journal of Visualized Experiments : JoVE* 2009, (23).
8. Kolmakov, K.; Belov, V. N.; Bierwagen, J.; Ringemann, C.; Mueller, V.; Eggeling, C.; Hell, S. W. Red-Emitting Rhodamine Dyes for Fluorescence Microscopy and Nanoscopy. *Chemistry - A European Journal* 2010, *16* (1), 158-166.
9. Heng, S.; Mak, A. M.; Stubing, D. B.; Monro, T. M.; Abell, A. D. Dual Sensor for Cd(II) and Ca(II): Selective Nanoliter-Scale Sensing of Metal Ions. *Analytical Chemistry* 2014, *86* (7), 3268-3272.
10. Mao, H.; Thorne, J. B.; Pharr, J. S.; Gawley, R. E. Effect of Crown Ether Ring Size on Binding and Fluorescence Response to Saxitoxin in Anthracylmethyl Monoaza Crown Ether Chemosensors. *Canadian Journal of Chemistry* 2006, *84*, 1273-1279.
11. Heng, S.; Nguyen, M. C.; Kostecki, R.; Monro, T. M.; Abell, A. D. Nanoliter-scale, regenerable ion sensor: sensing with a surface

functionalized microstructured optical fibre. *RSC Advances* 2013, *3* (22), 8308-8317.

12. Stubing, D. B.; Heng, S.; Abell, A. D. Crowned spiropyran fluoroionophores with a carboxyl moiety for the selective detection of lithium ions. *Organic & Biomolecular Chemistry* 2016, 14 (15), 3752-7.
13. Kostecki, R.; Ebendorff-Heidepriem, H.; Warren-Smith, S. C.; Monro, T. M. Predicting the drawing conditions for Microstructured Optical Fiber fabrication. *Optical Materials Express* 2014, *4* (1), 29-40.
14. Monro, T. M.; Warren-Smith, S.; Schartner, E. P.; Francois, A.; Heng, S.; Ebendorff-Heidepriem, H.; Afshar, S. Sensing with suspended-core optical fibers. *Optical Fiber Technology* 2010, *16* (6), 343-356.
15. Heng, S.; McDevitt, C. A.; Kostecki, R.; Morey, J. R.; Eijkelkamp, B. A.; Ebendorff-Heidepriem, H.; Monro, T. M.; Abell, A. D. Microstructured Optical Fiber-based Biosensors: Reversible and Nanoliter-Scale Measurement of Zinc Ions. *ACS Applied Materials & Interfaces* 2016, *8* (20), 12727-32.
16. Yoshida, S.; Plant, S. Mechanism of release of Ca2+ from intracellular stores in response to ionomycin in oocytes of the frog Xenopus laevis. *The Journal of Physiology* 1992, *458*, 307-18.